https://doi.org/10.35662/unine-thesis-2660

UNIVERSITÉ DE NEUCHÂTEL

Bacterial iron reduction and biogenic mineral formation for the stabilization of corroded iron objects

Wafa M. Kooli

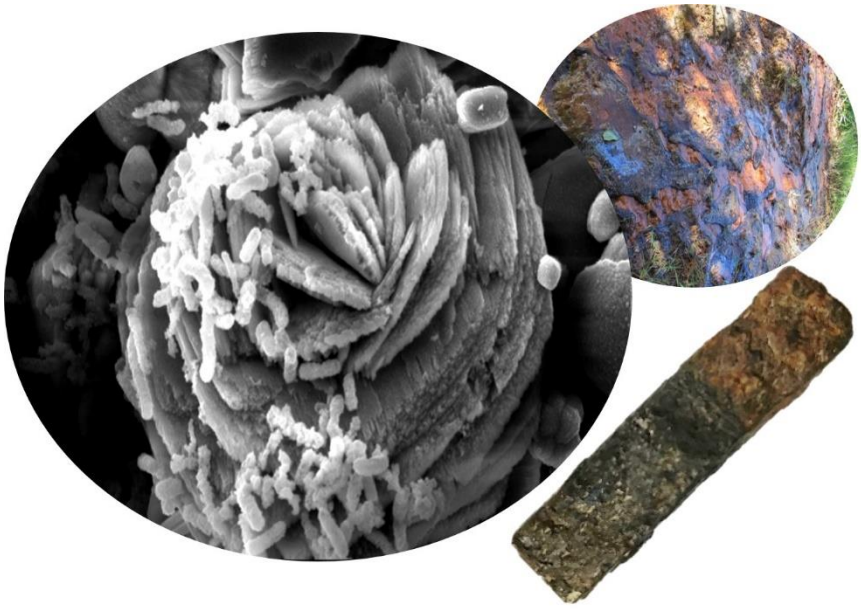

Jury committee members:

Prof. Pilar Junier, thesis co-director, University of Neuchâtel

Prof. Edith Joseph, thesis co-director, University of Neuchâtel

Prof. Geoffrey Gadd, University of Dundee, United Kingdom

Prof. Karim Benzerara, University Pierre et Marie Curie, CNRS, France

Dr. Saskia Bindschedler, University of Neuchâtel

April 11th, 2018

IMPRIMATUR POUR THESE DE DOCTORAT

La Faculté des sciences de l'Université de Neuchâtel autorise l'impression de la présente thèse soutenue par

Madame Wafa M. Kooli

Titre:

“Bacterial iron reduction and biogenic mineral formation for the stabilization of corroded iron objects”

sur le rapport des membres du jury composé comme suit:

- Prof. Pilar Junier, co-directrice de thèse, Université de Neuchâtel, Suisse
- Prof. ass. Edith Joseph, co-directrice de thèse, Université de Neuchâtel, Suisse
- Dr Saskia Bindschedler, Université de Neuchâtel, Suisse
- Dr Karim Benzerara, Université Pierre et Marie Curie, Paris VI
- Prof. Geoffrey M. Gadd, University of Dundee, UK

Neuchâtel, le 27 avril 2018 Le Doyen, Prof. R. Bshary

Bacterial iron reduction and biogenic mineral formation for the stabilization of corroded iron objects

A dissertation submitted to the University of Neuchâtel

For the degree of

Docteur ès Sciences

Presented by Wafa M. kooli, Msc Microbiology

Jury committee members:

Prof. Dr. Pilar Junier, thesis co-director, University of Neuchâtel

Prof Dr. Edith Joseph, thesis co-director, University of Neuchâtel

Prof. Dr. Geoffrey Gadd, University of Dundee, United Kingdom

Prof. Dr. Karim Benzerara, University Pierre et Marie Curie, CNRS, France

Dr. Saskia Bindschedler, University of Neuchâtel

April 11th, 2018

” One day we will be old and think of all the stories that we could have told”
Asaf Avidan

Acknowledgments

I would like to start my acknowledgments by sincerely thanking my thesis committee: **Prof. Geoffrey Gadd, Prof. Karim Benzerara, and Dr. Saskia Bindschedler**. It's an honour for me to be evaluated by great researchers that with their insightful comments will encourage me to widen my research from various perspectives.

During these four years of PhD, I met such great people, that helped me, each one in his or her own way, to become a better researcher and a better person. I learned a lot scientifically but also personally. For that, I would like to thank sincerely also:

Dr. Julien Maillard who introduced me to the polyphosphate world and who supported me during my research but also helped me with great ideas and comments.
Dr. Patrick Chain who gave me the opportunity to improve my bioinformatic skills and his amazing team members, especially **Karen Davenport, Dr. Migun Shakya and Paul Li.** Helped me with their precious support and bioinformatic patience, I had a great experience (even if Patrick (and Armand) were making fun of my bread drawing skills). An experience that allowed me to meet other researchers like Dr **Armand Dichosa, Grace Vuyisich, Tracy Erkkila, Cheryl Gleasner, Kim Mcmurry** that I would like also to thank.
Dr Kaushik Vaideeswaran, Dr Olha Sereda and Dr Massoud Dadras for their help with the XRD and SEM analyses.

All the collaborators of LATHEMA for their smile and kindness, **Mathilde Monachon** for her help for Raman analyses and especially to my co supervisor **Prof Edith Joseph** for giving the opportunity to do this PhD study and work on this amazing project. Thank you for teaching me to pay attention on the details and for the advices during these four years.

All the collaborators of LAMUN and by mean: Nicole Janneret, Teddy Monrouzeau, Andrej Al-dourobi, Sevasti Filippidou, Kelly Mottier for their help and support, **Fabio Palmeri** and **Coralie Montavon**, for staying with me in the lab till late and for all the funny moments and laughs about perfume advertisements that we had. My thanks go also to **Dr Saskia Bindschedler** for her humour and polite attitude that made some of my days better. **Dr. Thomas Junier**, for his patience, kindness and help during my bioinformatic trek. My friend and co-worker **Andrea Lohberger** for supporting and taking care of me during my sickness as well as teaching me that there's no age for climbing. My office mate **Isha Jamil** for bearing me during the writing period for her kindness and for her delicious Biryani.

My friends **Aymen Gabsi, Selim Bouslema, Sawssen Ben Dhia, Ziad Hassan, Hajer Salama, Mahdi Gharbi, Alain Dondo, Tugce Beycan, Anaele Simon, Vincent Hervé, Morgan Kelly, Martha Chan** for the laughing moments and their support. A special thanks to my BFF **Hela Azaeiz** for her continuous support, for listening to my sorrows and not hanging up even when she wanted to, for her honesty and kindness and for standing the bad mood that I had during my writing period.

My sisters, **Yosra and Dorra Kooli** for their continuous support and even if we are far away, they are always in my heart.
My parents, **Amor Kooli and Najoua Jemour** because without their love and support I would not be able to pursue my dreams and follow my career path. This PhD is the result of their sacrifices.
My grandparents, I was lucky to be loved so unconditionally and to receive my cultural heritage from them and even if they are not from this world anymore, they are still in my mind.

And last but not the least, I would like to express my gratitude to **Prof. Pilar Junier** for her motivation, and broad knowledge. Her involvement for improving my scientific skills and her patience for my "I don't know if I'll make it "moments. Her continuous investment made me feel really glad to have a supervisor, that no matter what, when I really needed help, she did not hesitate.

Summary

Due to the reactivity of iron to some compounds (oxygen, water, chlorine), this metal could be easily corroded and thus endangered. Many fields like food industry or water supply encounter severe problems due to iron corrosion that engenders important economic losses. In cultural heritage, iron artifacts and especially archaeological iron objects suffer from corrosion and could be irreversibly damaged. In order to remediate to these issues, different conventional conservation-restoration methods exist. However, these techniques present some caveats and/or are not completely efficient in terms of chlorine removal or corrosion inhibition.

Nowadays, the use of biotechnology represents a promising approach. Indeed, there is a growing interest in the synthesis of inorganic components by biological systems in processes that are respectful of the environment. The use of microorganisms with the ability to transform reactive corrosion products into chemically stable and insoluble compounds with a lower molar volume represents an alternative approach to the traditional methods employed in the field of iron conservation. The overall aim of this study is to contribute to the development of a biotechnological approach for the conservation-restoration of corroded iron items (outdoor monuments and archaeological objects). For this purpose, iron reduction by bacteria was selected as an interesting metabolic process underlying the transformation of Fe(III) corrosion products (such as akageneite and lepidocrocite present in corroded iron objects) into Fe(II) minerals (such as magnetite and siderite). The hypothesis tested considers that using iron-reducing bacteria, biologically-induced Fe(II) minerals will be formed from the corrosion products present on the objects and thus these latter will be stabilized and protected further corrosion.

Two main strategies were considered during this project. The first approach was the study of a known bacterium *Shewanella loihica* as a model iron reducer given that it is known to be a facultative anaerobe, halophilic and was used for the production of Fe(II) minerals in other studies. During this PhD project, interesting additional results were obtained: the iron reduction with *S. loihica* was solely possible in presence of NaCl and unexpected Fe(II) phosphate minerals were formed. The suitability of the proposed stabilization process was hence demonstrated and complemented with the investigation of the role of salt on iron reduction and of the accumulation of polyphosphates in this micro-organism. The second approach was the isolation of iron-reducing bacterial candidates from environmental samples. The screening resulted in the selection of two strains from the genus *Aeromonas*. Both isolated strains were employed in the experimental testing of the iron reduction process on archaeological objects allowing the setting-up of a prototype treatment that can be applied by conservator-restorers.

Keywords: iron, corrosion, reduction, biotechnology, heritage conservation, bacteria, biogenic minerals.

Résumé

En raison de la réactivité du fer à certains composés (oxygène, eau, chlore), ce métal pourrait être facilement corrodé et endommagé. De nombreux domaines tels que l'industrie alimentaire ou l'approvisionnement en eau rencontrent de graves problèmes dus à la corrosion du fer. La corrosion du fer engendre ainsi des pertes économiques importantes. Cela concerne aussi le patrimoine culturel oú les objets en fer et surtout les objets archéologiques souffrent également de la corrosion et peuvent être détruits de façon irréversible. Afin de remédier à ces problèmes de corrosion, différentes méthodes conventionnelles de conservation-restauration existent. Cependant, ces techniques présentent certains inconvénients ou ne sont pas totalement efficaces en termes d'inhibition de la corrosion ou de déchloruration des objets.

De nos jours, l'utilisation de la biotechnologie représente une approche prometteuse. En effet, il y a un intérêt croissant pour la synthèse de composés inorganiques par des systèmes biologiques dans des processus qui sont respectueux de l'environnement et des personnes. L'utilisation de micro-organismes ayant la capacité de transformer des produits de corrosion réactifs en composés chimiquement stables et insolubles avec un volume molaire inférieur représente une approche alternative aux méthodes traditionnelles utilisées dans le domaine de la conservation du fer. L'objectif global de cette étude est de contribuer au développement d'une approche biotechnologique pour la conservation-restauration des éléments en fer corrodés (monuments extérieurs et objets archéologiques). Pour cela, la réduction du fer par les bactéries a été choisie comme processus métabolique sous-jacent à la transformation des produits de corrosion réactifs (principalement akaganeite et lépidocrocite présents sur les objets en fer corrodés) en minéraux de Fe(II) (tels que magnétite et sidérite). L'hypothèse testée considère qu'en utilisant des bactéries réductrices du fer, des minéraux Fe(II) biogéniques seront formés permettant la conversion des produits de corrosion présents sur les objets, et qu'ainsi les objets en fer seront stabilisés et empêchés de corrosion ultérieure.

Deux principales stratégies ont été étudiées au cours de ce projet. La première approche étant l'utilisation de *Shewanella loihica* comme modèle de bactérie réductrice du fer, notamment car elle est également connue pour être anaérobe facultative, halophile et a été utilisée pour la production de minéraux de Fe(II) dans d'autres études. Au cours de ce projet de doctorat, des résultats additionnels intéressants ont été obtenus : la réduction du fer avec *S. loihica* n'était possible qu'en présence de NaCl et des phosphates de Fe(II) inattendus se sont formés. La pertinence du processus de stabilisation proposé a donc été démontrée et complétée par l'étude du rôle du sel dans la réduction du fer et de l'accumulation de polyphosphates dans cet organisme. La deuxième approche consistait à isoler à partir d'échantillons environnementaux d'autres candidats bactériens réduisant le fer. L'échantillonnage a abouti à la sélection de deux de deux souches du genre *Aeromonas*. Les deux souches isolées ont été alors employées dans la démonstration expérimentale du processus de réduction du fer sur des objets archéologiques une avec ces deux bactéries sélectionnées permettant la mise en place d'un prototype de traitement applicable par les conservateurs-restaurateurs.

Mots clés : fer, corrosion, réduction, biotechnologie, conservation du patrimoine, bactéries, minéraux biogénique

Table of Contents

Chapter 1

General Introduction

"Energy capture based on Fe/S compounds, now and perhaps before there was life, is as important as DNA in life's history". RJP Williams (Nature 1990)

Iron Pilar, 3 B.C. New Delhi, India © Prachodayat

Cosmology studies report that the Universe was born around 13.7 billion years ago and entered its own "Iron Age" 200 million years after the Big Bang [1]. Iron is an abundant element in the solar system [2]. It is present in the Sun [3] and other stars [4], as well as in some planets like Mercury, Venus [5] and most importantly on Earth [6–8]. Iron is one of the main compounds present in the Earth's crust (5.1%) [8] and the most abundant one in the Earth's core and mantle (88.8% [57]) [1]. The presence of iron guards the Earth against solar winds and radiations, which allows our planet to be suitable for life [1].

Life on Earth started some 3.5 billion years ago in an oxygen-free atmosphere, likely within a hyperthermic and hyperbaric environment. These conditions were favorable for a cycle of chemical reactions that generate exploitable energy. A key process in the development of life under these conditions was the transfer of electrons from ferrous or sulfide sources (e.g. hydrogen sulfide) to electron acceptors, leading to the fixation of carbon oxides that dissipated the redox gradient and simultaneously produced organic compounds. According to RJP Williams (Nature 1990) "*Energy capture based on Fe/S compounds, now and perhaps before there was life, is as important as DNA in life's history*".

Originally, in the anoxic Earth, soluble ferrous iron was abundant and easily available for the first life forms, but this "ferrous supply" started to decrease due to the generation of oxygen into the atmosphere by photosynthesizing cyanobacteria. Over the next 1.5 billion years, this phenomenon led to an increase in the oxygen atmospheric content to 21%, dramatically affecting life by oxidizing ferrous iron to insoluble ferric iron. The consequences of this event had an impact on both the geology ("banded iron formations") and the life of our planet. From this time to our days strictly aerobic organisms struggle to acquire, transfer, and store iron [1].

Since this period, about 200,000 years were needed for the evolution of *Homo sapiens*. Many decades later some civilizations entered into the Iron Age (~1200–1000 BC) were iron was used mostly for therapeutic purposes (e.g. as a cure for gout and acne), without full awareness of its importance for humans [1]. It was only in 1713 that iron was discovered as being part of the human body by Lemery and Geoffrey [9] and since then it is considered as an essential nutrient for all living organisms [10 11]. Iron participates to diverse physiological process such as oxygen transfer [10] (between 7 and 11 mg are daily required [12] for hemoglobin synthesis[11]), DNA synthesis, electron transport [11], photosynthesis, or the formation of chloroplasts and vacuoles[13]. For bacteria, iron plays also an important role. It influences the composition of the cells (effect on growth, sporulation, DNA synthesis, cell morphology), metabolism (electron transport chain, nitrogen fixation, phosphorylation, methanogenesis, production of vitamins, antibiotics, siderophores, or cytochromes), or enzymatic activity (catalytic role on peroxidase, superoxide dismutase, nitrogenase) [14].

The iron biogeochemical

Living organisms are part of the biogeochemical cycle of iron, which is crucial to maintain a balance between the sources and sinks of this element. Besides the main geological reservoirs of iron on Earth (Earth's core and mantle), iron is the fourth most abundant element in the Earth's crust. Iron is also present in soils (between 0.5 and 5%), atmosphere (traces), and water (sea water contains 2.5 ppb) [12]. Despite its abundance, it is biologically relatively scarce. Iron is an extremely redox-sensitive element and in its elemental form, it oxidizes instantly in the presence of oxygen. Two oxidation states can be distinguished for this element: ferrous (Fe(II)) or ferric (Fe(III)) iron. In nature, iron is usually found in the form of Fe(II)- or Fe(III)-bearing minerals or dissolved as an ion in water. The prevalence of each redox state depends mainly on factors such as oxygen concentration, pH, and microbial activity [15].

When in contact with water and atmospheric oxygen, elemental Fe is rapidly oxidized into Fe(II). The latter reacts with hydroxide ions and oxygen to form Fe(III) minerals.

$$Fe + 2OH^- \rightarrow Fe(OH)_2 + 2e^- \qquad 4Fe(OH)_2 + 2H_2O + O_2 \rightarrow 4Fe(OH)_3$$

The transition between Fe(II) and Fe(III) is fundamental for environmental biogeochemistry and plays an important role in redox processes in anoxic environments. Fe(III) is the thermodynamically stable form of iron and predominates in oxic environments (at neural pH) in the form of poorly soluble Fe(III) oxides. Due to weathering and erosion Fe(III) particles are transported to the soil and ocean/lakes from volcano ashes and iron primary rocks (Fig. 1). Then a continuous exchange between the Fe(III) and Fe(II) states takes place in what is known as the "ferrous wheel" [15]. Under anoxic conditions, Fe(III) from Fe(III) oxides can become biologically available for assimilation via uptake with microbial chelators (e.g. siderophores) [16,17]. Alternative, Fe(III) can be reduced to Fe(II) due to the activity of dissimilatory iron reducing bacteria (DIRB). Fe(II) is more stable under anoxic conditions [18,19]. The generated Fe(II) can be: i) abiotically reoxidized by oxidized manganese Mn(IV) species or by the diffusion of Fe(II) into an oxic environment where it will react with molecular oxygen; ii) biotically oxidized by chemolithotrophic bacteria (aerobically using oxygen as electron acceptor and anaerobically using nitrate or chlorate ions as electron acceptors) and anoxygenic phototrophic bacteria (using light energy to convert inorganic carbon (CO_2) into biomass (CH_2O)); and iii) reacts with some elements present in the environment to form Fe(II) minerals. Indeed, in anoxic habitats under circumneutral pH conditions most of the ferrous iron produced by microbial Fe(III) reduction would be found in solid phases such as magnetite, siderite or vivianite [20,21]. This process could lead to the immobilization and scavenging of other essential elements like phosphorus [22,23] (Fig. 1).

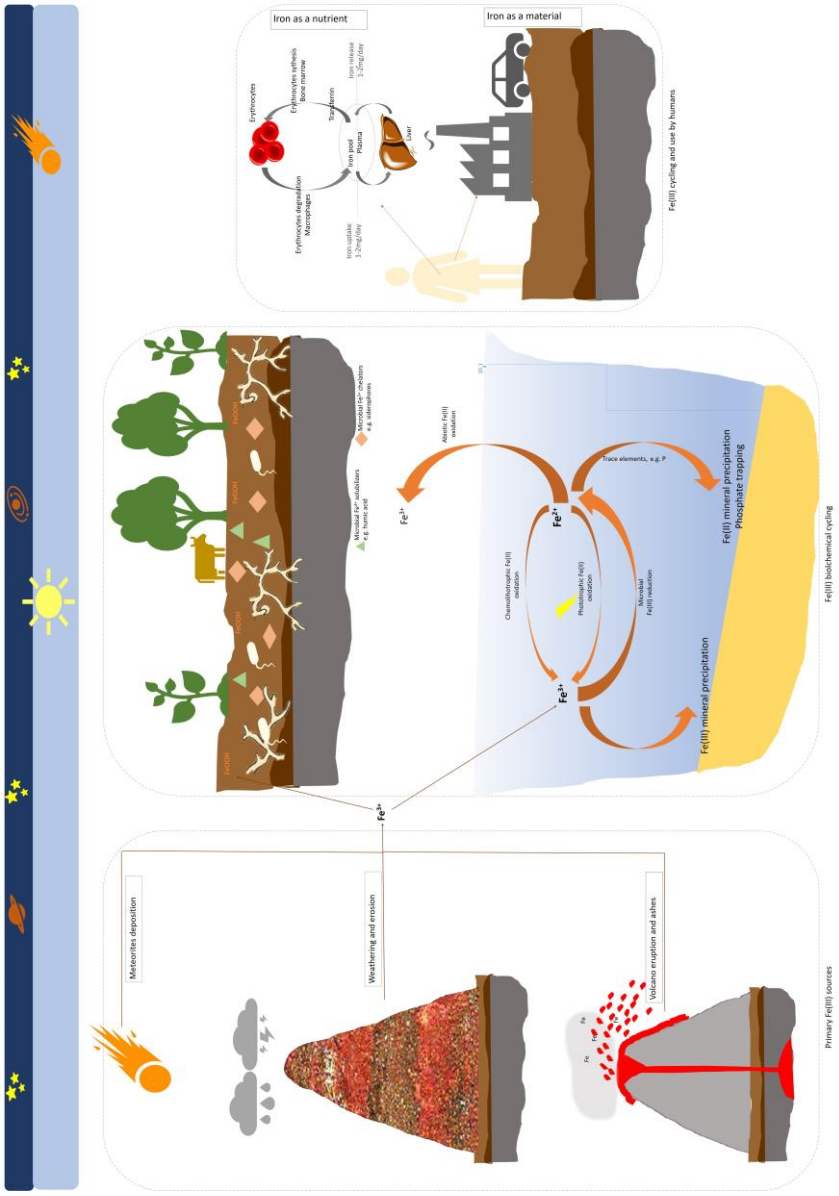

Figure 1: Schematic representation of the iron cycle. Primary iron sources: iron is deposited mainly in the form of Fe(III) in the water (ocean, lakes) and soils from the weathering of primary rocks, volcanic ashes and meteoric activity. Wind can also play a role in the transport of iron. Biochemical iron cycling: under anoxic conditions, in aquatic or soil environments, Fe(III) enters in the ferrous wheel where there is a reversible state exchange from Fe(III) to Fe(II) mainly due to microbial activity. Fe(II) could be reoxidized by some photolithotrophic bacteria and part of it is released to the oxic environment where it is reoxidized in contact to oxygen. Fe(III) undergo bacterial iron reduction, consequently, Fe(II) is produced which leads, in contact with the surrounding elements, to the scavenging and immobilization of other trace elements by producing Fe(II)-bearing minerals (e.g. Fe(II) carbonates and phosphates). Fe(III) could also be sequestrated by microbially secreted iron chelators (e.g. siderophores). In soil, fungi play an important role in scavenging Fe(III), while bacteria are known to reduce Fe(III) and secrete scavengers. Plants also can uptake iron from the root by secreting humic acids for example. Plants are then consumed by animals and both are a source of iron uptake by humans. Use of iron by humans, for 2 purposes: (i) iron is an essential nutrient for survival, in our body, it is used for muscles and hemoglobin synthesis. It is also important in Liver content. (ii) as a material for manufacturing purposes: iron is extracted from ores to be used by different fields (e.g. transport).

Assimilatory metabolism of iron

Despite the abundance of iron, its cellular uptake is compromised because this element occurs as Fe(III) in a mostly insoluble form under physiological pH and oxidizing conditions. [24]. In response, various cellular mechanisms have evolved to capture iron from the environment [25]. To assimilate iron from their environment, bacteria and fungi have developed specific strategies. They produce low-molecular mass chelators (e.g. siderophores) that have high affinity for ferric iron. In addition to their own siderophores, some bacteria have evolved the ability to utilize heterologous siderophores (xenosiderophores) from other bacteria or of

fungal origin [11] [25]. Bacteria have also developed other mechanisms to uptake ferric iron from the surrounding environment. For example; heme-mediated iron uptake, where bacteria express outer membrane receptors specific for heme and secrete hemophores, that sequester heme from the environment and transport it to its specific outer membrane receptors [26].
The acquisition of iron is recognized also as one of the key steps for the survival of microbial pathogens within their hosts and contributes significantly to virulence [14]. Thus, bacterial pathogens have various mechanisms to acquire iron from their hosts [27]. To survive in this harsh environment, in Gram-negative bacteria, for example, the cell envelope proteins, including periplasmic, outer and inner membrane proteins, are essential in the transport of iron related compounds into the intracellular environment [28]. To prevent the invasion of pathogens, hosts developed strategies to minimize the concentration of free iron by secreting transferrin and lactoferrin, molecules with high affinity for this element. However, some pathogenic bacteria uptake iron from their hosts via the expression of outer membrane receptors of transferrin and lactoferrin [26].

Dissimilatory metabolism of iron

The Fe(II)/Fe(III) redox cycling represents an important energy flux on Earth's surface and microbial reductive dissolution is the major mechanism under anoxic conditions to overcome the low solubility of Fe(III)-bearing minerals in the cycling of Fe [29]. Even if plants play an important role in iron cycling [15], oxidative and reductive reactions mediated by micro-organisms are considered as main mediators in the iron cycle [19], and the formation of some iron deposits has been attributed directly to microbial iron oxidation and reduction [16].

Fe(II) is used as an electron donor by chemolithotrophic Fe(II)-oxidizing bacteria to provide reducing equivalents for the assimilation of carbon into biomass under both oxic and anoxic conditions. Under oxic conditions, some bacteria oxidize Fe(II) with the reduction of oxygen at acidic and circumneutral pH. Indeed, microbial Fe(II) oxidation of both soluble and insoluble Fe(II) is coupled to nitrate reduction (and less commonly to chlorate or perchlorate reduction). This process is energetically favorable and produce enough energy to support carbon fixation and microbial growth [22]. In anoxic environments with sufficient light penetration, anoxygenic photoautotrophic microorganisms such as *Chlorobium ferrooxidans* and *Rhodopseudomonas palustris*, [19] oxidize Fe(II) and use light as energy to fix CO_2 into biomass.

In the absence of oxygen, bacteria can use soluble, amorphous and crystalline Fe(III) sources as terminal electron acceptors for respiration. The ability of microbes to use iron oxides as terminal electron acceptors is a process referred to as dissimilatory iron reduction (DIR) [30]. Iron respiration is considered as one of the first forms of microbial metabolisms preceding oxygen, nitrate and sulfate respiration. Up to 50% of carbon remineralization in marine sediments can be explained by microbial iron reduction, and this number is expected to be even higher in low-sulfate, freshwater ecosystems [19]. Indeed, Fe(III) respiration has been identified for a wide range of micro-organisms. Extracellular electron transfer to insoluble Fe(III) oxide minerals has been observed in hyperthermophilic archaea and is widely distributed among bacteria, suggesting that it is an ancient metabolism that has expanded during evolution between microorganisms [22].

Mechanisms of Dissimilatory Iron Reduction

Dissimilatory iron reduction (DIR) is one of the most important reactions of the iron cycle [31]. During DIR, microorganisms use different strategies to transfer electrons to iron. Microorganisms and especially bacteria capable of iron reduction are diverse. For example, spores of the bacterium *Desulfotomaculum reducens* MI-1 are able to reduce Fe(III) citrate [32]. Also, members of the *Geobacteraceae* have a significant role in DIR and the oxidation of organic matter in soils and sediments. Outside the δ-proteobacteria, the genus *Shewanella* in the γ-proteobacteria is another well-characterized group of ferric iron-reducing bacteria. *Shewanella oneidensis* and *Geobacter sulfurreducens* represent the most studied bacterial models concerning DIR [22] (Fig. 2).

Reduction of insoluble Fe(III) oxides is conducted via extracellular electron transport to the solid Fe(III) electron acceptor, and requires a terminal iron reductase localized in the outer membrane. On the contrary, the reduction of the soluble Fe(III) phase occurs in the periplasm. Accordingly, it has been postulated that different electron transport mechanisms are used to reduce insoluble and soluble Fe(III) sources [22]. The mechanisms by which bacteria reduce insoluble Fe(III) bearing minerals include: the direct contact of the bacterial cell with the mineral through cytochromes located at the external membrane; the use of a cellular appendage (e.g. pili/nanowires) that forms a bridge between the bacterial cell and the substrate, catalyzing the electron transfer; the use of Fe(III) chelators (e.g. siderophores) that dissolve and transport Fe(III) to the bacterial cell for subsequent reduction; and the use of electron shuttles to transfer electrons from the bacterial cell to the Fe(III)-containing substrate [29]. Some researchers suggested that the export of *c*-type cytochromes to the outer membrane is essential in Fe(III) reduction in the model DIR organism *S. oneidensis.* Other studies mentioned that these *c*-type cytochromes are an intermediate in electron transfer to metals in the same bacterium, and a terminal metal reductase is required [33].

Focusing on *S. oneidensis*, the gene cluster *mtrCAB* and *omcA* are the main genes encoding the proteins participating in electron transfer (Fig. 2). Direct electron transfer in *Shewanella* involves cytosolic membrane, periplasmic and outer membrane proteins that transfer electrons from the cytoplasm to the extracellular substrate [30]. Quinones are used as electron shuttle in Fe(III) reduction for the bacteria *S. oneidensis* and *Shewanella alga* [33]. The current knowledge on the mechanism of Fe(III) oxides reduction involves the transfer of electrons from a dehydrogenase to a quinone pool in the cytoplasmic membrane, to *c*-type cytochromes and finally to a reductase in the outer membrane (Fig. 2). The electrons are transferred from the menaquinone to CymA, a *c*-type cytochrome located in the cytoplasmic membrane. The electrons are then passed to electron carriers in the periplasm. Two *c*-type cytochromes in the periplasm have been identified as potential electron carriers: MtrA and Cytc3. Cytc3, a small tetraheme *c*-type cytochrome in the periplasm, acts as an electron shuttle between electron carriers. MtrA is a decaheme *c*-type cytochrome that accepts electrons from the cytoplasmic membrane electron carrier CymA. The electrons are then transferred through the porin MtrB to reach the outer membrane cytochrome MtrC. From here electrons can pass from MtrC to OmcA, or transferred directly to the Fe(III) solid phase. Flavins are part of the iron reduction mechanism, interacting with cytochromes to exchange electrons. In the absence of oxygen, secreted flavins bind to OmcA and MtrC, which enhances the mineral reductase activity of these cytochromes [17,22].

The genome of *G. sulfurreducens* possesses 111 putative *c*-type cytochromes (in comparison to 39 in the genome of *S. oneidensis*) suggesting that the high number of *c*-type cytochromes supports the existence of multiple electron-transport pathways. MacA, a periplasmic

cytochrome, was involved in the electron transfer to Fe(III) by transferring electrons to other periplasmic proteins such as PpcA, a tri-heme periplasmic *c*-type cytochrome involved in electron transport to OMPs and especially to OmcB (involved in insoluble Fe(III) reduction), OmcE and OmcS [17,22]. Some studies proposed that attachment of *Geobacter* spp. to Fe(III) oxides could involve flagella and pili. But most importantly, it has been proven that pili are required for the electron transfer to the insoluble Fe(III) phases. Conductive nanowires were considered to be exclusive to *Geobacter* spp. as pili produced by other metal-reducing organisms tested, including *S. oneidensis*, were not conductive [17,22,34]

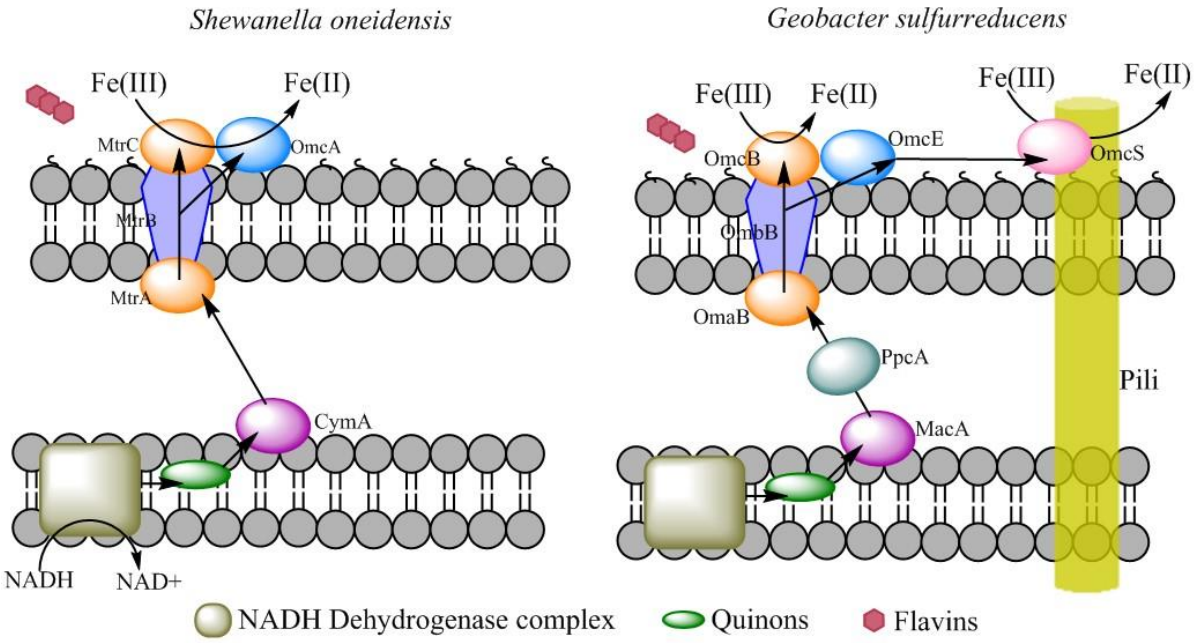

Figure 2: Mechanisms of iron reduction in *S. oneidensis* and *G. sulfurreducens* [17,22].

Iron minerals and biogenic mineral formation

Fe(II) and Fe(III) minerals form depending on the oxygen content, pH, ions present in the surrounding environment and microbial activity. Table 1 summarizes the most common iron minerals found in nature.

Table 1: Common iron minerals found in Nature and known involved in the biogeochemical cycle of iron [15,16,18,35]

Mineral group	Name	Formula	Solubility product* log K_{sp} [36–40]
Fe(III)oxides	Hematite	α-Fe_2O_3	0.09
	Maghemite	γ-Fe_2O_3	1.59
Fe(III)oxyhydroxides	Goetite	α-FeOOH	-0.02
	Akaganeite	β- FeOOH(Cl)	
	Lepidocrocite	γ-FeOOH	1.39
	Schwertmannite	δ-FeOOH	
	Ferrihydrite	$Fe_4HO_8 \cdot 4H_2O$	3.54
Fe(III)hydroxides	bernalite	$Fe(OH)_3$. nH_2O	
Fe(II) oxides	Wüstite	FeO	
Fe(II)hydroxides		$Fe(OH)_2$	
Fe(II)Fe(III)oxides	Magnetite	Fe_3O_4	12.02
Fe(II)Fe(III)hydroxides	Green rust	Fe(III)Fe(II)OHA - A^- is Cl^- or SO_4^{2-}or CO_3^-	
Sulfides	Pyrite	FeS_2	16.4
	Mackinawite	FeS	3.6
	Greigite	Fe_3S_4	4.4
Phosphates	Vivianite	$Fe_3(PO_4)_2 \cdot 8H_2O$	-36
Carbonates	Siderite	$FeCO_3$	-10.68
Silicates	Illite (others: smectite, chorite)	(K, H_3O) (Al, Mg, $Fe)_2$ (Si, $Al)_4$ O10 $(OH)_2$ (H_2O)	

*: the values of the solubility products depend on the conditions tested and the size of the minerals

Crystalline Fe(III) oxides and oxyhydroxides, such as Goethite, Hematite and Lepidocrocite are present in rocks, soil, sediments and rust (Fig. 3); Hematite is the oldest known iron oxide, Goethite is considered as the most thermodynamically stable and Lepidocrocite is mainly formed due to the oxidation of ferrous ions. Akaganeite is formed in Cl^- rich environments and as a consequence of rust of iron objects in marine habitats, Schwertmannite is often formed due to the oxidation of pyrite [41].

Figure 3: Examples of occurrence of iron oxides and oxyhydroxides in natural environments located near the region of Davos, Switzerland. Upper line, Totalp region near Kolsters: on the left a dolomite rock containing magnetite (black spots) and on the right a serpentine rock containing iron oxides (orange color). Middle line: presence of iron oxides and oxyhydroxides in Rablönch (left) and Arvadi (right) springs. Bottom line represents Jöri Lake 13.

The formation of iron minerals through biological processes has been commonly divided into two modes: i) biologically controlled mineralization in which bacteria genetically control the mineralization process; and ii) biologically mediated mineralization (or biogenic mineral formation) in which bacteria facilitate mineral formation by producing extracellular products that will interact with the surrounding environment and lead to mineral precipitation [42]. The formation of magnetite by magnetotactic bacteria represents an example of biologically controlled mineralization in which the particles are formed inside bacterial cells templated by a specific internal membrane [43]. In contrast, the formation of magnetite and siderite by Fe(III)-reducing bacteria, such as a *Thermoanerobacter ethanolicus*, TOR-39, *Shewanella pealeana* or *S. alga*, represents biologically facilitated mineralization in which the particles are formed extracellularly as a byproduct of microbial Fe(III) respiration [44]. In this case, if the external environment is suitable for mineral precipitation, Fe(II)-bearing minerals will be produced (Fig. 4).

The formation of magnetite, siderite and vivianite has been extensively associated with bacterial iron reduction [16,45,46]. Magnetite, for example was produced in Fe(III) chloride solution by the fungi *Fusarium oxysporum* and *Verticillium* sp. [16]. Magnetotactic bacteria (MTB) as *Magnetovibrio blakemoreii* MV-1 and *Magnetospirillum gryphiswaldense* are

known to synthetize magnetite under anaerobic conditions and at neutral pH, via controlled mineralization and to use this mineral for orientation purposes (same as for pigeons) [24,47,48]. Magnetite is also produced from Fe(III) oxides through biologically mediated mineralization by iron-reducing bacteria such as *Geobacter metallireducens*, *Rhodobacter* sp., *Thermoanaerobacter ethanolicus* and *Shewanella* spp. [16,47,49,50]. According to the literature, the bacteria *Shewanella* sp. HN-41, *Shewanella* sp. PV-4 and *Thermoanaerobacter ethanolicus* have the property of reducing Fe(III) oxides by converting akaganeite β-FeOOH(Cl) into magnetite with a higher yield than MTB [51,52].

Vivianite and siderite were reported to be formed as by-product minerals of dissimilatory Fe(III) reduction by diverse bacteria (Fig. 4), including: *S. oneidensis*, *Shewanella putrefaciens*, *G. sulfurreducens*, *Rhodococcus* sp. *strain C125*, *Pseudomonas putida mt2*, *Aeromonas hydrophila*, *Serratia fonticola*, and *Clostridium celerecrescens* [20,46,53–56].

Figure 4: Scanning electron microscopy image taken during our experiments and showing the formation of iron phosphate minerals as by-products of the reduction of insoluble Fe(III) oxides by *Shewanella loihica.*

The interaction between iron and microorganisms engenders by-products that have an important environmental and applied significance. This relationship was exploited for bioremediation purposes; the immobilization of heavy metals [16], the degradation of contaminants, the scavenging of essential traces elements [22], or the bioleaching of iron from ores [16]. It was also demonstrated that bacterial iron reduction could protect steel from corrosion [45] and more recently it was exploited for stabilizing corroded and archeological iron objects [57,58].

Iron and cultural heritage

Even if the oldest archaeological trace of iron dates to 3200 BC and corresponds to meteoric iron in Egypt [59], thanks to its widespread and metallurgical properties [8] (ductility, hardness, strength), evidence for the climax in production of iron (and iron alloys) weapons and tools is found in the so-called Iron Age [60–62]. The role of iron as a fundamental material for

civilizations starts with this period, which is characterized by the development of iron metallurgy.
We distinguish the Early Iron Age or Hallstatt period and the second Iron Age, or La Tène period (the name of a Swiss village on the shore of Lake Neuchâtel) [63].

Since the industrial revolution in the 18th century iron alloys (especially steel and cast) have been used at large scale and became a part of human activities in different fields like: architecture (e.g. Eiffel tower in 1889), civil engineering (e.g. construction with the first iron bridge built in 1778), transport (e.g. cars, railways, boats with the first example built with iron dating from 1818), food industry (e.g. cans), cutlery, jewelry, dye industry, mechanical tool production (e.g. screws) and art [12]. Iron constitutes nowadays 90% of all metals refined. It is the most mined element in the world (1.34 million tons of steel in 2007). Per year, the world production is estimated at 2.4 billion tons with 1.3 billion tons for steel (addition of about 1.7% of carbon making the iron more durable, resistant to corrosion and less harsh) [12].

Its metallurgical properties make iron and its alloys highly malleable, but due to its reactivity to some compounds (oxygen, humidity, chlorine), iron could be easily corroded and thus endangered [12,64] (Fig. 5). Many fields like food industry or water supply encounter severe problems due to iron corrosion [64]. For example, because of the extensive use of cast-iron pipes in water distribution networks [64], iron corrosion causes huge economic losses [65]: The American Water Works Association (AWWA) estimated in 2001 that USA has to spend $325 billion to upgrade water distribution system for the next 20 years due to iron corrosion [66]. In cultural heritage archeological iron also suffers from corrosion and in this case the whole object could be irreversibly damaged (Fig. 5). This also results in an important economic loss if we consider that cultural heritage has an important worldwide impact especially on tourism and socio-economic development (cultural heritage of a country is considered as a source of economic revenue, and for example, over 50% of the European tourism industry is based on cultural heritage [67]) [68–71].

Iron archaeological artifacts could encounter serious corrosion issues, especially after burial, due to the formation of different iron oxides and oxyhydroxides species depending on oxygen concentration, relative humidity, and contaminants [64,72]. The exposure of these iron items to higher oxygen concentrations and lower relative humidity cause the disruption of the stability of corrosion layers formed during burial resulting in physical and chemical changes damaging the object. This disruption is enhanced when the burial environment is contaminated by chlorine (contained in soil) [64,72,73]. Chloride ions (Cl^-) present as an acidic solution ($HCl/FeCl_2$) leads to the formation of iron oxyhydroxides [74]. At high concentrations of Cl^- ions, an active and unstable corrosion layer composed of akageneite β- FeOOH(Cl) is preferentially formed, but at low concentrations of Cl^- the formation of α-goethite FeOOH and/γ-lepidocrocite FeOOH prevails. Due to their high molar volume (higher than elemental iron's molar volume), these molecules generate cracks and destroy of the shape of the artifact if no intervention is engaged [64,74–77].

In order to remediate these corrosion problems, different conventional methods exist. This include alkaline immersion baths, electrolysis, plasma treatment, coatings using waxes and acrylic resins such as Paraloid, and use of anti-corrosion agents [73,74,78]. These treatments present many caveats: alkaline immersion baths are not completely effective on cast iron composite objects with organic substrates (e.g. wood) and time consuming. Plasma reduction and electrolysis are complex with expensive facilities and time consuming. Waxes and

Paraloid formulations photo-oxidize. Concerning the anti-corrosion agents, they could rub off and do not dry easily [12,73,74,78]. Some of these methods are resumed in the Table 2.

Table 2*:* Summary of the traditional methods of iron stabilization [79–84]

Method	Principle	Advantages	Disadvantages
Storage at low relative humidity	Storage with HR<12%	Simple, provides good results if storage conditions are controlled.	Expensive, parameters hardly controlled.
Alkaline immersion bath	Immersion in an aqueous solution and diffusion of Cl^- ions by reverse osmosis.	Simple	Slow, laborious, expensive, waste disposal
Electrolysis (electrochemical method)	Immersion of the artifact in an alkaline solution and application of a voltage between an electrode and the artifact.	Formation of insoluble and reduced corrosion products.	The power flow applied isn't known in advance. Used for large marine archaeological objects. Effective on thick corrosion layers.
Elimination of dissolved oxygen	Boiling solutions, bubbling an inert gas or trapping O_2.	Quite effective	Require specific installations
Plasma treatment	Reduction of the corrosion products in an oxidized state.	Porosity of the corroded layers increased.	Mainly used only as a pretreatment. Expensive.

Based on the advantages and disadvantages of the methods listed previously, it is essential to improve the control of iron corrosion considering the environmental conditions, the rate of corrosion, the chloride content and the physical integrity of the objects in order to develop a more effective, gentler, faster and less expensive stabilization method.

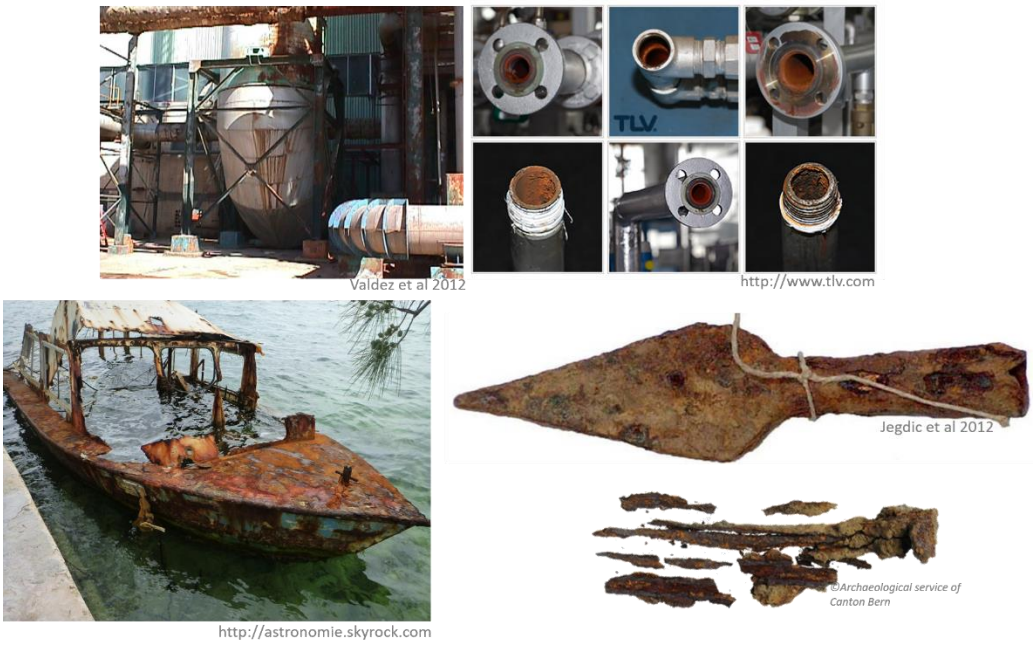

Figure 5: Examples of unstable iron corrosion consequences in industries (upper part), transport (down left) and archeological objects (down right).

Aim of this study

Iron corrosion is primarily an electrochemical process that involves redox reactions leading to the transformation of elemental iron into other composite iron minerals (e.g. magnetite, siderite, goethite or lepidocrocite) [19,73]. Although some corrosion products can be protective (e.g. magnetite, siderite, vivanite [85–89]), others, including iron oxides and oxyhydroxides like lepidocrocite or akaganeite, are minerals that cause unstable iron corrosion (commonly called rust [90]) [74,76,77]. The latter could be enhanced by some compounds like chloride ions [64,72,73].

Currently, there is a growing interest in the synthesis of inorganic components by biological systems in processes that have a higher respect for the preservation of the environment [76]. Bacterial iron reduction has been used as a low-cost and environmentally friendly biotechnological approach for iron extraction from ores [20]. This is why the use of microorganisms with the ability to transform unstable and reactive corrosion products such as akaganeite into more stable insoluble compounds with lower molar volume represents an alternative to traditional iron conservation methods [57].

The overall aim of this study is to contribute to the development of a biotechnological approach for the conservation-restoration of corroded iron items (outdoor monuments and archaeological artifacts). For this, dissimilatory iron reduction by bacteria was selected as metabolic process underlying the transformation of reactive and unstable Fe(III) corrosion products (such as akaganeite) present in corroded iron objects into more stable Fe(II) minerals (such as siderite). The hypothesis tested considers that by using iron-reducing bacteria, biologically-induced Fe(II) minerals will be formed allowing the conversion of the unstable corrosion products, present on the objects, into stable iron minerals which will stabilize the objects and prevent further corrosion.

This study was part of the MAIA project (Microbes for Archaeological Iron Artifacts; PI: Edith Joseph) that aimed at developing innovative methods for the use of microbe iron-related metabolisms in conservation-restoration to control the reactive corrosion present in archaeological iron artifacts. To do so, two approaches were considered, the first approach consists on the reductive dissolution of the Fe(III) reactive minerals present in the corrosion layer of the objects and their conversion into more stable compounds and with reduced molar volume. This generates an increase in the porosity of corrosion layers. As consequence, the extraction of chloride ions outside the archaeological artifact would occur by osmotic diffusion into an alkaline immersion baths. Although the increase in porosity is essential for the elimination of chloride ions, a simple osmotic diffusion does not allow a good extraction of these ions. That is the reason why a second approach focused on the direct extraction of chlorine by microorganisms.

The first strategy consists on studying the bacterial and fungal iron metabolisms targeting the reactive solid Fe(III) phases. Using alkaliphilic fungi that tolerate chlorine, Dr. Lucrezia Comensoli studied the ability of fungi to adsorb Fe(III) by secreting chelating substances (e.g. siderophores). The dissociation of Fe(III) and chlorine containing minerals was also investigated using bacteria. Indeed, under anaerobic conditions, bacteria can reduce Fe(III) into Fe(II). Fe(II) might interact with the environment to form Fe(II) biogenic minerals. My PhD work was included in this part of the project where I used facultative anaerobic bacteria to perform iron reduction and to favor the formation of biologically induced Fe(II) minerals.

The second strategy, performed by Dr. Lucrezia Comensoli, consisted on studying the active removal of chloride ions by uptake, translocation or volatilization using alkaliphilic fungi.

The MAIA project was inspired by previous studies (BIOPATINA and BAHAMAS projects; PI: Edith Joseph) that investigated the use of fungi for the stabilization of copper surfaces. These three projects have a significant contribution to the field of biotechnological innovation in conservation science and as such they have been presented in conferences and published in the form of articles in which I participated as a co-author (see Annex).

Research strategy

Nowadays, the use of microorganisms for biotechnological purposes represents a promising approach. Particularly in cultural heritage, exploiting specific bacterial abilities for the transformation of unstable corrosion products such as akaganeite into more stable iron minerals represents an alternative to the caveats of traditional conservation-restoration methods. The main goal is to stabilize the corroded iron objects by converting the reactive corrosion layer mainly composed of Fe(III) oxyhydroxides into Fe(II) biogenic minerals less reactive to the surrounding environment and thus more chemically stable. The stability depends on the composition (solubility product constants of principal iron compounds reported in Table 1) and the size of the minerals produced (Ksp may drastically increase with decreasing crystal size [36]). The strategy for the protection of archaeological/corroded iron objects by bacteria consists on the dissociation of instable Fe(III) oxides and oxyhydroxides, especially the ones containing chloride species, by iron reduction and biogenic mineral formation. The process is performed under anaerobic conditions to avoid further damage upon oxygen exposition of the corroded/archaeological iron object. These stable Fe(II) minerals with lower molar volume will generate an increase in the porosity of the corrosion layers allowing for the diffusion of chloride ions (if present) outside the object and also act as a passivation layer on the corroded surface.

A previous PhD thesis also in the frame of the MAIA project used *Desulfitobacterium hafniense* and demonstrated that this bacterium reduces reactive Fe(III) oxyhydroxides from corroded iron objects, favouring the biogenic production of vivianite [57]. However, due of the complex composition of the growth medium, abiotic reduction and undesirable formation of additional corrosion products were observed alongside biological iron reduction. In addition, working with a strict anaerobe such as *D. hafniense* was challenging to scale-up the biotechnological treatment into conservation praxis.

An alternative in this case is to perform bacterial iron-reduction under non-growing conditions and with a controlled chemical matrix with the hypothesis that under these conditions, iron reduction will induce the formation of specific Fe(II) minerals as by-products of the interaction with the chemical precursors present in the environment. For this, facultative anaerobes were deemed more suitable. Two strategies were considered. First, we used *Shewanella loihica* as a model organism given that this bacterium is known to be a facultative anaerobe, halophilic iron reducer and was used for magnetite production in previous studies [51,91]. In this case, demonstrating the suitability of the proposed stabilization process (Chapter 2) was complemented with the investigation of the role of salt on iron reduction (Chapter 3) and accumulation of polyphosphates (Chapter 4) in this organism. Second, the isolation of novel candidate species for the stabilization method from environmental samples was undertaken (Chapters 5). This was followed by the experimental demonstration of the process with selected candidate species allowing for the development of a prototype treatment (Chapter 6).

References

1. Sheftel, A. D., Mason, A. B. & Ponka, P. The long history of iron in the Universe and in health and disease. *Biochim. Biophys. Acta* **1820,** 161–187 (2012).
2. Anders, E. & Grevesse, N. Abundances of the elements: Meteoritic and solar. *Geochim. Cosmochim. Acta* **53,** 197–214 (1989).
3. Asplund, M., Grevesse, N., Sauval, A. J. & Scott, P. The chemical composition of the Sun. *Annu. Rev. Astron. Astrophys.* **47,** 481–522 (2009).
4. Santos N.C, I. G. and M. M. The metal-rich nature of stars with planets. *Astron. Astrophys.* **373,** 1019–1031 (2001).
5. Morgan, J. W. & Anders, E. Chemical composition of Earth, Venus, and Mercury. *Proc. Natl. Acad. Sci. U. S. A.* **77,** 6973–6977 (1980).
6. McDonough W.F and Sun S.-s. The composition of the Earth. *Chem. Geol.* **120,** 223–253 (1995).
7. Allègre C.J., Poirier J.P., H. E. and H. A. W. The Chemical Composition of the Interior Shells of the Earth. *Earth Planet. Sci. Lett.* **134,** 515–526 (1995).
8. Nielsen J.M. *The Radiochemistry of Iron. Chemistry, radiation and radiochemistry* (1960).
9. Ferreira Glória C. *Handbook of Porphyrin Science: With Applications to Chemistry, Physics, Materials Science, Engineering, Biology and Medicine*. (2013).
10. Abbaspour N, H. R. and K. R. Review on iron and its importance for human health. *J Res Med Sci* **19,** 164–74 (2014).
11. Lieu, P. T., Heiskala, M., Peterson, P. A. & Yang, Y. The roles of iron in health and disease. *Mol. Aspects Med.* **22,** 1–87 (2001).
12. John, E. An A-Z Guide to The Elements. *Oxford Univ. Press* 539 (2001). doi:978-0-19-960563-7
13. Morrissey, J. & Guerinot, M. Lou. Iron uptake and transport in plants: the good, the bad and the ionome. *Chem Rev* **109,** 4553–4567 (2009).
14. Messenger, A. J. & Barclay, R. Bacteria, iron and pathogenicity. *Biochem. Educ.* **11,** 54–63 (1983).
15. Pérez-Guzmán, L., Bogner, K. R. & Lower, B. H. Earth's Ferrous Wheel. *Nat. Educ. Knowl.* **3,** 32 (2010).
16. Gadd, G. M. Metals, minerals and microbes: Geomicrobiology and bioremediation. *Microbiology* **156,** 609–643 (2010).
17. White, G. F. *et al.* in *Advances in Microbial Physiology* **68,** 87–138 (Elsevier Ltd., 2016).
18. Raiswell, R. & Canfield, D. E. The Iron Biogeochemical Cycle Past and Present. *Geochemical Perspect.* **1,** 1–220 (2012).
19. S. Berg, J. *et al.* Intensive cryptic microbial iron reduction in the low iron water column of the meromictic Lake Cadagno. *Environ. Microbiol.* **18,** 5288–5302 (2016).
20. García-Balboa, C. *et al.* Bio-reduction of Fe(III) ores using three pure strains of *Aeromonas hydrophila*, *Serratia fonticola* and *Clostridium celerecrescens* and a natural consortium. *Bioresour. Technol.* **101,** 7864–7871 (2010).
21. Straub, K. L., Benz, M. & Schink, B. Iron metabolism in anoxic environments at near neutral pH. *FEMS Microbiol. Ecol.* **34,** 181–186 (2001).
22. Weber, K. a., Achenbach, L. a. & Coates, J. D. Microorganisms pumping iron: anaerobic microbial iron oxidation and reduction. *Nat. Rev. Microbiol.* **4,** 752–764 (2006).

23. Cosmidis, J. *et al.* Biomineralization of iron-phosphates in the water column of Lake Pavin (Massif Central, France). *Geochim. Cosmochim. Acta* **126,** 78–96 (2014).

24. Zeth, K., Offermann, S., Essen, L.-O. & Oesterhelt, D. Iron-oxo clusters biomineralizing on protein surfaces: structural analysis of *Halobacterium salinarum* DpsA in its low- and high-iron states. *Proc. Natl. Acad. Sci. U. S. A.* **101,** 13780–13785 (2004).

25. Funahashi, T. *et al.* Identification and characterization of *Aeromonas hydrophila* genes encoding the outer membrane receptor of ferrioxamine B and an AraC-type transcriptional regulator. *Biosci. Biotechnol. Biochem.* **78,** 1777–1787 (2014).

26. Sandy, M. & Butler, A. Microbial Iron Acquisition: Marine and Terrestrial Siderophores. *Chem Rev* **109,** 4580–4595 (2009).

27. Najimi, M., Lemos, M. L. & Osorio, C. R. Identification of siderophore biosynthesis genes essential for growth of *Aeromonas salmonicida* under iron limitation conditions. *Appl. Environ. Microbiol.* **74,** 2341–2348 (2008).

28. Yao, Z. *et al.* Quantitative proteomic analysis of cell envelope preparations under iron starvation stress in *Aeromonas hydrophila*. *BMC Microbiol.* **16,** 161 (2016).

29. Schütz, M. K., Bildstein, O., Schlegel, M. L. & Libert, M. Biotic Fe(III) reduction of magnetite coupled to H2 oxidation: Implication for radioactive waste geological disposal. *Chem. Geol.* **419,** 67–74 (2015).

30. Ruebush, S. S., Brantley, S. L. & Tien, M. Reduction of Soluble and Insoluble Iron Forms by Membrane Fractions of *Shewanella oneidensis* Grown under Aerobic and Anaerobic Conditions. *App* **72,** 2925–2935 (2006).

31. Tao, L., Zhu, Z.-K., Li, F.-B. & Wang, S.-L. Fe(II)/Cu(II) interaction on goethite stimulated by an iron-reducing bacteria *Aeromonas Hydrophila* HS01 under anaerobic conditions. *Chemosphere* **187,** 43–51 (2017).

32. Junier, P. *et al.* Metal reduction by spores of *Desulfotomaculum reducens*. *Environ. Microbiol.* **11,** 3007–3017 (2009).

33. Lovley, D. R. Dissimilatory metal reduction: from early life to bioremediation. Volume 68, number 5, 231-237 (2002).

34. Pirbadian, S. *et al. Shewanella oneidensis* MR-1 nanowires are outer membrane and periplasmic extensions of the extracellular electron transport components. *Proc. Natl. Acad. Sci.* **111,** 1–6 (2014).

35. Cornell, R.M., Schwertmann, U. The iron oxides: structure, properties, reactions, occurrence and uses. *Mineral. Mag.* **61,** 741 (2003).

36. Schwertmann, U. Solubility and dissolution of iron-oxides. *Plant Soil* **130,** 1–25 (1991).

37. Kraemer, S. M. Iron oxide dissolution and solubility in the presence of siderophores. *Aquat. Sci.* **66,** 3–18 (2004).

38. Bolt, G. H. *Soil Chemistry: A. Basic Elements*. *Developments in Soil Science* **5,** (1976).

39. Davison, W. The Solubility of Iron Sulfides in Synthetic and Natural-Waters at Ambient-Temperature. *Aquat. Sci.* **53,** 309–329 (1991).

40. Mahdavi, M. *et al.* Heat treatment effects on Fe3O4 nanoparticles structure and magnetic properties prepared by carbothermal reduction. *Lehigh Rev.* **3,** 208–211 (2012).

41. Cornell, R. M. & Schwertmann, U. *The Iron Oxides*. (1996).

42. Frankel, R. B. & Bazylinski, D. a. Biologically induced mineralization by bacteria. *Rev. Mineral. Geochemistry* **54,** 95–114 (2003).

43. Blakemore, R. Magnetotactic Bacteria. *Science (80-.).* **190,** 377–379 (1982).

44. Roh, Y. *et al.* Biogeochemical and environmental factors in Fe biomineralization: magnetite and siderite formartion. *Clays Clay Miner.* **51,** 83–95 (2003).

45. Dubiel, M., Hsu, C. H., Chien, C. C., Mansfeld, F. & Newman, D. K. Microbial respiration can protect steel from corrosion. *Appl. Environ. Microbiol.* **68,** 1440–1445 (2002).

46. Konhauser, K. O. Diversity of bacterial iron mineralization. *Earth Sci. Rev.* **43,** 91–121 (1998).

47. Moskowitz, B. M., Frankel, R. B., Bazylinski, D. a., Jannasch, H. W. & Lovley, D. R. A comparison of magnetite particles produced anaerobically by magnetotactic and dissimilatory iron- reducing bacteria. *Geophys. Res. Lett.* **16,** 665 (1989).

48. Moisescu, C., Bonneville, S., Tobler, D., Ardelean, I. & Benning, L. G. Controlled biomineralization of magnetite (Fe3O4) by *Magnetospirillum gryphiswaldense*. *Mineral. Mag.* **72,** 333–336 (2008).

49. Hedrich, S., Schlomann, M. & Johnson, D. B. The iron-oxidizing proteobacteria. *Microbiology* **157,** 1551–1564 (2011).

50. Roh, Y., Vali, H., Phelps, T. J. & Moon, J.-W. Extracellular Synthesis of Magnetite and Metal-Substituted Magnetite Nanoparticles. *J. Nanosci. Nanotechnol.* **6,** 3517–3520 (2006).

51. Moon, J.-W. *et al.* Microbial preparation of metal-substituted magnetite nanoparticles. *J. Microbiol. Methods* **70,** 150–158 (2007).

52. Ma, Y., Galinski, E. a., Grant, W. D., Oren, a. & Ventosa, a. Halophiles 2010: Life in Saline Environments. *Appl. Environ. Microbiol.* **76,** 6971–6981 (2010).

53. Zachara, J. M. *et al.* Bacterial reduction of crystalline Fe3+ oxides in single phase suspensions and subsurface materials. *Am. Mineral.* **83,** 1426–1443 (1998).

54. Köhler, I., Konhauser, K. O., Papineau, D., Bekker, A. & Kappler, A. Biological carbon precursor to diagenetic siderite with spherical structures in iron formations. *Nat. Commun.* **4,** 1741 (2013).

55. Volkland, H. P. *et al.* Bacterial phosphating of mild (unalloyed) steel. *Appl. Environ. Microbiol.* **66,** 4389–4395 (2000).

56. Fu, L. *et al.* Iron reduction in the DAMO/*Shewanella oneidensis* MR-1 coculture system and the fate of Fe(II). *Water Res.* **88,** 808–815 (2016).

57. Comensoli, L. *et al.* Use of bacteria to stabilize archaeological iron. *Appl. Environ. Microbiol.* (2017). doi:10.1128/AEM.03478-16

58. Kooli, W. M. *et al.* Bacterial iron reduction and biogenic mineral formation for the stabilisation of corroded iron objects. *Sci. Rep.* **8,** 764 (2018).

59. Rehren, T. *et al.* 5,000 years old Egyptian iron beads made from hammered meteoritic iron. *J. Archaeol. Sci.* **40,** 4785–4792 (2013).

60. Pons, E., Graells, R. & Valldeperez, M. Fin de l'âge du bronze et début de l'âge du fer dans le nord-est de la péninsule ibérique: nouvelles données et nouvelles approches (1100-550 av. J.-C.). *Rev. archéologique l'Est. Supplément* 541–558 (2009).

61. Richards, M. P., Fuller, B. T. & Molleson, T. I. Stable isotope palaeodietary study of humans and fauna from the multi-period (Iron Age, Viking and Late Medieval) site of Newark Bay, Orkney. *J. Archaeol. Sci.* **33,** 122–131 (2006).

62. Veen, P. Van Der. Early Iron Age Epigraphy and Chronological Revision : a summary article. **1567,** 190–198 (1994).

63. Councilparis, E. N. Position Paper on the Encouragement of Cultural Tourism. *Forum Am. Bar Assoc.* 1–20 (2006).

64. Sarin, P., Snoeyink, V. L., Lytle, D. A. & Kriven, W. M. Iron corrosion scales: model for sclae

growth, iron release and colored water formation. *J. Environ. Eng.* **130,** 364–373 (2004).

65. Dinh, H. T. *et al.* Iron corrosion by novel anaerobic microorganisms. *Nature* **427,** 829–832 (2004).

66. McNeill, L. S. & Edwards, M. Iron pipe corrosion in distribution systems. *Am. Water Work. Assoc.* **93,** 88–100 (2001).

67. Scicluna, M. Position paper on the encouragement of cultural tourism and the mitigation of its effects. Paris: Europa Nostra Council. (2006).

68. Murzyn-kupisz, M. & Murzyn-kupisz, M. Cultural , economic and social sustainability of heritage tourism : issues and challenges. *Econ. Environ. Stud.* **12,** 113–133 (2012).

69. Tweed, C. & Sutherland, M. Built cultural heritage and sustainable urban development. *Landsc. Urban Plan.* **83,** 62–69 (2007).

70. Goral, A. Research on cultural tourism development in sacral and spiritual sites from the UNESCO World Heritage List. *Int. J. Herit. Sustain. Dev.* **1,** 49–59 (2011).

71. Chhabra, D., Healy, R. & Sills, E. Staged authenticity and heritage tourism. *Ann. Tour. Res.* **30,** 702–719 (2003).

72. Selwyn, L. S., Sirois, P. J. & Argyropoulos, V. Maney Publishing The Corrosion of Excavated Archaeological Iron with Details on Weeping and Akaganéite. *Stud. Conserv.* **44,** 217–232 (1999).

73. Selwyn, L. overview of archeological iron: the corrosion problem, key factors affecting treatment and gaps in current knowledge. *Natl. museum Aust. Canberra* 294–306 (2004).

74. Pienimäki, A. Desalination of iron. A comparison of fresh, wet finds and dry storage ones. (Helsinki Metropolia University of Applied Sciences, 2016).

75. Joseph, E. Microbes for Archaeological Iron Artworks. *FNS – Ambizione* p: 1-16 (2012).

76. Watkinson, D. & Lewis, M. ss Great Britain iron hull: modelling corrosion to define storage relative humidity. *Met. 2004* **44,** 88–102 (2004).

77. Chaudhuri, S. K., Lack, J. G. & Coates, J. D. Formation through Anaerobic Biooxidation of Fe (II) Biogenic Magnetite. *Appl. Environ. Microbiol.* **67,** 2844–2948 (2001).

78. Einarsdóttir, S. S. Mass-Conservation of Archaeological Iron Artefacts: A Case Study at the National Museum of Iceland. (University of Gothenburg, 2012).

79. Joseph, E. *et al.* Protection of Metal Artifacts with the Formation of Metal–Oxalates Complexes by Beauveria bassiana. *Front. Microbiol.* **2,** 1–8 (2012).

80. Rimmer, M. & Wang, Q. Assessing the effects of alkaline desalination treatments for archaeological iron using scanning electron microscopy. *Br. museum, Tech. Res. Bull.* **4,** p: 79-86 (2010).

81. Rimmer, M. B. Investigating the treatment of chloride-infested archaeological iron objects. (Cardiff University, 2010).

82. Watkinson, D. Measuring effectiveness of washing methods for corrosion control of archaeological iron: problems and challenges. *Corros. Eng. Sci. Technol.* **45,** 400–406 (2010).

83. Paris-est, U. & Kergourlay, F. Étude des mécanismes de déchloruration d ’objets Cas des traitements en solutions alcalines aérée et désaérée. (2012).

84. Watkinson, D. *et al.* The Use of Neutron Analysis Techniques for Detecting The Concentration And Distribution of Chloride Ions in Archaeological Iron. *Archaeometry* (2013). doi:10.1111/arcm.12058

85. Hermansson, H. *The stability of Magnetite and its significance as a passivating film in the repository environment*. (2004).

86. Muxworthy, A. R. & Dunlop, D. J. High-temperature magnetic stability of small magnetite particles. *J. Geophys. Res.* **108,** 2281 (2003).

87. Kang, N., Schmidt, M. W., Poli, S., Franzolin, E. & Connolly, J. A. D. Melting of siderite to 20 GPa and thermodynamic properties of FeCO 3 -melt. *Chem. Geol.* **400,** 34–43 (2015).

88. Miot, J. *et al.* Transformation of vivianite by anaerobic nitrate-reducing iron-oxidizing bacteria. *Geobiology* **7,** 373–384 (2009).

89. Butler, I. B. & Rickard, D. Framboidal pyrite formation via the oxidation of iron (II) monosulfide by hydrogen sulphide. *Geochim. Cosmochim. Acta* **64,** 2665–2672 (2000).

90. Uhlig, H. H. & Revie, R. W. *Corrosion and corrosion control: an introduction to corrosion science and engineering. 4th Edition* (Wiley, 2008). doi:10.1108/eb044062

91. Gao, H. *et al. Shewanella loihica* sp. nov., isolated from iron-rich microbial mats in the Pacific Ocean. *Int. J. Syst. Evol. Microbiol.* **56,** 1911–1916 (2006).

Chapter 2

Bacterial iron reduction and biogenic mineral formation for the stabilization of corroded iron objects

"As early as 1836 it was found by Ehrenberg that certain bacteria have the power of withdrawing iron from solution and causing its precipitation as ferric hydroxide". Edmund C. Harder (1919)

Based on the following published article:

Kooli, W. M., Comensoli L., Maillard J., Albini M., Gelb A., Junier P. and Joseph E.. Bacterial iron reduction and biogenic mineral formation for the stabilisation of corroded iron objects. Sci. Rep. 8, 764 (2018)

Abstract

Exploiting bacterial metabolism for the stabilization of corroded iron artifacts is a promising alternative to conventional conservation-restoration methods. Bacterial iron reduction coupled to biogenic mineral formation has been shown to promote the conversion of reactive into stable corrosion products that are integrated into the natural corrosion layer of the object. However, in order to stabilize iron corrosion, the formation of specific biogenic minerals is essential. In this study, we used the facultative anaerobe *Shewanella loihica* for the production of stable biogenic iron minerals under controlled chemical conditions. The biogenic formation of crystalline iron phosphates was observed after iron reduction in a solution containing Fe(III) citrate. When the same biological treatment was applied on corroded iron plates, a layer composed of iron phosphates and iron carbonates was formed. Surface and cross-section analyses demonstrated that these two stable corrosion products replaced 81% of the reactive corrosion layer after two weeks of treatment. Such results demonstrate the potential of a biological treatment in the development of a stabilization method to preserve corroded iron objects.

Introduction

Iron is a ubiquitous material. Since the industrial revolution, iron alloys (especially steel and cast) have been used at a large scale in fields as diverse as architecture, civil engineering, transport, food industry, and art[1]. Nowadays, iron is the most mined element in the world and constitutes 90% of all refined metals[1]. The widespread use of iron is explained by its metallurgical properties (ductility, hardness, strength)[2]. However, iron can be easily corroded by electrochemical reactions or by microbiologically influenced corrosion (MIC)[3,4]. Corrosion of metals leads to the modification of the exposed surface and the formation of a corrosion layer[5]. Depending on the environmental conditions, the corrosion products formed can protect the surface from further change (chemically stable corrosion products)[3,6,7]. Indeed, some studies have demonstrated that the presence of magnetite (Fe_3O_4), siderite ($FeCO_3$) or vivianite ($Fe_3(PO_4)\cdot 2H_2O$) plays a significant role in the preservation of archaeological iron objects and of iron water pipes[8,9]. These minerals are less reactive (especially to oxygen and humidity), and their formation leads to the preservation of the object[8]. In other cases, the corrosion products formed can cause degradation and irreversible damage (active corrosion)[1,10]. Examples of such active corrosion products include some Fe(III) oxyhydroxides, goethite α-FeO(OH), and lepidocrocite γ-FeO(OH)[11]. In particular, active corrosion is promoted by chloride ions that can be part of the formed corrosion products (for instance in akageneite β-FeO(OH)Cl)[10,12–15]. When the relative humidity is high, Fe(II) chloride salts absorb water vapor, dissolve, and form wet droplets of an orange color causing a phenomenon described as weeping of iron[16]. Ultimately, if no conservation-restoration intervention is undertaken, these reactive corrosion products create physical stress and can lead to the integrity loss of the artifact[17].

Iron corrosion causes considerable economic losses due to the costs of maintenance and replacement of damaged of iron items[12,9-18]. Therefore, limiting the formation of reactive corrosion products or converting those into more stable ones are two key issues for the preservation of iron surfaces. The former can be achieved by storage under anoxic conditions, increasing pH (passivation), or by applying coatings or anticorrosion agents. Chemical transformation of the reactive corrosion products promotes the latter. Given that the procedures used so far for limiting iron corrosion can be harmful, costly, time consuming, and also produce large amounts of waste[1,14,17,19-16], there is a growing interest in developing green alternatives to traditional iron stabilization methods[20].

Using bacteria or bacterial enzymes to stabilise iron surfaces has been investigated previously[3]. For example, the iron reducing bacterium *Geobacter sulfurreducens* or a purified hydrogenase obtained from *Ralstonia eutropha* were used in separate studies to produce iron phosphates on steel[6,7]. Likewise, the incubation of mild steel on a biofilm composed of *Rhodococcus* sp. strain C125 and *Pseudomonas putida* mt2 led to the formation of a protective surface layer of the mineral vivianite[21]. Recently a study with *Desulfitobacterium hafniense* showed that this bacterium can reduce reactive Fe(III) oxyhydroxides from corroded iron objects, favouring the biogenic production of vivianite[22]. However, abiotic reduction and undesirable formation of additional corrosion products were observed alongside biological iron reduction due to the composition of the growth medium. In addition, working with a strictly anaerobic bacterium such as *D. hafniense* could be challenging for the transfer of a biotechnological solution from the laboratory into real conservation praxis. Using a facultative anaerobe to perform iron reduction in a two-step procedure is an alternative to solve both of these issues. In the first step biomass can be produced aerobically in optimal growth conditions. After recovery and cleaning of the bacterial biomass, iron reduction and crystalline mineral formation can be performed in a second step under anaerobic conditions and in a controlled chemical environment. Handling of a facultative anaerobe under these conditions facilitates the transfer of technology into praxis. The overall hypothesis in this approach is that active biomass will still perform iron reduction with minimal growth requirements, inducing the formation of specific minerals as by-products of the interaction with the chemical precursors present in the matrix. This hypothesis was tested here. We evaluated iron reduction and biogenic iron mineral formation using *Shewanella loihica* strain PV-4, a halophilic facultative anaerobe that reduces iron and was involved in magnetite production[23,24]. Active biomass of *S. loihica* was obtained from aerobic batch cultures and used for the production of crystalline iron minerals in various chemical matrices. Finally, conditions leading to the formation of crystalline minerals were applied on corroded iron coupons to demonstrate the performance of the proposed treatment.

Results

Reduction of ferric citrate and ferric chloride and characterization of the minerals formed

S. loihica is known for its ability to grow using iron as electron acceptor for respiration and to form doped magnetite particles after 75 days of incubation[24]. We first investigated iron reduction in three chemically defined matrices using biomass produced under aerobic conditions. For this, we first grew *S. loihica* aerobically in LB medium overnight and collected the biomass. Biomass (10^8 cells for 20 mL) was washed to avoid any carry over of the spent growth medium and then transferred to anaerobic bottles containing three different anoxic chemical matrices. These chemical matrices were designed to favor the production of iron oxides (IOx), iron carbonates (ICarb), or iron sulfides (ISulp) as biogenic minerals. Ferric citrate (Fe citrate) or $FeCl_3$ were used as iron sources. Controls were performed using the same chemical matrices in the absence of bacteria. Iron reduction was monitored for 24 h by measuring the concentration of Fe(II) in solution. The increase of Fe(II) in the bottles containing the bacterium confirmed that *S. loihica* could reduce the two iron sources (Fig. SI1).

Biogenic mineral formation was assessed after one, two, and six weeks of incubation. The formation of crystalline mineral phases was only observed in the IOx (after six weeks) and ICarb (visible from two weeks onwards) matrices containing Fe citrate in presence of bacteria (Fig. 1A; SI2). The size of the mineral particles increased overtime in the ICarb solution (Fig.

1A). Elemental analyses (Energy Dispersive Spectroscopy-EDS) of the mineral particles indicated that they are composed of iron, oxygen, carbon, and phosphorus (Table 1). The latter was only detected when crystalline particles were observed (Fig. 1A, SI2, and Table SI1). In the controls without bacteria the composition of the particles observed after lyophilization suggested only the precipitation of the salts present in the medium (with Na and Cl among the major elements detected; Table SI1). The presence of phosphorus was unexpected, as no phosphate was added to the chemical matrices for performing iron reduction. This was confirmed by the EDS measurements in all the treatments without the formation of a crystalline mineral phase (Table SI1). Since the biomass was washed prior to the transfer into the iron reduction matrices, is unlikely that phosphate originates from spent medium used during the step of production of the biomass.

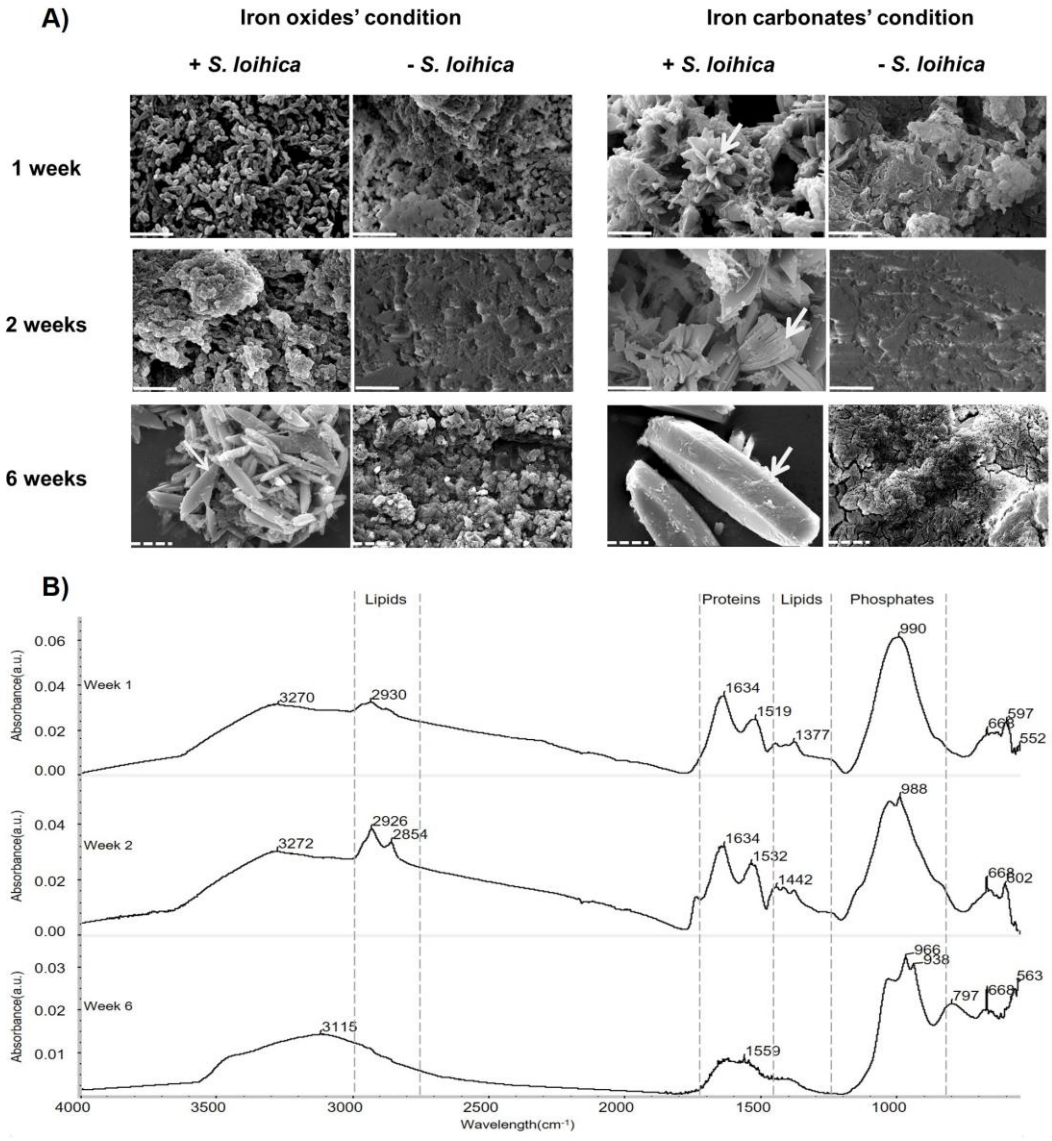

Figure 1. Soluble Fe(III) reduction and biogenic mineral formation. A. Scanning electron microscopy (SEM) images of samples collected during iron reduction in Fe citrate-containing iron oxides (IOx) and carbonate (ICarb) matrices in presence (+ *S. loihica*) or absence (- *S. loihica*) of *Shewanella loihica*. The results show the formation of minerals after 1, 2, and 6 weeks of incubation. The white arrows indicate the sites where elemental analysis was performed. Continuous and dashed white scale lines correspond respectively to 5 µm and 10 µm. **B.** ATR-FTIR spectra of culture pellets from iron-reducing ICarb solution contaning Fe

citrate after 1, 2 and 6 weeks of incubation. The spectral region corresponding to the absorbance peaks of lipids, proteins, and phosphates are marked out by dashed lines.
Fourier Transform Infrared Spectroscopy (FTIR) analyses were performed to identify the minerals formed. The results obtained with the IOx (Fig. SI3) and ICarb chemical matrices were comparable (Fig. 1B). After one and two weeks of incubation typical vibration bands for proteins (amide I peak around 1640 cm^{-1} and amide II peak around 1520 cm^{-1}) and lipids (C-H stretching around 2930, 2854 cm^{-1} and binding peaks at 1397 cm^{-1}) were observed, indicating the presence of bacteria. The peaks comprised between 1040 and 940 cm^{-1} correspond to the phosphate absorbance region[25,26], which confirmed the elemental analyses, and thus the formation of iron phosphates. Also, according to the differences observed in the spectra collected overtime, iron phosphates changed from an amorphous to a more crystalline phase. In amorphous compounds, water is not as coordinated as in crystalline forms. Absorbance bands corresponding to the coordinated water associated with iron phosphates can be observed at 3447 and 797 cm^{-1} only after six weeks of incubation. According to the obtained FTIR spectra the biogenic minerals belong to the family of vivianites or barbosalites[25,26].

Table 3: Elemental composition in terms of atomic percentage (AT%) obtained using energy-dispersive X-ray spectroscopy ***(****EDS) for the treatments* using Fe citrate with *S. loihica* (+), which resulted in the formation of biogenic minerals (ICarb and IOx conditions).

Elements (AT%)	ICarb condition			IOx condition
	1 week	2 weeks	6 weeks	6 weeks
Fe	15.37	15.26	19.18	15.61
O	24.00	33.66	46.42	51.02
C	33.74	26.64	19.22	20.75
P	5.60	9.89	12.77	11.23
Trace elements	21.29	14.55	2.41	1.39

Iron reduction with corroded iron plates and characterization of the minerals formed

As the aim of the study was the production of stable iron minerals by the conversion of reactive corrosion products, we performed further experiments with corroded iron plates using exclusively the ICarb chemical matrix, which clearly favored crystalline mineral formation in the previous experiment. The iron source was in this case the corrosion products (mainly goethite and lepidocrocite; FIG. SI4) formed on an iron plate corroded in a marine atmosphere. The plates were sterilized and added under anoxic conditions to anaerobic bottles containing the ICarb sterile matrix. Biomass of *S. loihica* was prepared and inoculated as described before (10^8 cells in 20 mL).

S. loihica is a halophile that requires the presence of salt for growth. We tested growth at different concentrations of NaCl (Fig. SI5) and with different sodium sources (Fig. SI6), confirming that 2% NaCl is the optimal salt concentration for bacterial growth. The addition of a salt containing chlorides to the reductive chemical matrix is not ideal given the deleterious role of chloride ions as active iron corrosion instigators. Therefore, we tested iron reduction without NaCl (0%) and 1% added NaCl on corroded iron coupons. In the treatment without NaCl we wanted to test if the salts potentially contained in the natural corrosion patina (i.e. salts deposited from aerosols produced by the marine environment in which the coupons were corroded) were enough to meet the salt requirements of a halophilic strain, such

as *S. loihica*. Iron reduction using corroded coupons as iron source was assessed by the increase of Fe(II) concentration in the solution. The results showed that *S. loihica* was only able to reduce solid Fe(III) when 1% NaCl was added (Fig. 2A). Therefore, salts present in the corrosion layer of the iron plates do not provide the required salt concentration for the metabolic activity of *S. loihica*. Without NaCl, no reduction was observed although the bacterial cells remained intact when observed under the microscope. The fact that iron reduction did not occur at 0% NaCl provided an ideal inactive biological control to establish the effect of the bacterial treatment (at 1% NaCl) on the conversion of the corrosion layer. As expected, no mineral formation was observed for the treatment with bacteria at 0% NaCl (Fig. SI7). On the contrary, with 1% NaCl, SEM observations of the coupons' surface confirmed the presence of a crystalline mineral phase already after one week of incubation (Fig. 2B). The production of minerals occurred alongside a change in the color of the iron plates, from red to dark grey (Fig. 2B). EDS analyses showed the presence of phosphorus associated to the production of crystalline mineral phases (Table 2). Phosphorus was absent from the plates incubated in the abiotic medium (Table 2; - *S. loihica*). Likewise, phosphorus was not detected by EDS analyses on the coupons treated at 0% NaCl, with and without the bacteria, as well as in the untreated coupons (Table SI2).

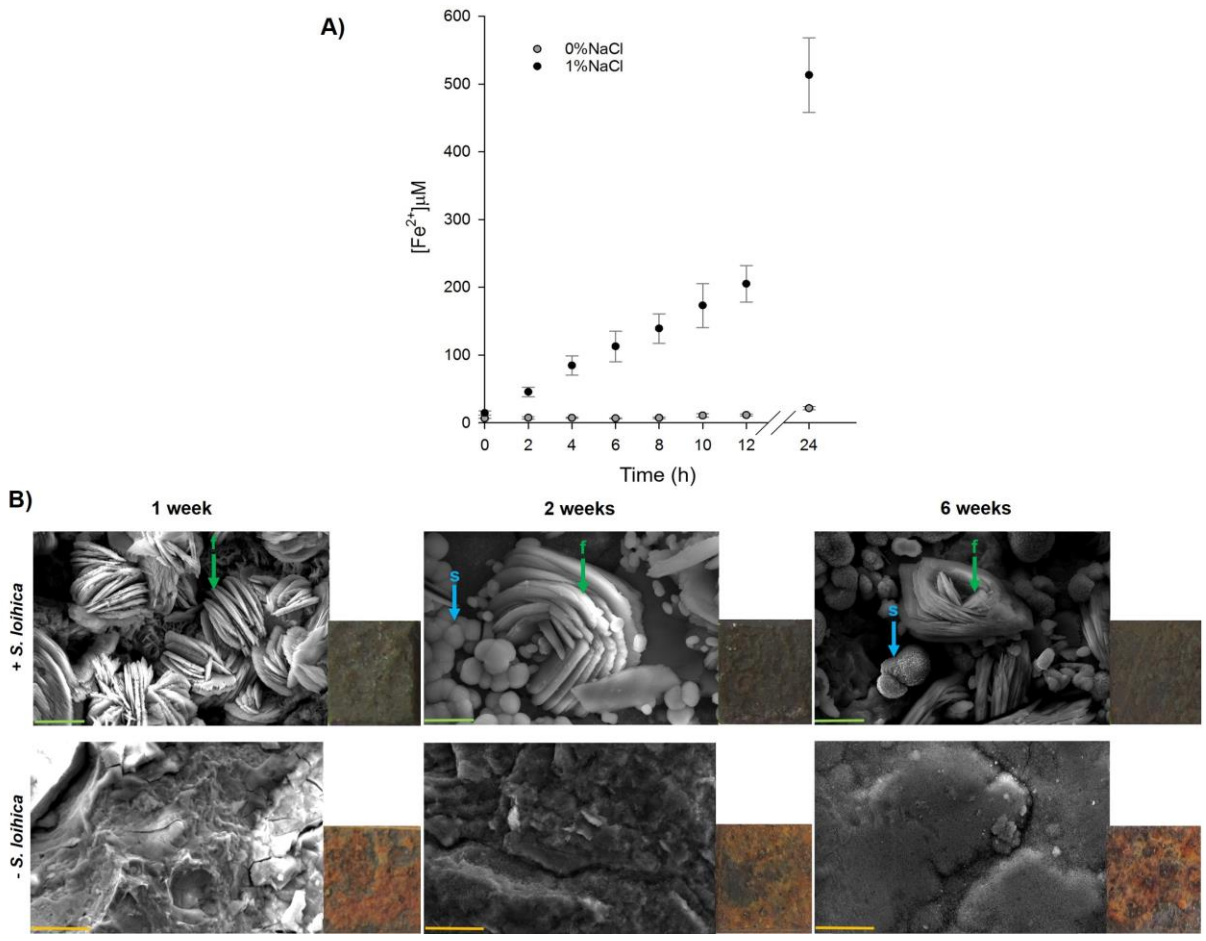

Figure 2. Solid Fe(III) reduction and biogenic mineral formation. (**A**) Iron reduction in cultures of *S. loihica* without (grey circles) and with 1% NaCl (black circles). (**B**) Scanning electron microscopy (SEM) images and visual aspect of the iron coupons treated with *S. loihica* (+*S. loihica*) and of the abiotic control (-*S. loihica*) in the presence of 1% NaCl, after

1, 2, and 6 weeks of incubation. The letters f and s indicate foil-like biogenic mineral habita and spherical agregates respectively. Scale bars: orange: 20µm and green: 10µm.

On the coupons treated with bacteria at 1% NaCl, two types of mineral forms were observed simultaneously after two and six weeks of incubation: foil-like habita (indicated as "f" in Fig. 2B and visible already at 1 week) and spherical aggregates (indicated as "s" in Fig. 2B). The EDS spectra of the two mineral phases differed. While the presence of phosphorus was a chemical signature of the foil-like habita (Table 2, f), the spherical-shaped aggregates contained only Fe, C, and O, but no traces of phosphorus (Table 2, s). As in the case of the soluble iron sources, the presence of phosphorus in the foil-like habita minerals was surprising given that no P source was added to the reductive chemical matrix. It is known that some bacteria are able to accumulate phosphate inside the cells in the form of polyphosphates. Depending on the metabolic state of the bacterial cells, phosphorus can later be released in the form of orthophosphates in the solution[27,28]. DAPI staining and microscopic observations of *S. loihica* showed that this bacterium is indeed able to accumulate polyphosphates in granules in oxic conditions, releasing orthophosphates in anoxic conditions during the treatment (Fig. SI8). These orthophosphates are a likely P source for the biogenic formation of iron phosphates.

Table 2. Elemental composition in terms of atomic percentage (AT%) obtained using energy-dispersive X-ray spectroscopy **(**EDS) for the minerals obtained in the treatment with 1% NaCl with (+) and without (-) *S. loihica*. "f" corresponds to the foil-like aggregates, while "s" refers to the spherical-shaped minerals. nd stands for "not detected".

Elements (AT%)	**1 week**		**2 weeks**			**6 weeks**		
	+	-	+		-	+		-
			f	s		f	s	
Fe	20.45	33.10	26.31	24.76	43.69	22.88	21.48	44.25
O	50.69	65.41	38.36	50.67	54.89	51.09	51.79	54.35
C	15.37	nd	23.09	24.57	nd	10.65	26.73	nd
P	12.49	nd	12.25	nd	nd	15.38	nd	nd
Cl	nd	0.37	nd	nd	nd	nd	nd	nd
Trace elements	1.00	1.12	0.00	0.00	1.42	0.00	0.00	1.4

Effect of biogenic mineral formation on the corrosion layer of iron coupons

Mineral identification before and after the bacterial treatment of iron coupons was conducted using XRD analysis. The results were consistent with the EDS analyses, showing the presence of a Fe(II) phosphate mineral (vivianite), already after one week of incubation (Fig. 3A). In addition, Fe(II) carbonate (siderite; $FeCO_3$), was detected on the treated coupons after two and six weeks of incubation (Fig. 3A). The XRD results also demonstrated the absence of Fe(II) phosphates or Fe(II) carbonates in the abiotic controls and on the untreated coupons (Fig. 3B). Moreover, the intensity of the XRD peaks related to reactive corrosion products (e.g. hematite and lepidocrocite) decreased over time in coupons treated with bacteria at 1%

NaCl (Fig. 3B). This result clearly demonstrated the effectiveness of the biological treatment to replace reactive corrosion products by stable biogenic minerals.

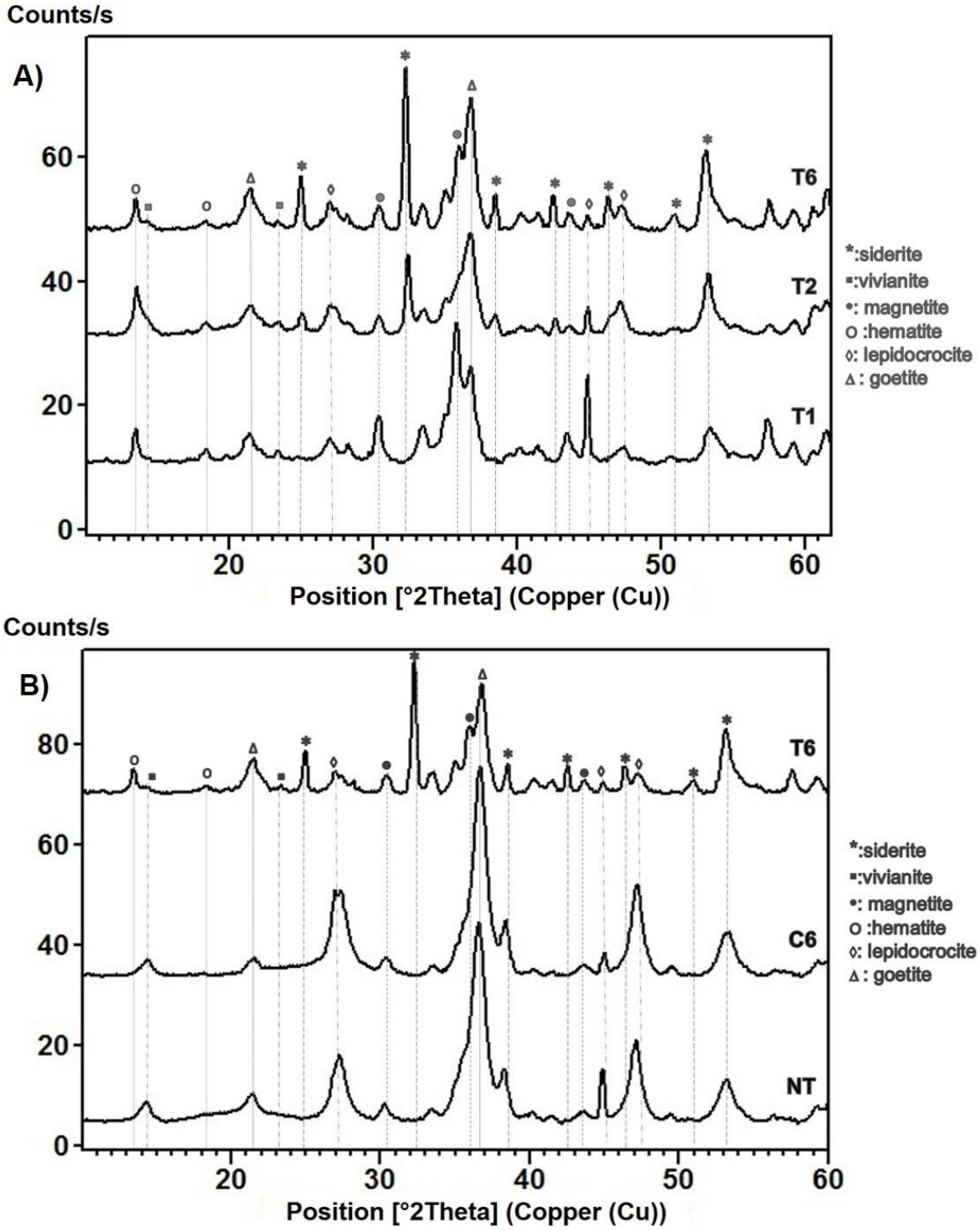

Figure 3. X-Ray diffraction (XRD) spectra of iron coupons. (A) Spectra recorded on the coupons treated with *S. loihica* after 1 (T1), 2 (T2) and 6 (T6) weeks of incubation. (B) Spectra recorded after 6 weeks of incubation of the coupons treated with *S. loihica* (T6), the abiotic control (C6), and the untreated coupons (NT).

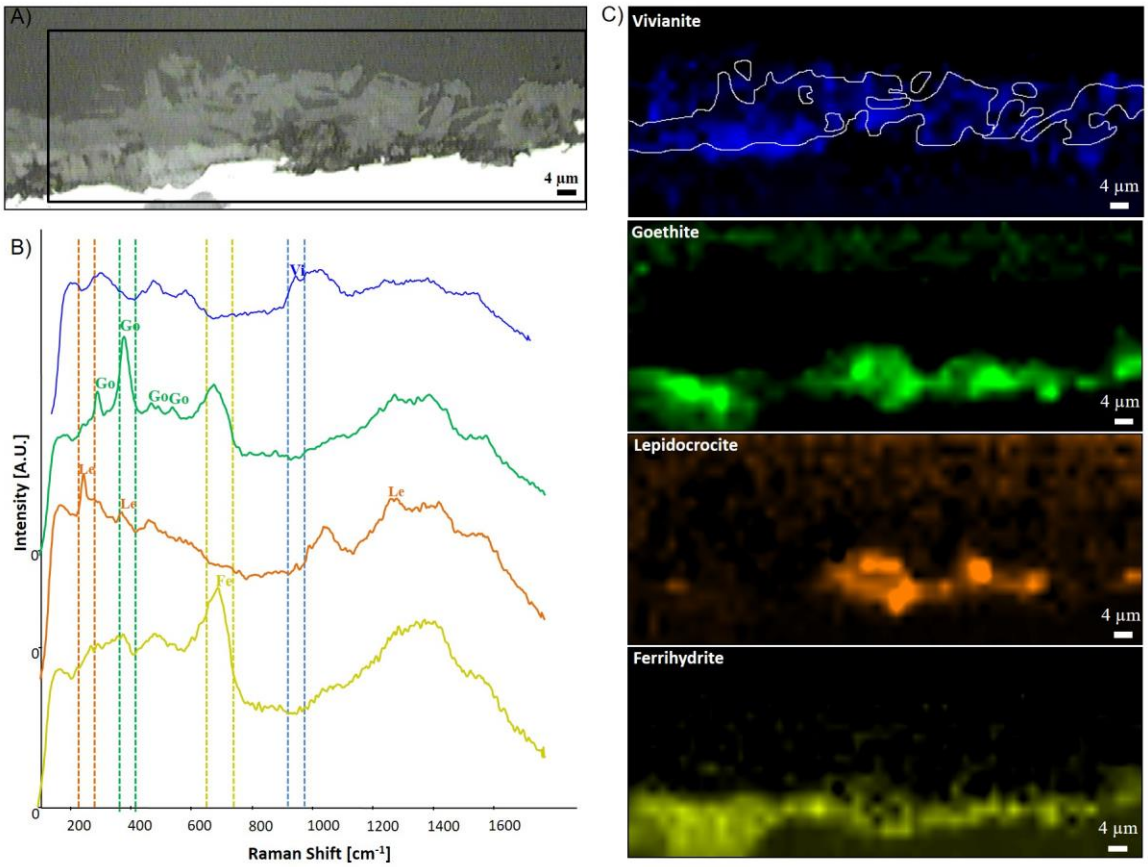

Figure 4. Raman mapping of a bacterial-treated coupon after 1 week of incubation. (A) Scanning electron microscopy image with the area analyzed by Raman mapping indicated by a black box. (B) Raman spectra of vivianite (Vi), goethite (Go), lepidocrocite (Le), and ferrihydrite (Fe), extracted from the map dataset and indicating the vibrational bands used for the elaboration of the chemical maps. (C) Raman chemical maps of vivianite (964 cm^{-1}) in blue, of goethite (384 cm^{-1}) in green, of lepidocrocite (248 cm^{-1}) in orange, and of ferrihydrite (705 cm^{-1}) in yellow.

In addition to the surface analyses, cross-section analyses were performed. Untreated iron coupons displayed a corrosion layer with dark-brown, red and orange tonalities (Fig. 5, SI9). The same was observed for the abiotic control coupons (Fig. SI9 and SI10). In contrast, a precipitation of grey-green minerals was observed on the outermost corrosion layer of the coupons treated with bacteria (Fig. SI9). Additional molecular analyses carried out on the cross-sectioned coupons after 1 week of treatment confirmed that the biogenic layer was mainly composed of vivianite with the presence of a characteristic Raman shift at 964 cm^{-1} (Fig. 4). Below this layer, the same corrosion products detected on the untreated coupons were also located and identified as goethite, lepidocrocite, and ferrihydrite (Fig. 4). No chlorinated compounds such as akageneite β-FeO(OH)Cl were individuated by Raman investigation, neither on the untreated nor on the treated coupons. This is probably due to the concomitant presence of ferrihydrite whose Raman shifts superimpose those of akageneite. An overall decrease on the thickness of the original corrosion layer was measured after the treatment with bacteria. The continuity of the biogenic layer was estimated and the results confirmed that bacteria produced a relatively homogeneous mineral layer on top of the original corrosion layer covering already 81% of the coupons' surface after 2 weeks of incubation (Fig. SI9).

SEM observations of the cross-sections after six weeks of treatment revealed that untreated coupons (Fig. 5) and abiotically treated coupons (Fig. SI10) had a corrosion layer mainly composed of iron, oxygen and chlorine. In contrast in the coupons treated with bacteria, Fe and O were found to be the main components of the corrosion layer (Fig. 5).

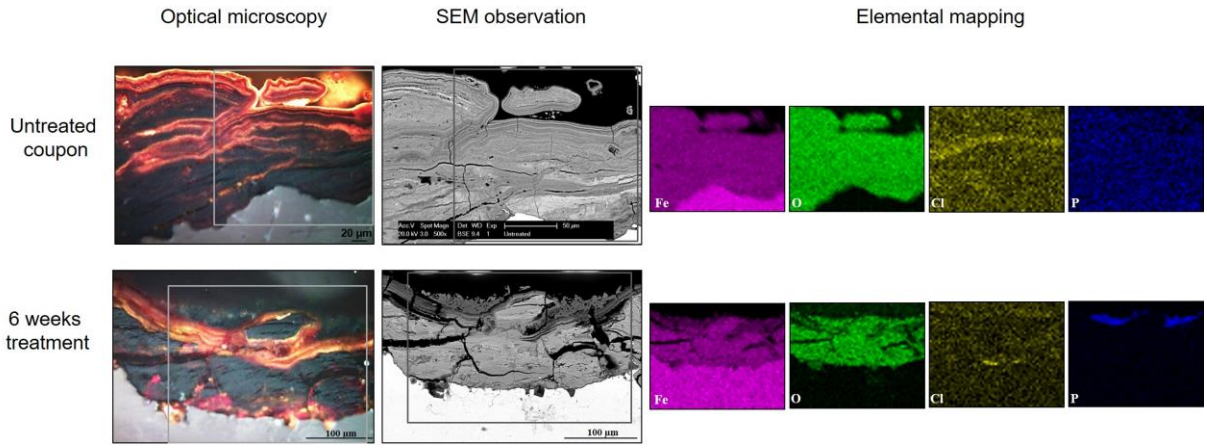

Figure 5. Cross-section analysis of the corrosion layer in iron coupons. Optical microscopy and scanning electron microscopy (SEM) images of the untreated and treated coupons after 6 weeks of incubation. The area where elemental mapping was performed is indicated by a grey box. Elemental mapping showing the presence of iron (pink), oxygen (green), chlorine (yellow), and phosphorus (blue).

Discussion

The aim of the proposed biological treatment to stabilize corroded iron is the production of specific iron minerals by the conversion of reactive corrosion products. Minerals such magnetite or siderite are desirable because they have a color similar to the native color of iron (black-grey). Moreover, these minerals are reported to be thermodynamically stable and are naturally found on iron objects acting as protective layer[11,8,16,29-30]. In this study, we developed a two-step approach based on the aerobic production of bacterial biomass followed by the anaerobic reduction of iron for the formation of specific biogenic minerals. Buffering the medium at the optimal pH reported for *S. loihica* (pH 6.5-7) precluded the formation of magnetite[24,31]. Also, recent studies have shown that under specific conditions (e.g. H_2 as electron donor) magnetite could be destabilized by iron reducing bacteria[32,33] and hence its formation may not be desirable. In the case of the chemical matrix to favor the production of iron sulfides, the formation of an amorphous phase of FeS instead of a crystalline one is probably the result of an insufficient concentration of dissolved sulphides[31]. The condition favoring the production of iron carbonates was suitable for biogenic mineral formation. However, in addition to the production of siderite after prolonged incubation (2 weeks onwards), vivianite was also precipitated. Vivianite (solubility constant -36.00[34]) is expected to be the initial Fe(II) phase to precipitate in a phosphorus-containing medium at a near neutral pH[8]. Experiments performed by Zachara et al[35] confirmed that in presence of 4 mM phosphates the formation of vivianite precedes the one of siderite (solubility constant -10.68)[34,36]), and that the latter precipitates only after the complete incorporation of phosphorus in vivianite[35]. Vivianite and siderite are biogenic by-product minerals of

dissimilatory Fe(III) reduction in bicarbonate buffers[31,35,37,38]. For instance, *Rhodococcu*s sp. C125 and *Pseudomonas putida* mt2 are able to induce vivianite formation on mild steel coupons in a phosphates-containing solution[39]. However, the production of iron phosphates under the treatment conditions used here was unexpected given the lack of added phosphorus in the reductive chemical matrix. Although dead bacterial biomass and/or the release of proteins containing phosphate groups as well as degradation of nucleic acids[40] are a possible source of phosphorus, accumulation of polyphosphates by *S. loihica* during aerobic growth and release of orthophosphates during the treatment under anoxic conditions is a more likely explanation as to the source of phosphorus for vivianite precipitation.

Production of vivianite has been proposed as an anti-corrosion treatment for steel[39]. Therefore, according to the results obtained, the proposed biological treatment seems to be a good alternative to stabilize corrosion of iron objects. Analyses performed on the corrosion layer of iron coupons demonstrated that the biological treatment led to the decrease of reactive corrosion products along with an increase in the formation of biogenic minerals that are integrated in the natural corrosion layer. This was accompanied by a pleasing aesthetical change in the color of the coupons to grey after 2 weeks of incubation. In addition, chlorides appeared to be almost completely extracted from the corrosion layer, avoiding any further harmful cyclic and active corrosion to start again. The biogenic minerals produced using *S. loihica*, vivianite and siderite, are reported to have a protective effect on water distribution pipes and archaeological iron objects[12,8]. Moreover, using a facultative anaerobe and the production of biomass under aerobic conditions facilitates the practical use of bacteria, compared to strict anaerobes[22]. Next, scaling up of the process and assessing the stability of the biogenic minerals produced and their long-term protective effect on corroded iron surfaces are required for the application of this stabilization method into real conservation-restoration praxis. Nevertheless, exploiting bacterial metabolic activity to stabilize corroded iron objects is an innovative biotechnological process that can have a significantly positive impact on the preservation and maintenance of iron-based surfaces.

Material and methods

Bacterial strain and aerobic growth conditions

Shewanella loihica PV-4 (DSM **17748)** was used in this study. The strain was purchased from the DSMZ (Deutsche Sammlung von Mikroorganismen und Zellkulturen GmbH,). Regular cultivation was performed aerobically using Luria-Bertani medium (LB; 1% (w/v) tryptone, 0.5% (w/v) yeast extract, and 1% (w/v) sodium chloride (NaCl)) at pH 7 and at 20°C under agitation at 130 rpm. For the experiments the bacterium was cultivated aerobically overnight. Cell biomass was then collected by centrifugation (1700 x *g* for 10 min) and the pellet was washed three times with an oxic basal solution containing 20 mM **1,4-Piperazinediethanesulfonic acid** (PIPES) and the same (w/v) concentration of NaCl of the reducing matrix (see below) to avoid the carryover of spent LB medium. Between the washing steps the cells were centrifuged at 1700 x g for 10 min, discarding the supernatant at every step. Finally, the pellet was resuspended in the same solution without NaCl and adjusted to a density of 10^8 cells/mL to be added to the defined chemical matrices containing iron (Fig. SI11).

Reduction of ferric citrate and ferric chloride

Three chemical matrices were used for iron reduction using ferric citrate and ferric chloride as electron acceptors. For this, 5 mM of sodium lactate as electron donor, and 10 mM of ferric citrate (Fe citrate) or ferric chloride ($FeCl_3$) as electron acceptors were added to the same basal solution (20 mM PIPES, 2% (w/v) NaCl). For the production of specific iron minerals, 20 mM NaOH or 50 mM sodium bicarbonate ($NaHCO_3$), were added to favor iron oxides (e.g. magnetite; IOx) or (e.g. siderite; ICarb), respectively. A third treatment consisted of 20 mM NaOH supplemented with 10 mM sodium sulfide (Na_2S) to induce the production of iron sulfides (ISulp) (SI-13). In the case of ISulp, after assessing iron reduction for 24 h in the (IOx) matrix, sodium sulfide was added to favor iron sulfide mineral production. The final pH of the three matrices was between 6.5 and 7 (optimal pH for *S. loihica*). To render the iron reduction matrices anoxic, the solutions were first boiled to remove dissolved oxygen and then flushed with nitrogen. The $FeCl_3$ stock solution was then filter sterilized under anoxic conditions as a precipitate was formed when autoclaving was performed. All the other solutions were sterilized by autoclaving at 120°C for 20 min. The $NaHCO_3$ solution was added after autoclaving to avoid CO_2 degassing. Biomass was prepared as described above and added to the reducing matrix to a final concentration of $5x10^6$ cells/mL. To evaluate iron reduction, 900 µL samples were collected every 2 h for 24 h to measure the concentration of Fe(II) in solution (see below). The production of iron minerals was evaluated after 1, 2, and 6 weeks of incubation at room temperature under agitation (120 rpm). Experiments were performed in triplicates including abiotic controls. In the latter the same defined matrices were incubated in the absence of bacteria to investigate abiotic iron reduction and chemical mineral formation.

Reduction of corroded iron plates

For the validation of the treatment on real objects, we used iron plates (50 x 50 x 2-3 mm) naturally corroded after one-year exposure in an outdoor marine environment containing chlorinated aerosols (French Institute of Corrosion, Brest, France). The orientation and position of the iron plates during exposure were selected according to ISO 9223 standard, which defines the standards for the corrosion of metals and alloys. Plates were exposed south

skyward at 45° from the horizontal. For the experiment, the plates were then cut in coupons of 10 x 10 x 2-3 mm. The preparation of the plates for the experiments was performed under oxic conditions.

Iron reduction and biogenic mineral formation with the corroded iron coupons was performed in a matrix composed of 20 mM PIPES, 5mM sodium lactate, and 50 mM $NaHCO_3$. In this case, two conditions were compared: no NaCl (0%) and 1% NaCl. The final pH of the matrices was between 6.6 and 7.4. For the sterilization of the iron coupons, autoclaving was avoided as an enhancement of the corrosion layer was observed under both oxic and anoxic conditions. Instead of autoclaving, coupons were washed with 70% (v/v) ethanol and dried under UV exposure for 1 h for each side. A control for this sterilization method was performed by incubating UV-sterilized plates on solid LB medium under oxic and anoxic conditions, which showed no bacterial growth after one week of incubation.

Biomass was prepared as described above and added to the reducing matrix to a final concentration of 5.10^6 cells/mL. To evaluate iron reduction, Fe(II) was measured in 900 µL samples collected every 2 h for 24 h (see below). The production of iron minerals was evaluated after 1, 2, and, 6 weeks of incubation at room temperature under agitation (120 rpm). Experiments were performed in triplicates including abiotic controls (without bacteria).

Measurements of Fe(II) concentration

To measure the reduction of Fe(III) into Fe(II), the ferrozine assay was performed following a modified protocol from Bell *et al.*[41]. First, 100 µL of 5 M HCl were added immediately after sampling to the 900 µL of collected samples and stored at 4°C. The samples were centrifuged for 1 min at 6700 x *g*, then 100 µL of the supernatant were taken and 900 µL of ferrozine solution (0.1% ferrozine in a 100 mM HEPES solution at pH 7) were added. Fe(II) concentration was determined by measuring the absorbance at 562 nm with a UV-Vis spectrophotometer (Thermo Scientific Genesis 10 s). A calibration curve was obtained using serial dilutions of 1 mM ferrous ammonium sulfate solution in acidic MilliQ water (pH 2).

Scanning Electron Microscopy coupled with Energy Dispersive X-Ray Spectroscopy (SEM-EDS) analyses

Samples from Fe citrate and $FeCl_3$ amended cultures were centrifuged and fixed for 1 h with 2.5% glutaraldehyde solution in 0.1 M sodium cacodylate, washed twice by centrifugation with the same solution and fixed again for 2 h with 1% osmium tetraoxide in 0.1 M sodium cacodylate. After the secondary fixation, the samples were washed twice with distilled water. Then dehydration steps were performed using different concentrations of ethanol (25%, 50%, 75%, 90%, 100% (v/v)) and then pure acetone following a modified protocol from Pearson *et al.*[42]. Finally, samples were mounted on stubs using carbon conductive tape and coated with a 23 nm layer of gold using a Bal-Tec sputter coater SCD 005 (60 mA current, distance of the gold pastille to the sample: 5 cm, 60 s duration, argon gas). As there were no precipitates in the abiotic controls with Fe citrate, samples were lyophilized prior to stub mounting. The iron coupons were washed twice with deionized water and ethanol 70% (v/v) before being mounted on stubs using carbon conductive tape without gold sputtering. To avoid humidification, the stubs were stored in desiccators with silica gel. A Philips ESEM XL30 FEG environmental scanning electron microscope equipped with an energy-dispersive X-ray analyzer was used. The samples and coupons were observed in secondary electrons mode at an acceleration potential of 10–25 keV and with a 10 mm working distance.

Fourier Transform Infrared Spectroscopy (FTIR) analyses

FTIR measurements were performed on the same samples used for SEM-EDS analyses. An iS5 Thermo Scientific spectrometer with a diamond Attenuated Total Reflectance (ATR) crystal plate (iD5™ ATR accessory) was used. All spectra were acquired in the range 4000–650 cm^{-1}, at a spectral resolution of 4 cm^{-1}. A total of 32 scans were recorded and the resulting interferograms averaged. Data collection and post-run processing were carried out using Omnic™ software.

X-Ray Diffraction crystallography (XRD) analyses

XRD analyses were performed on untreated, abiotic control and bacterially-treated iron coupons. The preparation of the iron coupons was the same as for SEM-EDS analyses. High-statistics -θ2θ (bulk) measurements were performed with a PANalytical X'Pert Pro MPD diffractometer equipped with a fast-linear detector and sample spinner. The measurement time was 60 h to acquire high statistics for better signal-to-noise ratio. The sensitivity of the XRD phase analyses was about 1 % weight. ICSD codes were used for the identification of siderite (98-004-6078), vivianite (98-004-6142), magnetite (98-001-1782), hematite (98-001-2733), lepidocrocite (98-000-0843) and goethite (98-001-7328).

Cross-section analyses

One sample for each condition tested (untreated, abiotic control and bacterial treatment) was embedded in methacrylate resin employing the EpoFix Kit (resin and hardener, Struers). Cross-polishing was performed with silicon carbide abrasive paper with 250, 500, and 1000 grit and Micro-Mesh abrasive cloths 1800, 2400, 3200, 3600, 4000, 6000, 8000, and 12000 grades. Microscopic observations on the cross-sectioned samples were carried out with a Polyvar MET optical microscope and microphotographs were collected with Axio Vision LE software. An estimation of the percentage of original corrosion layer covered by the biogenic crystals was extrapolated from the microscopic images. Using the working conditions indicated above, SEM-EDS mapping was carried out to ascertain the distribution and the elemental composition of the newly formed biogenic minerals. Non-destructive Raman spectroscopy was performed directly on the cross-sectioned samples to define the molecular composition of the corrosion layer before and after bacterial treatment. The analysis was carried out with a Horiba-Jobin Yvon Labram Aramis microscope equipped with a Nd:YAG laser of 532 nm at a power lower than 1 mW. The spectral interval analyzed was between 100 and 1600 cm^{-1}. Single points analyses were carried out with the following conditions: 400-µm hole, 200-µm slit, and 10 accumulations of 10 s. Raman mapping was performed in selected areas of cross-sectioned samples with a step size of 2.5 µm in x and y directions. The spectra recorded were corrected (automatic baseline correction) using LabSpec NGS spectral software. Reference spectra were used for identifying the compounds present and for elaborating chemical maps.

Polyphosphate staining with 4', 6-diamidino-2-phenylindole (DAPI)

Polyphosphate detection was performed in bacterial cultures cultivated overnight in LB medium. A washing step with 1× Phosphate-buffered saline (PBS buffer; 137mM NaCl, 10mM Na_2HPO_4, 2.7mM KCl, 1.8mM KH_2PO_4, pH 7.4) buffer was done twice in order to remove the media components. One mL from a bacterial culture of 1 OD unit (at 600 nm) was centrifuged, the pellet was collected, washed 2 times with 1 mL of ice-cold 1× PBS and resuspended in 1 mL of ice-cold 4% (w/v) paraformaldehyde (PFA).

The sample was incubated for 1 h at 4°C. The pellet was then collected by centrifugation and washed three times with 1× PBS. This washing step was repeated twice in order to remove residual PFA that would produce auto-fluorescent particles. For DAPI staining, a solution of 50 µg/mL DAPI was used. Cells were placed onto a microscope slide and left to dry at room temperature. Cells were then covered with the DAPI solution and incubated in the dark at room temperature for 30 min. The slides were washed by dipping into distilled water and then air-dried. An anti-fading agent (Citifluor AF2) was applied on the slides before placing the cover slip. Observations were done with an epi-fluorescence microscope Zeiss Axioplan2 imaging, using UV excitation light. Excitation wavelength was 350 nm. DNA-DAPI combination results in a blue color (maximum fluorescence emission at around 450 nm) while polyphosphate-DAPI complex has a bright yellow color (emission at around 550 nm)[43].

Quantification of orthophosphate (orthoP) release using malachite green

The orthoP released by the cells was measured every hour during 24 h following the same procedure of sample collection as for the iron reduction experiment. Cells were incubated in the anoxic ICarb solution (20 mM PIPES, 2% NaCl, 5mM sodium lactate, 10 mM Fe citrate and 50 mM $NaHCO_3$). The collected samples were filtered at 0.22 µm and mixed in a 1:1 ratio with malachite green solution (0.7 M HCl, 0.3 mM malachite green oxalate, 8.3 mM Na_2MoO_4, 0.05% (v⁄v) Triton X-100). After 15 min of incubation at room temperature, the absorbance was measured at 630 nm and compared with values obtained with a standard curve prepared with 10mM Na_2HPO_4[44].

Acknowledgments

The Swiss National Science Foundation (Ambizione grant PZ00P2_142514, P.I. Dr. Edith Joseph) for the funding of MAIA project (Microbes for archaeological iron Artifacts).
The Swiss Centre for Electronics and Microtechnology (CSEM) and especially Dr. M. Dadras, Dr. O. Sereda, Dr. I. Marozau and Dr. K. Vaideeswaran for SEM-EDS and XRD investigations.
The Swiss National Museum for Raman microscopy, especially Dr M. Wörle.

Author contribution

WMK performed the experiments, analysed the data and wrote the manuscript. LC performed the Raman analysis; JM performed the polyphosphate experiment; MA performed the SEM mapping; AG performed imaging of polyphosphate experiment; PJ and EJ designed the experiments, analysed the data and wrote the manuscript. All the co-authors corrected the manuscript.

References

1. John, E. An A-Z Guide to The Elements. *Oxford Univ. Press* 539 (2001). doi:978-0-19-960563-7

2. Nielsen J.M. *The Radiochemistry of Iron*. *Chemistry, radiation and radiochemistry* (1960).

3. Dubiel, M., Hsu, C. H., Chien, C. C., Mansfeld, F. & Newman, D. K. Microbial respiration can protect steel from corrosion. *Appl. Environ. Microbiol.* **68,** 1440–1445 (2002).

4. Esnault, L., Jullien, M., Mustin, C., Bildstein, O. & Libert, M. Metallic corrosion processes reactivation sustained by iron-reducing bacteria: Implication on long-term stability of protective layers. *Phys. Chem. Earth* **36,** 1624–1629 (2011).

5. Narain, S. & Jain, K. K. *Iron artifacts: History, metallurgy, corrosion and conservation*. (Agam Kala Prakashan, 2009).

6. Da Silva, S., Basséguy, R. & Bergel, A. Hydrogenase-catalysed deposition of vivianite on mild steel. *Electrochim. Acta* **49,** 2097–2103 (2004).

7. Cote, C., Rosas, O. & Basseguy, R. Geobacter sulfurreducens: An iron reducing bacterium that can protect carbon steel against corrosion? *Corros. Sci.* **94,** 104–113 (2015).

8. Scott, D. A. & Eggert, G. *Iron and steel in art: corrosion, colorants, conservation*. (Archetype Publications, 2009). doi:10.1016/S0953-7562(09)80810-1

9. Sun, H. *et al.* Formation and release behavior of iron corrosion products under the influence of bacterial communities in a simulated water distribution system. *Environ. Sci. Process. Impacts* **16,** 576 (2014).

10. Sarin, P., Snoeyink, V. L., Lytle, D. A. & Kriven, W. M. Iron corrosion scales: model for sclae growth, iron release and colored water formation. *J. Environ. Eng.* **130,** 364–373 (2004).

11. Neff, D., Reguer, S., Bellot-Gurlet, L., Dillmann, P. & Bertholon, R. Structural characterisation of corrosion products on archaeological iron. An integrated analytical approach to establish corrosion forms. *J. Raman Spectrosc.* **35,** 739–745 (2004).

12. Lin, J., Ellaway, M. & Adrien, R. Study of corrosion material accumulated on the inner wall of steel water pipe. *Corros. Sci.* **43,** 2065–2081 (2001).

13. Jegdić, B., Polić-Radovanović, S., Ristić, S. & Alil, A. Corrosion Stability of Corrosion Products on an Archaeological Iron Artifact. *Int. J. Conserv. Sci.* **3,** 241–248 (2012).

14. Selwyn, L. overview of archeological iron: the corrosion problem, key factors affecting treatment and gaps in current knowledge. *Natl. museum Aust. Canberra* 294–306 (2004).

15. Selwyn, L. S., Sirois, P. J. & Argyropoulos, V. Maney Publishing The Corrosion of Excavated Archaeological Iron with Details on Weeping and Akaganéite. *Stud. Conserv.* **44,** 217–232 (1999).

16. Einarsdóttir, S. S. Mass-Conservation of Archaeological Iron Artifacts: A Case Study at the National Museum of Iceland. (University of Gothenburg, 2012).

17. Watkinson, D. Measuring effectiveness of washing methods for corrosion control of archaeological iron: problems and challenges. *Corros. Eng. Sci. Technol.* **45,** 400–406 (2010).

18. McNeill, L. S. & Edwards, M. Iron pipe corrosion in distribution systems. *Am. Water Work. Assoc.* **93,** 88–100 (2001).

19. Pienimäki, A. Desalination of iron. A comparison of fresh, wet finds and dry storage ones. (Helsinki Metropolia University of Applied Sciences, 2016).

20. Gadd, G. M. Metals, minerals and microbes: Geomicrobiology and bioremediation. *Microbiology* **156,** 609–643 (2010).

21. Volkland, H. P. *et al.* Bacterial phosphating of mild (unalloyed) steel. *Appl. Environ. Microbiol.* **66,** 4389–4395 (2000).

22. Comensoli, L. *et al.* Use of bacteria to stabilize archaeological iron. *Appl. Environ. Microbiol.* (2017). doi:10.1128/AEM.03478-16

23. Gao, H. *et al.* Shewanella loihica sp. nov., isolated from iron-rich microbial mats in the Pacific Ocean. *Int. J. Syst. Evol. Microbiol.* **56,** 1911–1916 (2006).

24. Moon, J.-W. *et al.* Microbial preparation of metal-substituted magnetite nanoparticles. *J. Microbiol. Methods* **70,** 150–158 (2007).

25. Frost, R., Martens, W., Williams, P. & Kloprogge, J. Raman and infrared spectroscopic study of the vivianite-group phosphates vivianite, baricite and bobierrite. *Mineral. Mag.* **66,** 1063–1073 (2002).

26. Frost, R. L. *et al.* Vibrational spectroscopic characterization of the phosphate mineral barbosalite Fe2+Fe3+2 (PO4)2(OH)2 -Implications for the molecular structure. *J. Mol. Struct.* **1051,** 292–298 (2013).

27. Seviour, R. J., Mino, T. & Onuki, M. The microbiology of biological phosphorus removal in activated sludge systems. *FEMS Microbiol. Rev.* **27,** 99–127 (2003).

28. Albi, T. & Serrano, A. Inorganic polyphosphate in the microbial world. Emerging roles for a multifaceted biopolymer. *World J. Microbiol. Biotechnol.* **32,** 1–12 (2016).

29. Watkinson, D. & Al-Zahrani, A. Toward quantified assessment of aqueous chloride extraction methods for archaeological iron: de-oxygenated tratment environments. *Conserv.* **31,** 75–86 (2008).

30. Rémazeilles, C. *et al.* Microbiologically influenced corrosion of archaeological artifacts:Characterisation of iron(II) sulfides by Raman spectroscopy. *J. Raman Spectrosc.* **41,** 1425–1433 (2010).

31. Konhauser, K. O. Diversity of bacterial iron mineralization. *Earth Sci. Rev.* **43,** 91–121 (1998).

32. Schütz, M. K. *et al.* Combined geochemical and electrochemical methodology to quantify corrosion of carbon steel by bacterial activity. *Bioelectrochemistry* **97,** 61–68 (2014).

33. Schütz, M. K., Bildstein, O., Schlegel, M. L. & Libert, M. Biotic Fe(III) reduction of magnetite coupled to H2 oxidation: Implication for radioactive waste geological disposal. *Chem. Geol.* **419,** 67–74 (2015).

34. Bolt, G. H. *Soil Chemistry: A. Basic Elements*. *Developments in Soil Science* **5,** (1976).

35. Zachara, J. M. *et al.* Bacterial reduction of crystalline Fe3+ oxides in single phase suspensions and subsurface materials. *Am. Mineral.* **83,** 1426–1443 (1998).

36. Bénézeth, P., Dandurand, J. L. & Harrichoury, J. C. Solubility product of siderite (FeCO3) as a function of temperature (25-250 °C). *Chem. Geol.* **265,** 3–12 (2009).

37. Köhler, I., Konhauser, K. O., Papineau, D., Bekker, A. & Kappler, A. Biological carbon precursor to diagenetic siderite with spherical structures in iron formations. *Nat. Commun.* **4,** 1741 (2013).

38. McGowan, G. & Prangnell, J. The significance of Vivianite in archaeological settings. *Geoarchaeology an intenational J.* **21,** 93–111 (2006).

39. Volkland, H. P., Harms, H., Kaufmann, K., Wanner, O. & Zehnder, A. J. B. Repair of damaged vivianite coatings on mild steel using bacteria. *Corros. Sci.* **43,** 2135–2146 (2001).

40. Chubar, N., Avramut, C. & Visser, T. Formation of manganese phosphate and manganese carbonate during long-term sorption of Mn(2+) by viable Shewanella putrefaciens: effects of contact time and temperature. *Environ. Sci. Process. Impacts* **17,** 780–90 (2015).

41. Bell, P. E., Mills, a L. & Herman, J. S. Biogeochemical Conditions Favoring Magnetite Formation during Anaerobic Iron Reduction. *Appl. Environ. Microbiol.* **53,** 2610–2616 (1987).

42. Pearson, V. K., KEARSLEY, A. T. & Sephton, M. A. The In-Situ Detection of Organic Material in Extraterrestrial Samples. *Microsc. Anal.* **18,** 5–8 (2004).

43. Gomes, F. M. *et al.* New insights into the in situ microscopic visualization and quantification of inorganic polyphosphate stores by 4',6-diamidino-2-phenylindole (DAPI)-staining. *Eur. J. Histochem.* **57,** 228–236 (2013).

44. Guymer, D., Maillard, J., Agacan, M. F., Brearley, C. A. & Sargent, F. Intrinsic GTPase activity of a bacterial twin-arginine translocation proofreading chaperone induced by domain swapping. *FEBS J.* **277,** 511–525 (2010).

Supplementary information

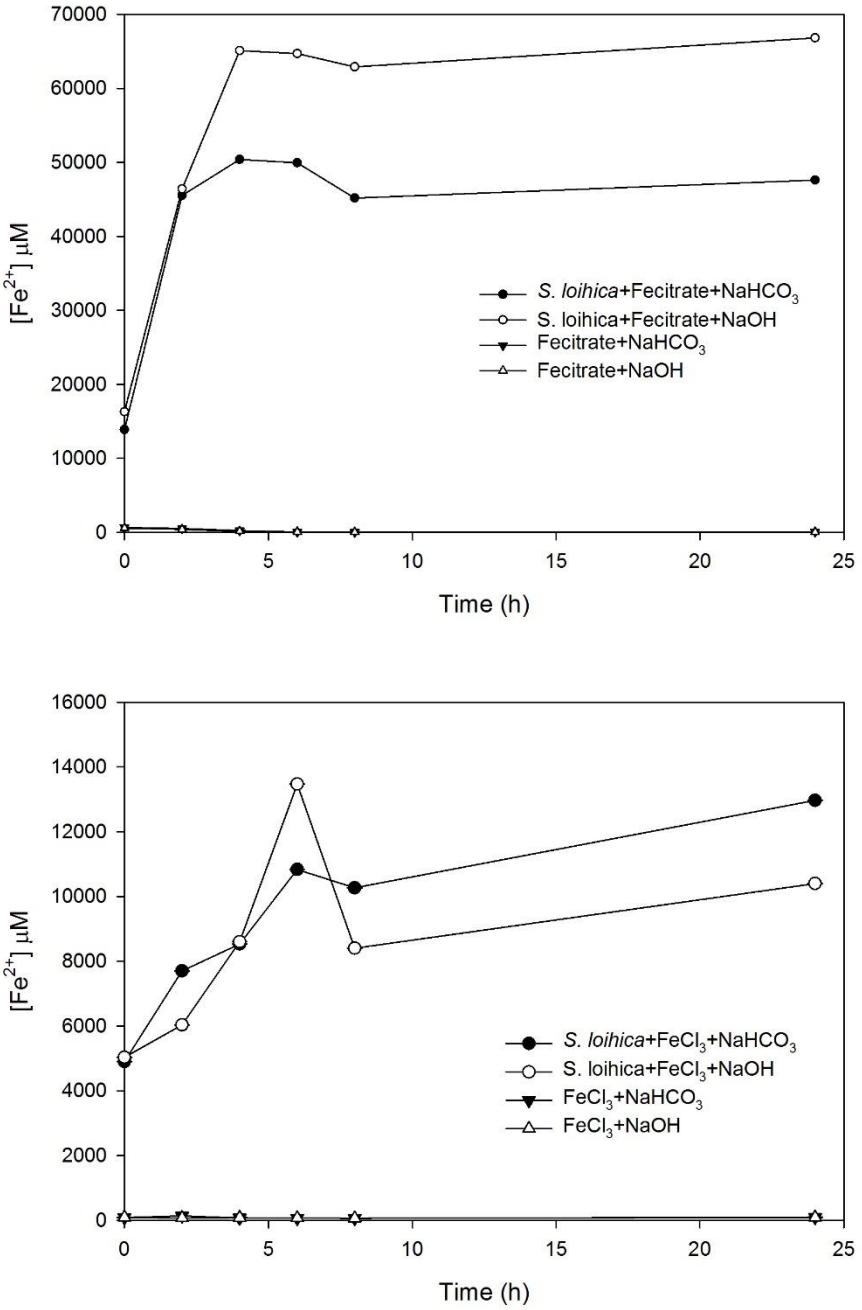

Figure SI1: Soluble Fe(III) reduction. Evolution of Fe^{2+} concentration in the chemical matrices favoring the production of iron oxides (IOx, addition of NaOH) or iron carbonates (ICarb, addition of $NaHCO_3$). The error bars correspond to the standard deviation of three independent measurements. These bars were however too small to be visible in the graphs.

A

Incubation	Visual observation	SEM pictures	EDS spectra
1 week		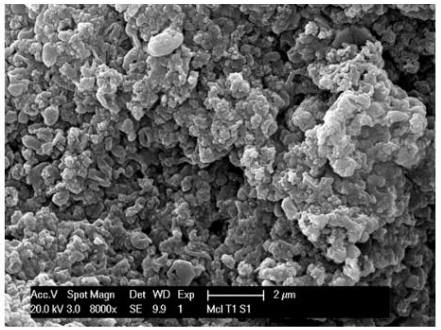	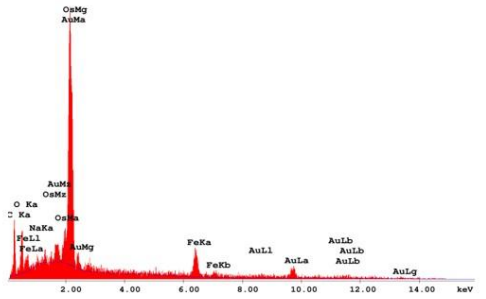
2 weeks		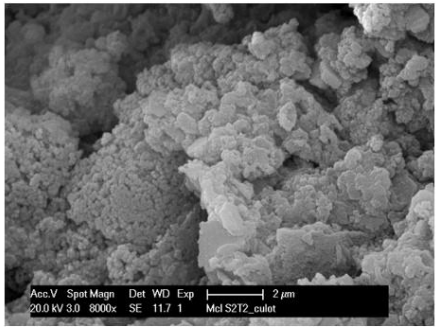	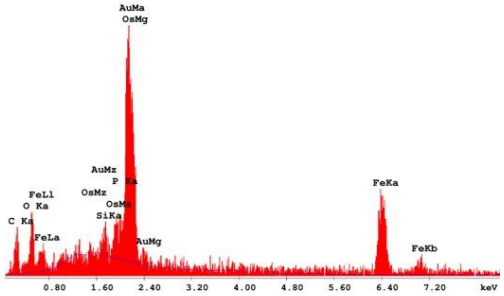
6 weeks		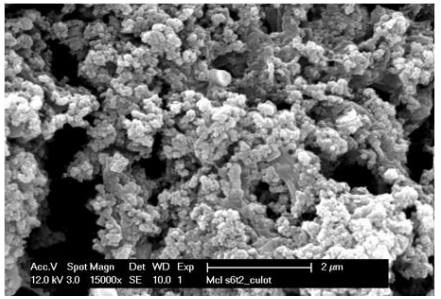	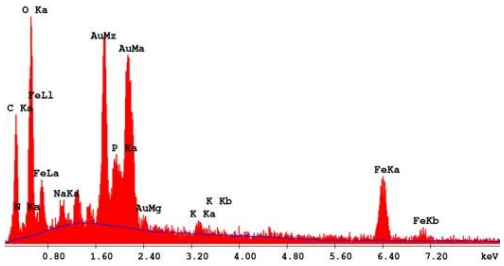

B

Incubation	Visual observation	SEM pictures	EDS spectra
1 week		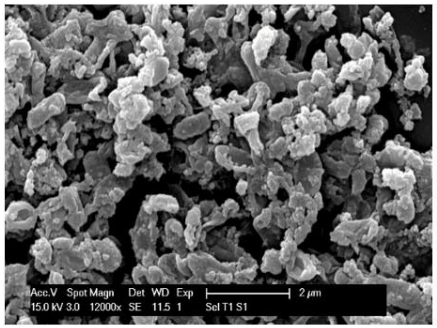	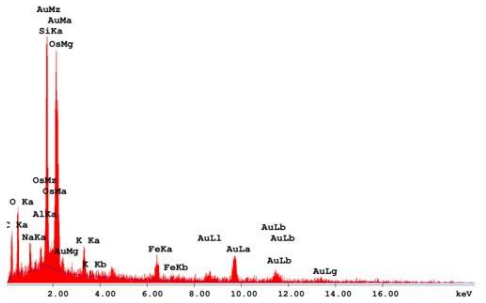
2 weeks		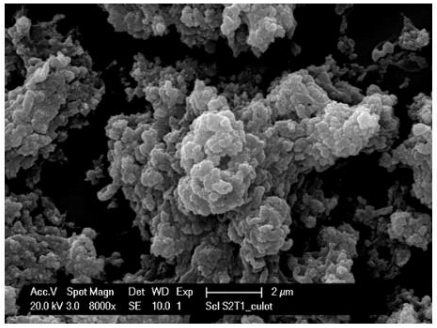	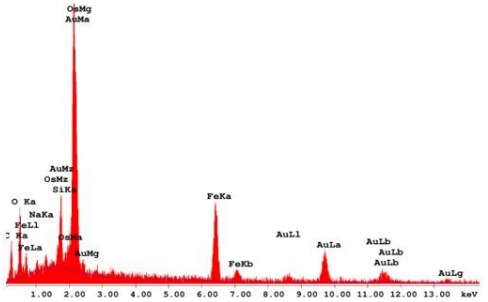
6 weeks		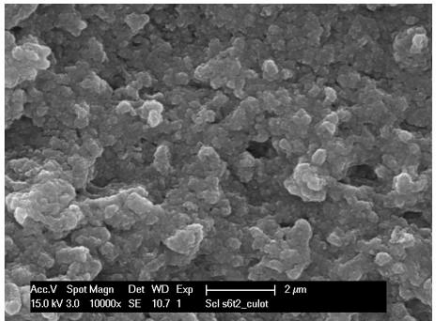	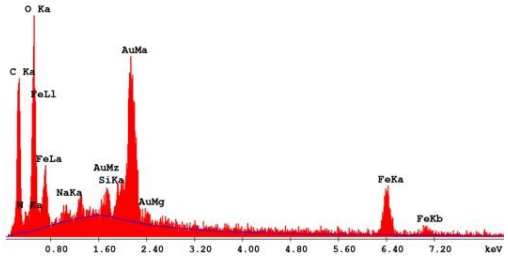

D

Incubation	Visual observation	SEM pictures	EDS spectra
1 week		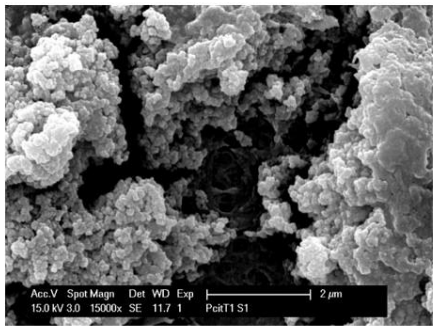	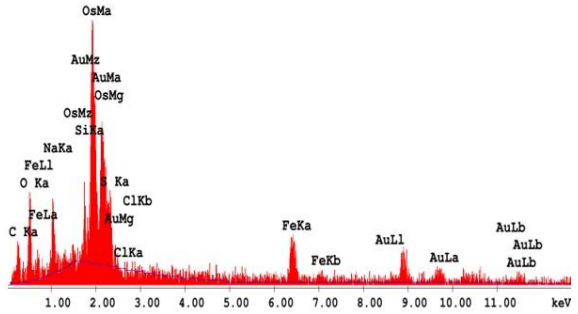
2 weeks		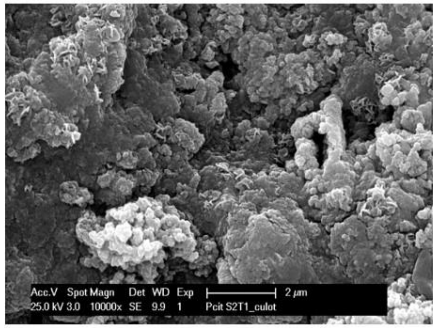	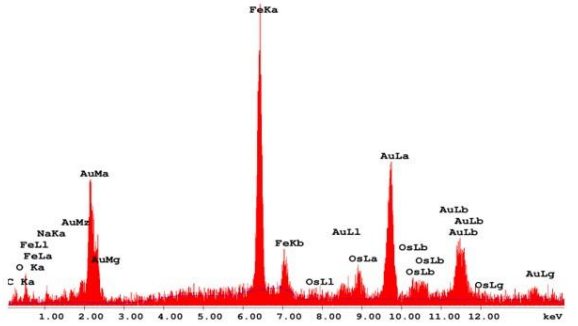
6 weeks		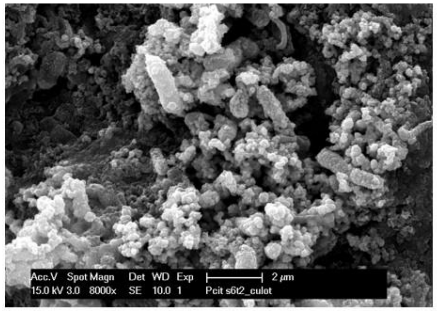	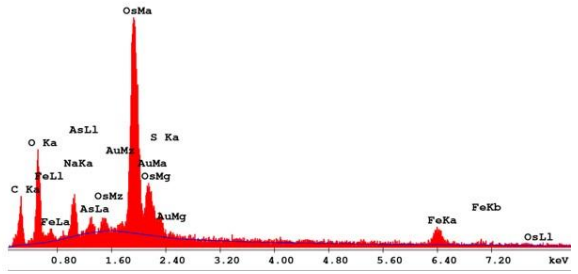

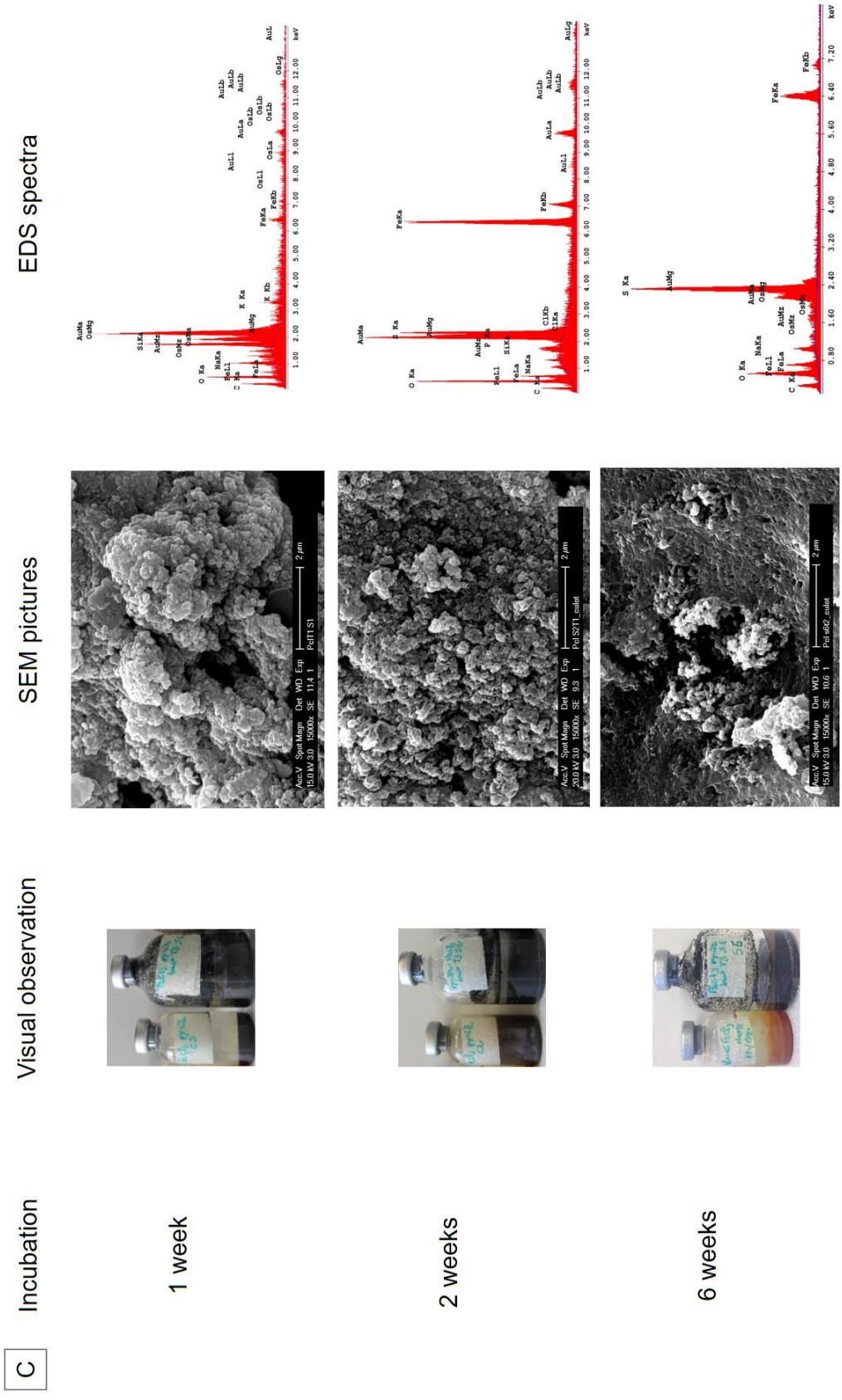

Figure SI2: Soluble Fe(III) reduction and biogenic mineral formation. Visual observations, scanning electron microscopy (SEM) images and EDS spectra of culture pellets of *S. loihica*, after 1, 2 and 6 weeks of incubation under the (A) IOx, (B) ICard and (C) ISulp conditions with $FeCl_3$, and (D) ISulp condition with Fe citrate.

Table SI1: Elemental composition in terms of atomic percentage (AT%) obtained using energy-dispersive X-ray spectroscopy (EDS), for the treatments using Fe citrate, which resulted in the formation of biogenic minerals (IOx and ICarb conditions).

ELEMENTS (AT%)	1 week				2 weeks				6 weeks			
	IOx conditions		ICarb conditions		IOx conditions		ICarb conditions		IOx conditions		ICarb conditions	
	+	-	+	-	+	-	+	-	+	-	+	-
Fe	1.97	2.51	**15.37**	2.11	2.09	-	**15.26**	-	**15.61**	-	**19.18**	-
O	22.30	10.65	24.00	-	9.86	-	33.66	8.90	51.02	5.50	46.42	14.29
C	35.25	33.48	33.74	33.01	67.15	-	26.64	30.52	20.75	30.00	19.22	30.79
P	-	-	**5.60**	-	-	-	**9.89**	-	**11.23**	-	**12.77**	-
Na	3.24	24.86	2.16	33.19	-	7.74	0.81	23.17	-	28.88	-	24.56
Si	9.57	-	3.11	-	-	-	1.34	-	-	-	-	-
Os	1.08	-	2.56	-	2.02	-	1.45	-	-	0.04	-	-
Al		-	0.62	-	-	-	-	-	-	-	-	-
K	1.18	-	-	-	0.37	-	-	-	-	-	-	-
Cl	-	25.17	-	29.56	-	68.91	-	23.82	-	31.50	-	27.43
N	-	-	-	-	-	-	4.28	6.47	-	-	-	-
Au	25.42	3.34	12.83	2.13	18.51	23.35	6.69	7.13	1.40	4.09	2.41	2.93

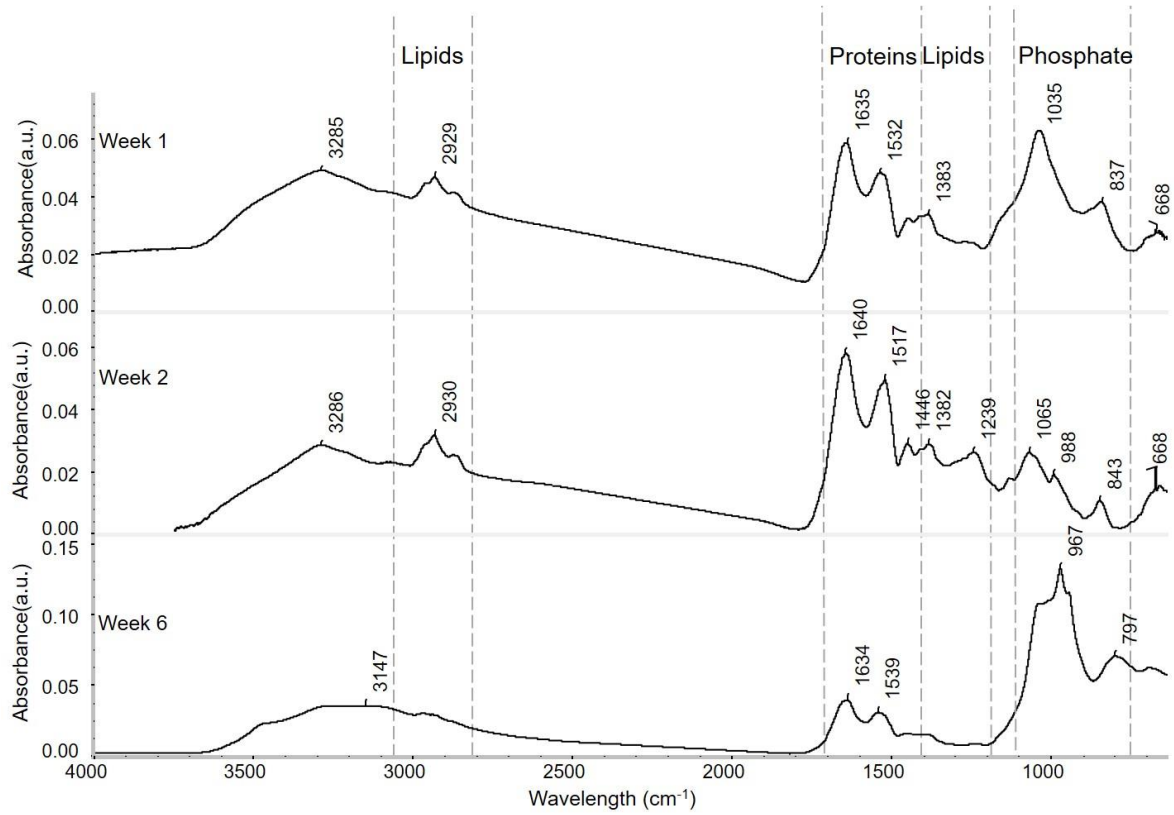

Figure SI3: ATR-FTIR spectra of culture pellets of *Shewanella loihica* after 1, 2 and 6 weeks of incubation in Fe citrate-amended solution under IOx condition. The region corresponding to the absorbance peaks of lipids, proteins, and phosphates are flanked by dashed lines as indicated in the graph.

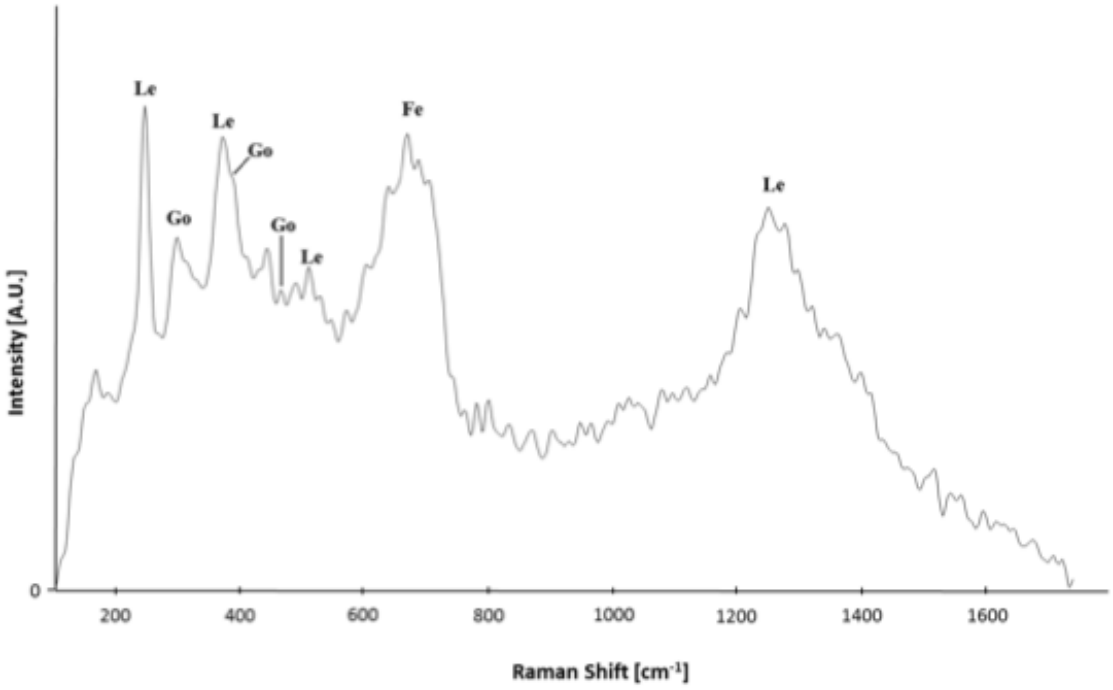

Figure SI4. Raman spectrum of the untreated iron coupon presenting a marine atmospheric corrosion. Corrosion compounds were identified as lepidocrocite (Le), goethite (Go), and ferrihydrite (Fe).

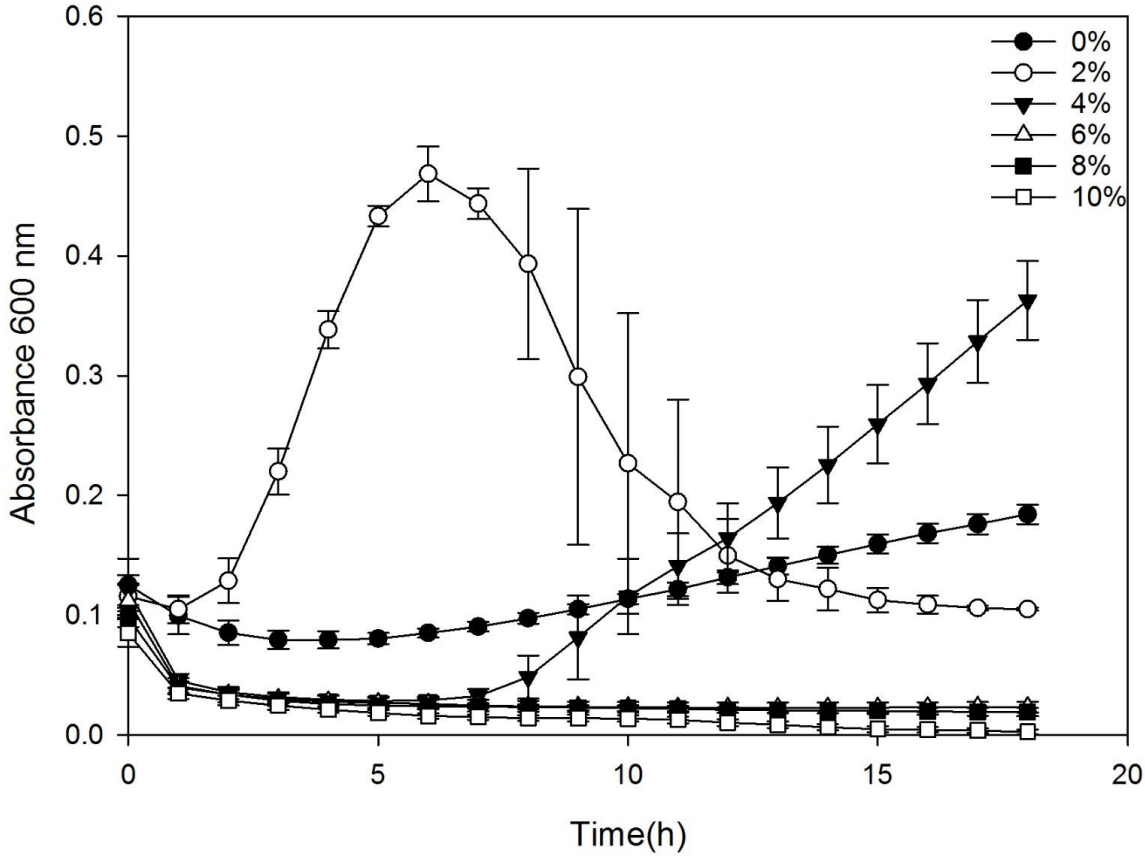

Figure SI5: Evaluation of the growth of *S. loihica* at different NaCl concentrations.

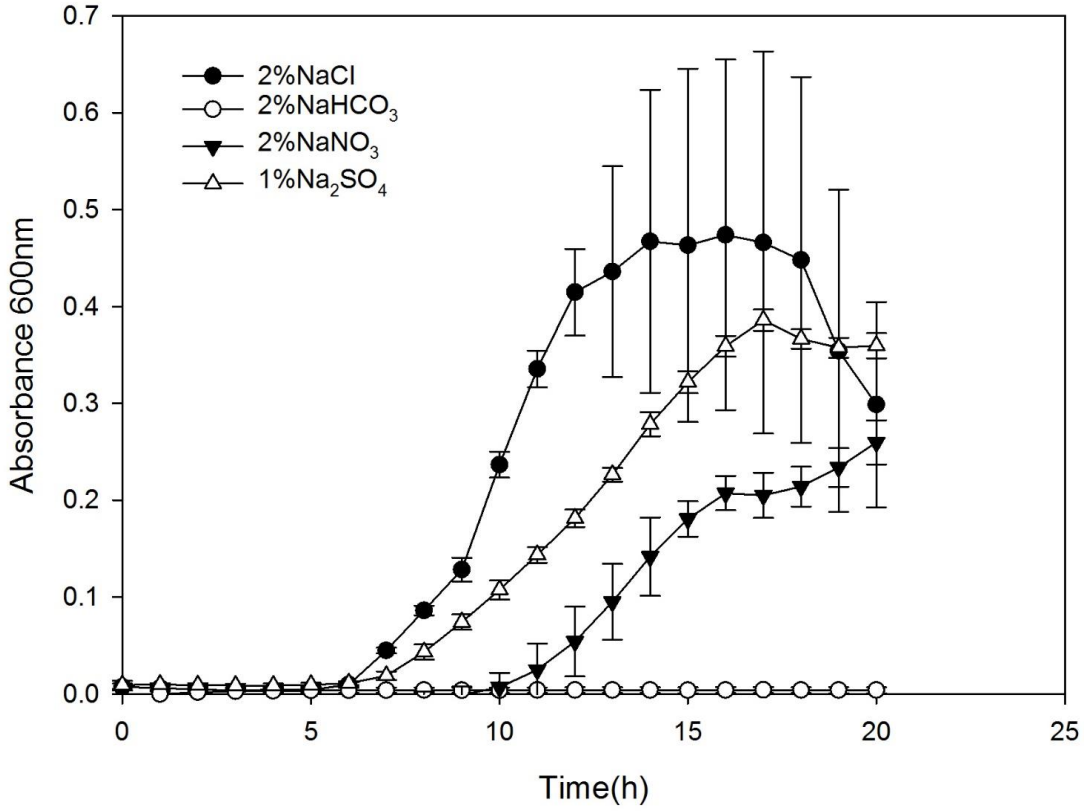

Figure SI6: Evaluation of the chlorides dependence of *S. loihica* growth.

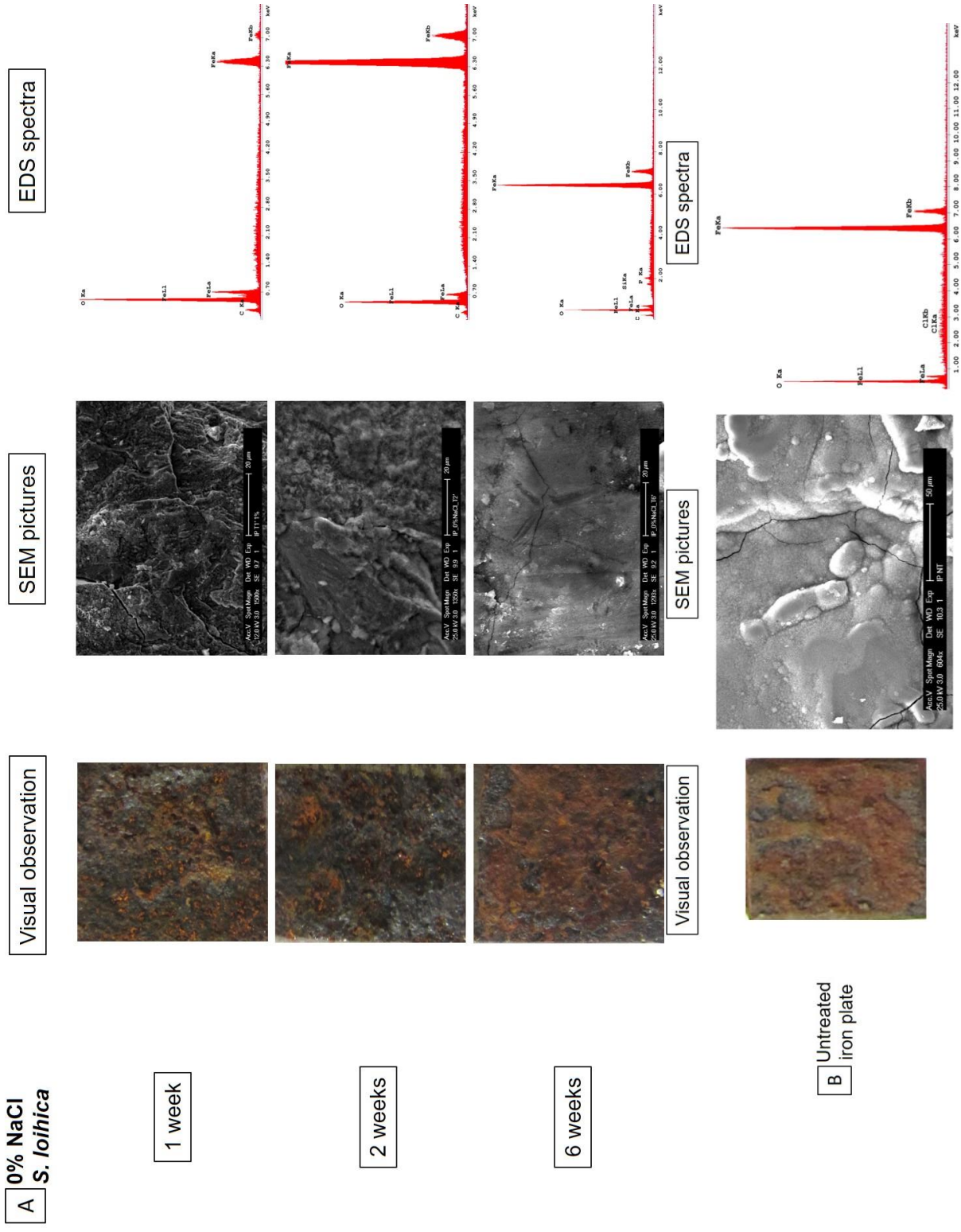

Figure SI7: **Solid Fe(III) reduction and biogenic mineral formation.** Visual observations, scanning electron microscopy (SEM) images and EDS spectra of (A) the iron coupons treated with *S. loihica* at 0% NaCl under ICarb condition after incubation of 1, 2 and 6 weeks and B) the untreated control iron coupon.

Table SI2: Atomic percentages (AT%) of the elements obtained from the Energy-dispersive X-ray spectroscopy (EDS) measurements performed on the iron coupons after 1, 2 and 6 weeks of incubation at 0% NaCl (+), on the abiotic control (-) and on the untreated coupon.

Elements (AT%)	1 week		2 weeks		6 weeks		Untreated iron coupon
	+	-	+	-	+	-	
Fe	45.31	53.80	42.00	58.41	29.50	48.63	27.20
O	40.08	46.20	43.07	41.59	37.27	47.42	50.56
C	14.62	-	14.93	-	32.25	-	19.68
P	-	-	-	-	0.98	-	-
Na	-	-	-	-	-	-	-
Si	-	-	-	-	-	3.95	1.04
Cl	-	-	-	-	-	-	1.53

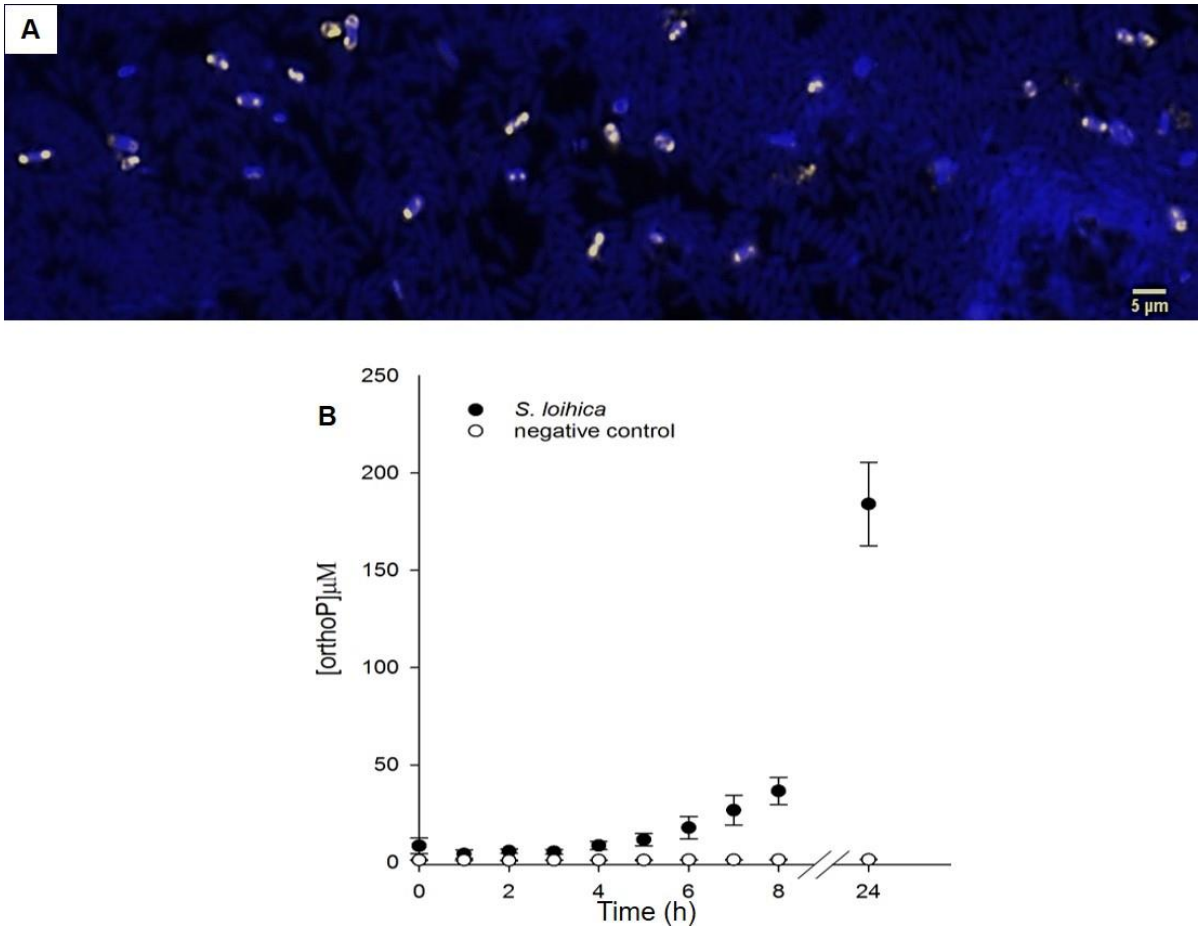

Figure SI8. Evaluation of polyphosphates accumulation and orthophosphates release by *S. loihica*. (A) Epifluorescence microscopy image showing polyphosphate granules (yellow spots) in the cells of *S. loihica* revealed by DAPI staining. (B) Evolution of orthophosphates concentration in the supernatant of *S. loihica* cultures incubated in anoxic ICarb solution.

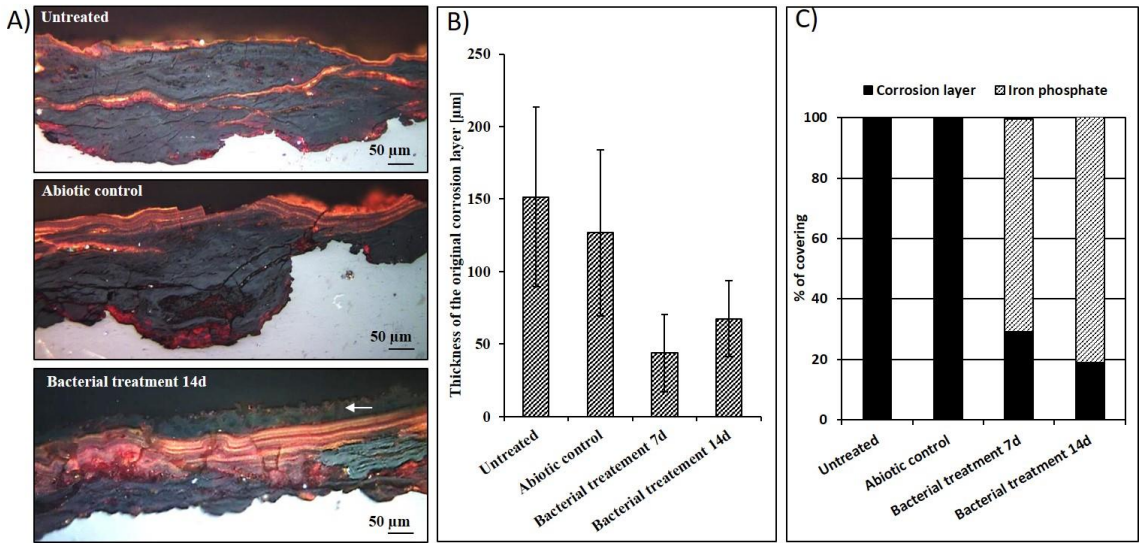

Figure SI9. Effect of biogenic mineral formation on the corrosion layer of iron coupons. A) Microscopic images of the untreated, abiotic control, and bacteria-treated iron coupons after 2 weeks of incubation. B) Measurement of the thickness of the original corrosion layer. C) Estimation of the coverage of the original corrosion layer by newly formed iron phosphates. 7d and 14d correspond to the treatment after 1 and 2 weeks respectively. The white arrow indicates the grey-black layer of iron minerals formed after 2 weeks of treatment.

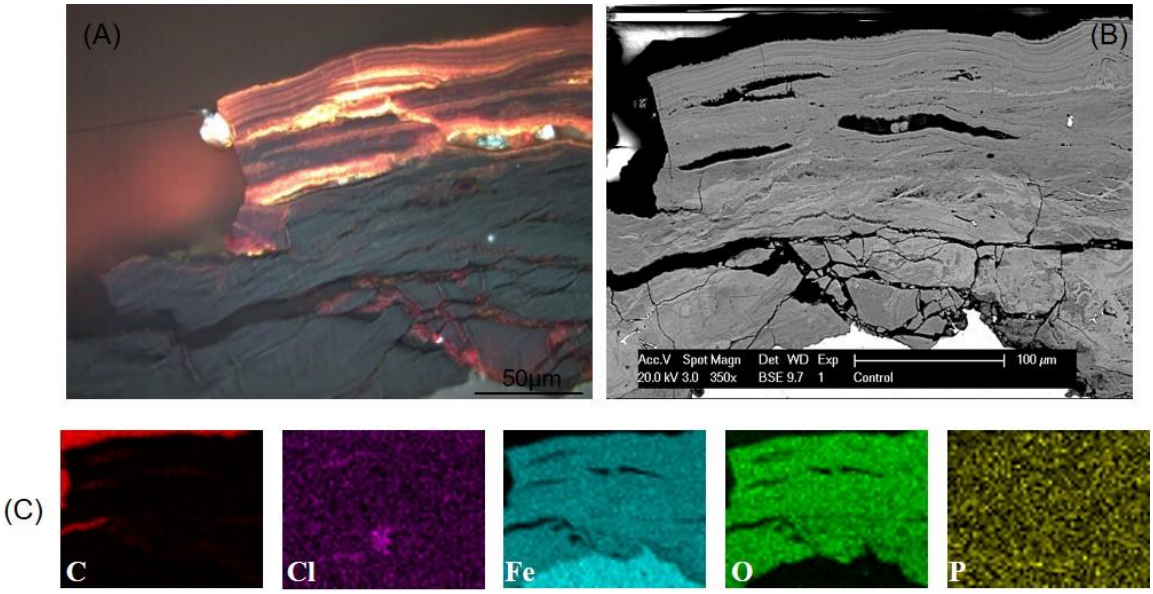

Figure SI10. **Cross-section analysis of the corrosion layer in abiotic iron coupons**. (A) Optical Microscopy and (B) scanning electron microscopy (SEM) images of the abiotic coupon after 6 weeks of incubation. (C) Elemental mapping showing the presence of carbon (red), chlorine (purple), iron (blue), oxygen (green) and phosphorus (yellow).

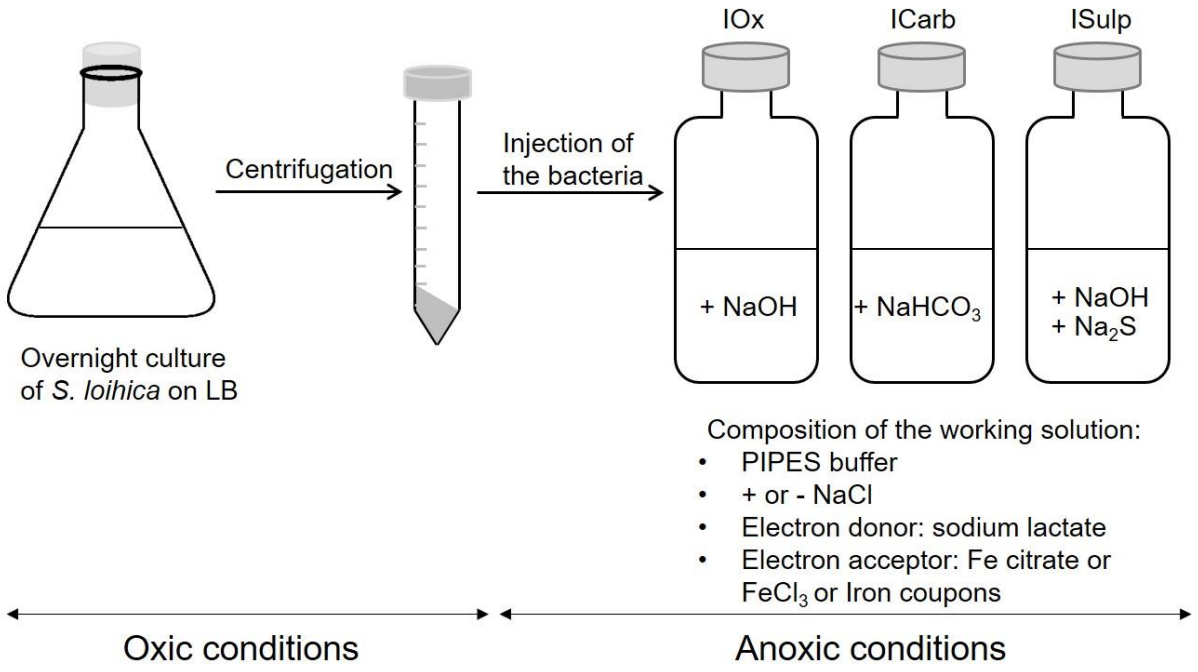

Figure SI11: Schematic representation of the procedure used to promote iron reduction and biogenic mineral formation by *S. loihica* in chemically controlled conditions. Iron coupons were only used with ICarb condition.

Chapter 3

Effect of NaCl on solid iron reduction in *Shewanella loihica* PV-4

"Let there be work, bread, water and salt for all" Nelson Mandela

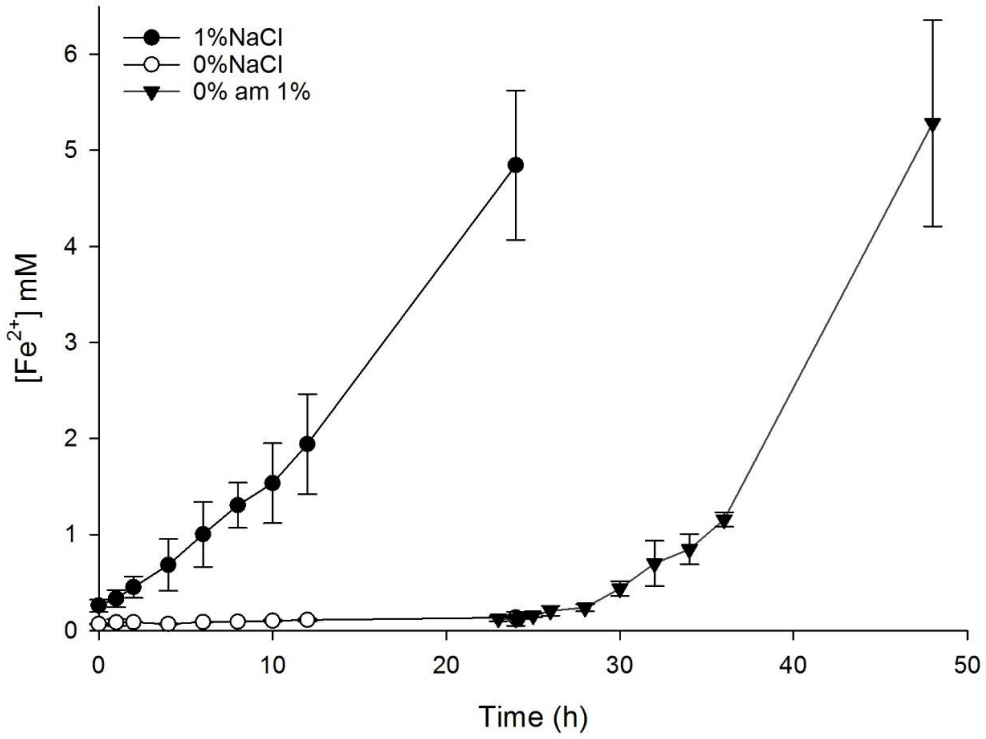

Co-Authors: Thomas Junier, Migun Shakya, Julien Maillard, Karen Davenport, Paul Li, Edith Joseph, Patrick S. Chain and Pilar Junier.
Status: in preparation for publication

Abstract

Salt is known to have a significant effect on bacterial metabolism. Even if sodium chloride is abundant in many natural environments, the effect of NaCl on iron reduction is poorly characterized. In this study we evaluated the impact of NaCl on solid iron reduction with the bacterium *Shewanella loihica.* In the previous chapter we have shown that this bacterium was unable to reduce iron without the addition of NaCl. Therefore, in this study we combined a comparative genomics approach with transcriptomic analysis to evaluate the effect of salt on iron metabolism under the conditions favoring biogenic mineral formation. In the transcriptomic study, the most significant effect was caused by the switch from aerobic to anaerobic conditions. A general stress response was observed that reflects the very limiting conditions used to stimulate mineral formation. Nevertheless, several genes were up regulated when salt was added to the iron-reducing medium. These included genes coding for transcriptional regulators (ArsR and TetR), methyl-accepting chemotaxis proteins, *c*-type cytochromes, acyl-CoA and Glu/Leu/Phe/Val dehydrogenases, porins, and iron transporters. These genes were positively regulated by NaCl and could play a role in solid iron reduction in *S. loihica*.

Introduction

Salinity has an significant impact on the metabolic and physiological functions of living organisms [1–4]. High salinity has often deleterious effects on microbial activity [3]. For example, it was reported that in saline soils, carbon and nitrogen mineralization are repressed, while cell lysis and desiccation are major consequences of osmotic stress [2]. Nevertheless, some microorganisms have developed adaptive strategies (e.g. changes in physiology and/or morphology) allowing them to thrive in highly saline environments [2,5]. Two main adaptive mechanisms to compensate saline osmotic stress are described in literature. In the first one, the incorporated solute (e.g. Na^+, Cl^-) is excluded thanks to the accumulation of other ions necessary for the metabolism of the organism. In the second, organic compounds are produced to counterbalance the concentration gradient between the cell and its environment [6,7]. For example, Gram-negative bacteria respond to salt stress by increasing intracellular concentrations of potassium ions, which lead to the increase in the internal glutamate pool to maintain electrical neutrality [8]. Adaptations to salinity can also involve the modification of the cell envelope and behavior. For some bacteria like *Methylobacter* sp., the variation in salinity has an effect on the composition of phospholipids and motility [9]. The effect of salt on organisms adapted to high salt concentrations is entirely different. In halophiles or halotolerant micro-organisms sodium chloride (NaCl) not only prevents osmotic shock (e.g. deformation, bursting) [1,10,11], but it has also a physiological role. Sodium ions inhibit lytic enzymes responsible for mucopeptide degradation and also activate many enzymes like permeases, lipases, and cytochrome oxidases, all of which are essential for metabolic activity [1].

Bacterial iron reduction is an ubiquitous environmental process [12]. Even though iron reduction should be expected in environments with high salt concentrations, little is known regarding the effect of NaCl on this metabolism. The lack of general information linking the role of salt and iron reduction is surprising, given the importance of the use of metals as electron acceptors in the oxidation of organic matter in environments such as marine sediments [12,13].
Studies performed with *Bacillus subtilis* and *Chromohalobacter salexigens* demonstrated a link between iron homeostasis and salt stress. In *B. subtilis*, the Fur regulon, encoding the siderophore bacillibactin and putative iron uptake systems, were induced by high salinity

suggesting that cells growing under osmotic stress experience severe iron limitation. The opposite was observed in *C. salexigens*, in which siderophore and protein production were repressed under salt-stress [14]. Another study reported that *Desulfuromonas acetoxidans* reduce Fe(III)-oxides in presence of NaCl (0.6-2% w/v), but no reduction was observed in medium without NaCl addition [15]. Likewise, iron reduction and Fe(II) mineral formation by *Thermoanerobacter ethanolicus* (TOR-39) and *Shewanella* sp. (W3-7-1 and NV-1) occurred at a salinity range between 0.05- 5% NaCl (w/v) using lactate as an electron donor and akaganeite as an electron acceptor [16].

Many *Shewanella* species are known for their ability to reduce a large diversity of electron acceptors, including iron [17]. Some species are at the same time slightly to moderate halophiles [18]. This includes *Shewanella frigidimarina* [19], *Shewanella gelidimarina* [19], *Shewanella baltica* [17,20], *Shewanella algae* [21,22], *Shewanella putrefaciens* [13,23], and *Shewanella loihica* [24,25]. These properties render this genus a useful model to investigate the role of salt on dissimilatory reduction of iron oxides. In our previous work [26], we exploited the iron reduction capabilities of the bacterium *S. loihica* to stabilize corroded iron objects by converting the corrosion layer composed of reactive Fe(III) oxides and oxyhydroxides into more stable Fe(II) minerals (siderite and vivianite). Interestingly we found that addition of 1% NaCl to the medium was essential for iron reduction and mineral formation. Despite of the large body of literature concerning iron reduction in the genus *Shewanella*, little is known about the effect of salt on this metabolism. The aim of this work was to investigate the effect of NaCl on solid iron reduction in the bacterium *S. loihica*. For this, we first analyzed and proposed a potential pathway for solid iron reduction by comparing the genomic information of *S. loihica* with the model *Shewanella oneidensis* strain MR-1. Further, we performed a transcriptomic analysis to infer the mechanisms explaining the effect of NaCl on iron reduction under the conditions used for the production of selected Fe(II) minerals in our previous work (iron reduction using a defined chemical matrix).

Results and discussion

Physiological effect of NaCl on iron reduction

Previous work with *S. loihica* has demonstrated that this bacterium can derive energy for growth using solid iron reduction under anaerobic conditions [25]. However, in the context of conversion of iron oxides into stable minerals, we modified the incubation conditions to accelerate mineral production of specific iron minerals (Chapter 2). Under these conditions we investigated the effect of NaCl on iron reduction. For this, we first grew the biomass under aerobic conditions in the presence of 1% NaCl and collected and washed the cells to transfer them into a defined anaerobic iron reduction matrix in the presence or absence of NaCl. Iron reduction of Fe(III) insoluble minerals was assessed by measuring the concentration of Fe(II) in solution. Iron reduction was immediately observed at 1% NaCl, while at 0%, no increase of Fe(II) concentration was measured (Fig. 1). This confirmed our previous results (Chapter 2). Nevertheless, the metabolic potential of cells at 0% NaCl was demonstrated, as the amendment with 1% NaCl after 24 hours of incubation, led to the immediate restitution of iron reduction activity. This experiment clearly shows that the presence of NaCl is essential for iron reduction in this halophilic bacterium. These results agreed with other bacterial iron reducers (*D. acetoxidans* [15] and *Shewanella* sp. W3-7-1 and NV-1 [16]) in which a minimal concentration of salt is required for iron reduction.

The role of salt on the biology of halophilic bacteria has been reviewed [27]. In most cases Na^+ is essential for growth because of the requirement of Na^+ gradients to drive process of cellular transport across the membrane (for example, by use of $Na^{+/}H^+$ antiporters) [27]. A study evaluating the effect of salt on aerobic respiration of an unidentified halophilic bacterium showed that neither potassium chloride nor sucrose could replace sodium salts for recovering respiratory rates [28]. In addition, a study with *Pseudomonas salinaria* showed that dehydrogenases and cytochrome oxidase are more active at high NaCl concentrations (2 to 3 M) [29]. However, the precise mechanisms by which sodium salts stimulate the electron transport chain are still unknown.

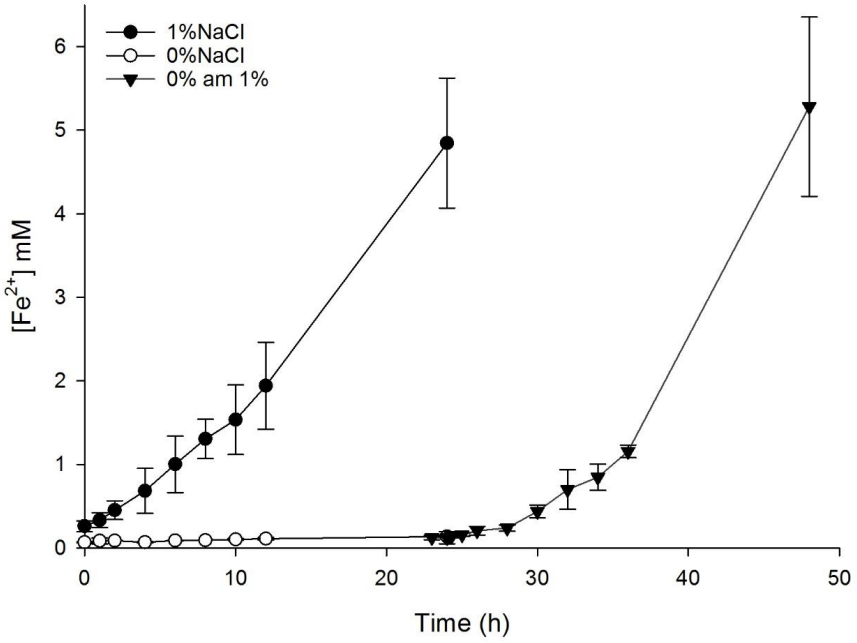

Figure 1. Solid Fe(III) reduction. Iron reduction of *S. loihica* in cultures without NaCl (white circles), with 1% NaCl (black circles) and in cultures without salt but amended with 1%NaCl after 24 hours of incubation (black triangles).

Transcriptomic analysis of *S. loihica*

In order to gain an insight into the potential mechanisms by which NaCl regulates iron reduction in *S. loihica*, we performed a transcriptomic study for three time points (0, 12 and 24 hours) comparing the cultures incubated without (0% NaCl) and with 1% NaCl, as well as the 1% amended cultures (Fig. 1). In addition, given that we grew the cells overnight aerobically, we compared the overnight culture with the iron reduction treatments previously mentioned. Overall 45 pairwise comparisons were generated, (Fig. SI1) but only 20 were deemed relevant for the analysis (Fig. 2). These 20 comparisons were grouped into four main clusters. The first one grouped two comparisons representing the change overtime on gene expression under iron reduction conditions (1% NaCl); the second included six comparisons representing the switch between aerobic (overnight) and anaerobic conditions; the third and fourth includes the comparisons with the amended 1% NaCl. Therefore, the transcriptomic analysis was focused on this grouping.

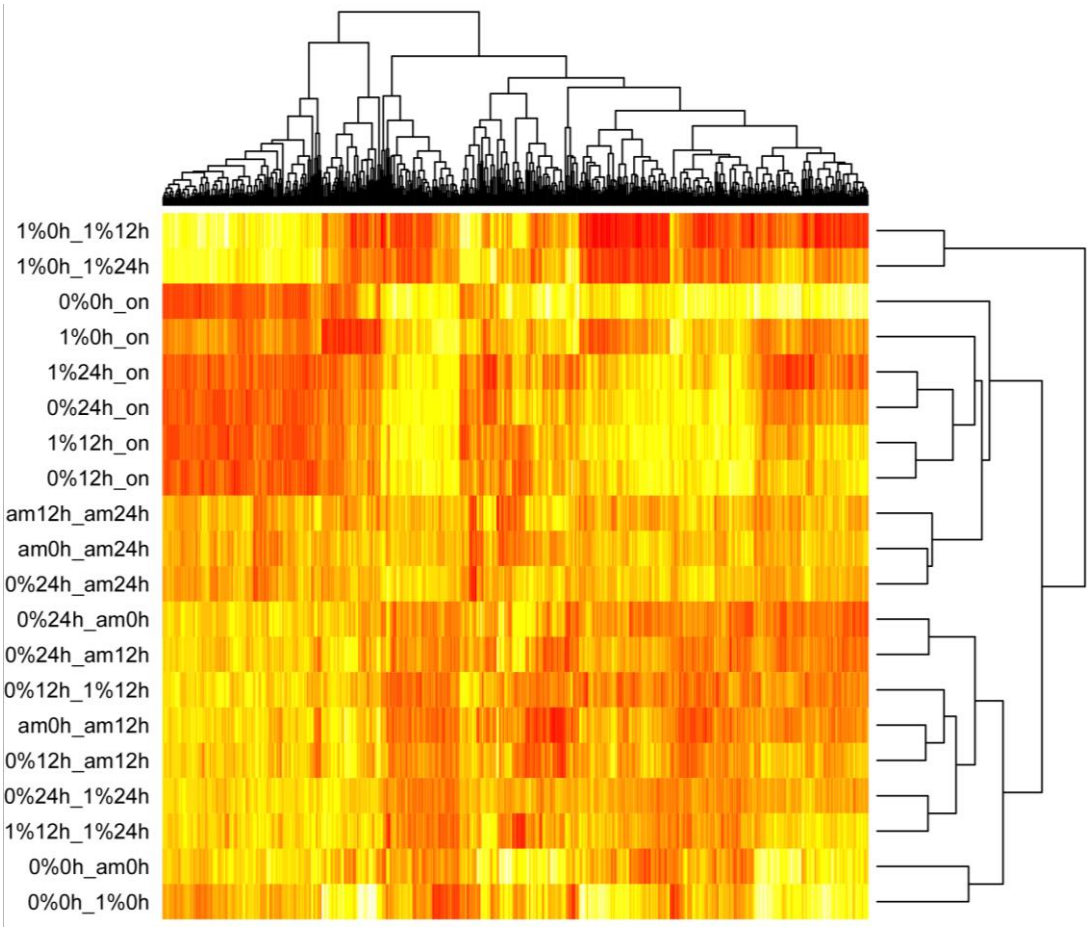

Figure 2: Comparisons of transcriptional profiles across samples. Hierarchical clustering of transcripts and samples. The heatmap shows the relative expression levels of each transcript (columns) in each pairwise comparison (rows). Rows and columns are hierarchically clustered. Each cell in the matrix represents the expression level of a gene feature. Red and white in cells reflect low and high expression levels, respectively. |log(FC)|>2. Sample codes: 1%0h_1%12h, 1%0h_1%24h and 1%12h_1%24h: 1%NaCl condition with a comparison between 0, 12 and 24h, 0%0h_on, 1%0h_on, 1%24h_on, 0%24h_on, 1%12h_on and 0%12h_on: 0%NaCl condition and 1%NaCl conditions at 0,12 or 24h in comparison to the overnight culture, am12h_am24h, am0h_am24h and am0h_am12h: amended 1%NaCl condition in comparison between 0,12 and 24h, 0%24h_am24h, 0%24h_am0h, 0%24h_am12h, 0%12h_am12h, 0%0h_am0h: comparison between 0%NaCl at 0,12 and 24h with amended 1%NaCl at 0,12 and 24h, 0%0h_1%0h, 0%12h_1%12h, 0%24h_1%24h: comparison between 0 and 1% NaCl conditions at 0, 12 and 24h.

Effect of the transition from aerobic to anaerobic conditions

The effect of the aerobic-anaerobic shift appears to have a major impact on the global gene expression of the organism. In response to the oxygen-no oxygen shift, more genes were differentially expressed (up and down regulation) in the condition with 0% NaCl, compared to 1% NaCl (303 genes versus 122 genes, respectively, Table 1, Fig. 3).

Figure 3: Pairwise comparison on the transcriptomic data using volcano plots (-log10Pvalue, Y axis, logFC, X axis) representing the comparison between 0% and 1% NaCl (at 0 hour) with the overnight conditions (0%0h_on and 1%0h_on, respectively). For the genes with a more significant change in gene expression, the function is indicated. Genes encoding hypothetical proteins or proteins with unknown function are shown with an *. For the specific information see Table SI1.

For the gene expression analysis of the overnight-anaerobic shift a selection of genes based on nine functional categories was made. Those categories included transcriptional regulators, sigma factors, ribosomal proteins, ATP synthase, chemotaxis, sodium/cation transporters, outer membrane proteins, cytochromes and energy metabolism, iron and metal transporters, oxygen tolerance and stress response (Table 1). In addition, 50 and 20 genes coding for hypothetical proteins were also differentially expressed in 0% and 1 % NaCl, respectively.

In *S. loihica*, most of the genes coding for transcriptional regulators were down regulated after the transition from overnight to anaerobic conditions (e.g. transcriptional regulators of the LysR family, CdaR, AraC, and Xre). In contrast, the transcriptional regulators Crp, ArsR, and AsnC were up regulated in 0 % NaCl, while GntR was up regulated in 0 % and 1% NaCl. Transcriptional regulators could be very versatile. LysR family of transcriptional regulators, contain more than 50 members with different functions (e.g. exopolysaccharide synthesis, sodium/proton antiporters, iron-regulated virulence factors, quorum sensing). In many studies, it was reported that some of them were overexpressed in stationary phase [30, 31], which is consistent with the results. In a study with *S. oneidensis*, a large number of transcriptional regulators were activated under anaerobic and Fe(III)-reducing conditions, including GntR and Crp [32], both upregulated in the shift from overnight to anaerobic conditions in *S. loihica*. The Crp, (cyclic-AMP receptor protein) transcriptional regulator was reported to be up regulated under anaerobic conditions and *crp* mutants are defective in utilizing several electron acceptors, including Fe^{3+} , Mn^{4+} , nitrate [33]. Crp also regulates gene expression in response to limitations in glucose, resulting in increased expression of genes involved in carbon catabolism [34]. Crp regulator respond to a wide range of endogenous and exogenous signals such as anoxia, oxidative stress, carbon monoxide, and temperature [35]. In *E. coli*, Crp regulates expression of the carbon regulon in response to carbon availability [36].

In the case of genes encoding sigma factors, those were all up regulation in anaerobic Fe(III)-containing solution non-amended with salt. The up-regulation of some genes coding for sigma factors (e.g. *rpoH* and *rpoE*) and stress-response related genes in the presence of metal electron acceptors is consistent with an accumulation of divalent metal cations that initiate global stress-related response leading to induction of a variety of detoxification, resistance and transport functions. In *S. oneidensis* MR-1, RpoE might function by signaling the initial response to oxygen limitation and activates transcription of *mtrC* and *omcA*. The sigma factor genes in this bacterium were reported to be the key factor for the adaptation to anoxic metal-reducing conditions in aquatic sediment and submerged soil systems where substantial amounts of Fe(II) and Mn(IV) can be generated. During a study with *S. oneidensis* MR-1, four genes encoding sigma factors were up regulated under anaerobic Fe(III) reducing conditions [37]. However, from all the sigma factors mentioned above, only RpoS and the Rsd/Alg anti-sigma factors were upregulated in the presence of 1% NaCl and only at 12 h (Table 2).

In a study with *D. vulgaris*, most ribosomal proteins encoding genes were repressed under salt adaptation conditions [38]. Similarly, genes encoding ribosomal proteins and ATP synthase were down regulated at stationary phase and this was linked to the reduction of the growth rate [39] [40]. These results are coherent with our data. We observed up regulation under anaerobic conditions, but mostly in the 0% NaCl (Table 1). Indeed, other studies reported that ribosomal proteins are up regulated under anaerobic conditions and that the accumulation of these proteins is due in this case to a stressful environment. Ribosomal proteins were also reported to accumulate under phosphate starvation [41].

In *E. coli*, it was reported that the *nhaA* gene (coding for sodium/proton antiporter) was overexpressed in stationary phase. This gene was involved in the survival of this bacterium to high salt and alkaline pH (conditions close to its natural habitats such as the sea) [37] . These results are in accordance with the up regulation of the sodium/proton antiporters in the overnight stationary phase of *S. loihica*.

The outer membrane adhesin-like protein (SHEW_RS01640) was highly upregulated at 1% NaCl when comparing with the overnight culture. Suggesting that this gene encoding this adhesin may play a role in the attachment to the Fe(III) minerals in presence of salt. Indeed, it was reported that MtrC protein in *S. oneidensis* contains a putative Fe(III)-binding motif, indicating that the adhesion of this bacterium to Fe(III) oxides and oxyhydroxides may be facilitated by cell surface-exposed MtrC. Nevertheless another mechanism for bacterial adhesion to insoluble Fe(III) involves interaction between the latter and outer membrane adhesins [42]. A study on *S. aureus* demonstrated that the cells were more attached on stainless steel coupons when they are in solution containing 40 mM (0.25%) NaCl then in sterile distilled water [43]. Besides this study, no clear evidence on the effect of salt in presence of iron source on the adhesin-like outer membrane proteins was reported.

Interestingly, according to the Table 1, many cytochromes were up regulated under anaerobic conditions, suggesting that the ones that were up regulated at 1%NaCl condition could be involved in the physiologically observed iron reduction in Fig. 1. Many studies reported that oxidoreductases, porins, and iron/metal transporters are up regulated under anaerobic conditions [44] [45] and that the up regulation of some porins is correlated with the positive activity of Crp transcriptional regulators under anaerobic conditions [45]. Even if the Crp transcriptional regulator coding gene (SHEW_RS03010) was up regulated under anaerobic conditions at 0% NaCl, most of the oxidoreductases, porins, and iron/metal transporters

(including TonB receptors, biopolymer and ferric chelates transporters) were down regulated, suggesting that they could be already expressed in the overnight culture. Indeed, some studies revealed that particular oxidoreductases (e.g. quinone oxidoreductase) and ABC transporters (acting as permease when some elements like sulfate are limited) could be up regulated during stationary phase [39, 46]. The stationary phase represent also a stress condition for bacteria, where nutritional elements tend to decrease, Thus bacterial cells may overexpress particular genes to overcome these limitations [46]. It was the case in a study with *D. vulgaris* where the up regulation of TonB receptor was observed after 23 hours of culture [39]. TonB could also be repressed under anaerobic conditions due to Fur action [47].

The up regulation of detoxification genes such as iron superoxide dismutase, peroxidase, thioredoxin has been reported under anaerobic conditions [32 48]. Peroxidase and thioredoxin were also reported to be up regulated under an anoxic metal-reducing environment in *S. oneidensis* [48]. These genes, involved in the protection of cells against oxidative stress, were up regulated in the anaerobic iron reducing condition at 0% NaCl.

Stress proteins are important in the bacterial adaptation to growth-limiting conditions, which are common in natural environments [49]. The solutions used to perform solid iron reduction with *S. loihica* have a minimal composition and do not sustain bacterial growth constituting a source of stress. Indeed, several stress response proteins are upregulated according to the results obtained (Table 1). When the bacterial cells were transferred from an overnight aerobic culture to anaerobic 0% and 1% NaCl iron reduction matrix, universal stress proteins (SHEW_RS16040, SHEW_RS16640), phage shock protein PspA (SHEW_RS12910), and carbon starvation protein A (SHEW_RS12055) were upregulated. It is known that bacterial growth in natural environments is restricted by nutrient scarcity, especially in aquatic environments where carbon concentration can be as low as 6-10 µg/l [50]. In *Vibrio* sp., carbon starvation is essential for the expression of starvation and stress resistance genes [51]. Two genes encoding putative carbon starvation proteins were down regulated in a study on *Desulfovibrio vulgaris* under salt adaptation conditions and low carbon availability, which is consistent with slow cell growth [38]. Very little is known about the effect of salt on carbon starvation genes. Interestingly, our results suggest that the up regulation of the gene coding for the carbon starvation protein A was not influenced by salt but rather by the absence of oxygen and/or the presence of iron. Indeed, studies on *D. vulgaris* and *Yersinia intermedia* indicate that carbon starvation genes are upregulated under oxygen limitation [39, 52], suggesting that these genes could be involved in stress-related functions associated with aerobic cellular metabolism. According to He *et al.* (2010), the major responses of *D. vulgaris* to salt adaptation (250 mM corresponding to 1.5% NaCl) were the decrease in cell growth and overexpression of genes related to heat shock and phage shock (*pspA* and *pspC*) [38]. The phage shock operon *psp* in *Escherichia coli* is induced by impaired inner membrane integrity and by the decrease in proton motive force (PMF). PspA and PspG react to diverse inducing stimuli in the switching of cells to anaerobic respiration and fermentation, down-regulating motility, a high consuming PMF process. Genes involved in iron transport and metabolism were highly down regulated only when *pspG* is overexpressed and not *pspA* [53]. These findings support our results that demonstrate a down regulation of the motility coding genes and an up regulation of some genes involved in iron metabolism and transport in presence of Fe(III), but the overexpression is not linked to salt but rather to the anaerobic conditions as mentioned by Clark et al (2006) [39].

Table 1: Differential gene expression data between 0%NaCl at 0h and overnight conditions (0%_on) and 1%NaCl at 0h and overnight conditions (1%_on). The values represent the log(FC) that was selected to be |log(FC)|>2

Function	Gene_locus	Gene_product	0%_on	1%_on
Transcriptional regulators	SHEW_RS01160	LysR family	-2.25	
	SHEW_RS04270	LysR family	-2.654	-2.33
	SHEW_RS06415	LysR family	-2.224	
	SHEW_RS12755	LysR family	-3.083	-2.274
	SHEW_RS03010	Crp	3.124	
	SHEW_RS05640	ArsR family	2.292	
	SHEW_RS09405	GntR family	3.305	2.483
	SHEW_RS10485	AsnC family	3.948	
	SHEW_RS13085	CdaR family	-3.011	-2.105
	SHEW_RS19610	AraC family	-2.465	
	SHEW_RS00360	AraC family	-2.714	
	SHEW_RS19895	XRE family	-2.075	-2.182
	SHEW_RS17640	heavy metal-responsive		-2.936
Sigma factors	SHEW_RS05405	RNA polymerase sigma factor RpoE	2.167	
	SHEW_RS06230	RNA polymerase sigma factor RpoS	2.608	
	SHEW_RS06890	flagellar biosynthesis anti-sigma factor FlgM	3.364	
	SHEW_RS07100	RNA polymerase sigma factor FliA	2.514	
	SHEW_RS17700	Rsd/AlgQ family anti-sigma factor	2.251	
	SHEW_RS18675	RNA polymerase sigma factor RpoH	3.052	
Ribosomal proteins	SHEW_RS00775	50S ribosomal protein L11 rplK	2.891	
	SHEW_RS00780	50S ribosomal protein L1	3.296	2.088
	SHEW_RS00785	50S ribosomal protein L10	3.619	
	SHEW_RS00790	50S ribosomal protein L7/L12	3.399	
	SHEW_RS00805	30S ribosomal protein S12	3.347	
	SHEW_RS00810	30S ribosomal protein S7	2.127	
	SHEW_RS00825	30S ribosomal protein S10	2.846	
	SHEW_RS00830	50S ribosomal protein L3	2.150	
	SHEW_RS00835	50S ribosomal protein L4	2.294	
	SHEW_RS00845	50S ribosomal protein L2	2.138	
	SHEW_RS00855	50S ribosomal protein L22	2.834	
	SHEW_RS00875	30S ribosomal protein S17 rpsQ	2.302	
	SHEW_RS00880	50S ribosomal protein L14	3.601	
	SHEW_RS00885	50S ribosomal protein L24	3.524	
	SHEW_RS00890	50S ribosomal protein L5	2.938	
	SHEW_RS00895	30S ribosomal protein S14	2.841	
	SHEW_RS00900	30S ribosomal protein S8 rpsH	3.207	
	SHEW_RS00905	50S ribosomal protein L6	3.008	
	SHEW_RS00910	50S ribosomal protein L18	2.930	
	SHEW_RS00915	30S ribosomal protein S5	2.553	
	SHEW_RS00920	50S ribosomal protein L15	3.038	
	SHEW_RS00930	30S ribosomal protein S13	3.335	
	SHEW_RS00935	30S ribosomal protein S11	2.266	
	SHEW_RS00940	30S ribosomal protein S4	3.093	
	SHEW_RS00950	50S ribosomal protein L17 rplQ	2.412	
	SHEW_RS04470	50S ribosomal protein L21 rplU	2.705	
	SHEW_RS04475	50S ribosomal protein L27 rpmA	2.535	
	SHEW_RS05480	30S ribosomal protein S16	3.519	
	SHEW_RS05485	ribosome maturation factor rimM	2.418	
	SHEW_RS05645	30S ribosomal protein S20	2.685	
	SHEW_RS10115	30S ribosomal protein S1	3.376	
	SHEW_RS10505	50S ribosomal protein L20	4.626	2.515
	SHEW_RS14575	30S ribosomal protein S15	2.295	
	SHEW_RS16980	50S ribosomal protein L9	2.716	
	SHEW_RS16995	30S ribosomal protein S6	2.528	
	SHEW_RS17040	30S ribosomal protein S9	3.105	2.586
	SHEW_RS17045	50S ribosomal protein L13	2.763	
	SHEW_RS18045	50S ribosomal protein L28	3.625	
	SHEW_RS20215	50S ribosomal protein L30	2.153	
	SHEW_RS20415	50S ribosomal protein L35	2.872	
	SHEW_RS16710	ribosomal RNA small subunit methyltransferase C	-2.207	-2.054
ATP synthase	SHEW_RS19920	ATP synthase subunit beta	2.036	
	SHEW_RS19925	ATP synthase subunit gamma	2.413	
	SHEW_RS19930	ATP synthase subunit alpha	2.068	
	SHEW_RS19935	ATP synthase subunit delta	2.224	

	SHEW_RS19940	ATP synthase subunit B	2.935	
	SHEW_RS19945	ATP synthase subunit C	2.484	
	SHEW_RS19950	ATP synthase subunit A	2.569	
Chemotaxis	SHEW_RS06885	flagellar protein FlgN	2.685	
	SHEW_RS06890	flagellar biosynthesis anti-sigma factor FlgM	3.364	
	SHEW_RS06910	flagellar basal body rod protein FlgB	2.324	
	SHEW_RS06915	flagellar basal body rod protein FlgC	2.667	
	SHEW_RS06960	flagellar hook-associated protein FlgL	2.862	
	SHEW_RS06965	flagellin	3.148	
	SHEW_RS06970	flagellin	3.663	
	SHEW_RS06975	flagellar protein FlaG	3.263	
	SHEW_RS06980	flagellar hook protein FliD	2.780	
	SHEW_RS06990	flagellar protein FliS	3.270	
	SHEW_RS07020	flagellar motor switch protein FliG	2.267	
	SHEW_RS01090	pilus assembly protein PilM	2.888	
	SHEW_RS01100	pilus assembly protein PilO	2.870	
	SHEW_RS01105	pilus assembly protein PilP	3.089	
	SHEW_RS01110	type IV pilus secretin PilQ	2.679	
	SHEW_RS12025	pilus assembly protein PilZ	2.684	
	SHEW_RS01100	pilus assembly protein PilO		2.061
	SHEW_RS06900	chemotaxis protein CheV	2.155	
	SHEW_RS06905	chemotaxis protein CheR	2.030	
	SHEW_RS07105	chemotaxis protein CheY	2.671	
	SHEW_RS07140	chemotaxis protein CheW	2.363	
	SHEW_RS00550	chemotaxis protein CheR		2.373
	SHEW_RS00555	methyl-accepting chemotaxis protein		2.463
Sodium, cation transporter/antiporter	SHEW_RS01785	Na+/H+ antiporter NhaC	-2.039	
	SHEW_RS10580	cation transporter	-2.431	-3.984
	SHEW_RS16910	potassium transporter Kef	-2.873	-2.312
	SHEW_RS03580	sodium:proton antiporter		-2.717
	SHEW_RS07840	sodium:proton antiporter		-4.822
Outer membrane proteins	SHEW_RS01615	OmpA family protein	2.931	2.132
	SHEW_RS05615	OmpA family protein	4.033	2.526
	SHEW_RS07870	OmpA family protein	2.081	
	SHEW_RS13220	outer membrane protein OmpW	3.381	
	SHEW_RS01640	outer membrane adhesin-like protein	3.884	4.076
	SHEW_RS16435	outer membrane porin%2C OprD family	-2.138	
Cytochromes and energy metabolism	SHEW_RS00985	cytochrome c5 family protein	2.530	
	SHEW_RS02945	cytochrome c	2.160	
	SHEW_RS04350	ammonia-forming cytochrome c nitrite reductase subunit c552	4.096	2.832
	SHEW_RS04715	cytochrome c	4.669	3.307
	SHEW_RS08930	cytochrome c	3.564	
	SHEW_RS10265	cytochrome c oxidase%2C cbb3-type subunit I ccoN	2.142	
	SHEW_RS10280	cytochrome-c oxidase%2C cbb3-type subunit III ccoP	2.198	
	SHEW_RS13920	cytochrome b561	3.384	3.586
	SHEW_RS18345	cytochrome c	3.452	
	SHEW_RS06810	NAD(P)-dependent oxidoreductase	2.245	
	SHEW_RS07705	FAD-binding oxidoreductase	2.075	
	SHEW_RS07990	FAD-binding oxidoreductase	-2.267	
	SHEW_RS03130	thiosulfate reductase	-3.387	-2.626
	SHEW_RS03375	nitric-oxide reductase large subunit	-2.344	
	SHEW_RS05510	hydroxylamine reductase	-2.254	
	SHEW_RS11785	glutathione-dependent reductase	-2.599	
	SHEW_RS01060	N-acetyl-gamma-glutamyl-phosphate reductase		-3.926
	SHEW_RS09115	Ni/Fe-hydrogenase%2C b-type cytochrome subunit cybH	3.749	3.044
	SHEW_RS09120	nickel-dependent hydrogenase large subunit	2.112	
	SHEW_RS09125	quinone-reactive Ni/Fe-hydrogenase small chain	2.618	
	SHEW_RS08555	succinate dehydrogenase cytochrome b556 large subunit	2.183	
	SHEW_RS00300	formate dehydrogenase	2.402	2.215
	SHEW_RS00310	formate dehydrogenase subunit gamma	2.443	
	SHEW_RS10490	alanine dehydrogenase ald	2.552	
	SHEW_RS10940	acyl-CoA dehydrogenase fadE	2.162	2.707
	SHEW_RS18515	aldehyde dehydrogenase	2.890	2.988

	SHEW_RS06000	L-threonine dehydrogenase		2.491
	SHEW_RS08645	acyl-CoA dehydrogenase		-2.126
	SHEW_RS13260	phosphogluconate dehydrogenase		-2.445
	SHEW_RS13375	electron transfer flavoprotein subunit beta	2.541	
	SHEW_RS16140	porin	-2.232	-3.353
	SHEW_RS16435	outer membrane porin%2C OprD family	-2.138	
	SHEW_RS16835	porin	-2.732	
	SHEW_RS16875	porin	3.560	
	SHEW_RS14030	putative porin		2.342
	SHEW_RS14205	porin		-3.025
Iron and metal transporters	SHEW_RS03670	iron ABC transporter permease	-3.395	-2.520
	SHEW_RS04430	iron ABC transporter substrate-binding protein	-2.971	-4.428
	SHEW_RS13030	ferrous iron transporter B	-2.328	-2.969
	SHEW_RS19505	metal transporter	3.115	3.731
	SHEW_RS19515	CusA/CzcA family heavy metal efflux RND transporter		2.230
	SHEW_RS15135	cobalt transporter	2.411	
	SHEW_RS19080	tungsten ABC transporter substrate-binding protein		-2.199
	SHEW_RS10580	cation transporter	-2.431	-3.984
	SHEW_RS03070	MFS transporter	-2.267	
	SHEW_RS04630	MFS transporter	-2.102	
	SHEW_RS14925	MFS transporter	-2.449	
	SHEW_RS04440	ABC transporter ATP-binding protein	-2.593	-2.097
	SHEW_RS08545	efflux RND transporter periplasmic adaptor subunit		2.292
	SHEW_RS08740	TonB-dependent receptor	-2.653	-3.74
	SHEW_RS12830	TonB-dependent receptor	3.076	
	SHEW_RS13910	TonB-dependent receptor	-2.531	-3.647
	SHEW_RS19045	TonB-dependent receptor	-2.493	-2.633
	SHEW_RS19450	TonB-dependent receptor	-2.027	
	SHEW_RS16020	TonB-dependent siderophore receptor	-3.79	-4.969
	SHEW_RS19900	TonB-dependent siderophore receptor	-4.525	-5.899
Oxygen tolerance	SHEW_RS07845	peroxidase	2.009	
	SHEW_RS09495	superoxide dismutase [Fe]	2.509	
	SHEW_RS01755	thioredoxin	2.262	
Stress response	SHEW_RS10310	universal stress protein E	2.971	
	SHEW_RS12900	envelope stress response membrane protein PspC	2.095	
	SHEW_RS16035	universal stress protein	2.161	
	SHEW_RS16040	universal stress protein	2.822	2.297
	SHEW_RS16640	universal stress protein UspA	2.134	2.252
	SHEW_RS08370	cold-shock protein	2.379	
	SHEW_RS12910	phage shock protein PspA	2.164	2.424
	SHEW_RS12055	carbon starvation protein A	2.324	3.273
Number of genes differentially expressed coding for hypothetical proteins			50	20

Effect of NaCl on iron reduction

Shewanella spp. are often characterized by their diverse respiratory capabilities and their ability to sense and respond to environmental stimuli, particularly the availability of different electron acceptors [54]. Nevertheless, very little is known about the effect of salt on iron reduction. For the analysis of the effect of salt on iron reduction, we compared gene expression at 1%NaCl overtime and the comparison of the 0% NaCl 24 h culture with the 1% amended NaCl cultures to identify the most significant differences in gene expression (Table SI2, Table SI3, Table 2 and Fig. SI2).

Members of the *Shewanella* genus have complex electron transport networks for the use of different electron acceptors. Biochemical and transcriptomic studies of *S. oneidensis* concluded that even if many genes and proteins exhibited altered expression levels as a result of the switch from aerobic to anaerobic respiration, a number of genes are up regulated as part of the electron transport chain (ETC) to reduce nitrate, fumarate, and Fe(III) [44].

Among them: *c*-type cytochromes, hydrogenases, dehydrogenases and outer-membrane proteins [44]. These findings are consistent with our results (Table 2) indicating that genes are part of ETC and energy metabolism for the respiration of Fe(III), the sole electron acceptor in our iron reducing matrix.

Some genes potentially involved in solid iron reduction of *S. loihica* (Fig. SI2) appear to respond differentially to the presence of NaCl (Table 2). When 1% NaCl was amended to the iron reduction culture of *S. loihica* after being incubated for 24 hours without salt, ArsR (SHEW_RS05640) and TetR/AcrR (SHEW_RS08695) transcriptional regulators were up regulated. In the literature, ArsR transcriptional regulators were reported to be involved in metal ion detoxification, efflux and sequestration. In *Shewanella* sp. strain ANA-3, the *ars* operon encodes an arsenate detoxification pathway where the ArsR transcriptional regulator regulates the arsenate respiratory reduction pathway in response to elevated arsenite concentrations under anaerobic conditions [55, 56]. A study on *Geobacter sulfurreduces* demonstrated that the absence of *orfR* (GSU2741, a member of TetR trannscriptional regulators family) affected the expression of the *c*-type cytochrome *omcB* and thus iron reduction rate [57]. TetR (tetracycline transcriptional regulators) family proteins are also known to be involved in different metabolic pathways like osmotic stress sensing [58]. Thus, these two transcriptional regulators could be involved in regulating the expression of genes involved in iron reduction when salt was added.

Chemotaxis is a behavioral response that allows bacteria to migrate towards or against chemical stimuli and it is considered as an indicator of changing environments [59, 60]. The up regulation of methyl-accepting chemotaxis (SHEW_RS18855) gene in the amended in comparison to 0% NaCl conditions, could signal the role of chemotaxis for the reduction of a solid electron acceptor. According to a recent study on *Shewanella* spp., the genes coding for *mcp* (methyl-accepting chemotaxis proteins) are essential for the attachment and congregation (accumulation of cells around insoluble electron acceptors) of *S. oneidensis* MR-1 to insoluble electron acceptors and particularly to $Fe(OH)_3$ [61]. This study also showed that *S. loihica* PV-4, in addition to *S. oneidensis* MR-1, are able to congregate around both MnO2 and $Fe(OH)_3$ [61]. Hence, these genes could play role in the physiological observation of iron reduction in presence of 1% NaCl. Under anaerobic and iron reducing conditions, some chemotaxis genes were up regulated in *S. oneidensis* MR-1 [32]. In addition, studies with *D. vulgaris* demonstrate a down regulation of chemotaxis genes in a medium containing 250 mM NaCl [38]. This suggests that *S. loihica* sensed the electron acceptor Fe(III) but NaCl repressed the involvement of chemotaxis genes in iron reduction.

The involvement of cytochromes in iron reduction is known not only for *S. oneidensis*, but also other bacteria [62]. From our differential gene expression data, three *c*-type cytochromes (SHEW_RS00985, SHEW_RS10280, SHEW_RS05540) are up regulated at 1% NaCl after 12 hours of incubation (Table 2) as well as two cytochromes (SHEW_RS13355, SHEW_RS01905) when 1% NaCl was amended to 0% NaCl condition after 12 and 24 hours (Table 2, Table SI2). As none of the homologues of *mtrCB* were up regulated, these cytochromes could therefore be involved in solid iron reduction of *S. loihica*. NaCl in this case could have a role in their up regulation.

Dehydrogenases, quinones, porins and flavoproteins play also an important role in the ETC for the reduction of insoluble Fe(III) minerals in *S. oneidensis* [62]. According to the results shown in Table 2, two dehydrogenases were up-regulated in presence of salt: acyl-CoA dehydrogenase (SHEW_RS08645) and Glu/Leu/Phe/Val dehydrogenase (SHEW_RS08080) as well as two electron-transferring flavoproteins (ETF) subunits (SHEW_RS13370,

SHEW_RS13375) and one flavodoxin (SHEW_RS09920). In *Clostridium* Acyl-CoA dehydrogenase (containing a FAD: flavin adenine dinucleotide) along with electron-transferring flavoproteins were reported to form a stable complex. Electron transfer flavoprotein is reduced by NADH and conducts the electrons to the acyl-CoA dehydrogenase and to ferredoxin [63]. These genes could thus play a role in the ETC for the reduction of insoluble iron minerals in presence of salt in *S. loihica.* In a study with *D. vulgaris,* Glu/Leu/Phe/Val dehydrogenase family protein was overexpressed at 250 mM (1.5%) NaCl. The increase in expression might result in an increase in the biosynthesis of glutamate, leucine, phenylalanine, and/or valine. In the same study, an iron-repressed flavodoxin (DVU2680) was also overexpressed [38]. Flavodoxins are small electron transfer proteins containing flavin mononucleotide as the prosthetic group. While ferrodoxin is down-regulated, flavodoxin is overexpressed under iron-limiting conditions in many bacteria as well as phytoplankton [64,65]. In the cyanobacterium *Synechocystis* the flavodoxin protein acts as stress indicator; accumulating under high salt conditions, heat shock and iron limitations [66]. The up regulation of these genes in our data set is likely due to the effect of NaCl, in particular, as flavodoxin is overexpressed at 12h at 1% NaCl, this protein could sense a reduction in the concentration of Fe (III) or an increase of Fe(II) concentrations, in addition to the salt presence, which is consistent with what we obtained physiologically (Fig. 1).

The porin MtrA in *S. oneidensis*, is crucial in the electron transport to the cytochrome MtrC and thus solid iron reduction [62]. According to the results obtained in Table SI1 and Table 2, no homologous to *mtrA* gene was found but three genes coding for porins are up-regulated in presence of 1%NaCl (SHEW_RS16140, SHEW_RS16875, SHEW_RS14205, SHEW_RS10205). Suggesting that these porins could play a role in the physiological iron reduction observed when salt was present.

In bacteria, ATP synthase generates ATP thanks to the proton motive force (pmf) created by the electron transport chain as a source of energy [67]. ATP synthase plays vital functions in the energy-transducing membranes of bacteria by catalyzing ATP synthesis and hydrolysis coupled with transmembrane proton or sodium ion transport [68]. All these newly identified ABC-transporter proteins were enhanced in salt-acclimated cells (Table SI2 and Table 2). Two subunits of ATP synthase were reported to be overexpressed in contact with salt [68,69], confirming the upregulation of ATP synthase gene *atpC* obtained in our data. However, a study on *Mycoplasma genitalium*, found that *atpC* gene was down-regulated at 0.3 M NaCl without further investigations.

No quinones were differentially expressed in presence of salt as well as pili genes, suggesting that the latter is not involved in solid iron reduction in presence of salt for the bacterium *S. loihica*, which was also the case for *S. oneidensis*, in the contrary of *G. sulfurreducens* [12,62].

Table 2: Differential gene expression data in 1%NaCl condition between 0 and 12h (1%0h_1%12h), 0 and 24h (1%0h_1%24h) and between 0%NaCl at 24h and amended 1%NaCl at 24h (0%24h_Am24h), conditions. The values represent the log(FC) that was selected to be log(FC)<2 (For the genes with values of log(FC)>2, see Table SI3)

Function	Gene_locus	Gene product	1%0h-1%12h	1%0-1%24h	0%24h_am24h
Transcriptional regulators	SHEW_RS06415	LysR family			-2.584
	SHEW_RS09405	GntR family			2.642
	SHEW_RS19820	XRE family	2.107	-2.131	
	SHEW_RS17640	heavy metal-responsive	-3.512		
Chemotaxis	SHEW_RS06910	flagellar basal body rod protein FlgB	-2.692	-2.473	
	SHEW_RS06915	flagellar basal body rod protein FlgC	-2.159	-2.013	
	SHEW_RS06960	flagellar hook-associated protein FlgL	-2.054		
	SHEW_RS18855	methyl-accepting chemotaxis protein			-2.246
Cytochromes and energy metabolism	SHEW_RS00985	cytochrome c5 family protein	-2.094		
	SHEW_RS10280	cytochrome-c oxidase%2C cbb3-type subunit III ccoP	-2.210		
	SHEW_RS05540	cytochrome c	-2.152		
	SHEW_RS01905	cytochrome ubiquinol oxidase subunit I cyoB			-2.044
	SHEW_RS02675	5,10-methylenetetrahydrofolate reductase metF			-2.269
	SHEW_RS08645	acyl-CoA dehydrogenase	-2.101		
	SHEW_RS08080	Glu/Leu/Phe/Val dehydrogenase	-2.534		
	SHEW_RS13375	electron transfer flavoprotein subunit beta	-2.420		2.802
	SHEW_RS13370	electron transfer flavoprotein subunit alpha	-3.121	-2.111	
	SHEW_RS09920	flavodoxin	-2.575		
	SHEW_RS19915	ATP synthase epsilon chain atpC	-3.044	-2.223	
	SHEW_RS16140	porin	-2.305		
	SHEW_RS14205	porin			-2.059
	SHEW_RS19785	porin family		2.344	
	SHEW_RS10205	porin			-2.298
Iron and metal transporters	SHEW_RS04430	iron ABC transporter substrate-binding protein	-3.022	-3.318	
	SHEW_RS19080	tungsten ABC transporter substrate-binding protein	-3.012	-2.966	
	SHEW_RS09580	MexH family multidrug efflux RND transporter periplasmic adaptor subunit	-2.166		
	SHEW_RS08740	TonB-dependent receptor	-2.406	-2.408	
	SHEW_RS12830	TonB-dependent receptor	-3.014		2.449
	SHEW_RS13910	TonB-dependent receptor	-2.03	-2.306	
	SHEW_RS16020	TonB-dependent siderophore receptor	-4.159	-3.563	
	SHEW_RS19900	TonB-dependent siderophore receptor	-2.898		
Number of genes differentially expressed coding for hypothetical proteins			16	10	13

Iron uptake mechanisms are key factors for the regulation of intracellular iron concentration. These transport systems are subject to adaptations to environmental conditions. Fe(III) is usually sequestrated as iron salts and iron oxides or it is found bound to host iron-binding proteins such as hemoglobin, ferritin and transferrin, and thus unavailable. To transport these different iron complexes, bacteria can synthesize specific receptors and transporters. The Fe(III) uptake from the periplasm into the cytoplasm is mediated by an ATP binding cassette (ABC) transporter system. With TonB-ExbB-ExbD complex, the ABC transport system, constitute a common factor for all Gram-negative bacterial transport systems, both of which located in the inner membrane. Free intracellular iron is then incorporated into various metallo-proteins to be used for many biological processes. Alternatively bacteria can store the iron in bacterioferritin [70]. Despite the importance of Fe(III) ions as electron acceptors under anoxic conditions, it was reported that *S. oneidensis* does not have a high number of metal ion transporters, which is in accordance with the fact that the metal reduction capability of this bacterium occurs by direct contact rather than by metal ions transport into the cells [71]. In contrast to *S. oneidensis*, a general screening in the genome of *S. loihica* revealed a large number of transporters (246 hits versus 66 in the case of *S. oneidensis*).

Interestingly, our results suggest that iron ABC transporter substrate-binding protein (SHEW_RS04430) is overexpressed in presence of salt especially at 12 and 24 hours in comparison to 0 hour and 0%NaCl conditions. This was also the case for MexH family multidrug efflux RND transporter periplasmic adaptor subunit (SHEW_RS09580, only at 12h). The metal transporter (SHEW_RS19505) was overexpressed only when comparing 0 and 1%NaCl with overnight culture, suggesting that the up regulation of this gene could be link to the presence of iron and/or to the oxygen limitations. According to some studies, iron ABC transporter substrate-binding protein, utilize the energy of ATP hydrolysis to pump iron through the membrane and import it to the cells [72]. Iron chelates, generally scarce and required in small amounts, could be taken up via an ABC transporter [72]. In the cyanobacterium *Synechocystis* sp. strain PCC 6803, the expression of iron ABC transporter was highly enhanced with 684 mM (4%) NaCl [69].

In *S. oneidensis* genome, there are 9 genes encoding MexH family multidrug efflux RND (resistance nodulation cell division) pump. Their involvement in drug resistance, secondary metabolite or hydrophobic compound secretion remains unclear regarding this bacterium [71]. Extrusion of toxic compounds from bacterial cells is a mechanism of drug resistance. One of the most important drug extrusion systems are the MFS (major facilitator super), SMR (small multidrug resistance) and RND (resistance nodulation cell division) [73]. The latter is also reported to act as transporters for metal ions [74] and to involved in maintaining metal homeostasis of zinc, copper, cadmium, nickel and iron [75]. A study with the halophilic bacterium *Chromohalobacter* sp. showed that a multidrug resistance Hrd efflux pump was induced by 1 M and 2 M NaCl [76]. Despite this information, little is known about the effect of salt on MexH family multidrug efflux RND. In this case, this study shows that the gene SHEW_RS09580 in *S. loihica* encoding for MexH family multidrug efflux RND pump is up_regulated in presence of iron and salt.

Potential electron transport pathway for solid iron reduction in *S. loihica*

S. oneidensis is one of the best studied model microorganisms in terms of the electron transport chain (ETC) involved in the reduction of different kinds of electron acceptors. The mechanism of reduction of soluble iron chelates (e.g. Fe(III) citrate) versus insoluble Fe(III) minerals are clearly distinct [12,62]. Physical and chemical properties determine the bioavailability of different insoluble iron minerals and how readily they can be used as a substrate for anaerobic respiration [62]. Nevertheless, one common point to the reduction of insoluble iron minerals is the need for the cell to transport electrons generated in the cytoplasm to the cell surface, where the catalytic reactions will take place [12, 62]. Starting with the electrons generated by the oxidation of the electron donor, the ETC proposed for *S. oneidensis* MR-1 includes a NADH dehydrogenase complex that transfer electrons to the quinone pool in the cell membrane. In this way, electrons are directed towards the *c*-type cytochrome CymA, located also in the cytoplasmic membrane. MtrA, a decaheme *c*-type cytochrome, accepts electrons from CymA and transports those through the porin MtrB to the outer membrane cytochrome MtrC. From here electrons can pass from MtrC to OmcA, an extracellular decaheme cytochrome involved in mineral reduction, or be transferred directly to the Fe(III) solid phase if there is contact with the cell surface. Flavins are also part of the iron reduction mechanism by interacting with OmcA and MtrC to shuttle electrons to the acceptor (Fig. 1). Based on this model, we analyzed the genome of *S. loihica* to propose a potential ETC for the reduction of insoluble iron minerals.

The proposed pathway includes homologues to the MtrCAB complex (SHEW_RS13070, SHEW_RS13080 and SHEW_RS13075 respectively), and homologs to OmcA (SHEW_RS13065) and CymA (SHEW_RS18345) (Fig. 4A and B). In the model mechanism the involvement of conductive Pili was also considered as Pili have been involved in iron reduction in other bacteria such as *Geobacter sulfurreducens*. However, in the case of *S. oneidensis*, conductive Pili have not been yet unequivocally shown to be involved in solid iron reduction [62]. According to the Table 2, genes coding for cytochromes, porins, dehydrogenases, as well as flavoproteins and iron transporters were up regulated in presence of salt suggesting that they could be involved in the physiologically observed iron reduction shown Fig. 1. Thus, according to these results, we propose a solid iron reduction pathway for *S. loihica* in our treatment conditions (Fig. 4C).

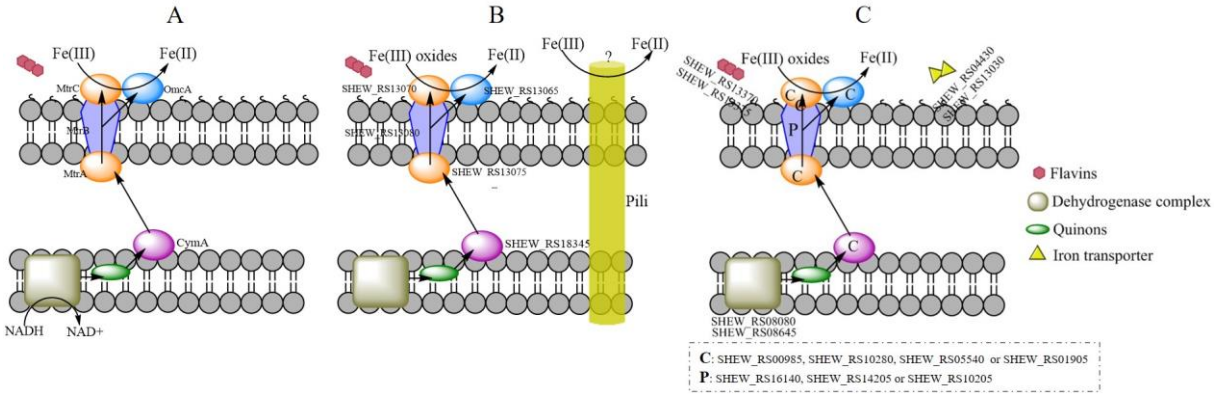

Figure 4. Comparison of the electron transport chain involved in reduction of solid iron substrates in A) *Shewanella oneidensis* B) the homologs identified in the genome of *Shewanella loihica* and C) a proposed solid iron reduction pathway of *S. loihica* according to our transcriptomic data. The pathway for *S. oneidensis* was based on [12,62].

Conclusion

We found that *S. loihica* recovered completely its iron reduction capabilities after amending 1% NaCl, to a culture incubated for 24 hours in a solution without NaCl. Moreover, some genes coding for transcriptional regulators (ArsR and TetR), methyl-accepting chemotaxis proteins, *c*-type cytochromes, acyl-CoA dehydrogenase and Glu/Leu/Phe/Val dehydrogenase and porins as well as iron ABC were only activated in presence of NaCl, suggesting that they play a key role in iron reduction observed in 1% NaCl and 1% NaCl amended conditions. Surprisingly, none of the genes that were up regulated in presence of salt, corresponded to the homologues of the *mtrCAB* operon, which is reported in the literature to be involved in iron reduction in *S. oneidensis*. Nevertheless, due to the minimal composition of the iron reduction solution, the bacterial cells are confronted to several stresses and thus, the conditions tested were not ideal for determining the effect of salt on growth of *S. loihica* using solid iron as final electron acceptor.

Material and methods

Bacterial strain

Shewanella loihica PV-4 (DSM 17748) was used in this study. The strain was purchased from DSMZ (Deutsche Sammlung von Mikroorganismen und Zellkulturen GmbH). Regular cultivation was performed aerobically using Luria-Bertani medium (LB; 1% tryptone, 0.5% yeast extract, and 1% NaCl) at pH 7 and at 20°C under agitation at 130 rpm.

Genomic analysis of solid iron reduction mechanism

Genomic analysis was performed in order to identify the potential genes involved in reduction of solid iron in *S. loihica* PV-4. Based on a literature review, the proteins involved in iron reduction in the model bacterium *S. oneidensis* MR-1 were identified and extracted from the genome available in NCBI (Genome accession number: NC_004347.2; MtrA NP_717386.1, MtrB NP_717385.1, MtrC NP_717387.1,OmcA NP_717388.1, CymA NP_720107.1). A similarity search against the proteome of *S. loihica* (NC_009092.1) was performed using protein BLAST program blastp [77]. The iron reduction pathways of both *S. oneidensis* and *S. loihica* were drown using ChemDraw Professional software (version 16.0.0.82(68)) [78].

Iron reduction of solid Fe(III)

Iron reduction using iron coupons corroded in marine environment as solid iron source (see Chapter 2) was performed in a matrix composed of 20 mM PIPES, 5mM sodium lactate, and 50 mM $NaHCO_3$. Three conditions were tested: matrix amended with 1% NaCl, non-amended matrix and matrix amended with 1% NaCl after 24 hours of incubation. All the experiments were performed in triplicates.

Bacterial cells were grown in 450 ml LB broth overnight under agitation and at room temperature. Cells were harvested by centrifugation at 1700 × g for 10 minutes at room temperature. Pellets were washed with a 20 mM PIPES solution. The pellets were resuspended in a solution of 20 mM PIPES and inoculated in the three iron reduction matrices (with and without NaCl). To evaluate iron reduction, samples were collected every 2 hours for 24 hours. For RNA sequencing, the samples were collect from the overnight culture, and at 0, 12 and 24 h after inoculating the strains. For RNA sequencing 1 ml of the culture was collected and stored at -80°C.

Measurements of Fe(II) concentration

To measure the reduction of Fe(III) into Fe(II), the ferrozine assay was performed following a modified protocol from Bell *et al.*[79]. First, 100 µL of 5 M HCl were added to 900 µL of collected samples and stored at 4°C. The samples were centrifuged for 1 minute at 6700 x *g*, then 100 µL of the supernatant were taken and 900 µL of ferrozine solution (0.1% ferrozine in a 100 mM HEPES solution at pH 7) were added. Fe(II) concentration was determined by measuring the absorbance at 562 nm with a UV-Vis spectrophotometer (Fisher Scientific Genesys^{TM} 10 s). A calibration curve was obtained using serial dilutions of 1 mM ferrous ammonium sulphate solution in acidic MilliQ water (pH 2).

RNA extraction and rRNA removal

The RNA sequencing consisted on the extraction of RNA, removal of rRNA and library preparation and sequencing. Bacterial cell stored at -80°C were thawed on ice and then briefly centrifuged (10000 x g for 1 minute) prior to RNA extraction. RNA extraction was done using a Zymo Research Direct-zol kit with TRIzol® reagent according to the manufacturer's instructions.

A Ribo-Zero™ Magnetic kit for Gram-negative bacteria (Illumina) was used for rRNA removal, according to the manufacturer's instructions. The concentration of RNA from the extraction was considered to calculate the reagents used for the preparation of the magnetic beads and for the treatment of total RNA with Ribo-Zero rRNA removal solution (4 µl rRNA removal solution for 0.25 to 1 µg total RNA per reaction). Samples in Ribo-Zero rRNA removal solution were incubated at 68°C for 10 minutes followed by 5 minutes of incubation at 20°C. To remove rRNA, the Ribo-Zero mix incubated previously was mixed with the prepared magnetic beads and placed at room temperature for 5 minutes, then at 50°C for 5 minutes. The rRNA-depleted samples were purified using RNeasy MinElute Kit (Qiagen). The final mRNA eluted was quantified using Qubit-IT RNA HS assay kit (ThermoFisher Scientific) and Bioanalyzer RNA 6000 Pico kit (Agilent).

Illumina indexed library preparation

The preparation of indexed libraries from RNA and sequencing using ScriptSeq v2 Sample Preparation Kit (Illumina) follows these steps: fragmentation of RNA and primer hybridization, cDNA synthesis where RNA is converted to cDNA, then adapter sequences and indexes are added onto the ends of the fragments to generate libraries using PCR that was run as multiplexed paired-end sequencing libraries on an Illumina sequencer. RNA fragmentation step depends on the size of the RNA fragments. As less than 40% of the RNA obtained was more than 600 nt, no fragmentation was done. Nevertheless, A maximum of 5 µg of RNA was mixed 2µl of cDNA primer (200 µM) and incubated at 65°C for 5 minutes on a thermal cycler, then placed on ice (1 µl of fragmentation solution was added after incubation according to the manufacturer's instructions). 3 µl of the cDNA synthesis premix obtained previously was mixed with 0.5 µl DTT 100 mM and 0.5 µl StarScript Reverse Transcriptase. The reaction was incubated at 25°C for 5 minutes, by 42°C for 20 minutes and hold at 37°C. Then 1 µl of finishing solution was added and the reaction was incubated at 37°C for 10 minutes, 95°C for 3 minutes and hold at 25°C. 8 µl of Tagging Master mix (7.5 µl Terminal Tagging Premix and 0.5 µl DNA polymerase was added and the tubes were incubated at 25°C for 15 minutes, 95°C for 3 minutes and hold on ice. The purification of the cDNA was performed using Agencourt AMPure XP beads. PCR was performed using Failsafe PCR Enzyme Mix (Illumina). It starts by preparing a PCR Master Mix (25 µl of PCR Premix E, 1 µl of forward PCR primer and 0.5 µl of Failsafe enzyme (2.5U/µl) and adding 1 µl of Index Primer (Script Seq Index PCR primers, Illumina). The reaction was incubated in the thermocycler as follows: 95°C for 1 minute, 15 cycles of 95°C for 30 seconds, 55°C for 30 seconds and 68°C for 3 minutes. The samples were then incubated at 68°C for 7 minutes and hold at 4°C. The PCR products clean-up was done using AMPure XP beads. The validation and the quality control of the library was done using Qubit-IT dsDNA HS assay kit and BioAnalyzer DNA high sensitivity kit (Agilent). Accurate quantification of the amplified library products is important for the sequencing results on the Illumina next-generation sequencing platforms. A qPCR (using KAPA SYBR FAST universal qPCR kit for illumine libraries) was performed in order to obtain an accurate quantification of the amplifiable molecules in the DNA libraries.

Illumina sequencing and data analysis pipeline

Libraries were sequenced on Illumina NextSeq 500 instrument, using Nextseq Sequencing Kit HO 300 cycles (Illumina) according to the manufacturer's instruction (paired end sequencing mode).

The raw reads of RNA-seq data were processed using Pipeline for Reference based Transcriptomics (PiReT) sowftware (https://github.com/mshakya/PyPiReT).

Briefly, the reads were aligned and assigned to the reference genomes using HISAT2 version [version information is available in github repo].

Aligned reads were then analyzed and assigned to individual genes according to the genome annotations provided by GenBank (*Shewanella loihica* PV-4, NC_009092.1). The normalized read counts for each gene, RPKM, was calculated by an R [80] package EdgeR.

Graphical representations of differential gene expression data obtained from pairwise comparison (Volcano plots, Principal Component Analysis (PCA), Heatmaps) were created using R including the ggplot 2 package [81].

Author contribution

WMK designed and performed the experiments, analyzed the data and wrote the manuscript. TJ, MS, KD, PL and PC performed the RNA sequencing data analysis; JM performed protein migration, Heme staining experiment; EJ corrected the manuscript and PJ designed the experiments, analyzed the data, wrote and corrected the manuscript.

References

1. Mudryk, Z. & Donderski, W. Effect of Sodium Chloride on the Metabolic Activity of Halophilic Bacteria Isolated From the Lake Gardno Estuary. *Estuaries* **14,** 495–496 (1991).

2. Wichern, J., Wichern, F. & Joergensen, R. G. Impact of salinity on soil microbial communities and the decomposition of maize in acidic soils. *Geoderma* **137,** 100–108 (2006).

3. Yan, N., Marschner, P., Cao, W., Zuo, C. & Qin, W. Influence of salinity and water content on soil microorganisms. *Int. soil water Conserv. Res.* **3,** 316–323 (2015).

4. Urbina, M. A. & Glover, C. N. Effect of salinity on osmoregulation, metabolism and nitrogen excretion in the amphidromous fish, inanga (*Galaxias maculatus*). *J. Exp. Mar. Bio. Ecol.* **473,** 7–15 (2015).

5. Casamayor, E. O. *et al.* Changes in archaeal, bacterial and eukaryal assemblages along a salinity gradient by comparison of genetic fingerprinting methods in a multipond solar saltern. *Environ. Microbiol.* **4,** 338–348 (2002).

6. Killham, K. *Soil Ecology*. *Nature* **455,** (1994).

7. Rath, K. M. & Rousk, J. Salt effects on the soil microbial decomposer community and their role in organic carbon cycling: A review. *Soil Biol. Biochem.* **81,** 108–123 (2015).

8. Hua, S. T., Tsai, V. Y., Lichens, G. M. & Noma, A. T. Accumulation of Amino-Acids in *Rhizobium* Sp Strain WR1001 in Response to Sodium Chloride Salinity. *Appl. Environ. Microbiol.* **44,** 135–140 (1982).

9. Khmelenina, V. N., Kalyuzhnaya, M. G., Starostina, N. G., Suzina, N. E. & Trotsenko, Y. A. Isolation and characterization of halotolerant alkaliphilic methanotrophic bacteria from Tuva soda lakes. *Curr. Microbiol.* **35,** 257–261 (1997).

10. Brown, a. D. Aspects of Bacterial Response To the Ionic Environment. *Bacteriol. Rev.* **28,** 296–329 (1964).

11. Molina-H *et al.* Protective Effect of Sucrose and Sodium Chloride for *Lactococcus lactis* during Sublethal and Lethal High-Pressure Treatments. *Appl. Environ. Microbiol.* **70,** 2013–2020 (2004).

12. Weber, K. a., Achenbach, L. a. & Coates, J. D. Microorganisms pumping iron: anaerobic microbial iron oxidation and reduction. *Nat. Rev. Microbiol.* **4,** 752–764 (2006).

13. Lovley, D. R. Dissimilatory Fe(III) and Mn(IV) reduction. *Microbiol. Rev.* **55,** 259–287 (1991).

14. Argandoña, M. *et al.* Interplay between iron homeostasis and the osmotic stress response in the halophilic bacterium *Chromohalobacter salexigens*. *Appl. Environ. Microbiol.* **76,** 3575–3589 (2010).

15. Roden, E. E. & Lovley, D. R. Dissimilatory Fe(III) Reduction by the Marine Microorganism *Desulfuromonas acetoxidans*. *Appl. Environ. Microbiol.* **59,** 734–742 (1993).

16. Roh, Y. *et al.* Biogeochemical and environmental factors in Fe biomineralization:

magnetite and siderite formartion. *Clays Clay Miner.* **51,** 83–95 (2003).

17. Ziemke, F., Hofle, M. G., Lalucat, J. & Rossello-moras, R. Reclassification of *Shewanella putrefaciens* Owen's genomic group II a *Shewanella baltica*. *Int. J. Syst. Bacteriol.* **48,** 179–186 (1998).

18. DasSarma, S. & DasSarma, P. Halophiles. *eLS* 1–13 (2017). doi:10.1002/9780470015902.a0000394.pub4

19. Bowman, J. P. *et al. Shewanella gelidimarina* sp. nov. and *Shewanella frigidimarina* sp. nov., Novel Antarctic species with the ability to produce eicosapentaenoic acid (20: 5ω3) and grow anaerobically by dissimilatory Fe (III) reduction. *Int. J. Syst. Bacteriol.* **47,** 1040–1047 (1997).

20. Jiang, H. *et al.* Microbial response to salinity change in Lake Chaka, a hypersaline lake on Tibetan plateau. *Environ. Microbiol.* **9,** 2603–2621 (2007).

21. Holt, H. M., Gahrn-Hansen, B. & Bruun, B. *Shewanella algae* and *Shewanella putrefaciens*: Clinical and microbiological characteristics. *Clin. Microbiol. Infect.* **11,** 347–352 (2005).

22. Cummings, D. E., Caccavo, F., Fendorf, S. & Rosenzweig, R. F. Arsenic mobilization by the dissimilatory Fe(III)-reducing bacterium *Shewanella alga* BrY. *Environ. Sci. Technol.* **33,** 723–729 (1999).

23. L., L. *et al.* Do stresses encountered during the smoked salmon process influence the survival of the spoiling bacterium *Shewanella putrefaciens*? *Lett. Appl. Microbiol.* **30,** 437–42 (2000).

24. Gao, H. *et al. Shewanella loihica* sp. nov., isolated from iron-rich microbial mats in the Pacific Ocean. *Int. J. Syst. Evol. Microbiol.* **56,** 1911–1916 (2006).

25. Moon, J.-W. *et al.* Microbial preparation of metal-substituted magnetite nanoparticles. *J. Microbiol. Methods* **70,** 150–158 (2007).

26. Kooli, W. M. *et al.* Bacterial iron reduction and biogenic mineral formation for the stabilisation of corroded iron objects. *Sci. Rep.* **8,** 764 (2018).

27. Ventosa, A., Nieto, J. J. & Oren, A. Biology of moderately halophilic aerobic bacteria. *Microbiol. Mol. Biol. Rev.* **62,** 504–44 (1998).

28. Rafaeli-eshkol, B. Y. D. Studies on Halotolerance in a Moderately Halophilic Bacterium. Effect of growth conditions on salt resistance of the respiratory system. *Biochem. J* **109,** 679–685 (1968).

29. Baxter, R. M. & Gibbons, N. E. Effects of Sodium and Potassium Chloride on Certain Enzymes of *Micrococcus Halodenitrificans* and *Pseudomonas Salinaria*. *Can. J. Microbiol.* **2,** 599–606 (1956).

30. Schell, M. Molecular Biology of the LysR Family of Transcriptional Regulators. *Annu. Rev. Microbiol.* **47,** 597–626 (1993).

31. Cao, H. *et al.* A quorum sensing-associated virulence gene of *Pseudomonas aeruginosa* encodes a LysR-like transcription regulator with a unique self-regulatory mechanism. *Proc. Natl. Acad. Sci.* **98,** 14613–14618 (2001).

32. Beliaev, a S. *et al.* Global Transcriptome Analysis of Shewanella oneidensis MR-1

Exposed to Different Terminal Electron Acceptors Global Transcriptome Analysis of *Shewanella oneidensis* MR-1 Exposed to Different Terminal Electron Acceptors †. *J. Bacteriol.* **187,** 7138–7145 (2005).

33. Gao, H. *et al.* Physiological roles of ArcA, Crp, and EtrA and their interactive control on aerobic and anaerobic respiration in *Shewanella oneidensis*. *PLoS One* **5,** (2010).

34. Saffarini, D. a, Schultz, R. & Beliaev, A. Involvement of Cyclic AMP (cAMP) and cAMP Receptor Protein in Anaerobic Respiration of *Shewanella oneidensi*s *J. Bacteriol.* **185,** 3668–3671 (2003).

35. Agari, Y., Kashihara, A., Yokoyama, S., Kuramitsu, S. & Shinkai, A. Global gene expression mediated by Thermus thermophilus SdrP, a CRP/FNR family transcriptional regulator. *Mol. Microbiol.* **70,** 60–75 (2008).

36. Zhang, Z. *et al.* Functional Interactions between the Carbon and Iron Utilization Regulators , Crp and Fur , *in Escherichia coli J. Bacteriol.* **187,** 980–990 (2005).

37. Padan, E., Venturi, M., Gerchman, Y. & Dover, N. Na+/H+ antiporters. *Biochim. Biophys. Acta* **1505,** 144–157 (2001).

38. He, Z. *et al.* Global transcriptional, physiological and metabolite analyses of the responses of *Desulfovibrio vulgaris* Hildenborough to salt adaptation. *Appl. Environ. Microbiol.* **76,** 1574–1586 (2010).

39. Clark, M. E. *et al.* Temporal transcriptomic analysis as Desulfovibrio vulgaris Hildenborough transitions into stationary phase during electron donor depletion. *Appl. Environ. Microbiol.* **72,** 5578–5588 (2006).

40. Johnson, D. R. *et al.* Temporal transcriptomic microarray analysis of *Dehalococcoides ethenogenes* strain 195 during the transition into stationary phase. *Appl. Environ. Microbiol.* **74,** 2864–2872 (2008).

41. Happe, T. & Kaminski, A. Differential regulation of the Fe-hydrogenase during anaerobic adaptation in the green alga *Chlamydomonas reinhardtii*. *Eur. J. Biochem.* **269,** 1022–1032 (2002).

42. Burns, J. L. *et al.* Outer membrane-associated serine protease involved in adhesion of *Shewanella oneidensis* to Fe(III) oxides. *Environ. Sci. Technol.* **44,** 68–73 (2010).

43. Barnes, L.-M., Lo, M. F., Adams, M. R. & Chamberlain, A. H. L. Effect of Milk Proteins on Adhesion of Bacteria to Stainless Steel Surfaces. *Appl. Environ. Microbiol.* **65,** 4543–4548 (1999).

44. Beliaev, A. S. *et al.* Gene and Protein Expression Profiles of *Shewanella* Electron Acceptors. *J. Integr. Biol.* **6,** 39–60 (2002).

45. Gao, T., Ju, L., Yin, J. & Gao, H. Positive regulation of the *Shewanella oneidensis* OmpS38, a major porin facilitating anaerobic respiration, by Crp and fur. *Sci. Rep.* **5,** 1–13 (2015).

46. Nyström, T. Stationary-Phase Physiology. *Annu. Rev. Microbiol.* **58,** 161–181 (2004).

47. Young, G. M. & Postle, K. Repression of tonB transcription during anaerobic growth requires Fur binding at the promoter and a second factor binding upstream. *Mol. Microbiol.* **11,** 943–954 (1994).

48. Hantke, K. Iron and metal regulation in bacteria. *Curr. Opin. Microbiol.* **4,** 172–177 (2001).

49. Völker, U., Mach, H., Roland, S. & Hecker, M. Stress proteins and cross-protection by heat shock and salt stress in *Bacillus subtilis*. *J. Gen. Microbiol.* **138,** 2125–2135 (1992).

50. Matin, A. The molecular basis of carbon-starvation-induced general resistance in *Escherichia coli*. *Mol. Microbiol.* **5,** 3–10 (1991).

51. Flardh, K., Cohen, P. S. & Kjelleberg, S. Ribosomes exist in large excess over the apparent demand for protein synthesis during carbon starvation in marine Vibrio sp. strain CCUG 15956. *J. Bacteriol.* **174,** 6780–6788 (1992).

52. Babujee, L., Balakrishnan, V., Kiley, P. J., Glasner, J. D. & Perna, N. T. Transcriptome Changes Associated with Anaerobic Growth in Yersinia intermedia (ATCC29909). *PLoS One* **8,** 1–12 (2013).

53. Jovanovic, G., Lloyd, L. J., Stumpf, M. P. H., Mayhew, A. J. & Buck, M. Induction and function of the phage shock protein extracytoplasmic stress response in Escherichia coli. *J. Biol. Chem.* **281,** 21147–21161 (2006).

54. Li, J., Romine, M. F. & Ward, M. J. Identification and analysis of a highly conserved chemotaxis gene cluster in *Shewanella* species. *FEMS Microbiol. Lett.* **273,** 180–186 (2007).

55. Pennella, M. A. & Giedroc, D. P. Structural determinants of metal selectivity in prokaryotic metal-responsive transcriptional regulators. *BioMetals* **18,** 413–428 (2005).

56. Murphy, J. N. & Saltikov, C. W. The ArsR repressor mediates arsenite-dependent regulation of arsenate respiration and detoxification operons of *Shewanella* sp. strain ANA-3. *J. Bacteriol.* **191,** 6722–6731 (2009).

57. Deng, W., Li, C. & Xie, J. The underling mechanism of bacterial TetR/AcrR family transcriptional repressors. *Cell. Signal.* **25,** 1608–1613 (2013).

58. Ramos, J. L. *et al.* The TetR Family of Transcriptional Repressors The TetR Family of Transcriptional Repressors. *Microbiol. Mol. Biol. Rev.* **69,** 326–356 (2005).

59. Hong, C. S. *et al.* Chemotaxis proteins and transducers for aerotaxis in *Pseudomonas aeruginosa*. *FEMS Microbiol. Lett.* **231,** 247–252 (2004).

60. Springer, W. R. & Koshland, D. E. Identification of a protein methyltransferase as the cheR gene product in the bacterial sensing system. *Proc. Natl. Acad. Sci.* **74,** 533–537 (1977).

61. Harris, H. W. *et al.* Redox sensing within the genus *Shewanella*. *Front. Microbiol.* **8,** 1–11 (2018).

62. White, G. F. *et al.* in *Advances in Microbial Physiology* **68,** 87–138 (Elsevier Ltd., 2016).

63. Herrmann, G., Jayamani, E., Mai, G. & Buckel, W. Energy conservation via electron-transferring flavoprotein in anaerobic bacteria. *J. Bacteriol.* **190,** 784–791 (2008).

64. Geider, R. J. & La Roche, J. The role of iron in phytoplankton photosynthesis, and the potential for iron-limitation of primary productivity in the sea. *Photosynth. Res.* **39,**

275–301 (1994).

65. La Roche, J., Boyd, P. W., McKay, R. M. L. & Geider, R. J. Flavodoxin as an in situ marker for iron stress in phytoplankton. *Nature* **382,** 802–805 (1996).

66. Erdner, D. L., Price, N. M., Doucette, G. J., Peleato, M. L. & Anderson, D. M. Characterization of ferredoxin and flavodoxin as markers of iron limitation in marine phytoplankton. *Mar. Ecol. Prog. Ser.* **184,** 43–53 (1999).

67. Yoshida, M., Muneyuki, E. & Hisabori, T. ATP synthase - A marvellous rotary engine of the cell. *Nat. Rev. Mol. Cell Biol.* **2,** 669–677 (2001).

68. Soontharapirakkul, K. *et al.* Halotolerant cyanobacterium *Aphanothece halophytica* contains an Na+-dependent F1F0-ATP synthase with a potential role in salt-stress tolerance. *J. Biol. Chem.* **286,** 10169–10176 (2011).

69. Huang, F., Fulda, S., Hagemann, M. & Norling, B. Proteomic screening of salt-stress-induced changes in plasma membranes of *Synechocystis* sp. strain PCC 6803. *Proteomics* **6,** 910–920 (2006).

70. Lau, C. K. Y., Krewulak, K. D. & Vogel, H. J. Bacterial ferrous iron transport: The Feo system. *FEMS Microbiol. Rev.* **40,** 273–298 (2016).

71. Heidelberg, J. F. *et al.* Genome sequence of the dissimilatory metal ion-reducing bacterium *Shewanella oneidensis*. *Nat. Biotechnol.* **20,** 1118–1123 (2002).

72. Higgins, C. F. ABC Transporters: From Microorganisms to Man. *Annu. Rev. Cell Biol.* **8,** 67–113 (1992).

73. Sekiya, H. *et al.* Functional Cloning and Characterization of a Multidrug Efflux Pump , MexHI-OpmD , from a *Pseudomonas aeruginosa* Mutant. *Antimicrob. Agents Chemother*. **47,** 2990–2992 (2003).

74. Saier, M. H. *et al.* Evolutionary origins of multidrug and drug-specific efflux pumps in bacteria. *FASEB J.* **12,** 265–274 (1998).

75. Alvarez-Ortega, C., Olivares, J. & Martínez, J. L. RND multidrug efflux pumps: What are they good for? *Front. Microbiol.* **4,** 1–11 (2013).

76. Tokunaga, H. *et al.* Salt-Inducible Multidrug Efflux Pump Protein in the Moderately Halophilic Bacterium *Chromohalobacter* sp . *Appl. Environ. Microbiol.* **70,** 4424–4431 (2004).

77. Johnson, M. *et al.* NCBI BLAST: a better web interface. *Nucleic Acids Res.* **36,** 5–9 (2008).

78. Mills, N. ChemDraw Ultra 10.0. *J. Am. Chem. Soc.* **128,** 13649–13650 (2006).

79. Bell, P. E., Mills, a L. & Herman, J. S. Biogeochemical Conditions Favoring Magnetite Formation during Anaerobic Iron Reduction. *Appl. Environ. Microbiol.* **53,** 2610–2616 (1987).

80. R Core Team. R Core Team (2017). R: A language and environment for statistical computing. *R Found. Stat. Comput. Vienna, Austria.*

81. Wickham, H. *ggplot2:Elegant Graphics for Data Analysis*. *Media* **35,** (2009).

Supplementary information

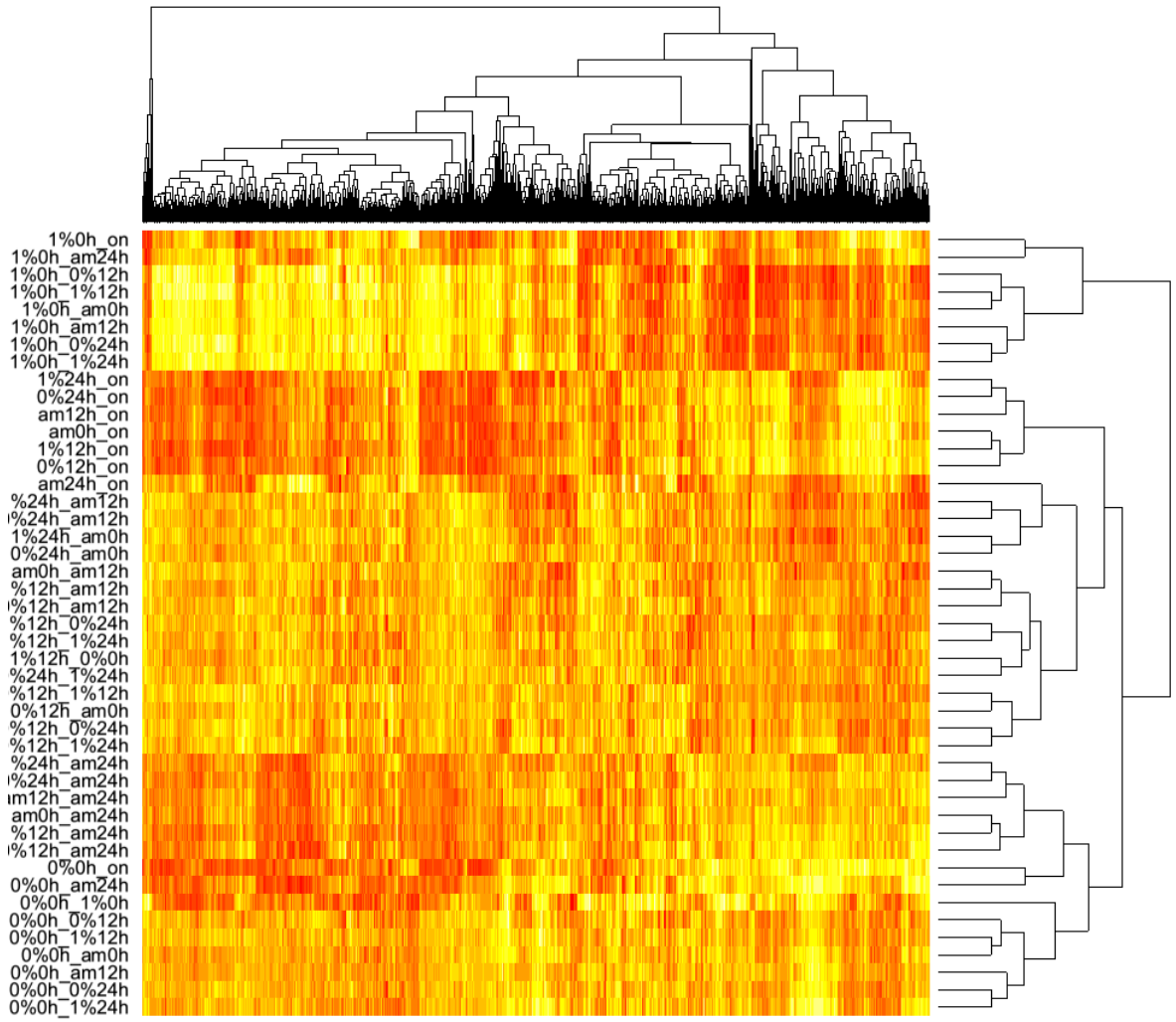

Figure SI1: Heatmap without filtering the genes with |log(FC)|>2 and showing all the conditions generated with our transcriptomic analysis.

Table SI1: Table showing the genes with a more significant change in gene expression presented in Fig. 3, as well as their function, log(FC) and P values.

Gene_locus	Function	LogFC	Pvalue
SHEW_RS09485	Hypothetical protein	3.161	6.32E-11
SHEW_RS12055	Carbon starvation	3.272	3.92E-10
SHEW_RS04425	Hypothetical protein	3.081	8.29E-10
SHEW_RS14545	TatD family deoxyribonuclease	2.812 (1%0h_on) 2.279 (0%0h_on)	2.37E-09 1.06E-06
SHEW_RS06300	Hypothetical protein	3.607 (1%0h_on) 3.409 (0%0h_on)	2.91E-09 1.16E-08
SHEW_RS00575	STAS domain-containing protein	2.988	1.13E-08
SHEW_RS09070	Hypothetical protein	3.499	7.37E-08
SHEW_RS09480	SpoVR family protein	3.377	1.13E-07
SHEW_RS01100	Pilus assembly protein PilO	2.869	1.25E-07
SHEW_RS06000	L-threonine dehydrogenase	2.490	2.18E-07
SHEW_RS09490	PrkA family serine protein kinase	3.857	5.96E-07
SHEW_RS07995	DUF465 domain-containing protein	3.973	9.00E-05
SHEW_RS10505	50S ribosomal protein L20	4.626	0.000427842
SHEW_RS11475	Integration host factor subunit alpha ihfA	3.871	0.000277592
SHEW_RS16875	Porin	3.560	0.046241738
SHEW_RS03580	Sodium:proton antiporter	-2.716	1.37E-05
SHEW_RS03130	Thiosulfate reductase	-3.387	1.93E-05
SHEW_RS16835	Porin	-2.731	7.93E-05
SHEW_RS10580	Cation transporter	-3.984	9.50E-05
SHEW_RS08880	Alpha/beta hydrolase	-3.852	0.000189479
SHEW_RS03465	Hypothetical protein	-5.767 (1%0h_on) -4.501 (0%0h_on)	0.000136156 0.00168838
SHEW_RS19900	TonB- dependent siderophore receptor	-5.899 (1%0h_on) -4.525 (0%0h_on)	0.001582157 0.009555356
SHEW_RS16020	TonB- dependent siderophore receptor	-4.968 (1%0h_on) -3.790 (0%0h_on)	0.003073772 0.016669938
SHEW_RS05130	KfrA protein	-3.272	0.185528704
SHEW_RS07840	Sodium:proton antiporter	-4.821	0.009512029

Table SI2: Differential gene expression data between 0, 12 and 24h in 0%NaCl condition (0-12h, 0-24h, 12-24h), between 0% and 1%NaCl at 0h (0%_1%), between 0, 12 and 24h in Amended 1%NaCl condition (0-12h, 0-24h, 12-24h), between 0%NaCl and Amended 1%NaCl (0h_0h, 12h_12h, 24h_0h, 24h_12h) and between 1%NaCl and amended 1%NaCl (0h_0h, 12h_12h, 24h_24h). The values represent the log(FC) that was selected to be |log(FC)|>2

Function	Gene_locus	Gene product	Conditions												
			0% NaCl			0% versus 1%	Amended			0% versus Amended				1% versus Amended		
			0-12h	0-24h	12-24h	0% 0h_1% 0h	0-12h	0-24h	12-24h	0h_0h	12h_12h	24h_0h	24h_12h	0h_0h	12h_12h	24h_24h
Transcriptional regulators	SHEW_RS06415	LysR family						-2.118	-2.030							-2.262
	SHEW_RS03010	Crp	2.463							2.478						
	SHEW_RS05640	ArsR family	2.918			2.361	-2.762		2.066	3.638	-2.042				-2.338	
	SHEW_RS08695	TetR/AcrR family						-2.087						2.334		
	SHEW_RS09405	GntR family						2.742	2.280							3.064
	SHEW_RS10485	AsnC family	2.401	2.632		2.062				2.968						
	SHEW_RS19820	XRE family					-2.142			2.511				3.208		
	SHEW_RS17640	heavy metal-responsive													2.530	
	SHEW_RS17745	PdhR		2.047												
Sigma factors	SHEW_RS05405	RNA polymerase sigma factor RpoE	2.243			2.705										
	SHEW_RS06230	RNA polymerase sigma factor RpoS				2.036		2.021						-2.869		
	SHEW_RS06890	flagellar biosynthesis anti-sigma factor FlgM														2.281
	SHEW_RS18675	RNA polymerase sigma factor RpoH				2.351										
	SHEW_RS15310	RNA polymerase sigma factor	2.138							2.169						
Ribosomal proteins	SHEW_RS00775	50S ribosomal protein L11 rplK		2.329					2.124							
	SHEW_RS00780	50S ribosomal protein L1		2.086					2.300							
	SHEW_RS00785	50S ribosomal protein L10		3.773	2.241	2.749			2.773							
	SHEW_RS00790	50S ribosomal protein L7/L12		2.495		2.734			2.352							
	SHEW_RS00805	30S ribosomal protein S12		3.083		2.623			2.664							
	SHEW_RS00810	30S ribosomal protein S7		2.117		3.037			2.007							
	SHEW_RS00825	30S ribosomal protein S10		2.503		3.143			2.294							
	SHEW_RS00830	50S ribosomal protein L3		2.228												
	SHEW_RS00835	50S ribosomal protein L4		2.386		2.546			2.383							
	SHEW_RS00845	50S ribosomal protein L2							2.407							
	SHEW_RS00855	50S ribosomal protein L22		2.420					2.634							
	SHEW_RS00875	30S ribosomal protein S17 rpsQ		2.200					2.667							
	SHEW_RS00880	50S ribosomal protein L14		3.309		3.217			2.772							
	SHEW_RS00885	50S ribosomal protein L24	2.165	3.999		3.185			3.110							
	SHEW_RS00890	50S ribosomal protein L5		3.039					2.183							
	SHEW_RS00895	30S ribosomal protein S14		2.315		2.120			2.644							
	SHEW_RS00900	30S ribosomal protein S8 rpsH		2.825					2.382							
	SHEW_RS00905	50S ribosomal protein L6		2.734		2.156			2.675							
	SHEW_RS00910	50S ribosomal protein L18		2.908		2.002			3.225							
	SHEW_RS00915	30S ribosomal protein S5	2.114	2.793					2.552							
	SHEW_RS00920	50S ribosomal protein L15	2.182	2.534					2.958							
	SHEW_RS00930	30S ribosomal protein S13		2.590		2.452			2.765							
	SHEW_RS00935	30S ribosomal protein S11							2.014							
	SHEW_RS00940	30S ribosomal protein S4		2.741		2.330			2.546							
	SHEW_RS00950	50S ribosomal protein L17 rplQ		2.582		2.084			2.598							
	SHEW_RS04470	50S ribosomal protein L21 rplU		2.450		3.572			2.168							
	SHEW_RS04475	50S ribosomal protein L27 rpmA	2.191	2.223		2.117										
	SHEW_RS05480	30S ribosomal protein S16	2.008	3.521		2.712			3.433							
	SHEW_RS05485	ribosome maturation factor rimM														
	SHEW_RS05645	30S ribosomal protein S20	2.050	2.228		2.802			2.462							
	SHEW_RS10115	30S ribosomal protein S1		2.304												
	SHEW_RS10505	50S ribosomal protein L20				2.111		2.158								
	SHEW_RS14575	30S ribosomal protein S15	2.170	3.233		2.885			2.497							
	SHEW_RS16980	50S ribosomal protein L9		2.256		2.028										
	SHEW_RS16995	30S ribosomal protein S6		2.407		2.388										
	SHEW_RS17040	30S ribosomal protein S9		2.220		2.851										
	SHEW_RS17045	50S ribosomal protein L13	2.299	2.769		3.105			2.684							
	SHEW_RS18045	50S ribosomal protein L28	2.136	3.165					3.121							
	SHEW_RS20215	50S ribosomal protein L30	2.855	3.645		2.261			3.472							
	SHEW_RS20415	50S ribosomal protein L35		2.130												
	SHEW_RS00865	50S ribosomal protein L16		2.131		2.638			2.297							
	SHEW_RS05495	50S ribosomal protein L19		2.459		2.128			2.223							
	SHEW_RS09475	50S ribosomal protein L25		2.829		3.114			2.674							
	SHEW_RS00860	30S ribosomal protein S3							2.570							

Chemotaxis	SHEW_RS06890	flagellar biosynthesis anti-sigma factor FlgM																	2.281
	SHEW_RS06910	flagellar basal body rod protein FlgB				3.290											-2.357		
	SHEW_RS06915	flagellar basal body rod protein FlgC				2.361													
	SHEW_RS06960	flagellar hook-associated protein FlgL				2.522													
	SHEW_RS06970	flagellin				2.123					2.456								2.091
	SHEW_RS06975	flagellar protein FlaG	2.304								2.847								
	SHEW_RS06980	flagellar hook protein FliD	2.418			2.087					2.597								
	SHEW_RS06990	flagellar protein FliS				3.459					2.217								
	SHEW_RS01110	type IV pilus secretin PilQ						2.07	2.04										
	SHEW_RS18855	methyl-accepting chemotaxis protein						-2.24											
Sodium/cation transporter/antiporter	SHEW_RS07840	sodium:proton antiporter				4.111											-3.895		
	SHEW_RS04365	ammonium transporter						-2.001											
Cytochromes and energy metabolism	SHEW_RS00985	cytochrome c5 family protein		2.368		2.692					2.056								
	SHEW_RS04350	ammonia-forming cytochrome c nitrite reductase subunit c552						2.105	2.603										
	SHEW_RS04715	cytochrome c						2.721	3.081										
	SHEW_RS10280	cytochrome-c oxidase cbb3-type subunit III ccoP															-2.078		
	SHEW_RS13920	cytochrome b561																	
	SHEW_RS18345	cytochrome c	2.795			2.393					2.927								
	SHEW_RS13065	cytochrome c	2.248																
	SHEW_RS13355	cytochrome c	2.698									-2.583							
	SHEW_RS05540	cytochrome c				2.059													
	SHEW_RS19245	cytochrome c4				2.356													
	SHEW_RS01060	N-acetyl-gamma-glutamyl-phosphate reductase				2.211													
	SHEW_RS02675	5,10-methylenetetrahydrofolate reductase metF	2.312																-2.699
	SHEW_RS09115	Ni/Fe-hydrogenase b-type cytochrome subunit cybH						2.048											2.462
	SHEW_RS09120	nickel-dependent hydrogenase large subunit																	2.446
	SHEW_RS08645	acyl-CoA dehydrogenase															-2.337		
	SHEW_RS13260	phosphogluconate dehydrogenase																	
	SHEW_RS08080	Glu/Leu/Phe/Val dehydrogenase															-2.663		
	SHEW_RS14255	isocitrate dehydrogenase				2.137													
	SHEW_RS09965	2-oxoisovalerate dehydrogenase subunit beta															-2.044		
	SHEW_RS13375	electron transfer flavoprotein subunit beta						3.278									-2.201		
	SHEW_RS13370	electron transfer flavoprotein subunit alpha						2.542									-3.279		
	SHEW_RS09920	flavodoxin				2.773											-2.179		
	SHEW_RS19925	ATP synthase subunit gamma		2.418															
	SHEW_RS19935	ATP synthase subunit delta		2.083		2.802													
	SHEW_RS19940	ATP synthase subunit B		2.492		2.020					2.546								
	SHEW_RS19945	ATP synthase subunit C				2.391													
	SHEW_RS19950	ATP synthase subunit A		3.627							3.315								
	SHEW_RS19915	ATP synthase epsilon chain atpC				2.809											-2.583		
	SHEW_RS16140	porin															-2.802		
	SHEW_RS16835	porin									2.433								
	SHEW_RS16875	porin	2.578	3.797		2.469	-2.612		4.036		2.905	-2.285		-3.503		-2.129			
	SHEW_RS14030	putative porin		2.439							2.007						2.658		
	SHEW_RS14205	porin															-2.308		
	SHEW_RS01400	porin family protein	2.172			2.433					2.261								
	SHEW_RS19785	porin family protein		2.116															
	SHEW_RS10205	porin																	-2.047
Outer membrane proteins	SHEW_RS05615	OmpA family protein						2.299											
	SHEW_RS13220	outer membrane protein OmpW							2.479										
	SHEW_RS01640	outer membrane adhesin-like protein						2.268	2.206										2.955
Iron and metal transporters	SHEW_RS04430	iron ABC transporter substrate-binding protein					2.269	-2.459		-2.509							-3.966		
	SHEW_RS13030	ferrous iron transporter B															-2.170		
	SHEW_RS19080	tungsten ABC transporter substrate-binding protein				2.142											-2.680		
	SHEW_RS08545	efflux RND transporter periplasmic adaptor subunit	2.003		-2.792								2.0655	2.318					
	SHEW_RS09580	MexH family multidrug efflux RND transporter periplasmic adaptor subunit															-2.119		
	SHEW_RS08740	TonB-dependent receptor							-2.8474					2.346			-2.0786	2.05556	
	SHEW_RS12830	TonB-dependent receptor						3.36154									-3.4458		
	SHEW_RS13910	TonB-dependent receptor					2.46779		-2.9219								-3.1093		
	SHEW_RS12355	TonB-dependent receptor						2.45057											
	SHEW_RS16020	TonB-dependent siderophore receptor	-2.235	-2.168			3.161		-3.5387	-3.169	2.226			2.159			-4.3479	2.97215	
	SHEW_RS19900	TonB-dependent siderophore receptor	-2.024				2.41269		-2.1893	-2.093	2.3435						-3.4676		
Oxygen tolerance	SHEW_RS07845	peroxidase				2.221											-2.327		
	SHEW_RS09495	superoxide dismutase [Fe]		2.503		2.133													
	SHEW_RS04090	peroxiredoxin ahpC		2.584					3.168								2.616		
	SHEW_RS01755	thioredoxin	2.015			2.261													
Stress response	SHEW_RS10310	universal stress protein E											3.068	2.854					3.326
	SHEW_RS12900	envelope stress response membrane protein PspC	3.586		-3.682			2.4			2.972		2.654	3.005			2.748		
	SHEW_RS16035	universal stress protein																2.140	2.630
	SHEW_RS16040	universal stress protein																	2.250
	SHEW_RS16400	oxidative stress defense protein									2.037		2.061						
	SHEW_RS08370	cold-shock protein		2.288		2.630													
	SHEW_RS12910	phage shock protein PspA	3.225		-3.183						2.718		2.675	2.663			2.978		
	SHEW_RS11080	heat-shock protein IbpA	2.149			2.712													
	SHEW_RS08125	cold shock domain protein CspD				2.098		2.283									-2.698		
Number of genes differentially expressed coding for hypothetical proteins			13	6	6	23	1	3	10	10	1	2	3				12	1	5

Table SI3: Differential gene expression data in 1%NaCl condition between 0 and 12h (1%0h_1%12h), 0 and 24h (1%0h_1%24h) and between 0%NaCl at 24h and amended 1%NaCl at 24h (0%24h_Am24h), conditions. The values represent the log(FC) that was selected to be log(FC)>2

Function	Gene_locus	Gene product	1%0h-1%12h	1%0-1%24h	0%24h_am24h
Transcriptional regulators	SHEW_RS09405	GntR family			2.642
	SHEW_RS19820	XRE family	2.107	-2.131	
	SHEW_RS19800	MerR family		2.149	
Chemotaxis	SHEW_RS06890	flagellar biosynthesis anti-sigma factor FlgM			2.145
	SHEW_RS06970	flagellin			2.808
	SHEW_RS06990	flagellar protein FliS			2.303
	SHEW_RS01105	pilus assembly protein PilP			2.07
	SHEW_RS01110	type IV pilus secretin PilQ			2.345
Cytochromes and energy metabolism	SHEW_RS04350	ammonia-forming cytochrome c nitrite reductase subunit c552			2.209
	SHEW_RS04715	cytochrome c			3.239
	SHEW_RS18345	cytochrome c			2.172
	SHEW_RS09115	Ni/Fe-hydrogenase%2C b-type cytochrome subunit cybH			3.555
	SHEW_RS09120	nickel-dependent hydrogenase large subunit			2.447
	SHEW_RS00320	formate dehydrogenase	2.110		
	SHEW_RS13375	electron transfer flavoprotein subunit beta	-2.420		2.802
	SHEW_RS16875	porin		2.449	
	SHEW_RS14030	putative porin	2.693	3.734	
	SHEW_RS19785	porin family protein		2.344	
Outer membrane proteins	SHEW_RS13220	outer membrane protein OmpW			2.069
	SHEW_RS01640	outer membrane adhesin-like protein			2.943
Iron and metal transporters	SHEW_RS19505	metal transporter			2
	SHEW_RS08545	efflux RND transporter periplasmic adaptor subunit	2.052		
	SHEW_RS12830	TonB-dependent receptor	-3.014		2.449
Oxygen tolerance	SHEW_RS04090	peroxiredoxin ahpC		4.060	
Stress response	SHEW_RS10310	universal stress protein E			3.863
	SHEW_RS12900	envelope stress response membrane protein PspC	2.957		2.527
	SHEW_RS16035	universal stress protein			2.232
	SHEW_RS16040	universal stress protein			2.500
	SHEW_RS12910	phage shock protein PspA	3.268		2.314
Number of genes differentially expressed coding for hypothetical proteins			16	10	13

A)

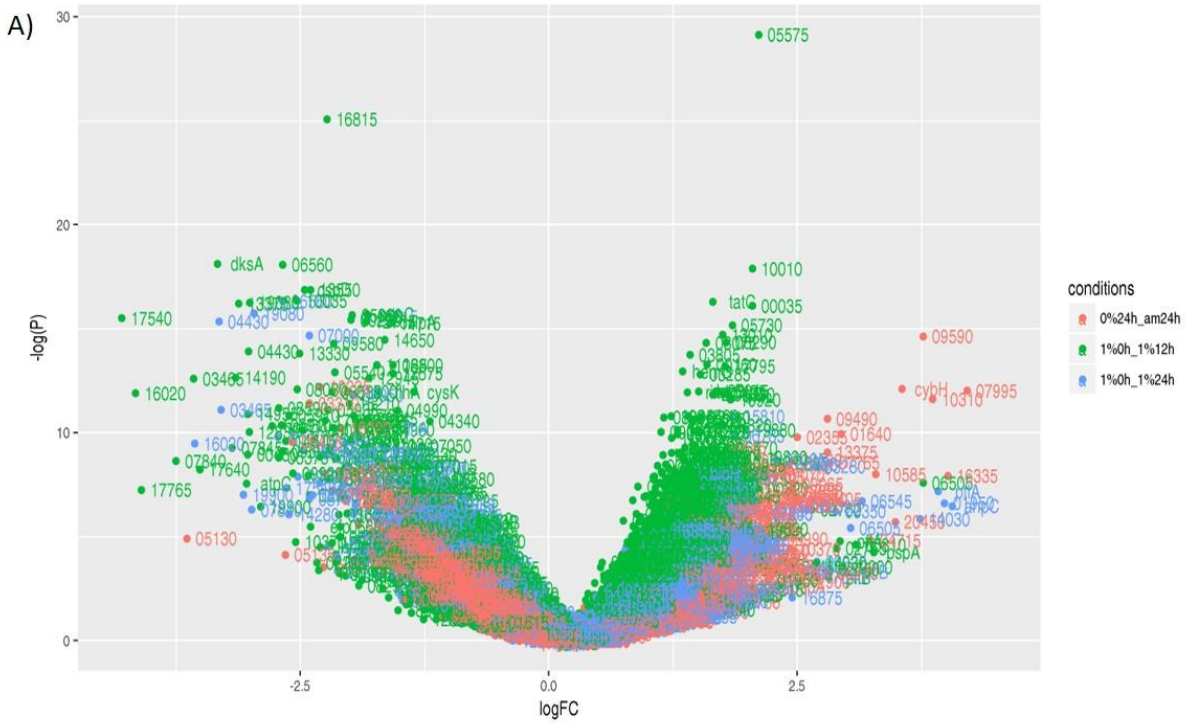

B)

Gene_locus	Function	Log(FC)	Pvalue
SHEW_RS05575	Hypothetical protein	2.110	2.21E-13
SHEW_RS10010	EEP domain-containing protein	2.047	1.71E-08
SHEW_RS00035	Hypothetical protein	2.047	1.01E-07
SHEW_RS17475	Twin-arginine translocase subunit TatC	1.649	8.36E-08
SHEW_RS09590	Hypothetical protein	3.766	4.40E-07
SHEW_RS07995	DUF465 domain-containing protein	4.208	6.03E-06
SHEW_RS10310	universal stress protein E	3.862	9.06E-06
SHEW_RS09115	Ni/Fe-hydrogenase b-type cytochrome subunit cybH	3.555	5.55E-06
SHEW_RS09490	PrkA family serine protein kinase	2.802	2.34E-05
SHEW_RS01640	Outer membrane adhesin-like protein	2.942	4.84E-05
SHEW_RS10585	Ecotin	3.290	0.000335
SHEW_RS16335	DUF2726 domain-containing protein	4.014	0.000359
SHEW_RS16815	Hypothetical protein	-2.232	1.29E-11
SHEW_RS06560	isocitrate lyase	-2.676	1.40E-08
SHEW_RS19080	tungsten ABC transporter substrate-binding protein	-2.965	1.46E-07
SHEW_RS16185	RNA polymerase-binding protein DksA	-3.333	1.34E-08
SHEW_RS04430	iron ABC transporter substrate-binding protein	-3.021(1%0h_1%12h) -3.318(1%0h_1%24h)	9.14E-07 2.17E-07
SHEW_RS14190	phosphate-binding protein	-3.150	3.20E-06
SHEW_RS03465	Hypothetical protein	-3.574(1%0h_1%12h) -3.298(1%0h_1%24h)	3.40E-06 1.52E-05
SHEW_RS17540	DUF465 domain-containing protein	-4.297	1.83E-07
SHEW_RS16020	TonB-dependent siderophore receptor	-4.159(1%0h_1%12h) -3.563(1%0h_1%24h)	6.82E-06 7.62E-05
SHEW_RS07840	sodium:proton antiporter	-3.751	0.000178
SHEW_RS17765	methylation site containing protein	-4.099	0.000708
SHEW_RS05130	KfrA protein	-3.642	0.007372

Figure SI2: A) Pairwise comparison on the Rna-seq data using volcano plots (-log10Pvalue, Y axis, logFC, X axis) representing comparisons at 24 hours between 0%NaCl and amended 1%NaCl (0%24h_am24h), at 1%NaCl, between 0 and 12h (1%0h_1%12h) and between 0 and 24h (1%0h_1%24h). B) For the genes with a more significant change in gene expression, the function, the values of log(FC) and P are indicated in the table

Chapter 4

Investigation of polyphosphate accumulation by *Shewanella loihica* and comparison *Shewanella oneidensis*

"Phosphate minerals have been known and prized since remote antiquity. Turquoise, has been found among the remains of many ancient civilizations, including Egypt, Mesopotamia, India and China. As early as 3400 B.C., it was obtained from the Sinai Peninsula, Egypt, in what was probably one of the earliest hard-rock mining operations in the world" J.O. Nriagu (1985) [1]

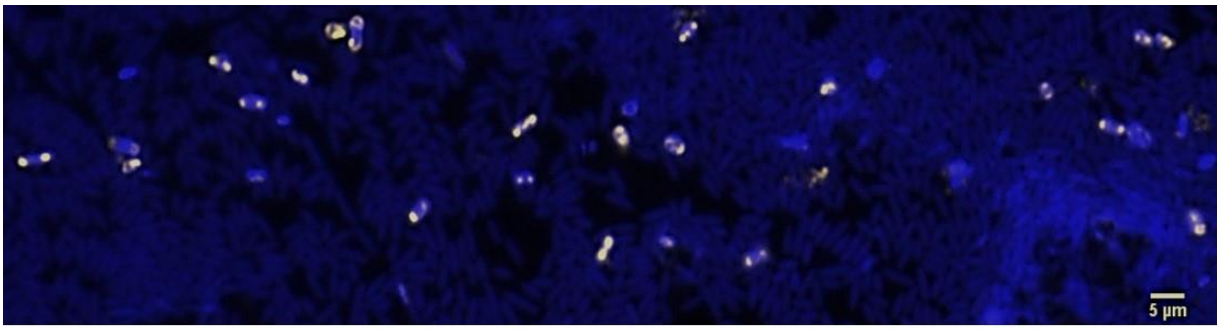

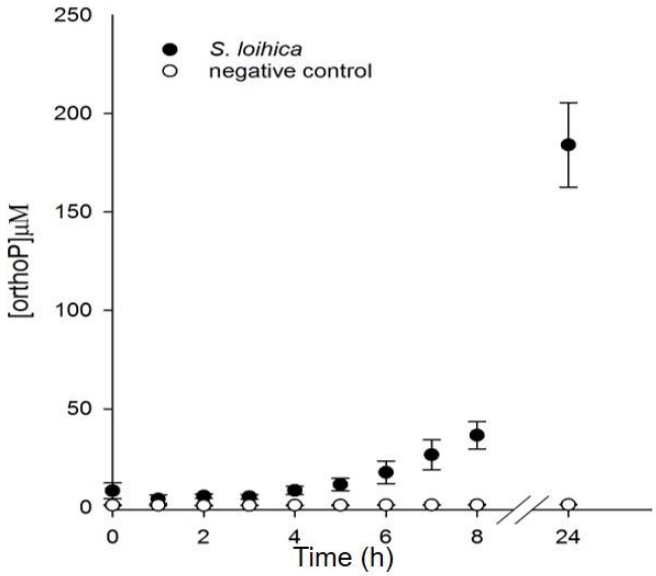

Co-authors: Julien Maillard, Paul Li, Edith Joseph, Patrick S. Chain and Pilar Junier.
Status: in preparation for publication

Abstract

Polyphosphate (polyP) plays an important role in the physiological adaptation of bacteria during growth and development, as well as in their response to nutritional and environmental stress. Moreover, polyP accumulation is of environmental relevance and might be linked to the formation of phosphate minerals. In particular, ferrous iron phosphate minerals represent a key stage in the recycling of phosphorus in aquatic and terrestrial ecosystems. In this study we investigated the polyP accumulation potential of two selected *Shewanella* species. We inferred polyP accumulation in *Shewanella loihica* by measuring the concentration of orthophosphate after polyP hydrolysis from cells cultivated aerobically. In contrast, the ability to accumulate polyP appears to be less pronounced in *Shewanella oneidensis*. Moreover, during iron reduction (and the production of Fe(II)), we observed a decrease in the concentration of the released orthophosphate compared to incubations in absence of iron. This result correlates well with the production of iron phosphate minerals observed under the same conditions. The physiological results could be correlated with the analysis of the genomes of both species. Polyphosphate kinase (accumulation and hydrolysis of polyP) and exopolyphosphatase (hydrolysis of polyP) were identified in the genome of *S. loihica*, but only the latter was found in the genome of *S. oneidensis*. We discuss the results in the context of biogenic mineral formation and the widespread detection of iron phosphates in natural and manmade ecosystems, in which iron phosphates could be used for the recovery and recycling of phosphorus.

Introduction

Phosphorus is essential to living organisms. It represents about 1% of the dry weight of bacterial cells and it is a structural component of several biopolymers (DNA, RNA, phospholipids, nucleotides, phosphoryl groups of signal molecules) [2]. However, phosphorus is a limiting nutrient in many environments [3]. Many bacterial species have developed strategies to cope with phosphorus limitation. Accumulation of polyphosphate (polyP) in form of granules in the cytosol represents a good solution to counteract phosphorus and energy shortage, as the granules can be consumed when the phosphate supply is limited [4]. Polyphosphate molecules are linear polymers consisting of two to thousands orthophosphate (Pi) residues, all linked by energy-rich phosphoanhydride bonds [5]. PolyP plays important roles in the physiology of prokaryotic and eukaryotic organisms [4]. The main role of polyP granules is to acts as a phosphate and energy reserve [4,6]. The hydrolysis of the energy-rich PolyP bonds is coupled to the production of ATP [6] and can in this way, supply energy for many biochemical reactions in the cell. In addition, many studies have demonstrated that polyP granules are also involved in other physiological and regulatory processes in bacteria. This include the response to oxidative, acid, osmotic, or UV stress, as well as nutrient starvation. In addition, polyP plays a role in motility, competence, biofilm formation, virulence, regulation of gene expression, cytoplasmic membrane stabilization, regulation of enzymatic activities, as well as ATP and metal homeostasis [4,6].

Polyphosphate is a biopolymer reported in diverse bacteria, fungi, plants, and animals [7]. Polyphosphate granules were first identified in the yeast *Saccharomyces cerevisiae* in 1888 [8]. Since then, the ability to store polyP as granules was found to be widespread among microorganisms and especially bacteria [8], including for example, *Ralstonia eutropha* [9], *Accumulibacter phosphatis*, *Gemmatimonas aurantiaca* [10], *Pseudomonas putida* [11], *Pseudomonas fluorescens* [12], *Bacillus sphaericus, Acidithiobacillus ferrooxidans* [13], and *Acinetobacter* spp. (e.g. *A. calcoaceticus* [12], *A. johnsonii* [13] and *A. baumannii* [14]).

One of the processes in which polyP accumulation has been studied in more detail is wastewater treatment. Domestic wastewater is one of the major sources of phosphate in natural environments [15]. Controlling phosphate levels in water bodies receiving treated wastewater is a major concern to prevent eutrophication. One of the promising strategies to remove phosphate is enhanced biological phosphorus removal (EBPR), which is largely based on polyP accumulation by polyphosphate-accumulating organisms (PAO) [15,16]. There is a link between polyP accumulation and the cycles of aerobic-anaerobic conditions used in wastewater treatment. Under anaerobic conditions, the hydrolysis of intracellular polyP enables PAO to obtain the energy required to uptake organic substrates [17,18]. In this way, carbon is assimilated and stored in absence of oxygen. For example, in wastewater, acetate is a major carbon source and is converted into acetyl-CoA. This reaction requires energy provided by the hydrolysis of ATP, leading to the production of ADP and the release of orthophosphate in the medium. Acetyl-CoA is next metabolized into β-polyhydroxyalkanoates (PHAs), which are carbon storage compounds. In aerobic conditions, this trend is reversed. PHAs are used for cell growth and the reconstitution of the polyP reserves. PHAs are hydrolyzed, which leads to the synthesis of acetyl-CoA, processed through the TCA cycle. The TCA cycle produces energy, a part of which is used to assimilate soluble phosphate from the environment and to incorporate it into polyP [19].

In bacteria, phosphorus uptake is controlled by two distinct transport systems: high affinity Pit and low affinity Pst phosphate transporters. The high affinity Pit system is activated when internal phosphorus is depleted and allows bacteria to accumulate phosphorus at a faster rate [20,21]. Polyphosphate accumulation could be divided in two mechanisms: (i) "luxury uptake" where the limitation of a different nutrient (e.g. carbon) results in formation of polyP granules, and (ii) "over plus accumulation" where, polyP accumulation is due to a sudden change from phosphate deprivation to phosphate availability [22]. PolyP accumulation involves two classes of polyphosphate kinases (PPK1 and PPK2). They catalyze the ATP-dependent formation of a phosphoanhydride bond between a polyP chain and orthophosphate [23]. The same enzymes can also work in the reverse direction to generate ATP from polyP. In contrast, the exopolyphosphatase (PPX) hydrolyzes the terminal phosphate from linear polyP mainly under anoxic and environmental phosphate-limited conditions [7]. Genes encoding PPK are present in many bacteria, including various human pathogens. Deletion of *ppk* genes affects growth, motility, quorum sensing, biofilm formation, and virulence. For example, in the opportunistic pathogen *Bacillus cereus*, the *ppx* mutant is also impaired in sporulation [24].

In our previous work, we used *Shewanella loihica*, a facultative anaerobe and iron reducer, for the treatment of corroded iron objects by the production of biogenic iron minerals. Among the Fe(II) minerals produced, we obtained vivianite, a Fe(II) phosphate mineral. The formation of vivianite was unexpected, as the anoxic solution used for iron reduction did not contain any phosphate source. Additional experiments suggested that this bacterium accumulates polyP granules inside the cells during aerobic growth and releases phosphate under anaerobic conditions (Chapter 2) [25]. Even if the phosphorus incorporated in vivianite could have other origins (recycling of DNA, RNA, phospholipids) [26], the possible correlation between polyP accumulation, iron reduction, and vivianite formation was further investigated here. This chapter presents the results of preliminary experiments aiming at better understanding the link between the formation of vivianite and polyP accumulation by *S. loihica*. For this, we first perform physiological studies to compare polyP accumulation in *S. loihica* and the well-studied model *Shewanella oneidensis* MR-1. This was complemented by the analysis of gene repertoires involved in polyP synthesis in both species, as well as of transcriptomics data obtained from *S. loihica* during the transition of aerobic to anaerobic conditions favoring or

not iron reduction. Understanding polyP accumulation in *S. loihica* in comparison to the model organism *S. oneidensis* is of great value from fundamental and applied points of view, as this genus is considered a prime model for biogenic mineral formation.

Results

Polyphosphate accumulation during aerobic growth by *S. loihica* and comparison with *S. oneidensis*

Although polyP accumulation appears to be widespread in many microorganisms [27], the conditions for polyP accumulation and the level of accumulation among bacteria differ [28]. It has been reported that intracellular synthesis of polyP granules occurs during aerobic growth [22,29], during exponential and/or stationary growth phases (luxury uptake), but also in response to environmental stress [7,28]. In the case of *S. loihica*, the indirect quantification of polyP in relationship to biomass production suggest a possible accumulation of polyP during aerobic growth in LB medium after 4 and 8 hours of incubation (Fig. 1). The quantity of polyP measured after 8 hours decreased but it was still higher than the value obtained for the inoculum. In contrast, in *S. oneidensis*, the quantity of polyP was only slightly higher than for the inoculum after 4 hours of incubation and decreased to the same level of the inoculum after 8 h. These results were not confirmed when using gel electrophoreses and toluidine blue staining to visualize polyP (Fig. 2). However, a more intense coloration of the gel was observed for the sample of *S. loihica* after 8 hours of incubation (well n°5) in comparison to *S. oneidensis*. Yet, the samples were not correlated with biomass. Since the amount of biomass was clearly higher after 8 h, a higher amount of polyP is expected at this time point. Thus, this experiment must be repeated in order to confirm the results considering the biomass load, additional and standardization of replicates.

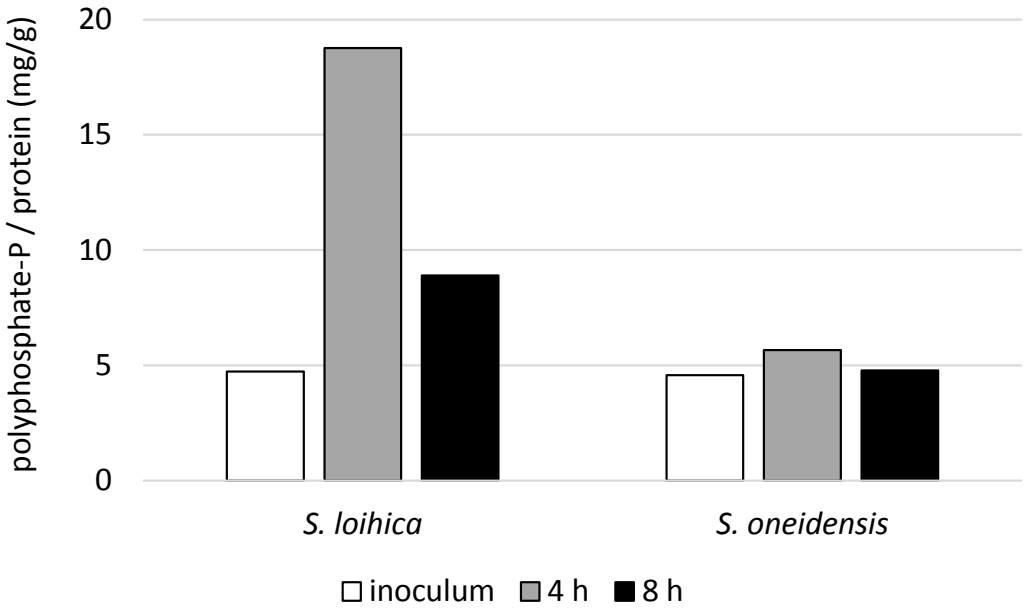

Figure 1. Polyphosphate accumulation during aerobic cultivation of *S. loihica* and *S. oneidensis*. Intracellular polyphosphate was quantified indirectly after hydrolysis to phosphate. The resulting phosphate concentration was corrected by the amount of biomass used in the analysis and expressed as mg of polyphosphate-P per g of total proteins.

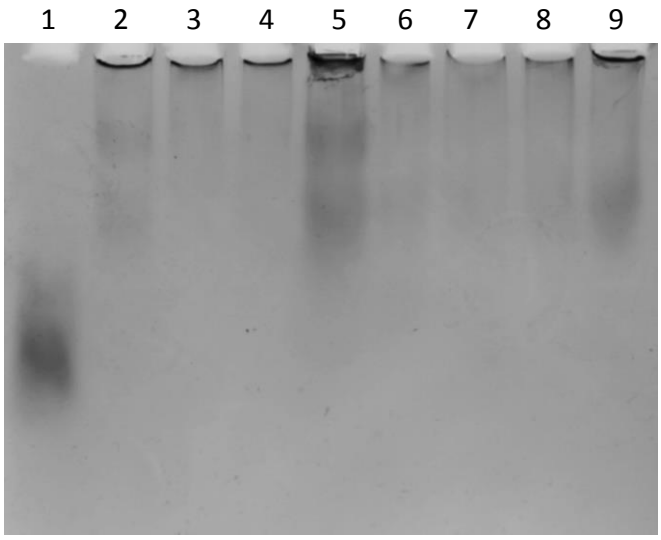

Figure 2. Gel electrophoresis analysis of polyphosphate extracted from *S. loihica* and *S. oneidensis* biomass samples. Samples obtained after NaOH treatment of cell suspensions were analyzed by gel electrophoresis and stained with Toluidine Blue. Lanes: 1, polyphosphate-700 (Sigma) as reference; 2-5, *S. loihica*; 6-9, *S. oneidensis*; 2 and 6, samples from overnight pre-cultures; 3-4 and 7-8, samples collected after 4 h of aerobic cultivation (two replicates for each strain); 5 and 9, samples collected after 8 h of aerobic cultivation (only one replicate for each strain).

Orthophosphate release in anaerobic iron reduction conditions

Given the iron reduction capabilities of *S. loihica* and *S. oneidensis*, the link between iron reduction and polyphosphate metabolism was investigated. In PAOs, polyP hydrolysis and orthophosphate release occur usually under anaerobic conditions [19,29] or when the surrounding environment is phosphate-limited [30–32]. The same could be the case for *S. loihica* and *S. oneidensis* under iron reducing conditions. As phosphate ions have a high affinity for ferrous iron, orthophosphate release during iron reduction could lead to the formation of Fe(II) phosphate minerals. This chelation is expected to render soluble/aqueous phosphate ions less available. To test this, cells from an overnight aerobic culture were resuspended in anaerobic buffer in the presence or absence of Fe(III) citrate and an electron donor (stimulation of iron reduction). In the anaerobic buffer lacking Fe(III) there was a notable increase overtime of the orthophosphate concentration for *S. loihica* (Fig. 3). In contrast, when an iron source was amended to the buffer, the concentration of released orthophosphate did not increase (Fig. 3). In the case of *S. oneidensis* the amount of released orthophosphate was significantly lower than for *S. loihica* with or without addition of iron. The lack of Fe(III) citrate in the anaerobic buffer resulted only in a slight increase of the phosphate release compared to the condition where iron was added (Fig. 3). The difference in the concentration of orthophosphate released between *S. loihica* and *S. oneidensis* is in agreement with the polyP accumulation capability of the former presented in Figures 1 and 2. While for both bacteria, iron was reduced (Fig. 4), reduction was associated with a decrease of the free phosphate in the medium only in the case of *S. loihica*. These results suggest that when an Fe(III) source is added to stimulate iron reduction, the latter leads to the production of Fe(II) in solution, which decreases the concentration of free orthophosphate detected from the degradation of polyP granules.

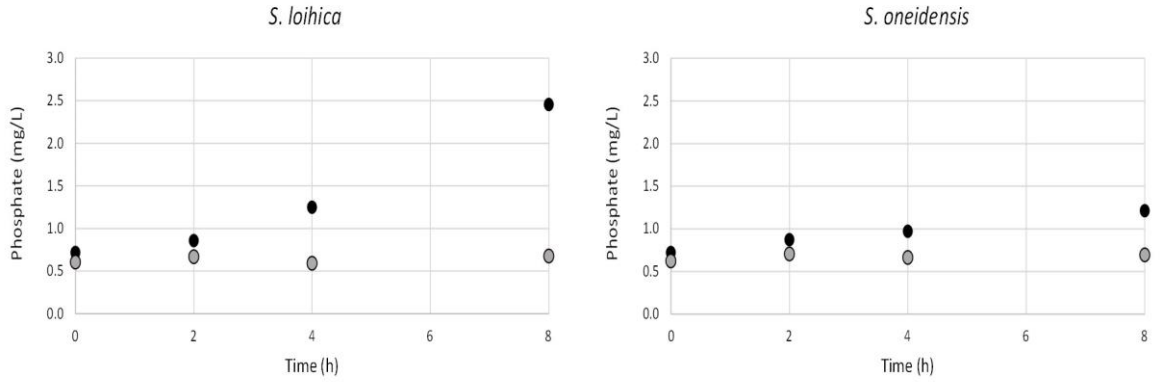

Figure 3. Phosphate release into the culture medium by *S. loihica* (left panel) and *S. oneidensis* (right panel) during anaerobic incubation. Phosphate was quantified in the culture medium during incubation of both strains in presence (grey circles) and absence (black circles) of Fe(III) citrate.

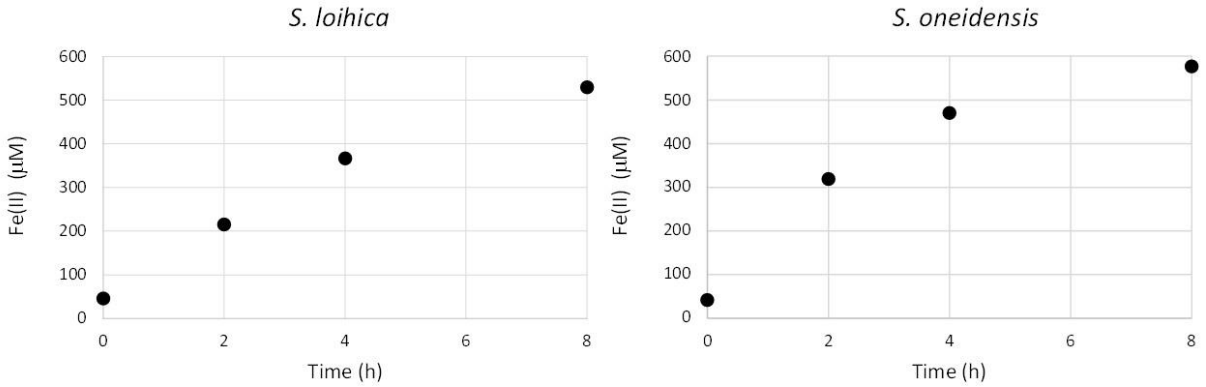

Figure 4. Iron reduction by *S. loihica* and *S. oneidensis* during anaerobic incubation.

Putative genes involved in polyphosphate accumulation and genome comparison of *S. loihica* with *S. oneidensis* and *S. putrefaciens*

Polyphosphate accumulation has been poorly studied in the case of the genus *Shewanella*. Polyphosphate accumulation and release in bacteria is directed by a set of genes, mainly *ppk* and *ppx*, coding for polyphosphate kinases and exopolyphosphatases, respectively. To investigate the presence of these genes in the genomes of *S. loihica* and *S. oneidensis*, we searched in the corresponding annotation files. We include as control the genome of *S. putrefaciens*, one of the few species for which indication of polyP accumulation has been suggested within the genus [32,33]. The analysis showed the presence of *ppx* genes in all three genomes (Table 1). The *ppk* gene, however, could only be clearly identified in *S. putrefaciens* and *S. loihica*. The presence of *ppk* and *ppx* genes in *S. putrefaciens* supports the hypothesis in polyP accumulation reported in the literature [32,33]. This is also in agreement with our results concerning polyP accumulation/orthophosphate release capabilities of *S. loihica* (Chapter 2). In *S. oneidensis*, *ppk* appears as a pseudogene as it is disrupted by an insertion sequence (Fig. 5). The disruption of *ppk* in *S. oneidensis* is coherent with the physiological results and would explain the low amounts of polyP and orthophosphate detected (Fig. 1 and Fig. 3).

Table 4: Putative genes involved in polyphosphate metabolism from the genomes of *S. loihica*, *S. oneidensis* and *S. putrefaciens*

Predicted function	Locus in *S. loihica* PV-4	Locus in *S. oneidensis* MR-1	Locus in *S. putrefaciens* CN-32
polyphosphate kinase (*ppk*)	SHEW_RS15930	-	SPUTCN32_RS08915 (this gene exhibits 81% identity with SHEW_RS15930 using Blastp)
Exopolyphosphatase (*ppx*)	SHEW_RS01765 SHEW_RS15925	SO_2185	SPUTCN32_RS08910 SPUTCN32_RS17810

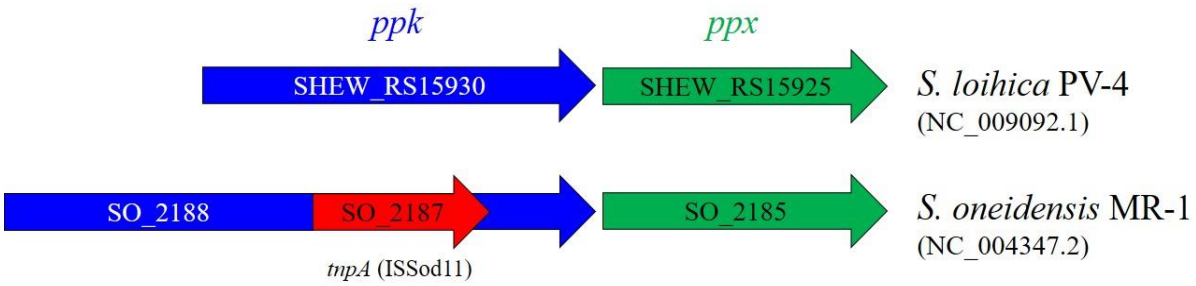

Figure 5. Genetic map of *ppk-ppx* gene clusters in *S. loihica* (top) and *S. oneidensis* (bottom). Note that the *ppk* gene in *S. oneidensis* is disrupted by the insertion of a transposase gene (*tnpA*) and therefore likely non-functional.

Expression of genes involved in polyP metabolisms in *S. loihica*

Based on transcriptomic data obtained during the transition of aerobic to anaerobic growth in conditions favoring iron reduction (Chapter 3), we analyzed the expression level of the genes SHEW_RS15930, SHEW_RS01765 and SHEW_RS15925 of *S. loihica*. The results showed that the gene SHEW_RS15930 coding for a PPK is not expressed in the differential gene expression analysis. However, it is likely that the cells were already under oxygen limitation and therefore, in a growth phase favoring the hydrolysis of polyP. The two genes encoding putative exopolyphosphatases (SHEW_RS01765 and SHEW_RS15925) were expressed, although the differences in expression levels during the transition were never significant. Overall, SHEW_RS01765 was up-regulated in the aerobic phase, as well as under iron reduction. In contrast, SHEW_RS15925 was down-regulated in the aerobic phase, and its expression varies under iron reduction (Table 2).

Table 5: log(FC) values obtained from the RNAseq results. The control represents the condition where no physiological iron reduction was observed.

Conditions	**SHEW_RS01765**	**SHEW_RS15925**
Aerobic versus anaerobic	0.362 ± 0.168	-0.950 ± 0.387
Control versus iron reduction	-0.178 ± 0.155	-0.125 ± 0.553

Discussion

Microorganisms are known to have a global impact in the phosphorus biogeochemical cycle. In particular, they participate to the mineralization of organic P compounds, generating local gradients of inorganic phosphate [3]. The storage of polyP and its hydrolysis back into orthophosphate in anoxic conditions is postulated to be involved in the precipitation of calcium and iron minerals such as apatite and vivianite [19]. These phosphate minerals represent a major sink in the global P cycle in aquatic environments [3,15,34]. The processes mediating the scavenging of phosphorus in this way constitute important regulators of internal phosphorus recycling and in consequence, of the trophic status of aquatic ecosystems [35]. The formation of phosphate minerals is tightly coupled to other microbial metabolisms. For example, bacterial iron respiration leads to the release of ferrous iron in the environment. Ferrous iron reacts with dissolved phosphate ions to form ferrous phosphate minerals. Iron phosphate minerals have a high environmental relevance, as the adsorptive affinity between iron and phosphate leads to the scavenging of the latter and become the primarily stock of potentially mobile phosphorus [35-36]. In this way, iron plays an important role in controlling the mobilization of P in aquatic systems, but also in soils and sediments [16,37].

Vivianite is the most common stable iron phosphate mineral in both terrestrial and aquatic ecosystems. Despite its widespread occurrence, the origin, mode of formation and significance of vivianite in the global phosphorus cycle are not well understood [38]. One of the processes that has recently being identified is the authigenic formation of reduced Fe(II) phosphates in anoxic environments [38]. In the environment, it has been postulated that Fe(III) oxyhydroxides can be an important precursor in vivianite formation. The reasons for this are, on the one hand, the role of these Fe(III) phases in the scavenging of orthophosphate, and on the second hand, the release of Fe(II) and orthophosphate upon chemical or biological iron reduction.

The direct role of polyP accumulation in the formation of phosphate minerals has been poorly studied. A study on the authigenic formation of calcium phosphates, suggest that accumulation of polyP by diatoms may represent a key process explaining the formation of these minerals in marine sediments [39]. Likewise, there is recent report suggesting that the activity of polyP-accumulating bacteria may trigger the precipitation of Fe(II) phosphates in the water column of an iron-rich sulfate-poor meromictic lake (Lake Pavin, France) [3].

In this study we investigated the possible link between polyP accumulation, iron reduction, and vivianite formation in the iron reducers *S. loihica* and *S. oneidensis*. Polyphosphate accumulation in relationship to biogenic mineral formation in *Shewanella* spp. has not been addressed so far. Studies on *Shewanella putrefaciens, Shewanella alga* and *S. oneidensis* have reported the formation of vivianite, but in all the cases, an external source of phosphate was provided in the culture medium [40–42]. Only a few studies reported the potential of *Shewanella* spp. (*S. putrefaciens* and *Shewanella* sp. HN-41) to accumulate polyP, but the evidence for this was not conclusive [32,33]. Our data suggest that not all *Shewanella* species would have the same capability to accumulate polyP and by this means, to release orthophosphate that can be a substrate for biogenic phosphate mineral formation. For example, the disruption of *ppk* gene in *S. oneidensis* could indicate that PPK enzyme is not functional which is coherent with the physiological results and could explains the low amounts of polyP and orthophosphate detected in the experiments performed (Fig. 1 and Fig. 3). In contrast, based on the genomic information *S. loihica* has the potential to accumulate polyP and our experimental data also suggest this. Even though, it will be tempting to generalize the correlation between the

genomic and experimental results, one has to be careful in doing so as it has been shown that a mutant *Pseudomonas putida* KT2440 Δ*ppk* was not deficient in polyP accumulation but had other pleiotropic effects [43].

Even if members of the genus *Shewanella* share some physiological properties that were relevant for this study (facultative anaerobes, metal reducers), the difference in polyP accumulation between these three *Shewanella* spp. reflects the divergence within the *Shewanella* genus. Indeed, ACT results (supplementary Fig. 5A,) showed that the gene order and orientation is not highly conserved between *S. loihica/S. oneidensis* and *S. loihica/S. putrefaciens*. In addition, several unique DNA regions were also observed in the comparison of the genomes. This is also confirmed by ANI test (supplementary Fig. 5B), where 78.03% average nucleotide identity between *S. loihica* and *S. oneidensis* and 77.81% between *S. loihica* and *S. putrefaciens* were calculated.

A better understanding of the relationship between iron reduction, polyP accumulation and biogenic mineral formation could have important repercussions in applied research. For example, iron and phosphorus are two of the main elements found in modern sewage treatment systems. In a recent study, the detection of vivianite in solids from two wastewater treatment plants was postulated to be associated to either chemical or biological Fe(III) reduction and phosphorus scavenging. This mineral phase appears to withstand the oxygenated treatment zones due to its slow oxidation kinetics and could offer a route towards the recovery of phosphorus downstream of the process [16,44]. This is relevant as the current use of phosphorus is not sustainable and its supply is not guaranteed in the future. However, an economically feasible recovery process is still technologically challenging [16]. Using *Shewanella* spp. as both a model of metal reduction and phosphate cycling could open the possibility to advance in this timely environmental issue. The preliminary results obtained during this study support our hypothesis for polyphosphate accumulation in *S. loihica* presented in chapter 2 and the link between polyphosphate accumulation and the formation on vivianite on corroded iron coupons. Vivianite can be an interesting mineral to be formed in terms of the conversion of reactive corrosion products on iron surfaces, both in terms of aesthetic change of the surface, as well as the stability and protective effect. However, the production of vivianite as a by-product of bacterial accumulation of polyphosphate raises a question in terms of our ability to control the biogenic minerals formed in a biotechnological treatment. Likewise, it suggests that iron phosphate formation can be avoided using a different bacterium like *S. oneidensis,* or by changing the conditions for iron reduction. This needs to be investigated in the future.

Conclusion

This is the first study that focuses on polyphosphate accumulation potential of some *Shewanella* species and suggests the possible polyphosphate accumulation in *Shewanella loihica.* Knowing that this bacterium was isolated from seawater could explain the need of this survival mechanism for this bacterium. Further investigations need to be done to confirm this polyphosphate biosynthesis potential, among which RNA extraction and RT-qPCR targeting the polyphosphate kinase and exopolyphosphatase genes of *S. loihica* and *S. oneidensis* are ongoing.

Material and methods

Bacterial cultivation and incubation for phosphate metabolism analysis

Liquid cultures of 50 mL LB medium in 250-mL Erlenmeyer flasks were inoculated with single colonies of *S. oneidensis* (abbreviated *Son*) and *S. loihica* (*Slo*) and incubated overnight at 150 rpm, and 30 and 20°C, respectively. The next day, three flasks containing fresh 50 mL LB medium were inoculated with 1 mL of the overnight pre-cultures. Aerobic cultivation of the two strains was performed as before and biomass samples were taken after 4 h (in duplicates) and after 8 h, as explained below. Biomass from the rest of the overnight pre-cultures was collected by 10 min centrifugation at 4500 × *g* and 4°C. Cells were washed in 20 mL of anaerobic buffer (50 mM HEPES, pH 7.0, 100 mM NaCl, flushed with N_2 gas) and collected by centrifugation as before. The biomass corresponding to 20 mL of overnight cultures was resuspended in 2.5 mL of anaerobic buffer and 1 mL of this biomass suspension was transferred in 100-mL serum flasks containing 50 mL of anaerobic buffer supplemented with either 20 mM lactate (buffer L) or 20 mM lactate and 5 mM Fe citrate (buffer L/F). Samples were collected as described below at the start of the experiment and after 2, 4 and 8 h of anaerobic incubation.

Sampling of biomass for analysis

From aerobic and anaerobic samples, 1 mL samples were taken for measurement of optical density at 600 nm. The same samples from aerobic cultivation were then filtered for the quantification of phosphate in the culture medium. For Fe(II) quantification, 0.5 mL aliquots were collected from anaerobic biomass suspensions and mixed with 0.5 mL of 1 M HCl to prevent Fe(II) oxidation. For indirect polyphosphate quantification, the biomass from 5 mL of overnight pre-cultures and 25 mL of aerobic cultures was collected by centrifugation as before. Biomass pellets were stored at -20°C until analysis.

Gel electrophoresis of polyphosphate

The gel mixture was composed of 1× TAN buffer (40 mM Tris-HCl, pH 8.0, 20 mM acetic acid and 18 mM NaCl), 2% acrylamide/bisacrylamide (37.5:1), 0.75% agarose, 0.04% ammonium persulfate and 0.0004% TEMED. The gel was run in 1× TAN buffer for 1 h at 100 V prior to load the samples. Aliquots of 8 µL of samples were mixed with 2 µL of 5× loading buffer (5× TAN buffer, 50% sucrose, 0.125% bromophenol blue) and loaded on the gel. Electrophoresis was run until the dye reached half-way through the gel length. The gel was then stained for 30 min in Toluidine Blue solution (0.25% Toluidine Blue O, 25% methanol and 5% glycerol) and finally washed twice for 30 min in destaining solution (25% methanol, 5% glycerol).

Phosphate quantification with Malachite Green

Aliquots of 0.25 mL of 0.22 µm filtered culture samples were mixed with 0.25 mL of ddH_2O water and 0.5 mL of Malachite Green solution (0.03% (w/v) of Malachite Green oxalate, 0.2% (w/v) di-sodium molybdate, 0.05% (v/v) Triton-X-100 in 0.7 M HCl). Samples were incubated 15 min at room temperature before spectrophotometric analysis at 630 nm. A 20 mM stock solution of Na_2HPO_4 was used as reference.

Indirect quantification of intracellular polyphosphate

Biomass samples collected for the quantification of intracellular polyphosphate were prepared as follows (modified from [45]). Biomass pellets from 5 mL of overnight pre-cultures were resuspended in a volume of ddH_2O corresponding to one fifth (in mL) of the respective OD_{600nm} values. Pellets collected from 25 mL of aerobic cultures were resuspended in a volume corresponding to the respective OD_{600nm} values. From the cell suspensions 0.8 mL

was mixed with 0.2 mL of 1 M NaOH for cell lysis and incubated for 20 h at room temperature in a rotary shaker.

Cell debris were removed by 3 min centrifugation at 2000 × *g* and 0.5 mL of the supernatant was collected for polyphosphate hydrolysis. To this purpose, 0.5 mL of 1 M HCl was added, mixed thoroughly by vortex, boiled for 10 min and centrifuged as before. Phosphate quantification was finally performed with the Malachite Green assay from the supernatants of NaOH-treated biomass samples (background phosphate concentration) and HCl-treated samples. Polyphosphate-derived phosphate concentrations were obtained by subtracting the background concentration for each HCl-treated samples.

Fe(II) quantification with ferrozine

Aliquots of 0.1 mL of HCl-acidified samples were mixed with 0.9 mL of ferrozine solution (0.5% (w/v) ferrozine in 100 mM HEPES buffer, pH 7.0), incubated 30 s and analyzed in a spectrophotometer at 562 nm. An acidified $FeCl_2$ solution was used as reference for calibration.

Protein quantification with the BCA assay

The BCA assay (Pierce) was used to quantify the protein concentration in biomass suspension samples. Aliquots of 0.1 mL of cell suspensions were boiled for 5 min and the protein concentration analyzed following the manufacturer's instructions. Bovine serum albumin was used as reference for calibration.

Genes and genomes comparison

To investigate the presence of genes involved in polyP synthesis and hydrolysis, the annotation files of *S. loihica* PV-4, *S. oneidensis* MR-1 and *S. putrefaciens* CN-32 (accession numbers GCF_000016065.1, GCF_000146165.2 and GCF_000016585.1, respectively) were used. Genomes comparison was performed using: (i) ACT (Artemis Comparison Tool) [46, 47], a pairwise comparisons tool between complete genome sequences and associated annotations. DNA sequences were used to identify and analyse regions of similarity and difference between genomes. (ii) ANI (average nucleotide identity) calculator from Kostas Lab [48,49] (http://enve-omics.ce.gatech.edu/ani/, used with default settings) was employed to measure the nucleotide genomic pairwise similarity between the coding regions of the genomes.

Author contribution

WMK performed the experiments, analyzed the data and wrote the manuscript. JM designed and performed the experiment and corrected the manuscript, EJ corrected the manuscript and PJ analyzed the data, wrote and corrected the manuscript.

References

1. Nriagu, J. O. & Moore, P. B. Phosphate Minerals. *Geological Magazine* **122,** 1–2 (1985).
2. Appenzeller, B. M. R. *et al.* Effect of adding phosphate to drinking water on bacterial growth in slightly and highly corroded pipes. *Water Res.* **35,** 1100–1105 (2001).
3. Cosmidis, J. *et al.* Biomineralization of iron-phosphates in the water column of Lake Pavin (Massif Central, France). *Geochim. Cosmochim. Acta* **126,** 78–96 (2014).
4. Gomes, F. M. *et al.* New insights into the in situ microscopic visualization and quantification of inorganic polyphosphate stores by 4',6-diamidino-2-phenylindole (DAPI)-staining. *Eur. J. Histochem.* **57,** 228–236 (2013).
5. Lubov, R. *et al.* The early stage of polyphosphate accumulation in *Saccharomyces cerevisiae*: comparative study by extraction and DAPI staining. *Adv. Biosci. Biotechnol.* **2,** 293–297 (2011).
6. Byung Hong, K. & Gadd, G. M. in *Bacterial physiology and metabolism* 488–489 (Cambridge University Press, 2008).
7. Mullan, A., Quinn, J. P. & McGrath, J. W. Enhanced phosphate uptake and polyphosphate accumulation in *Burkholderia cepacia* grown under low-pH conditions. *Microb. Ecol.* **44,** 69–77 (2002).
8. Günther, S. *et al.* Dynamics of polyphosphate-accumulating bacteria in wastewater treatment plant microbial communities detected via DAPI and tetracycline labeling. *Appl. Environ. Microbiol.* **75,** 2111–2121 (2009).
9. Tumlirsch, T., Sznajder, A. & Jendrossek, D. Formation of Polyphosphate by Polyphosphate kinases and its Relationship to PHB Accumulation in *Ralstonia eutropha* H16. *Appl. Environ. Microbiol.* **81,** 8277–8293 (2015).
10. Zhang, H. *et al. Gemmatimonas aurantiaca* gen. nov., sp. nov., a Gram-negative, aerobic, polyphosphate-accumulating micro-organism, the first cultured representative of the new bacterial phylum *Gemmatimonadetes* phyl. nov. *Int. J. Syst. Evol. Microbiol.* **53,** 1155–1163 (2003).
11. Tobin, K. M., McGrath, J. W., Mullan, A., Quinn, J. P. & O'Connor, K. E. Polyphosphate accumulation by *Pseudomonas putida* CA-3 and other medium-chain-length polyhydroxyalkanoate-accumulating bacteria under aerobic growth conditions. *Appl. Environ. Microbiol.* **73,** 1383–1387 (2007).
12. Sidat, M., Bux, F. & Kasan, H. C. Polyphosphate accumulation by bacteria isolated from activated sludge. *Water SA* **25,** 175–179 (1999).
13. Sivaswamy, V. *et al.* Multiple mechanisms of uranium immobilization by *Cellulomonas* sp. strain ES6. *Biotechnol. Bioeng.* **108,** 264–276 (2011).
14. Bojkovic, J. *et al.* Characterization of an *Acinetobacter baumannii* lptD deletion strain: Permeability defects and response to inhibition of lipopolysaccharide and fatty acid biosynthesis. *J. Bacteriol.* **198,** 731–741 (2016).
15. Azam, H. M. & Finneran, K. T. Fe(III) reduction-mediated phosphate removal as vivianite (Fe3(PO4)2.8H2O) in septic system wastewater. *Chemosphere* **97,** 1–9 (2014).
16. Wilfert, P., Kumar, P. S., Korving, L., Witkamp, G.-J. & Van Loosdrecht, M. C. M.

The relevance of phosphorus and iron chemistry to the recovery of phosphorus from wastewater: a review. *Environ. Sci. Technol.* 1–44 (2015).

17. Seviour, R. J., Mino, T. & Onuki, M. The microbiology of biological phosphorus removal in activated sludge systems. *FEMS Microbiol. Rev.* **27,** 99–127 (2003).

18. Kulakovskaya, T. V., Lichko, L. P. & Ryazanova, L. P. Diversity of phosphorus reserves in microorganisms. *Biochem.* **79,** 1602–1614 (2014).

19. Tarayre, C. *et al.* Characterisation of Phosphate Accumulating Organisms and Techniques for Polyphosphate Detection: A Review. *Sensors* **16,** 797 (2016).

20. Jansson, M. Phosphate uptake and utilization by bacteria and algae. *Hydrobiologia* **170,** 177–189 (1988).

21. Burow, L. C., Mabbett, A. N., McEwan, A. G., Bond, P. L. & Blackall, L. L. Bioenergetic models for acetate and phosphate transport in bacteria important in enhanced biological phosphorus removal. *Environ. Microbiol.* **10,** 87–98 (2008).

22. Comeau, Y., Hall, K., Hancock, R. & Oldham, W. Biochemical model for enhanced biological phosphorus removal. *Water Res.* **20,** 1511–1521 (1986).

23. Alcántara, C., Blasco, A., Zúñiga, M. & Monedero, V. Accumulation of polyphosphate in *Lactobacillus* spp. and its involvement in stress resistance. *Appl. Environ. Microbiol.* **80,** 1650–1659 (2014).

24. Shi, X., Rao, N. N. & Kornberg, A. Inorganic polyphosphate in *Bacillus cereus*: Motility, biofilm formation, and sporulation. *Proc. Natl. Acad. Sci.* **101,** 17061–17065 (2004).

25. Kooli, W. M. *et al.* Bacterial iron reduction and biogenic mineral formation for the stabilisation of corroded iron objects. *Sci. Rep.* **8,** 764 (2018).

26. Lee, J. H. & Hur, H. G. Intracellular uranium accumulation by *Shewanella* sp. HN-41 under the thiosulfate-reducing condition. *J. Korean Soc. Appl. Biol. Chem.* **57,** 117–121 (2014).

27. Rao, N. N., Roberts, M. F. & Torriani, A. Amount and Chain Length of Polyphosphates in *Escherchia coli* depend on cell growth conditions. *J. Bacteriol.* **162,** 242–247 (1985).

28. Deinema, M. H., Habets, L. H. A., Scholten, J., Turkstra, E. & Webers, H. A. A. M. The accumulation of polyphosphate in *Acinetobacter* spp. *FEMS Microbiol. Lett.* **9,** 275–279 (1980).

29. Smolders, G. J. F., van der Meij, J., van Loosdrecht, M. C. M. & Heijnen, J. J. Stoichiometric model of the aerobic metabolism of the biological phosphorus removal process. *Biotechnol. Bioeng.* **44,** 837–848 (1994).

30. Ohtake, H., Takahashi, K., Tsuzuki, Y. & Toda, K. Uptake and release of phosphate by a pure culture of *Acinetobacter calcoaceticus*. *Water Res.* **19,** 1587–1594 (1985).

31. Comeau, Y., Rabionwitz, B., Hall, K. J. & Oldham, W. K. Phosphate Release and Uptake in Enhanced Biological Phosphorus Removal from Wastewater. *ution Control Fed. Pumps* **59,** 707–715 (1987).

32. Chubar, N., Avramut, C. & Visser, T. Formation of manganese phosphate and manganese carbonate during long-term sorption of Mn(2+) by viable *Shewanella putrefaciens*: effects of contact time and temperature. *Environ. Sci. Process. Impacts*

17, 780–90 (2015).

33. Merzouki, M., Delgenès, J. P., Bernet, N., Moletta, R. & Benlemlih, M. Polyphosphate-accumulating and denitrifying bacteria isolated from anaerobic-anoxic and anaerobic-aerobic sequencing batch reactors. *Curr. Microbiol.* **38,** 9–17 (1999).

34. Konhauser, K. O. Diversity of bacterial iron mineralization. *Earth Sci. Rev.* **43,** 91–121 (1998).

35. Carey, C. C. & Rydin, E. Lake trophic status can be determined by the depth distribution of sediment phosphorus. *Limnol. Oceanogr.* **56,** 2051–2063 (2011).

36. Konhauser, K. *Introduction to geomicrobiology*. *European Journal of Soil Science* **58,** (Blackwell publishing, 2007).

37. Heiberg, L., Koch, C. B., Kjaergaard, C., Jensen, H. S. & Hans Christian, B. H. Vivianite Precipitation and Phosphate Sorption following Iron Reduction in Anoxic Soils. *J. Environ. Qual.* **41,** 938 (2012).

38. Rothe, M., Kleeberg, A. & Hupfer, M. The occurrence, identification and environmental relevance of vivianite in waterlogged soils and aquatic sediments. *Earth-Science Rev.* **158,** 51–64 (2016).

39. Diaz, J. *et al.* Marine polyphosphate: A key player in geologic phosphorus sequestration. *Science (80-.).* **320,** 652–655 (2008).

40. Jorand, F. *et al.* Assessment of vivianite formation in *Shewanella putrefaciens* culture. *Environ. Technol.* **21,** 1001–1005 (2000).

41. Urrutia, M. M., Roden, E. E., Fredrickson, J. K. & Zachara, J. M. Microbial and surface chemistry controls on reduction of synthetic Fe(III) oxide minerals by the dissimilatory iron-reducing bacterium *Shewanella alga*. *Geomicrobiol. J.* **15,** 269–291 (1998).

42. De Windt, W., Boon, N., Siciliano, S. D. & Verstraete, W. Cell density related H2 consumption in relation to anoxic Fe(0) corrosion and precipitation of corrosion products by <I>Shewanella oneidensis</i> MR-1. *Environ. Microbiol.* **5,** 1192–1202 (2003).

43. Casey, W. T. *et al.* The effect of polyphosphate kinase (*ppk*) deletion on polyhydroxyalkanoate accumulation and carbon metabolism in *Pseudomonas putida* KT2440. *Environ. Microbiol. Rep.* **5,** 740–746 (2013).

44. Wilfert, P. *et al.* Vivianite as an important iron phosphate precipitate in sewage treatment plants. *Water Res.* **104,** 449–460 (2016).

45. Aravind, J., Saranya, T. & Kanmani, P. Optimizing the production of Polyphosphate from *Acinetobacter towneri*. *Glob. J. Environ. Sci. Manag.* **1,** 63–70 (2015).

46. Carver, T. *et al.* Artemis and ACT: Viewing, annotating and comparing sequences stored in a relational database. *Bioinformatics* **24,** 2672–2676 (2008).

47. Carver, T. J. *et al.* ACT: The Artemis comparison tool. *Bioinformatics* **21,** 3422–3423 (2005).

48. Goris, J. *et al.* DNA-DNA hybridization values and their relationship to whole-genome sequence similarities. *Int. J. Syst. Evol. Microbiol.* **57,** 81–91 (2007).

49. Rodriguez-r, L. M. & Konstantinidis, K. T. Bypassing Cultivation To Identify Bacterial Species. *Microbe* **9,** 111–118 (2014).

Supplementary information

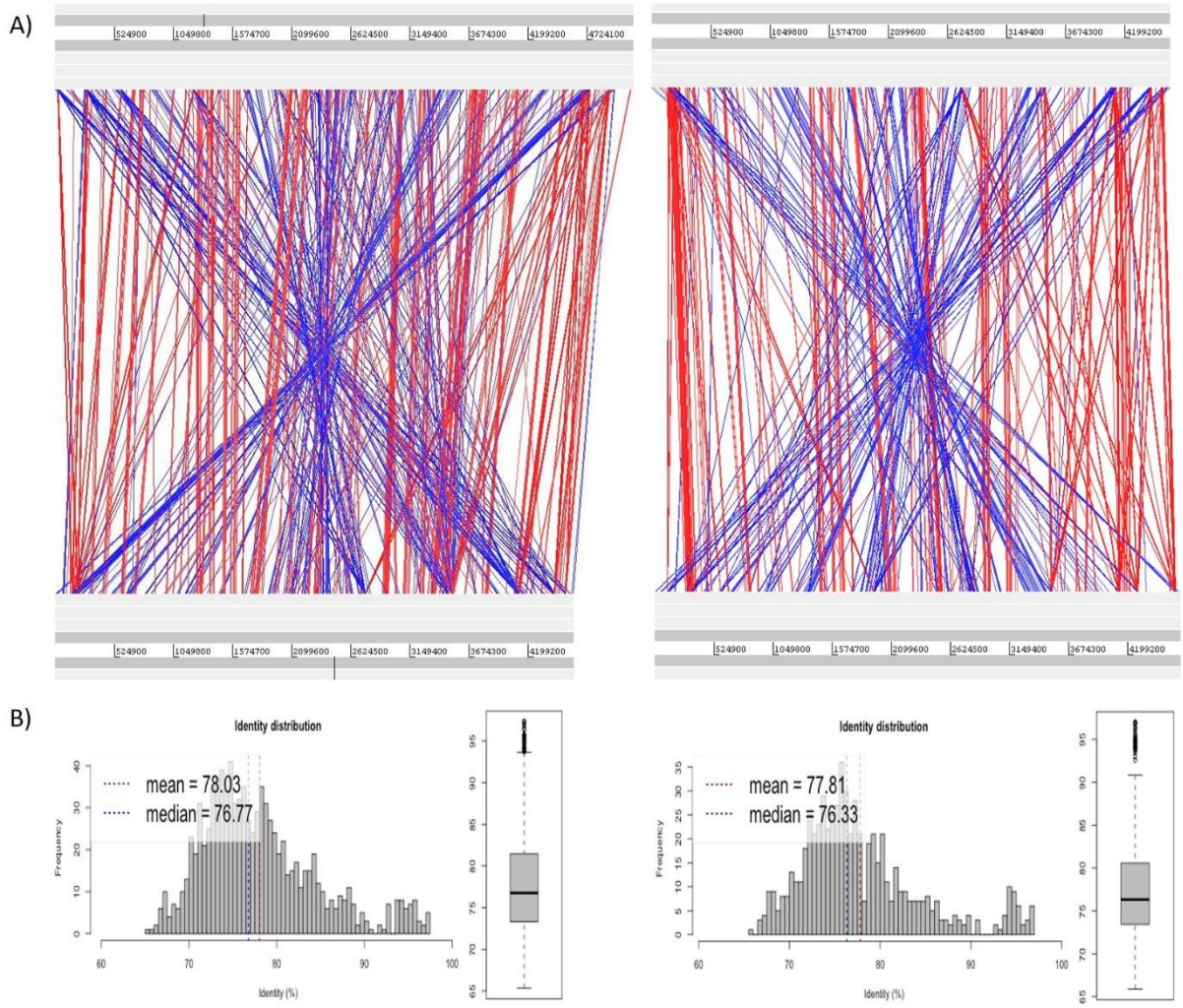

Figure SI1. Genomes comparison of *S. loihica* with *S. oneidensis* and *S. putrefaciens*. A) Genome comparison using ACT, of *S. loihica* (on the top) with: *S. oneidensis* (left image, on the bottom) and *S. putrefaciens* (right image, on the bottom). The red and blue bands represent the forward and reverse matches, respectively, the white colour represent the absence of matches. B) ANI results obtained when comparing *S. loihica* and *S. oneidensis* (left panel) and *S. loihica* and *S. putrefaciens* (right panel).

Chapter 5

Isolation of environmental iron reducing bacterial strains for biotechnological purposes

"The environment is everything that isn't me". Albert Einstein

Cudrefin, Neuchâtel

Co-authors: Nicole Jeanneret, Kelly Mottier, Sevasti Filippidou, Edith Joseph and Pilar Junier
Status: not intended for publication

Abstract

The use of *Shewanella loihica*, a halophilic microorganism for the treatment of corroded iron objects could be inconvenient because: (i) this bacterium needs salt for growth and for performing iron reduction and (ii) chloride ions are corrosive agents and should be removed from corroded iron objects. Thus, the need for other candidates that could perform iron reduction and biogenic mineral formation in the absence of a salt. A sampling of Swiss Lakes led to the selection of two environmental bacterial strains, CA23 and CU5, that reduced liquid and solid Fe(III) phases with and without NaCl addition to the reductive solution. Biochemical and physiological characterizations of these two strains were performed. Identification by sequencing analysis of the 16S rRNA gene showed that the two selected strains both belong to the *Aeromonas* Genus.

Introduction

In the field of metal conservation, many conservators are concerned with the phenomenon of corrosion of iron and its alloys, which are the most represented substrates for metal artworks. In fact, the preservation of iron artifacts encounters severe obstacles after excavation when different salt containing chloride ions contaminate the corrosion crust surrounding the object. As a result, flakes, cracks and finally loose of shape can be observed on the object [1].

Since conventional methods of iron conservation present some disadvantages [2,3], the use of microorganisms represents, nowadays, an environmentally friendly process that could be an alternative for the stabilization of corroded iron objects. Particularly, exploiting specific bacterial metabolisms for the transformation of reactive corrosion products such as lepidocrocite or akaganeite into more stable iron minerals represents a promising approach. To achieve this purpose, our previous studies focused on the capacities of two iron reducing bacteria (*Shewanella loihica* and *Desulfitobacterium hafniense*) to stabilize corrosion by forming stable iron minerals such as magnetite, siderite and vivianite [4,5]. Even if the results of these studies have demonstrated the feasibility of the concept in terms of the conversion of reactive corrosion products, these two candidates were not ideal. *S. loihica* needed salt to reduce reactive Fe(III) oxides and oxyhydroxides and *D. hafniense* required a complex medium for iron reduction and thus the culturing and mineral formation were difficult to control. Therefore, exploring other more suitable bacterial candidates was required.

The biological formation of minerals has been divided into two modes: biologically controlled mineralization in which bacteria genetically control the mineralization process, and biologically induced mineralization in which bacteria facilitate mineral formation by creating suitable external chemical environments [6]. The formation of magnetite by assimilatory iron reducing bacteria (AIRB) such as magnetotactic bacteria (e.g. *Magnetovibrio blakemoreii* MV-1 [7] and *Magnetospirillum gryphiswaldense* [8]) represent an example of biologically controlled mineralization. In magnetotatic bacteria, magnetite (Fe_3O_4) particles are formed inside bacterial cells within a specific internal membrane [9]. In contrast, the formation of magnetite and siderite by dissimilatory iron reduction bacteria (DIRB), such as *Shewanella alga* and *Thermoanaerobacter ethanolicus* represents a biologically facilitated mineralization in which the particles are formed extracellularly as a by-product of microbial Fe(III) respiration[10–13].

The formation of magnetite by magnetotactic bacteria (MTB) inside magnetosomes is a naturally occurring process [14,9] that could be a good alternative to the previous approaches

selected for our studies. MTB are naturally found in sediments of freshwater, or marine habitats as well as in stratified water columns. The occurrence of MTB depends on the presence of an oxic-anoxic interface (OAI). The largest numbers of MTB are typically found at or slightly below the OAI [15]. Some studies recommend to sample in sites with soft muddy sediments and with a water depth between 10 and 100 cm [16,17].

According to literature, an excess of Fe(III) ions as potential electron acceptors in the form of poorly crystalline Fe(III) oxides [18,19], makes of freshwater sediments a good source of dissimilatory metal reducers. Hence, in order to isolate MTB and DIRB, two sampling campaigns were conducted: in Lake Neuchâtel and in Lake Cadagno. Lake Neuchâtel presents numerous archaeological sites from La Tène period (Iron Age celtic civilization, 500 BC to 1 BC). This period was called la Tène due to the major discovery of a large number of iron objects excavated near a Swiss village called *La Tène* and belonging to the second Iron Age period (demonstrating that this lake has an evident metallurgical activity) [20,21].

Concerning Lake Cadagno, it is a meromictic lake hosting an interesting iron cycle. Various iron-reducing bacterial species were identified as part of the iron cycling system including representatives of *Magnetospirillum*, *Geobacter*, and *Rodoferax* [22]. We also simultaneously conducted a third isolation campaign for potential DIRB from the corrosion crust of iron plates naturally corroded in a marine environment. These plates were used in our previous studies as solid Fe(III) source.

In order to have candidates with the best performances for our proposed treatment, the aim of this work was to isolate new bacterial strains fulfilling simultaneously the following criteria: i) the strains should correspond to a facultative anaerobe. This was essential in order to use a simplified matrix for iron reduction as shown previously in the case of *S. lohica* (Chapter 2); ii) the strains should be halotolerant. This would ensure the tolerance to salt dislodged from the corrosion crust; and iii) the strains should reduce solid Fe(III) phases without the need of salt addition (in contrast to *S. loihica*; Chapter 2 and 3).

Results

NaCl tolerance

After testing the growth of bacterial isolates under anoxic and oxic conditions, we obtained 49 facultative anaerobe strains (SI1). The chloride tolerance experiment allowed us to select 22 interesting strains that could tolerate a salinity up to 4, 6 or 8% NaCl (no growth was observed beyond 8% NaCl). These 22 isolates demonstrated an optimal growth when NaCl concentration was between 0% and 2%. The results are presented in table 1 (see also Fig. SI1).

Table 1: NaCl tolerance of the studied isolates. The symbols highlighted in bold represent the optimal growth condition concerning the NaCl test. The symbol "+" means that we noticed a bacterial iron reduction, "+/-" means that the iron reduction capability was not clear and "-" means that we did not observe iron reduction. The symbols "+++", "++" and "+" represent the growth rate from higher to lower extent respectively.

Isolate ID	NaCl (%)					
	0	**2**	**4**	**6**	**8**	**10**
CA112	+	**++**	+	+/-	-	-
CA122	++	**+++**	+	+/-	-	-
CA142	+	**++**	+	+/-	-	-
CA23	++	**+++**	+	-	-	-
CA25	+	**++**	+/-	-	-	-
CA341	++	**+++**	+	-	-	-
CA421	**++**	+	+/-	+/-	+/-	+/-
CU1	**++**	**++**	+	-	-	-
CU1f	**++**	**++**	+	+/-	-	-
CU21	**++**	+	+	-	-	-
CU4	+	**++**	+	+/-	-	-
CU5	+	**++**	-	-	-	-
R1	++	**+++**	+	+/-	-	-
R5	**++**	**++**	+	-	-	-
R61	**++**	**++**	+	+/-	-	-
IPU1	**++**	**++**	+	+	+	+/-
IPU2	**++**	**++**	+	+	+	+/-
IPUE11	**++**	+	+	+	+	+
IPUE12	**++**	+	+	+	+	+
IPUE21	++	**+++**	**+++**	+	+	+
IPUE22	++	**+++**	**+++**	+	+	+
IPUE23	**++**	**++**	+	+/-	-	-

Morphological, physiological and biochemical characterization

The morphological, physiological and biochemical characterizations revealed that the 22 isolates have different properties and the results are shown in table 2.

Table 2: Morphological, physiological and biochemical characteristics of the bacterial isolates. "+" means that we noticed a positive reaction with the reagent, a motility and a presence of spores or that the bacterium is Gram positive."-" means that the bacterium is Gram negative or we observed a negative reaction with the chemicals tested. "+++", "++" and "+", "+/-" represent the growth rate from higher to lower extent respectively.

Isolate ID	Gram	KOH	Oxidase	Catalase	Microscopy	Motility	Spores	Aspect of colony	Nitrate reduction test			
									Growth NB+KNO3	N_2	Nitrites	+Zn
CA112	-	+	+	+	bacilli	+	-	Small, circular, smooth, raised, shiny	+++	-	-	-
CA122	-	+	+	+	Bacilli, slightly curved	+	-	Medium, circular, smooth, raised, shiny, mucoid	++	-	-	-
CA142	-	+	+	+	Bacilli, slightly curved	+	-	Medium, circular, smooth, raised, shiny, rhizoid	++	-	-	-
CA23	-	+	+	+	Bacilli, slightly spiral, form chains	+	-	Medium, circular, smooth, raised, shiny, mucoid	+++	-	+	-
CA25	-	+	+	+	Bacilli, slightly spiral	+	-	Medium, circular, smooth, raised, shiny, white	++++	-	+	-
CA341	-	+	+	+	Bacilli, slightly curved	+	-	Medium, circular, smooth, raised, shiny, mucoid	++++	+	-	+
CA421	+	-	-	+	Bacilli, slightly spiral, form chains	+	+	Large, smooth, very mucoid, orange	+/-	-	+	-
CU1	-	+	-	+	Bacilli, form chains	+	-	Small, circular, smooth, raised, shiny, yellowish	-	-	-	-
CU1f	-	+	-	+	Bacilli, form chains	+	-	Small, circular, smooth, raised, shiny, yellowish	-	-	-	-
CU21	-	+	-	-	Bacilli	+	-	Small, circular, smooth, raised, shiny, yellowish	+++	-	-	-
CU4	-	+	-	+	Bacilli	-	-	Small, circular, smooth, raised, shiny, yellowish	-	-	-	-
CU5	-	+	+	+	Bacilli	+	-	Medium, circular, smooth, raised, shiny	++	-	+	-
R1	-	+	+	+	Bacilli, slightly curved	+	-	Large, circular, smooth, raised, shiny, rhizoid	+++	-	-	-
R5	-	+	+	+	Bacilli, slightly curved	+	-	Medium, circular, smooth, transparent	+++	-	-	-
R61	-	+	+	+	Bacilli, slightly curved	+	-	Large, circular, smooth, raised, shiny	++	-	-	-
IPU1	+	-	-	+	Bacilli, slightly coiled, form chains	+	+	very small rhizoid colonies	+	-	+	-
IPU2	+	-	-	+	Bacilli, slightly coiled, form chains	+	+	very small rhizoid colonies	++	-	+	-
IPUE11	+	-	-	+	Bacilli, very motile	+	+	Medium, circular, smooth, raised, shiny, rhizoid	+	-	-	-
IPUE12	+	-	-	+	Bacilli, very motile	+	+	Medium, rhizoid, flat, transparent	+	-	+	-
IPUE21	+	-	-	+	Bacilli	-	+	Medium, circular, smooth, raised, shiny	+	-	+	-
IPUE22	+	-	-	+	Bacilli	+	+	Medium, circular, flat, shiny	+/-	-	+	-
IPUE23	+	-	-	+	Bacilli, form chains	+	+	Large, rhizoid, flat, opaque, dry	+	-	+	-

Iron reduction analyses

Fe(III) reduction was tested in a solution containing sodium lactate as the primary electron donor and with two Fe(III) sources: Fe(III) quinate as soluble source and corroded iron plates as solid source. This solution was amended or not with 2% NaCl (concentration observed for optimal growth for most of bacteria tested). The iron reduction test was performed under three conditions consecutively: a) Fe(III) quinate with 2%NaCl, b) Fe(III) quinate without NaCl and c) iron plates without NaCl addition to the culturing solution. Concerning the condition "a" Fe(III) reduction was observed for seven strains. The iron reduction capabilities of these seven strains were then tested under condition "b" and results showed that four strains were able to reduce soluble iron without salt addition (CA23, CA341, CU5 and IPU21) (Table 3, Fig. 1). Finally, the Fe(II) concentration was monitored under the condition "c" for these 4 strains. Its increase was indicative of Fe(III) reduction, allowing us to select two final candidates, CA23 and CU5 that could fulfil the criteria needed for the proposed treatment of corroded iron plates (Table 3, SI2-4).

Table 3: Fe(III) reduction of the studied isolates. The symbols highlighted in bold represent the strains that were able to reduce iron. The symbol "+" means that we noticed a bacterial iron reduction while "-" means that no iron reduction was observed. na= not applicable

Isolate ID	Fe(III) quinate reduction with 2%NaCl	Fe(III) quinate reduction without NaCl	Corroded IP reduction without NaCl
CA112	-	-	na
CA122	-	-	na
CA142	-	-	na
CA23	+	+	+
CA25	+	-	na
CA341	+	+	-
CA421	-	-	na
CU1	-	-	na
CU1f	-	-	na
CU21	-	-	na
CU4	-	-	na
CU5	+	+	+
R1	-	-	na
R5	-	-	na
R61	-	-	na
IPU1	-	-	na
IPU2	-	-	na
IPUE11	+	-	na
IPUE12	-	-	na
IPUE21	+	+	-
IPUE22	-	-	
IPUE23	+	-	na

Optimal growth conditions for the selected iron reducing bacteria

The seven isolates that previously showed a liquid Fe(III) reduction with 2% NaCl demonstrated an optimal growth when NaCl concentration was at 2% (except for IPUE11 and IPUE23) (table 2). Similarly, growth was noticed over a broad spectrum of temperature (17 to 40°C) and pH values (pH 5.5 to 9.5) for these same seven strains (SI5-6). Optimal growth was observed at temperatures between 30 and 40°C and pH between 6.5 and 8.5 (Table 4).

Table 4: Optimal temperature (°C) and pH, of selected isolates

Isolate ID	Optimal T°C	Optimal pH
CA23	30	7.5-8.5
CA25	37	7.5
CA341	40	7.5
CU5	30	7.5-8.5
IPUE11	40	6.5-7.5
IPUE21	40	6.5
IPUE23	30	7.5

Phylogenetic analysis

The phylogenetic tree in Fig. 1 shows that the 16S rRNA gene sequences of the strains placed the isolates within the *Bacillus, Stenotrophomonas, Aeromonas and Pseudomonas* genera respectively in the phyla of Firmicutes or Proteobacteria. The closest cultured relative, the percentage of similarity between the 16S rRNA gene sequence of the strain and its closest relative, as well as the 16S rRNA gene sequence length are summarized in table 5.

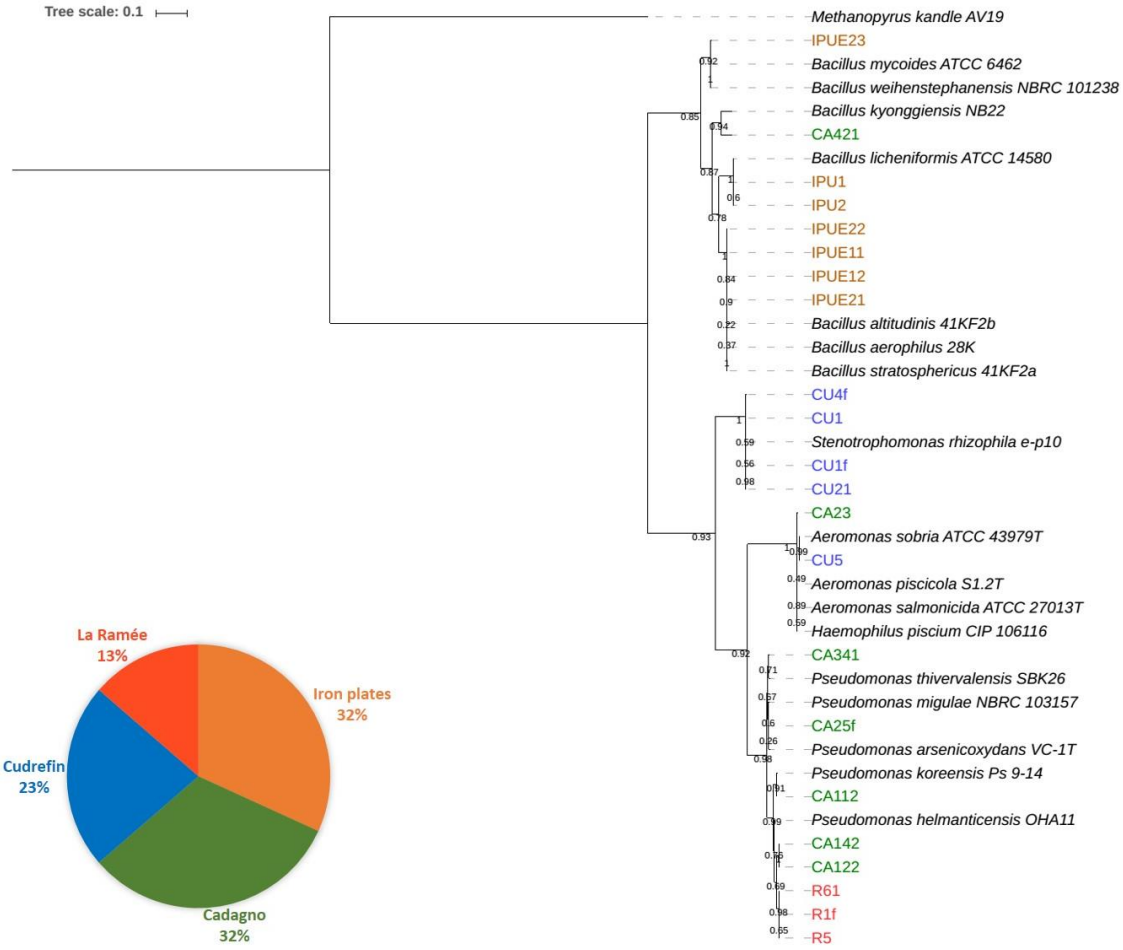

Figure 1: Maximum likelihood phylogenetic tree describing the phylogenetic relationship between isolates (code) and reference strains (species name indicated), the archaeon *Methanopyrus kandleri* was chosen as outgroup. Bootstrap values based on 100 replications were calculated and are expressed on the clades as decimal. The tree shows four main clusters: *Pseudomonas, Aeromonas, Stenotrophomonas* and *Bacillus*. Color codes for each isolate is described in the sector graph on the left where the percentage of selected isolates from each sampling location is mentioned.

Table 5: Similarity percentage, 16S sequence length and Genbank accession number of the isolates

Isolate ID	Closest relative	Similarity %	16S rDNA sequence lenght (bp)	Genbank Accession number
CA112	*Pseudomonas koreensis*	99.62	1325	KY457749
CA122	*Pseudomonas helmanticensis*	99.71	1399	KY457741
CA142	*Pseudomonas helmanticensis*	99.79	1403	KY457745
CA23	*Aeromonas piscicola*	100	1333	KY457758
CA25f	*Pseudomonas migulae*	99.56	1357	KY457746
CA341	*Pseudomonas thivervalensis*	99.49	1367	KY457754
CA421	*Bacillus kyonggiensis*	96.67	1419	KY457750
CU1	*Stenotrophomonas rhizophila*	99.93	1368	KY457759
CU1f	*Stenotrophomonas rhizophila*	99.79	1403	KY457743
CU21	*Stenotrophomonas rhizophila*	99.71	1402	KY457751
CU4f	*Stenotrophomonas rhizophila*	99.63	1362	KY457752
CU5	*Aeromonas sobria*	99.78	1366	KY457755
R1f	*Pseudomonas helmanticensis*	99.63	1358	KY457757
R5	*Pseudomonas helmanticensis*	98.93	1408	KY457748
R61	*Pseudomonas helmanticensis*	99.63	1362	KY457739
IPU1	*Bacillus licheniformis*	99.72	1414	KY457753
IPU2	*Bacillus licheniformis*	99.78	1369	KY457761
IPUE11	*Bacillus altitudinis*	100	1348	KY457742
IPUE12	*Bacillus altitudinis*	100	1376	KY457747
IPUE21	*Bacillus altitudinis*	100	1390	KY457740
IPUE22	*Bacillus altitudinis*	99.93	1345	KY457744
IPUE23	*Bacillus mycoides*	100	1386	KY457760

Discussion

In order to obtain bacterial strains that fulfil our requirements for the biotechnological treatment, the screening performed in this work followed these steps: selection of the facultative anaerobe isolates, then the chlorine tolerant ones, from these latter we performed a selection of iron reducers of soluble Fe(III) source (with 2% NaCl), followed by choosing the iron reducers of soluble Fe(III) without NaCl and finally the iron reducers of solid Fe(III) source without NaCl addition.

The selection of MTB as candidates for our treatment was not a successful strategy. Indeed, it is known that the cultivation of MTB could be delicate and difficult [23] and their use for our treatment could need an additional extraction step for obtaining magnetite, as this mineral is formed inside bacterial cells templated by a specific internal membrane [9]. In contrast, the formation of magnetite and siderite by Fe(III)-reducing bacteria, such as a *Thermoanerobacter ethanolicus*, TOR-39 or *Shewanella alga* (DIRB), represents biologically facilitated mineralization in which the particles are formed extracellularly as a byproduct of microbial Fe(III) respiration [13,24–26]. It was also reported that some dissimilatory iron reducing bacteria produce 5000 fold more magnetite per unit biomass than MTB [27]. For all these reasons, we directed our isolation to all the potential iron reducers that could be present in our samples, being sediments or corroded iron plates.

As a result of our sampling campaigns, we were able to isolate iron reducing bacteria from the genera *Bacillus*, *Pseudomonas, Stenotrophomonas* and *Aeromonas.* Many bacterial strains belonging to these genera were reported to reduce iron, like *Bacillus megaterium, Pseudomonas aeruginosa, Stenotrophomonas maltophilia* and *Aeromonas hydrophila* [28–31]. These results are in accordance with a previous study in Lake Cadagno where a 16S rRNA gene sequencing of the chemocline revealed the presence of an iron-reducing bacterial community including representatives of *Aeromonas* and *Pseudomonas* [22].

Many studies have reported that soluble iron reduction mechanism differ from those involved on the reduction of solid iron electron acceptors [32]. Indeed, the isolated strains behaved differently in contact with soluble or solid Fe(III) phases, suggesting their respective iron reduction mechanism could involve different components. Some of the strains were only able to reduce soluble Fe(III) species (CA341 and IPUE21) while CA23 and CU5, belonging to *Aeromonas* spp., were able to reduce both soluble and solid Fe(III) phases. These results suppose that the bacterial strains that do not reduce solid Fe(III) probably do not have the necessary molecules for that purposes like outer membrane cytochromes, external ferric reductase, electron shuttles or nanowires [32,33].

Iron reduction needs different environmental conditions to occur (pH, appropriate electron donor, among others) [32], less is known about the effect of sodium salt (Chapter 3). The results obtained regarding iron reduction with or without addition of sodium salt suggest that the presence of sodium salt influences bacterial ability to reduce iron. As an example, CA25 and IPUE23 were only able to reduce a soluble Fe(III) phase when sodium salt was added to the solution.

Aeromonas are known as human and animal pathogens (mainly fish) [34,35], but little is reported about the physiology and ecology of this group [28]. Iron-reducing *Aeromonas* spp. have been isolated from river sediments, heavy-metal-contaminated sites, and paddy soils [18,36,37], suggesting that *Aeromonas* could be an interesting group of Fe(III)-reducing bacteria along with other model groups such as *Geobacter* and *Shewanella* [36].

However, the iron reduction mechanism in *Aeromonas* has been poorly investigated and it would be important to determine whether iron reduction is linked to their potential pathogenicity and if these isolates are member of the predominant populations of iron reducers present in Lake Neuchâtel and Lake Cadagno.

The screening performed allowed us to select promising candidates for the stabilization of corroded iron objects. Some preliminary experiments showed that after few weeks of incubation with CA23 and CU5 a reactive corrosion layer was transformed into stable Fe(II) minerals. Further investigation on the minerals formed and a deeper understanding of the iron reduction mechanism is developed in Chapter 6.

Material and methods

Sampling

The sampling of water and sediments was performed in Lakes Neuchâtel and Cadagno in May and July 2014, respectively. From each location, sediment and water were collected in 3x1l plastic jars with loosened caps and stored at room temperature in the dark (Fig. 2A and 2B). Measurements of pH, conductivity, temperature and O_2 content were performed (Table 6).

Another sampling strategy was set up for the extraction of potential iron reducing bacteria from marine corroded iron plates. These iron plates (50 x 50 x 2-3 mm) were naturally corroded after one-year exposure in a marine environment containing chlorinated aerosols (French Institute of Corrosion, Brest, France). The orientation and position of the iron plates during exposure to marine environment were selected according to ISO 9223 standard. Plates were exposed south skyward at 45° from the horizontal. For the experiment, the plates were then cut in coupons of 10 x 10 x 2-3 mm and some of them were used as substrate after sterilization for our reduction test experiment.

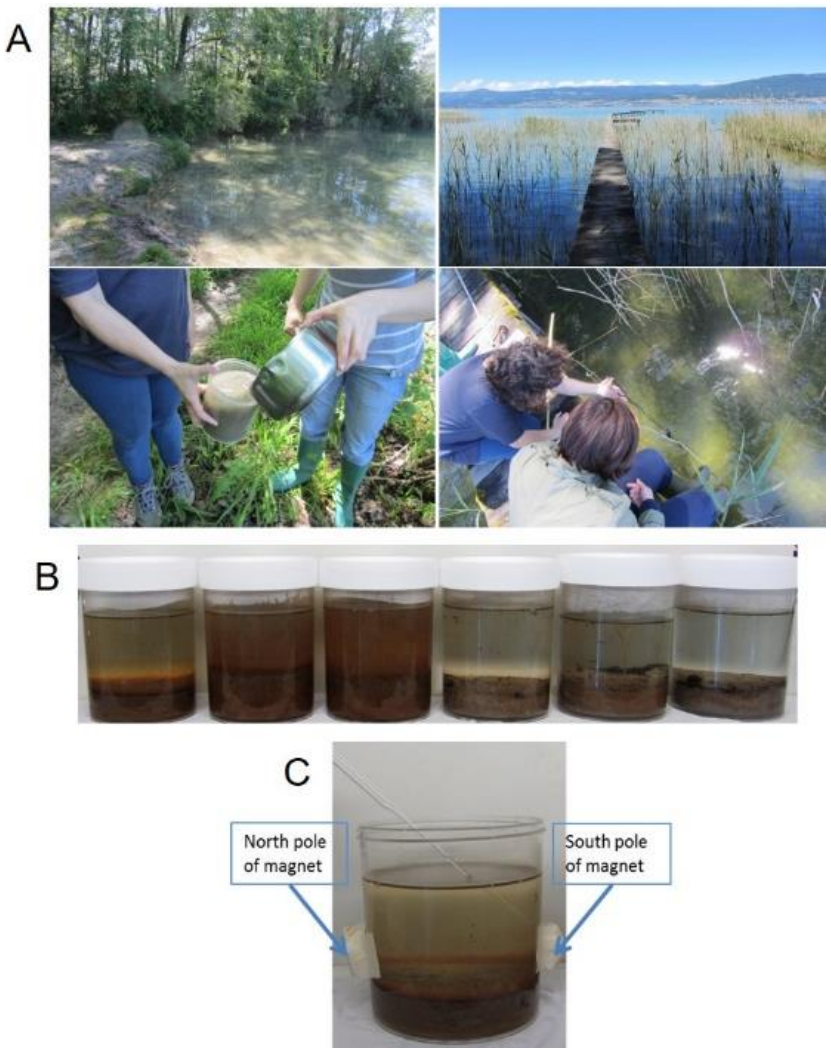

Figure 2: Sampling campaign performed in Lake Neuchâtel: A) La Ramée (left) and Cudrefin (right) sampling sites. B) Water and sediment samples collected from Lakes. C) Position of the magnets and collection of water sample during the MTB enrichment.

Table 6: Parameters values of the water in Lakes Neuchâtel (La Ramée and Cudrefin) and Cadagno recorded during sampling

	La Ramée 46° 0′ N, 6° 59′ E	**Cudrefin** 46° 57′ N, 7° 1′ E	**Cadagno** 46° 33′ N, 8° 43′ E
TºC	15.6	17.2	12
pH	8.24	8.19	8.48
O_2(mg/L)	8.10	9.32	11.84
Conductivity (µS/cm)	307	308	107

Enrichment and purification of MTB

The enrichment step (magnet collection technique) consisted on placing magnets on the sides of a plastic container, approximately 1 cm above the sediment-water interface (Figure 2C). After 30 min to 1 hour and using a sterile Pasteur pipette, the water was collected near the position of the south-pole bar magnet (for samples collected in the Northern hemisphere). Then, a capillary racetrack was used as a purification technique, where a sealed end Pasteur pipette was placed horizontally and plugged with cotton. After collecting a water sample with the pipette, a south magnet was placed near to the sealed end. According to the literature, a duration of 30 minutes is needed for allowing the migration of potential magnetotactic bacteria toward closed end of the Pasteur pipette. Finally, with a diamond pen, the sealed end was opened and the filtrate collected [14]. ¨

Enrichment of dissimilatory iron reducing bacteria

The enrichment of DIRB was done using either the water collected from the MTB enrichment step or the iron coupons. The latter consisted on incubating the coupons in sterile liquid LB medium (composition: 1% tryptone, 0.5% yeast extract, and 1% NaCl, seller LLG, no. 6271009) under agitation for 1 month. The liquid culture was collected then for the isolation and screening steps.

Isolation and screening of dissimilatory iron reducing bacteria

Screening for facultative anaerobes, halophilic and dissimilatory iron reducing bacteria was performed. The selection of facultative anaerobe bacteria from the different samples was initiated in solid ACA[38] and Farzan[39] media and incubated in anoxic 2.5 l jars at room temperature in the dark. Ferric citrate was the final electron acceptor (we also tested Sakaguchi media[40] but culturing was not successful as no growth was observed (data not shown). The 2.5 l jars were purchased from Sigma-Aldrich (reference: **28029 FLUKA)** An oxygen-depleted atmosphere was generated using anoxic sachets AnaerocultA® (Merck, reference: 1.13829.0001).

The composition of modified ACA medium per liter of deionized water is as follows: 2.38 g HEPES (*4-(2-hydroxyethyl)-1-piperazineethanesulfonic acid),* 3 g sodium pyruvate, 0.1g yeast extract, 3g soybean peptone (Merck), 0.34 g $NaNO_3$, 0.1 g KH_2PO_4, 0.15 g $MgSO_4 \cdot 7H_2O$, 3 g activated charcoal. The pH was adjusted to 7.0 with 1N NaOH. Ferric citrate (500 µM) and 1.4-dithiothreitol (DTT; 1 mM) were added aseptically after autoclaving[41]. Farzan medium contained the following in 983 ml of distilled water: 10 ml of vitamin solution, 5ml trace minerals solution, 2 ml 0.01M ferric quinate (see below), 0.45 ml 0.1% resazurin $C_{12}H_6NNaO_4$, 0.68 g potassium dihydrogen phosphate KH_2PO_4 0.12 g Sodium

nitrate $NaNO_3$, 0.37 g tartaric acid $C_4H_6O_6$, 0.37 g succinic acid $C_4H_6O_4$, 0.05 g sodium acetate $C_2H_3NaO_2$ and 0.05 g of Na-thioglycolate[39]. Ferric quinate (0.01M) contained in 100 ml distilled water: 0.27 g Fe(III) chloride $FeCl_3$ and 0.19 g quinic acid $C_7H_{12}O_6$[42]. The pH of the medium was adjusted to 6.8 with 1N NaOH. For preparation of solid media, 15 g/L agar (Difco) was added to the above liquid media. The media were autoclaved at 121°C for 15 min. Unless indicated otherwise, all chemicals were purchased from Sigma-Aldrich. Approximately after 1 month of incubation at room temperature and in the dark, colonies that developed in ACA and Farzan media were transferred into LB medium supplemented with 15 g/L agar. The bacteria that grew under oxic conditions on LB were characterized and tested for chlorides tolerance and then iron reduction.

NaCl tolerance

To evaluate the salt tolerance, the growth of the selected strains was monitored using modified tryptic soy broth (TSB) medium. Composition in one liter deionized water was 2.5 g glucose, 2.5 g K_2HPO_4, 3 g soy peptone, 17 g tryptic casein digest) supplemented with 0, 2, 4, 6, 8 or 10% (w/v) NaCl. The Absorbance was measured every hour for 24 h at 600nm using UV-Vis spectrophotometer (Fisher Scientific Genesys^{TM} 10s). The concentration at which growth appeared first was considered optimal; growth was considered positive when it was visible after 24 hours.

Morphological, physiological and Biochemical characterization

A light microscope (Leica DM R, Leica microsystems Wetzlar GmbH, Germany) was used to determine the motility (wet mounts) and evaluate Gram staining. In addition to NaCl tolerance and anaerobic/aerobic growth evaluation, a number of biochemical and physiological tests were made: Gram staining [43] and KOH reactions, cytochrome oxidase and catalase activities (determined using 1% TMPD (*N,N,N′,N′*-tetramethyl-*p*-phenylenediamine) reagent and 3% (w/v) H_2O_2 respectively)[44], nitrate reduction and sporulation tests. For the nitrate reduction test, nutrient broth (NB) medium (1 g/L beef extract, 2 g/L yeast extract, 5 g/L peptone and 5 g/L NaCl) was supplemented with 2g/L KNO_3. Nitrite was detected with naphthylamine/sulphanilic acid reagents and residual nitrate with zinc dust; production of N_2 was detected in inverted Durham tubes [45]. Sporulation test was done using nutrient agar medium (NB medium with 15 g/L agar) amended with $MnSO_4$ and observation was performed on wet mounts by phase contrast microscopy under oil immersion at 100×magnification. Commercial identification kit (API 20 NE, BioMerieux) were used for physiological and biochemical characterization of the final selected strains.

Iron reduction test

Subsequent to NaCl tolerance, isolates were transferred into a defined basal medium (BM) amended with sodium lactate (electron donor), Fe(III) quinate or iron coupons (electron acceptors) and sodium bicarbonate for iron reduction tests. BM contained the following (per liter of deionized water): 20 mM PIPES (piperazine-N,N′-bis(2-ethanesulfonic acid)) supplemented or not with 20 g NaCl. Preparation of anoxic liquid BM was achieved by heating the culture medium to 100°C, the culture media was then cooled to room temperature under a 100% N_2 headspace and subsequently dispensed under an anoxic atmosphere (100% N_2 headspace) into anoxic culture bottles sealed with thick butyl rubber stoppers (SUPELCO, no. 27232), crimped (using aluminum crimps, SUPELCO 508500), and autoclaved (20 min at 121°C).[46]

Electron donor, electron acceptor and sodium bicarbonate substrates were added to BM from sterile, anoxic (100% N_2 atmosphere) concentrated stock solutions to yield a final concentration of 5 mM, 10 mM and 50 mM respectively. Fe(III) was supplied in the form of soluble Fe(III) (Fe(III) quinate) or solid Fe(III) phases present on corroded iron coupons (that were sterilized under UV for two hours). The iron reduction experiments were performed first with 2% NaCl and Fe(III) quinate in the medium to test the iron reduction capabilities of the selected strains, then with Fe(III) quinate but without sodium salt to select strains that reduced Fe(III) without the need of sodium addition, and finally with iron plates and without sodium salt, as it is a requirement for the biotechnological treatment of corroded iron objects. To evaluate iron reduction, Fe(II) concentration was determined using the colorimetric Ferrozine assay [47].

Optimal temperature and pH selection

To determine the optimal temperature and pH, TSB medium was used (modified TSB amended with 2%NaCl). For the optimal temperature test, the pH was adjusted to 7. TSB medium was inoculated with overnight cultures of the selected strains (starting OD was 0.05). The temperatures chosen were 4, 17, room temperature (22-23°C) 30, 37, 40, 50 and 60°C and pH tested were 2.5, 3.5, 4.5, 5.5, 6.5, 7.5, 8.5, 9.5 and 10.5. The growth was monitored in 96 well plates under agitation using the spectrophotometer spectra xi3. The absorbance was measured every hour for 24h at 600nm. The temperature and pH at which growth appeared first was considered optimal; growth was considered positive when it was visible after 24 hours.

Sequence analysis of the 16S rRNA gene

Genomic DNA of the bacterial isolates was extracted using the Qiagen Qiamp DNA mini kit according to the manufacturer's instructions. A polymerase chain reaction (PCR)-mediated amplification was performed on the extracted DNA targeting the 16S rDNA, using GM3F and GM4R primer pairs [48]. Nearly full-length 16S rRNA sequences were obtained by sequencing the PCR products in addition with the primers 338F and 907R [48,49]. The amplicons were purified using a MultiScreen PCRμ96 filter plate (Millipore Cat n° SAVM 38401, USA) according to the manufacturer's instructions and sequenced using the services of GATC Biotech (Germany). The 16S rRNA genes were identified using EzTaxon, against EzTaxon's cultured isolates database[50]. The complete 16S rDNA sequences were deposited in GenBank under accession numbers listed in table 6.

Phylogenetic analysis

Sequences of the 16S rRNA gene corresponding to the 23 strains analyzed were aligned using MUSCLE software [51]. A maximum likelihood phylogenetic tree was built using PhyML software[52] with default parameters. Then an ornament tree was created using Newick utilities [53] and visualized using iTOLsoftware [54]. Reference sequences were obtained from the NCBI (National Center for Biotechnology Information).

Acknowledgments

The Swiss National Science Foundation (Ambizione grant PZ00P2_142514, P.I. Dr. Edith Joseph) for the funding of MAIA project (Microbes for archaeological iron Artifacts).
The Alpine Biology Centre Foundation for the infrastructure and Dr. Mauro Tonolla of the laboratory of applied microbiology of SUPSI and the microbiology unit of the university of Geneva, Switzerland.

Author contribution

WMK designed and performed the experiments, analyzed the data and wrote the manuscript. NJ and KM performed the experiment, SF helped in the DNA extraction, 16S amplification and analysis, EJ and PJ analyzed the data, wrote and corrected the manuscript.

References

1. Watkinson, D. & Lewis, M. ss Great Britain iron hull: modelling corrosion to define storage relative humidity. *Met. 2004* **44,** 88–102 (2004).

2. Selwyn, L. overview of archeological iron: the corrosion problem, key factors affecting treatment and gaps in current knowledge. *Natl. museum Aust. Canberra* 294–306 (2004).

3. Watkinson, D. Measuring effectiveness of washing methods for corrosion control of archaeological iron: problems and challenges. *Corros. Eng. Sci. Technol.* **45,** 400–406 (2010).

4. Kooli, W. M. *et al.* Bacterial iron reduction and biogenic mineral formation for the stabilisation of corroded iron objects. *Sci. Rep.* **8,** 764 (2018).

5. Comensoli, L. *et al.* Use of bacteria to stabilize archaeological iron. *Appl. Environ. Microbiol.* (2017). doi:10.1128/AEM.03478-16

6. Frankel, R. B. & Bazylinski, D. a. Biologically induced mineralization by bacteria. *Rev. Mineral. Geochemistry* **54,** 95–114 (2003).

7. Moisescu, C., Bonneville, S., Tobler, D., Ardelean, I. & Benning, L. G. Controlled biomineralization of magnetite (Fe3O4) by Magnetospirillum gryphiswaldense. *Mineral. Mag.* **72,** 333–336 (2008).

8. Hedrich, S., Schlomann, M. & Johnson, D. B. The iron-oxidizing proteobacteria. *Microbiology* **157,** 1551–1564 (2011).

9. Blakemore, R. Magnetotactic Bacteria. *Science (80-.).* **190,** 377–379 (1982).

10. Roh, Y., Vali, H., Phelps, T. J. & Moon, J.-W. Extracellular Synthesis of Magnetite and Metal-Substituted Magnetite Nanoparticles. *J. Nanosci. Nanotechnol.* **6,** 3517–3520 (2006).

11. Lee, J. H., Roh, Y. & Hur, H. G. Microbial production and characterization of superparamagnetic magnetite nanoparticles by *Shewanella* sp. HN-41. *J. Microbiol. Biotechnol.* **18,** 1572–1577 (2008).

12. Ma, Y., Galinski, E. a., Grant, W. D., Oren, a. & Ventosa, a. Halophiles 2010: Life in Saline Environments. *Appl. Environ. Microbiol.* **76,** 6971–6981 (2010).

13. Roh, Y. *et al.* Biogeochemical and environmental factors in Fe biomineralization: magnetite and siderite formartion. *Clays Clay Miner.* **51,** 83–95 (2003).

14. Oestreicher, Z., Lower, S. K., Lin, W. & Lower, B. H. Collection, Isolation and Enrichment of Naturally Occurring Magnetotactic Bacteria from the Environment. *J. Vis. Exp.* (2012). doi:10.3791/50123

15. Lefevre, C. T. & Bazylinski, D. a. Ecology, Diversity, and Evolution of Magnetotactic Bacteria. *Microbiol. Mol. Biol. Rev.* **77,** 497–526 (2013).

16. Schüler, D., Spring, S. & Bazylinski, D. a. Improved Technique for the Isolation of Magnetotactic Spirilla from a Freshwater Sediment and their Phylogenetic Characterization. *Syst. Appl. Microbiol.* **22,** 466–471 (1999).

17. Chavadar, M. S. & Bajekal, S. S. Magnetotactic bacteria from Lonar lake. *Curr. Sci.* **96,** 957–959 (2009).

18. Knight, V. & Blakemore, R. Reduction of diverse electron acceptors by *Aeromonas hydrophila*. *Arch. Microbiol.* **169,** 239–248 (1998).

19. Beliaev, A. S. & Saffarini, D. a. *Shewanella putrefaciens mtrB* encodes an outer Membrane Protein Required for Fe(III) and Mn(IV) Reduction. *J. Bacteriol* **180,** (1998).

20. Councilparis, E. N. Position Paper on the Encouragement of Cultural Tourism. *Forum Am. Bar Assoc.* 1–20 (2006).

21. Purdy, B. A. *Wet Site Archaeology*. (Taylor & Francis, 1990).

22. S. Berg, J. *et al.* Intensive cryptic microbial iron reduction in the low iron water column of the meromictic Lake Cadagno. *Environ. Microbiol.* **18,** 5288–5302 (2016).

23. Tajer Mohammad Ghazvini, P., Kasra Kermanshahi, R., Nozad Golikand, A. & Sadeghizadeh, M. Isolation and characterization of a novel magnetotactic bacterium from Iran: Iron uptake and producing magnetic nanoparticles in Alphaproteobacterium MTB-KTN90. *Jundishapur J. Microbiol.* **7,** 1–10 (2014).

24. Ruebush, S. S., Brantley, S. L. & Tien, M. Reduction of Soluble and Insoluble Iron Forms by Membrane Fractions of *Shewanella oneidensis* Grown under Aerobic and Anaerobic Conditions. *App* **72,** 2925–2935 (2006).

25. Lovley, D. R. Dissimilatory Fe(III) and Mn(IV) reduction. *Microbiol. Rev.* **55,** 259–287 (1991).

26. Lovley, D. R. Dissimilatory metal reduction: from early life to bioremediation. Volume 68, number 5, 231-237 (2002).

27. Moon, J.-W. *et al.* Microbial preparation of metal-substituted magnetite nanoparticles. *J. Microbiol. Methods* **70,** 150–158 (2007).

28. Wang, X. J., Chen, X. P., Kappler, A., Sun, G. X. & Zhu, Y. G. Arsenic binding to iron(II) minerals produced by an iron(III)reducing *Aeromonas* strain isolated from paddy soil. *Environ. Toxicol. Chem.* **28,** 2255–2262 (2009).

29. Lovley, D. R. Organic matter mineralization with the reduction of ferric iron: A review. *Geomicrobiol. J.* **5,** 375–399 (1987).

30. Ivanov, V., Stabnikov, V., Zhuang, W. Q., Tay, J. H. & Tay, S. T. L. Phosphate removal from the returned liquor of municipal wastewater treatment plant using iron-reducing bacteria. *J. Appl. Microbiol.* **98,** 1152–1161 (2005).

31. Valencia-Cantero, E. *et al.* Role of dissimilatory fermentative iron-reducing bacteria in Fe uptake by common bean (Phaseolus vulgaris L.) plants grown in alkaline soil. *Plant Soil* **291,** 263–273 (2007).

32. Weber, K. a., Achenbach, L. a. & Coates, J. D. Microorganisms pumping iron: anaerobic microbial iron oxidation and reduction. *Nat. Rev. Microbiol.* **4,** 752–764 (2006).

33. Pham, C. A. *et al.* A novel electrochemically active and Fe(III)-reducing bacterium phylogenetically related to *Aeromonas hydrophila*, isolated from a microbial fuel cell. *FEMS Microbiol. Lett.* **223,** 129–134 (2003).

34. Ding, T., Li, T., Wang, Z. & Li, J. Curcumin liposomes interfere with quorum sensing system of *Aeromonas sobria* and in silico analysis. *Sci. Rep.* **7,** 8612 (2017).

35. Igbinosa, I. H., Igumbor, E. U., Aghdasi, F., Tom, M. & Okoh, A. I. Emerging *Aeromonas* Species Infections and Their Significance in Public Health. *Sci. World J.* 1–13 (2012). doi:10.1100/2012/625023

36. Yao, Z. *et al.* Quantitative proteomic analysis of cell envelope preparations under iron starvation stress in *Aeromonas hydrophila*. *BMC Microbiol.* **16,** 161 (2016).

37. Scala, D. J., Hacherl, E. L., Cowan, R., Young, L. Y. & Kosson, D. S. Characterization of Fe(III)-reducing enrichment cultures and isolation of Fe(III)-reducing bacteria from the Savannah River site, South Carolina. *Res. Microbiol.* **157,** 772–783 (2006).

38. Lefevre, C. T. *et al.* Insight into the Evolution of Magnetotaxis in *Magnetospirillum* spp., Based on mam Gene Phylogeny. *Appl. Environ. Microbiol.* **78,** 7238–7248 (2012).

39. Farzan, F., Shojaosadati, S. A. & Tehrani, H. A. A preliminary report on the isolation and identification of magnetotactic bacteria from Iran environment. *Iran. J. Biotechnol.* **8,** 98–102 (2010).

40. Sakagushi., T., Tsujimura., N. & Matsunaga., T. A novel method for isolation of magnetic bacteria without magnetic collection using magnetotaxis. *Microbiol* **26,** 1996 (1996).

41. Schultheiss, D. & Schüler, D. Development of a genetic system for *Magnetospirillum gryphiswaldense*. *Arch. Microbiol.* **179,** 89–94 (2003).

42. Martins, J. L., Keim, C. N., Farina, M., Kachar, B. & Lins, U. Deep-etching electron microscopy of cells of *Magnetospirillum magnetotacticum*: Evidence for filamentous structures connecting the magnetosome chain to the cell surface. *Curr. Microbiol.* **54,** 1–4 (2007).

43. Dussault, H. P. An improved technique for staining red halophilic bacteria. *J. Bacteriol.* **70,** 484–485 (1955).

44. Matsunaga, T., Sakaguchi, T. & Tadakoro, F. Magnetite formation by a magnetic bacterium capable of growing aerobically. *Appl. Microbiol. Biotechnol.* **35,** 651–655 (1991).

45. Ventosa, A., Quesada, E., Rodriguez-Valera, F., Ruiz-Berraquero, F. & Ramos-Cormenzana, A. Numerical Taxonomy of Moderately Halophilic Gram-negative Rods. *J. Gen. Microbiol.* **128,** 1959–1968 (1982).

46. Hungate, R. E. Chapter IV A Roll Tube Method for Cultivation of Strict Anaerobes. *Methods Microbiol.* **3,** 117–132 (1969).

47. Bell, P. E., Mills, a L. & Herman, J. S. Biogeochemical Conditions Favoring Magnetite Formation during Anaerobic Iron Reduction. *Appl. Environ. Microbiol.* **53,** 2610–2616 (1987).

48. Muyzer, G., Teske, A., Wirsen, C. O. & Jannasch, H. W. Phylogenetic relationships of *Thiomicrospira* species and their identification in deep-sea hydrothermal vent samples by denaturing gradient gel electrophoresis of 16S rDNA fragments. *Arch. Microbiol.* **164,** 165–172 (1995).

49. Ovreås, L., Forney, L., Daae, F. L. & Torsvik, V. Distribution of bacteroplankton in meromictic lake Sælenvannet, as deteremined by denaturing gradient gel electrophorresis of PCR-amplified gene fragments coding for 16S rRNA. *Appl. Environ. Microbiol.* **63,** 3367–3373 (1997).

50. Kim, O. S. *et al.* Introducing EzTaxon-e: A prokaryotic 16s rRNA gene sequence database with phylotypes that represent uncultured species. *Int. J. Syst. Evol. Microbiol.* **62,** 716–721 (2012).

51. Edgar, R. C. MUSCLE: Multiple sequence alignment with high accuracy and high throughput. *Nucleic Acids Res.* **32,** 1792–1797 (2004).

52. Guindon, S. *et al.* New algorithms and methods to estimate maximum-likelihood phylogenies: Assessing the performance of PhyML 3.0. *Syst. Biol.* **59,** 307–321 (2010).

53. Junier, T. & Zdobnov, E. M. The Newick utilities: high-throughput phylogenetic tree processing in the UNIX shell. *Bioinformatics* **26,** 1669–1670 (2010).

54. Letunic, I. & Bork, P. Interactive Tree Of Life (iTOL): An online tool for phylogenetic tree display and annotation. *Bioinformatics* **23,** 127–128 (2007).

Supplementary information

Table SI1: Screening of facultative anaerobe bacteria

Isolate ID	Microaerobiosis	Aerobiosis	Anaerobiosis
CA111	+	+	+
CA11f	+	-	-
CA112	+	+	+
CA122	+	+	+
CA12f	+	+	-
CA131	+	+	+
CA132	+	+	-
CA142	+	+	+
CA15	+	+	-
CA15f	+	+	-
CA16	+	-	-
CA17	+	-	-
CA18	+	+	-
CA21	+	+	-
CA21f	+	+	+
CA22	+	+	-
CA22f	+	+	-
CA23	+	+	+
CA23f	+	+	-
CA24	+	-	-
CA24f	+	+	-
CA25f	+	+	+
CA261f	+	+	-
CA2621f	+	+	+
CA2622f	+	+	-
CA311	+	+	+
CA31f	+	+	-
CA312	+	+	+
CA321	+	+	+
CA322	+	+	+
CA32f	+	+	+
CA331f	+	+	+
CA332f	+	+	+
CA341	+	+	+
CA342	+	+	+
CA34f	+	+	+
CA35f	+	+	+
CA36f	+	+	+
CA41f	+	+	+
CA421	+	+	+
CA42f	+	-	-
CA43	+	+	+
CA43f	+	-	+
CA45	+	-	-

CA45f	+	+	+
CA46f	+	+	-
CA47	+	-	-
CA48	+	+	-
CU1	+	+	+
CU1f	+	+	+
CU21	+	+	+
CU22	+	+	+
CU2f	+	+	+
CU3	+	+	+
CU3f	+	+	-
CU4	+	+	+
CU4f	+	+	+
CU5	+	+	+
CU5f	+	+	-
CU6	+	+	+
CU6f	+	-	-
CU7	+	-	-
CU7f	+	-	-
CU8	+	+	+
CU8f	+	+	-
IPU1	+	+	+
IPU2	+	+	+
IPUE11	+	+	+
IPUE12	+	+	+
IPUE21	+	+	+
IPUE22	+	+	+
IPUE23	+	+	+
R1f	+	+	+
R2f	+	+	+
R4f	+	+	-
R5	+	+	+
R5f	+	+	+
R61	+	+	+
R62	+	-	-
R6f	+	+	-
R71	+	+	-
R72	+	+	-
R7f	+	+	-
R8	+	+	-
R8f	+	+	-

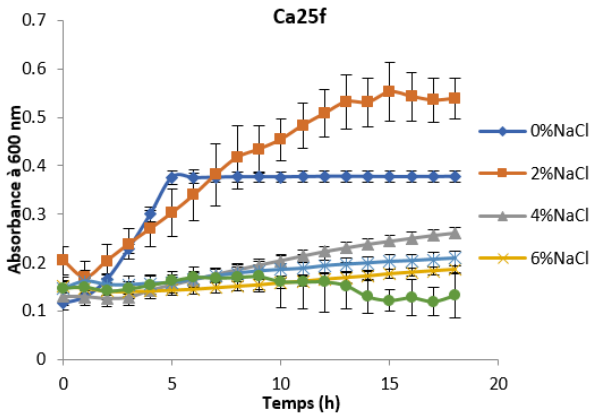
Ca25f
Absorbance à 600 nm
Temps (h)
0%NaCl
2%NaCl
4%NaCl
6%NaCl

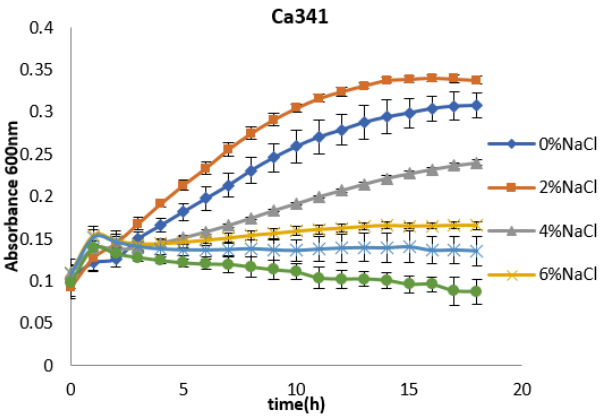
Ca341
Absorbance 600nm
time(h)
0%NaCl
2%NaCl
4%NaCl
6%NaCl

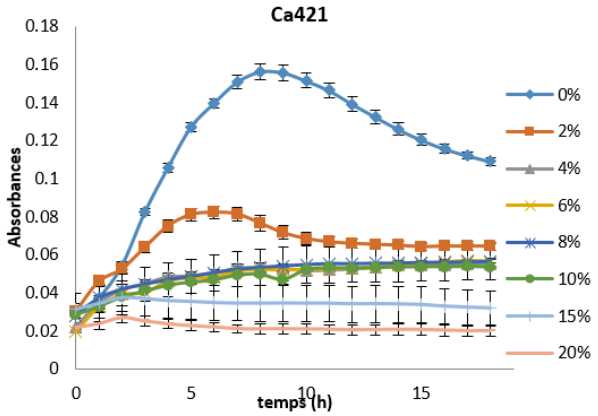
Ca421
Absorbances
temps (h)
0%
2%
4%
6%
8%
10%
15%
20%

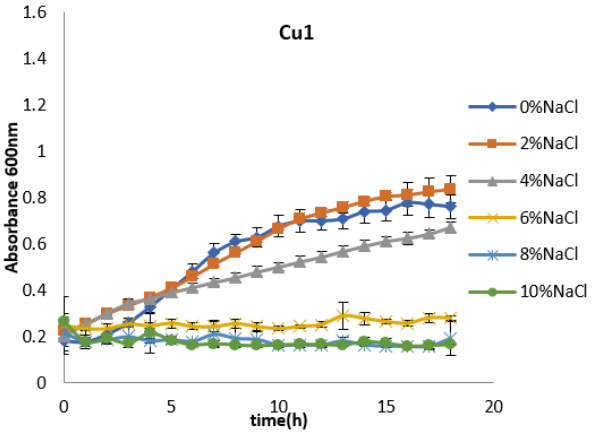
Cu1
Absorbance 600nm
time(h)
0%NaCl
2%NaCl
4%NaCl
6%NaCl
8%NaCl
10%NaCl

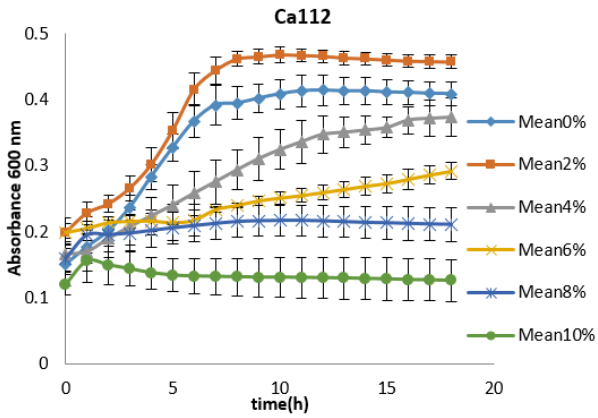
Ca112
Absorbance 600 nm
time(h)
Mean0%
Mean2%
Mean4%
Mean6%
Mean8%
Mean10%

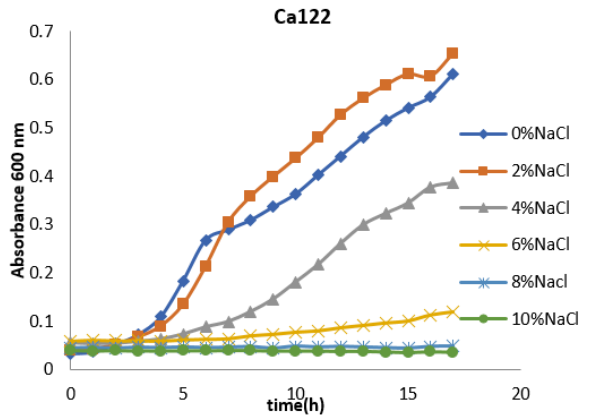
Ca122
Absorbance 600 nm
time(h)
0%NaCl
2%NaCl
4%NaCl
6%NaCl
8%Nacl
10%NaCl

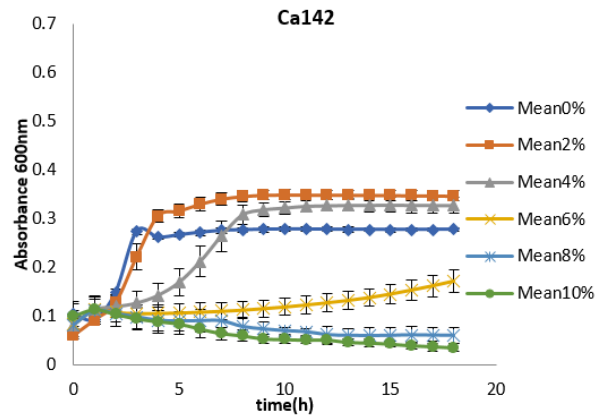
Ca142
Absorbance 600nm
time(h)
Mean0%
Mean2%
Mean4%
Mean6%
Mean8%
Mean10%

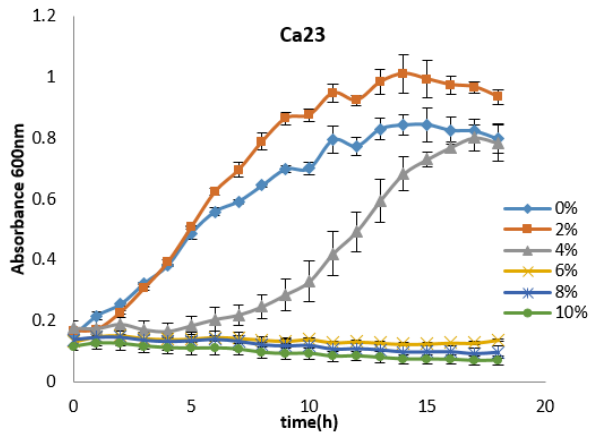
Ca23
Absorbance 600nm
time(h)
0%
2%
4%
6%
8%
10%

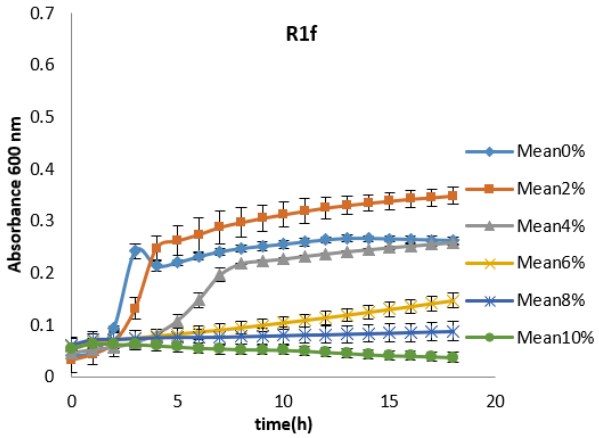
R1f
Absorbance 600 nm
time(h)
Mean0%
Mean2%
Mean4%
Mean6%
Mean8%
Mean10%

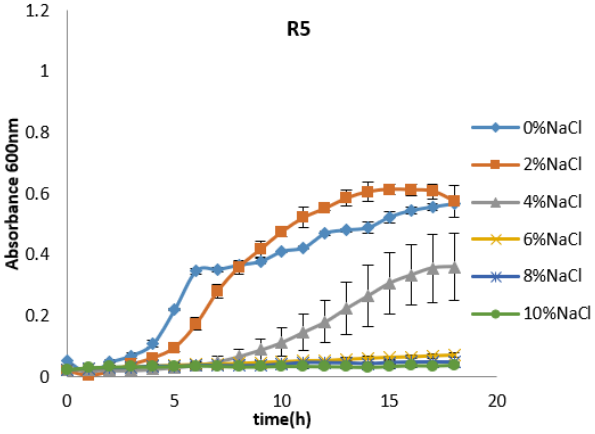
R5
Absorbance 600nm
time(h)
0%NaCl
2%NaCl
4%NaCl
6%NaCl
8%NaCl
10%NaCl

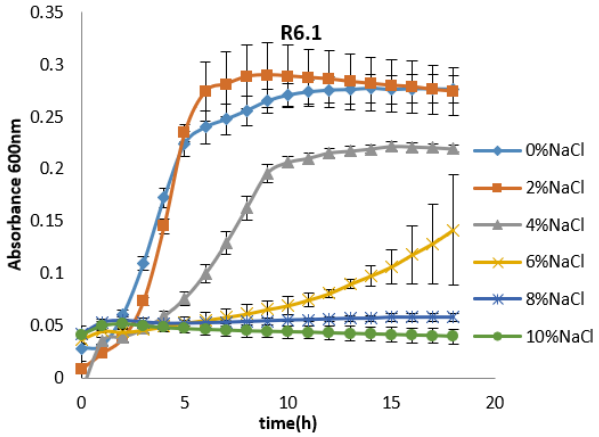
R6.1
Absorbance 600nm
time(h)
0%NaCl
2%NaCl
4%NaCl
6%NaCl
8%NaCl
10%NaCl

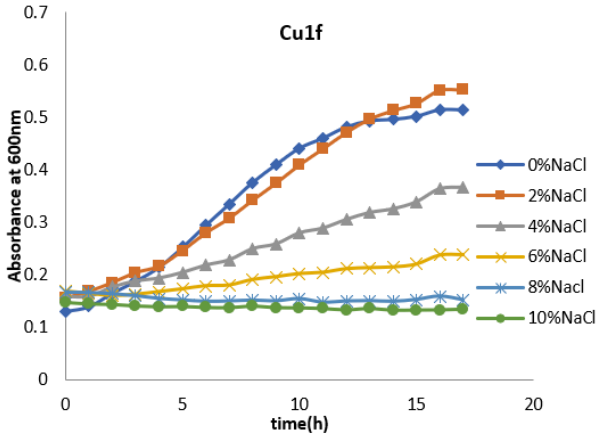
Cu1f
Absorbance at 600nm
time(h)
0%NaCl
2%NaCl
4%NaCl
6%NaCl
8%Nacl
10%NaCl

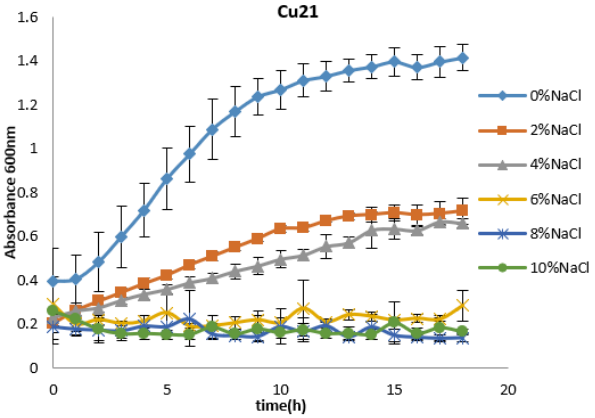
Cu21
Absorbance 600nm
time(h)
0%NaCl
2%NaCl
4%NaCl
6%NaCl
8%NaCl
10%NaCl

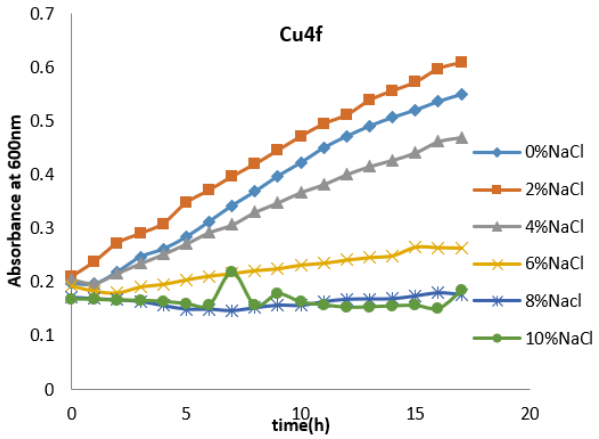
Cu4f
Absorbance at 600nm
time(h)
0%NaCl
2%NaCl
4%NaCl
6%NaCl
8%Nacl
10%NaCl

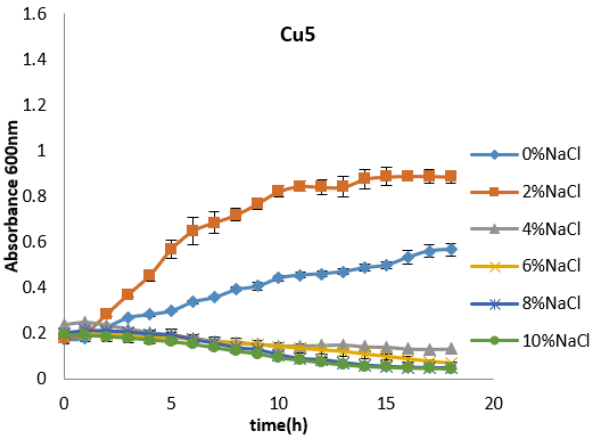
Cu5
Absorbance 600nm
time(h)
0%NaCl
2%NaCl
4%NaCl
6%NaCl
8%NaCl
10%NaCl

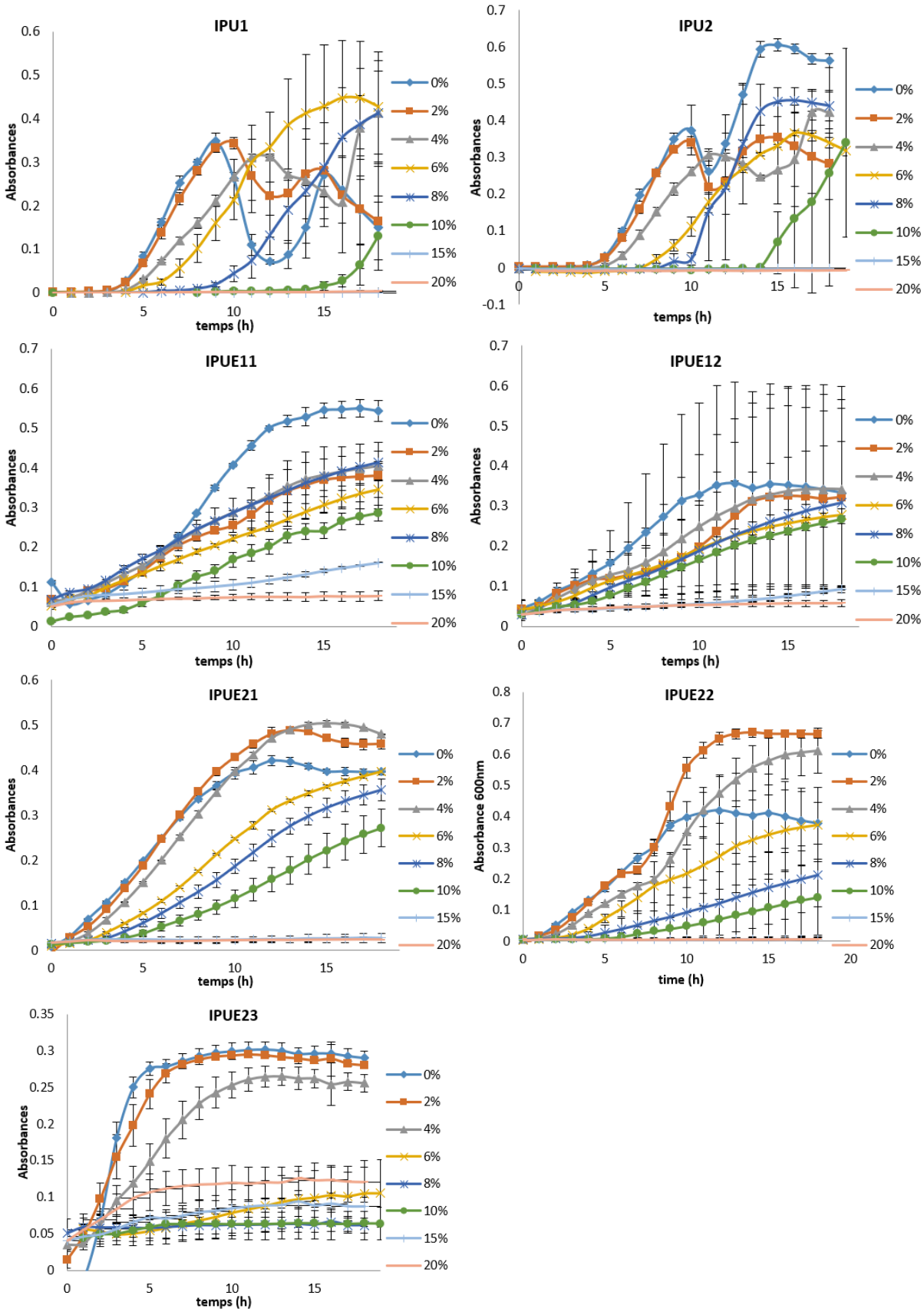

Figure SI1: Evaluation of NaCl tolerance of the bacterial isolate

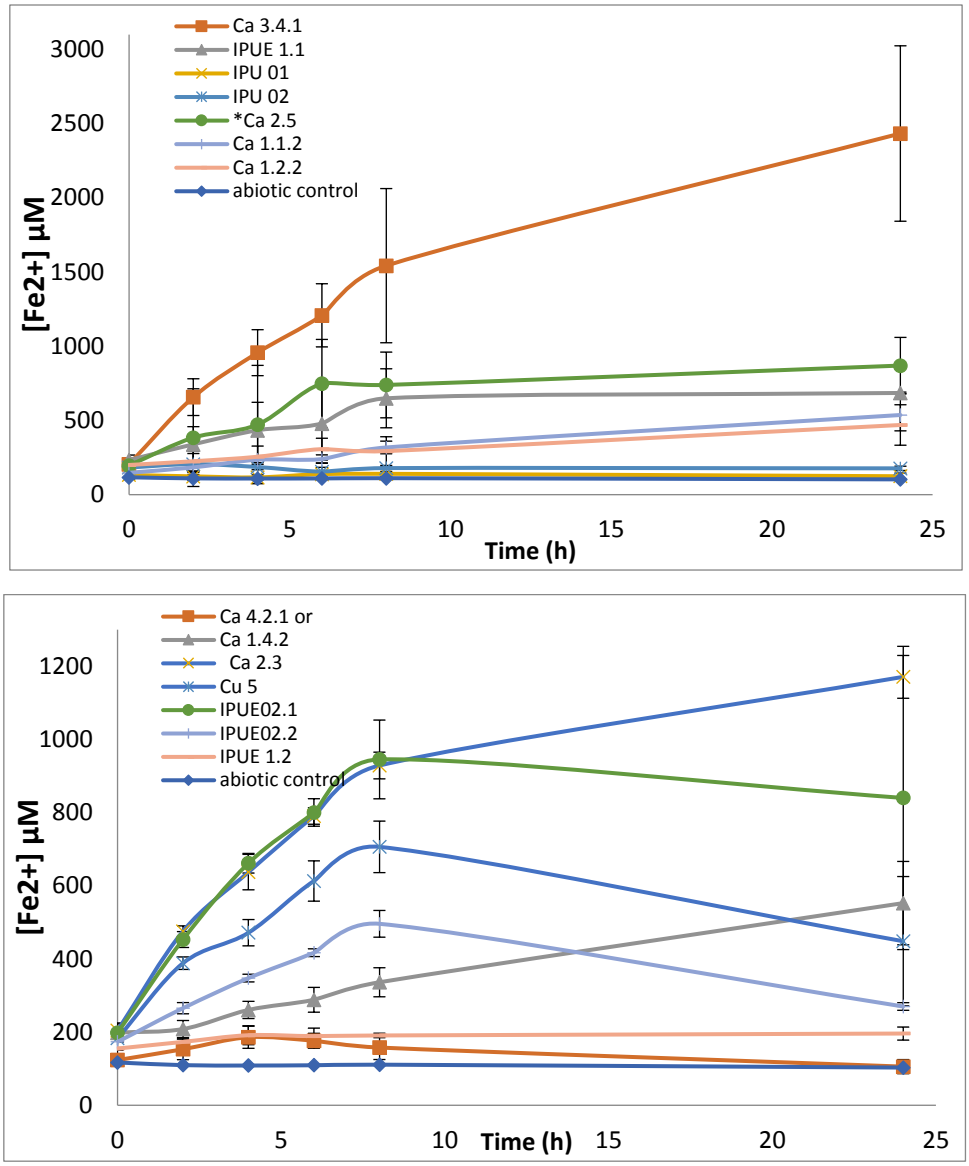

Figure SI2: Evaluation of soluble iron reduction with 2%NaCl of some bacterial isolates, using Fe(III) quinate.

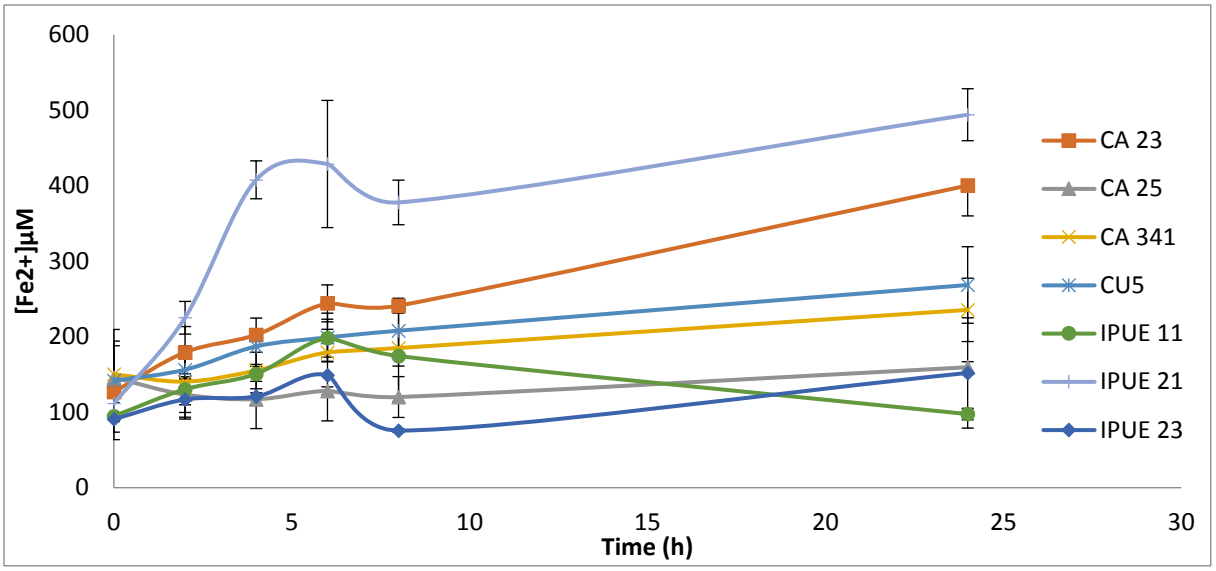

Figure SI3: Evaluation of soluble iron reduction with 0%NaCl of some bacterial isolates that were able to reduce Fe(III) quinate with 2%NaCl

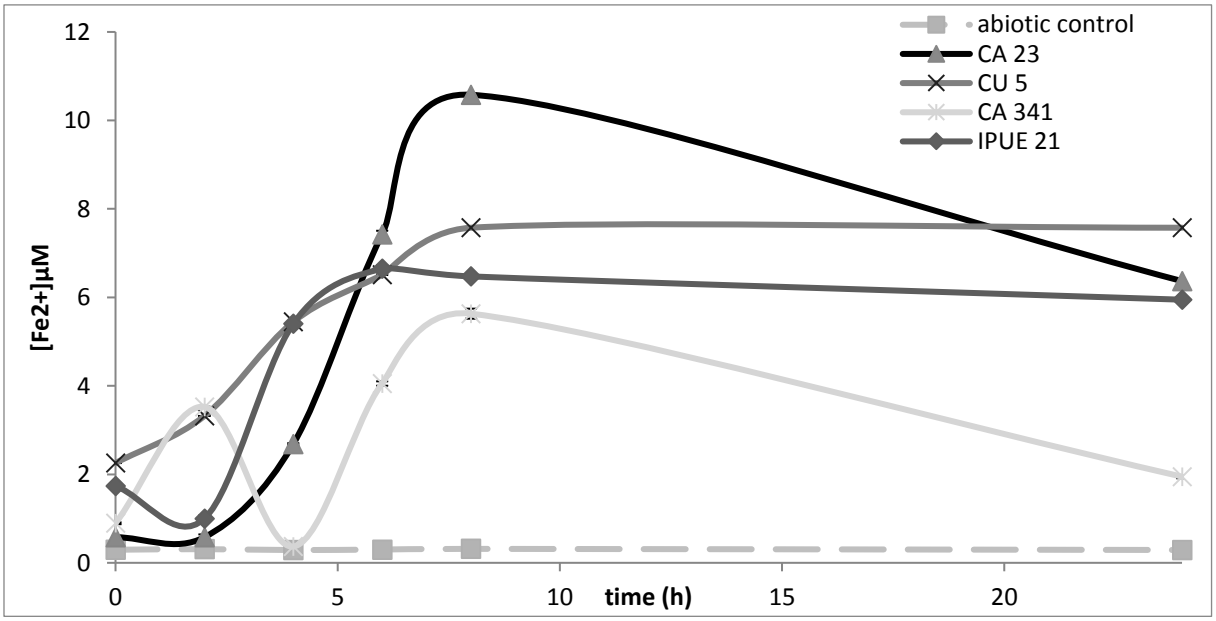

Figure SI4: Evaluation of solid iron reduction with 0%NaCl of CA341, IPUE21, CA23 and CU5

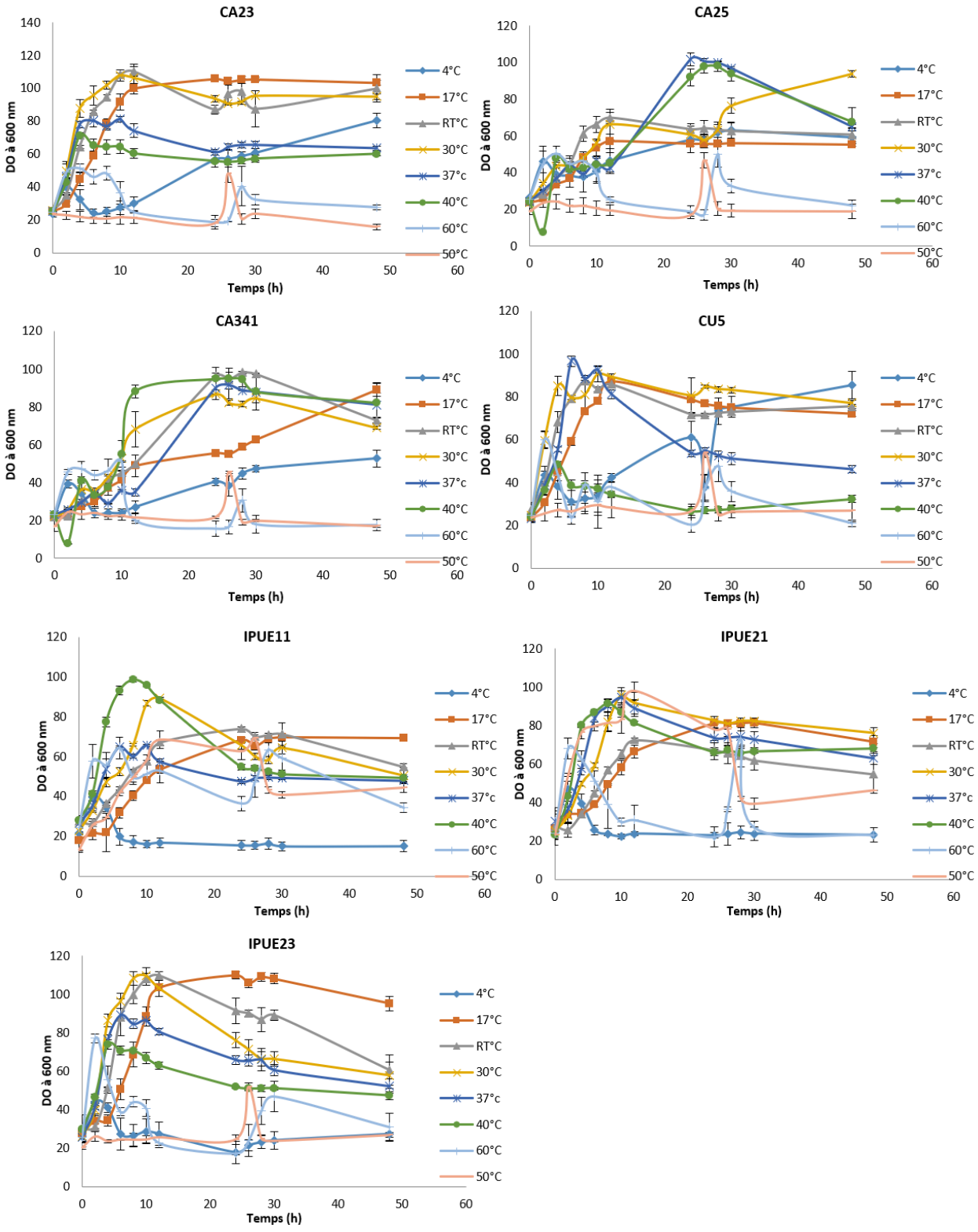

Figure SI5: Evaluation of optimal temperature of some bacterial isolates that were tested for their ability to reduce iron in figure SI2

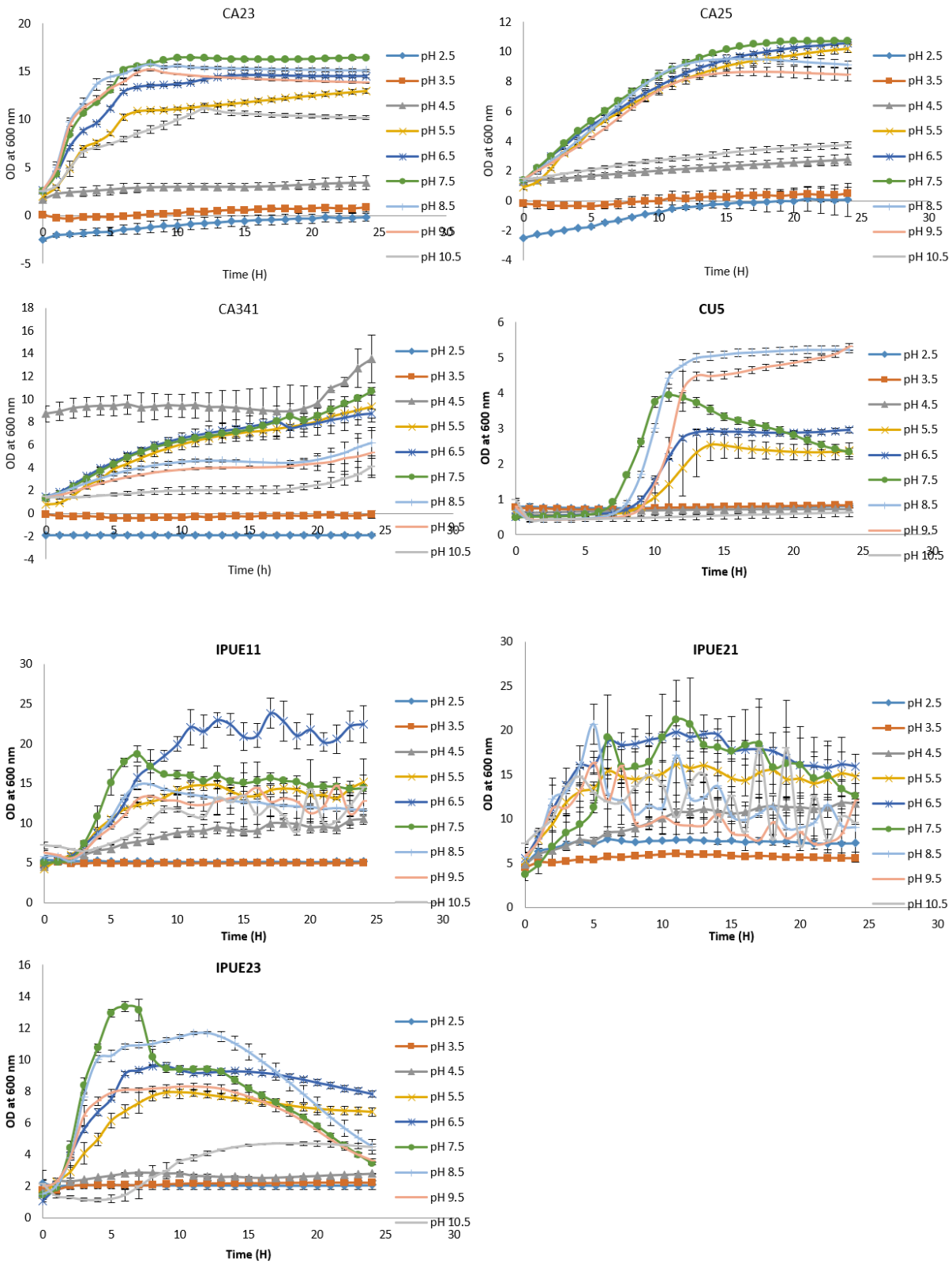

Figure SI6: Evaluation of the optimal pH of some bacterial isolates that were tested for their ability to reduce iron in figure SI2

Chapter 6

Reductive treatment of corroded iron objects by environmental *Aeromonas* isolates

"Look! Look deep into nature, and then you will understand everything better". Albert Einstein

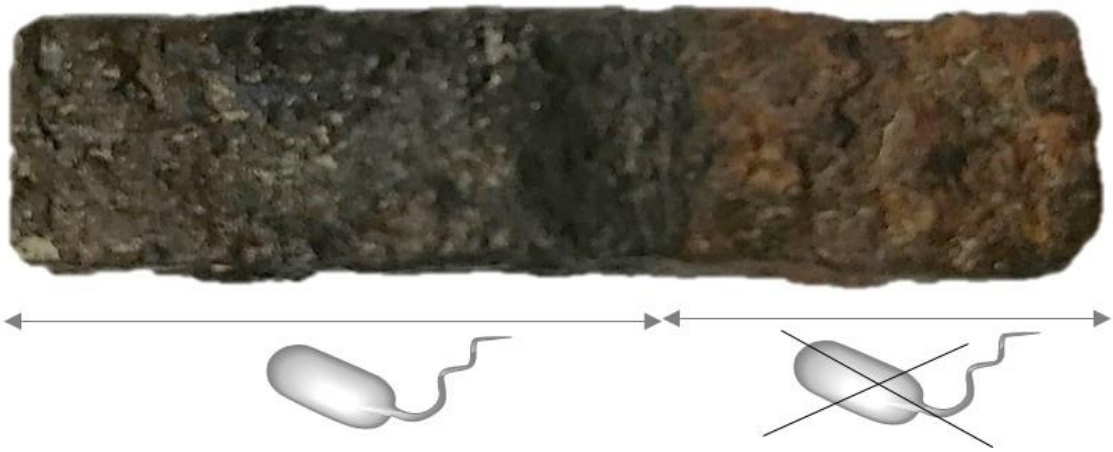

Co-Authors: Thomas Junier, Migun Shakya, Mathilde Monachon, Karen Davenport, Kaushik Vaideeswaran, Ivan Marozau, Teddy Monrouzeau, Olha Sereda, Patrick S. Chain, Edith Joseph and Pilar Junier

Status: in preparation for publication

Abstract

Two iron-reducing environmental strains (CA23 and CU5) belonging to the genus *Aeromonas* were enriched from sediments and tested for their ability to transform ferric iron insoluble corrosion products present on corroded iron objects into stable ferrous iron-bearing minerals. The results show that the two bacterial strains were able to transform the reactive corrosion layer of iron objects corroded in a marine environment into more stable ferrous minerals (vivianite and siderite). In parallel, an investigation of the virulence of the two isolates was conducted. Even if the genomes of CA23 and CU5 exhibit a wide range of virulence factors, none of the genes were expressed under the conditions used for iron reduction. These results allowed us to scale up the treatment by using CA23 and CU5 in a gel delivery system to treat archaeological iron objects. Promising results were obtained, as the surface appearance and composition of the artifacts was modified. The reactive corrosion composed of lepidocrocite and goethite decreased with the increase of vivianite and siderite, suggesting that the bacterial reduction of these Fe(III) oxyhydroxides lead to the formation of ferrous iron minerals. Nevertheless, the stability of the Fe(II) mineral layer needs to be optimized.

Introduction

In nature, the phenomenon of iron corrosion is an essential part of the biogeochemical cycling of iron. While aerobic corrosion is considered to be primarily a chemical process, anaerobic corrosion is often related to oxidative and/or reductive bacterial activity [1]. Iron is a redox-sensitive element. It oxidizes easily in the presence of oxygen to form poorly soluble Fe(III) oxides. The latter accumulate in sediments and soils [2] where iron can be actively remobilized through biotic and abiotic reactions [3, 4]. Even if the majority of iron is bound in a mineral form and therefore not easily available for living organisms [3], some bacteria are able to catalyze transformations of iron minerals under oxic and anoxic conditions [2]. In the presence of oxygen, some bacteria (e.g. *Thiobacillus ferrooxidans*) can oxidase ferrous iron to obtain energy for growth [5]. This explains the formation of Fe(III) oxides in specific environmental settings. Under anoxic conditions, ferric iron-reducing bacteria and anaerobic ferrous iron-oxidizing bacteria (e.g. phototrophic non-sulfur purple bacteria) are involved in the cycling of Fe [2]. Iron-reducing bacteria couple the oxidation of organic compounds or hydrogen to the reduction of ferric iron oxides as alternative terminal electron acceptors in respiration. Even though according to the literature, most of the Fe(II) produced by microbial Fe(III) reduction precipitates in solid phases such as magnetite, siderite or vivianite [6], part of it can remain in solution and could be used or mobilized by other organisms [6, 7]. Anaerobic iron-oxidizing bacteria use Fe(II) as electron donor for different reactions (e.g. anoxic photosynthesis in the presence of light) [8]. An understanding of the biogeochemical cycle of iron constitutes the base for exploiting specific bacterial metabolisms as an environmental solution to current issues of iron corrosion.

Iron corrosion has a major impact in man-made ecosystems and cause large economic losses in fields as diverse as water supply, food industries, transport, and cultural heritage [1, 9]. The latter has a worldwide impact especially on tourism and sustainable development [10–12]. The damage generated by uncontrolled corrosion of archeological objects is a clear example of the negative effects of iron corrosion. Unstable iron oxides and oxyhydroxides are the major unstable iron corrosion products reported for this type of objects. Due to their molar volume (higher than the metallic iron substrate) these corrosion products generate cracks and the destruction of the objects if no intervention is engaged [9, 13–15]. The use of microorganisms with

the ability to transform reactive corrosion products (e.g. lepidocrocite) into stable compounds with low molar volume represents a promising biotechnological approach [6, 7].
In previous studies [16, 17], we have shown the feasibility of a bacterial treatment for corroded iron objects. The strategy consists on the reduction of reactive Fe(III) oxides and oxyhydroxides and biogenic mineral formation under anaerobic conditions. In our previous work [16], we used the bacterium *Shewanella loihica* for treating corroded iron coupons in presence of 1% NaCl, as this bacterium could not reduce iron without salt addition. However, the addition of NaCl to the reducing medium was problematic as the presence of chlorides or chlorine-containing iron oxyhydroxides (e.g. akaganeite) enhances undesirable corrosion processes [9, 18, 19]. Hence, we were interested in finding a more suitable candidate by selecting a facultative anaerobe that could reduce iron in the absence of added salt. In order to select better candidates, a screening of bacterial isolates from two Swiss lakes was performed. As a result, two isolates belonging to the genus *Aeromonas* (*Aeromonas* sp. strain CA23 and *Aeromonas* sp. strain CU5) were identified. These facultative anaerobic bacteria were able to reduce soluble and solid Fe (III) (Chapter 5).

Aeromonas spp. are ubiquitous bacteria associated with aquatic environments [20, 21]. Some species are reported as facultative dissimilatory iron-reducing bacteria [21, 22]. Among the species known to reduce iron, *Aeromonas hydrophila* is the best-studied [23–25]. In *A. hydrophila* the mechanism for reduction of Fe(III)-bearing minerals involves a respiratory electron transport chain. Reducing equivalents that enter this respiratory chain via a succinate dehydrogenase are transferred from quinones via *c*-type cytochromes to a membrane-associated Fe(III) reductase [4]. Studies evaluating the reduction of Fe(III) citrate by *A. hydrophila* suggested that electron flow between formate dehydrogenase and the membrane-associated iron reductase is similar to the one involving a non-soluble Fe(III) source and occurs via molybdopteridin cofactors, quinones and a cytochrome complex [23]. The iron reduction mechanism in *Aeromonas* is less characterized than the mechanism described for the model iron-reducers *Shewanella* and *Geobacter*. In *Shewanella oneidensis*, the *mtrCAB* operon as well as *omcA* and *undA* genes encode the key proteins in iron reduction. In *A. hydrophila* it has been proposed that the cluster involved in iron reduction is homologue to the *mtrCAB* operon of *S. oneidensis*, but homologues to *omcA*, *undA* or *mtrDEF* have not been identified [26].

The pathogenic potential of the environmental isolates used is another consideration for the development of a biological approach for the transformation of iron corrosion products. Competition between bacteria and their host for available Fe(III) is known to increase the virulence of pathogenic bacteria [27]. The selection of iron-reducing bacteria from environmental samples could lead to the unintentional enrichment of pathogens. Indeed, *Aeromonas* can be found in many environmental niches [28]. Some *Aeromonas* species such as *Aeromonas sobria* or *Aeromonas salmonicida* are known to be pathogens of aquatic animals and especially of fish, while *A. hydrophila*, and *Aeromonas veronii* have been related to human infection [29–31]. The goals of this study consist on improving the development of a biotechnological treatment for the stabilization of corroded iron coupons and archaeological nails by testing the ability of the two *Aeromonas* isolates to convert reactive iron corrosion products in biogenic Fe(II) minerals. In addition, we investigated the iron reduction mechanism and the potential virulence of the these two *Aeromonas* isolates.

Results and discussion

Biogenic formation of Fe(II) minerals on corroded iron plates

The overall goal of the biotechnological treatment consists in transforming the reactive corrosion layer present in a corroded iron object by forming biogenic Fe(II) minerals as by-products of the reduction of reactive Fe(III) oxyhydroxides. This ought to be performed in a solution without NaCl addition as the negative effect of chloride ions on the stability of iron objects has been well established [18]. The results obtained showed that the macro- and microscopic visual aspects of corroded iron plates treated with the two selected *Aeromonas* strains changed starting from 2 weeks of incubation with the strain CU5 and after 4 weeks of incubation with strains CA23 (Fig. 1). In the abiotic control treatment, no change in the aspect of the iron coupons was observed, suggesting that the solution used for the reduction of reactive Fe(III) oxyhydroxides does not contribute to the transformation of the reactive corrosion layer (Fig. SI1, table SI1). In the plates treated with bacteria, the elemental composition of the surface changed (Table 1); EDS analysis showed the presence of phosphorus starting from 2 weeks with CU5 and after 4 weeks with CA23 when this measurement was performed on the foil "f" like habitus (Fig. 1). On the corroded iron plates treated with CA23, minerals with cubical "c" and spherical "s" like habita were also observed by SEM (Fig. 1). EDS analysis showed the presence of iron, oxygen, and carbon (Table 1; "s" and "c").

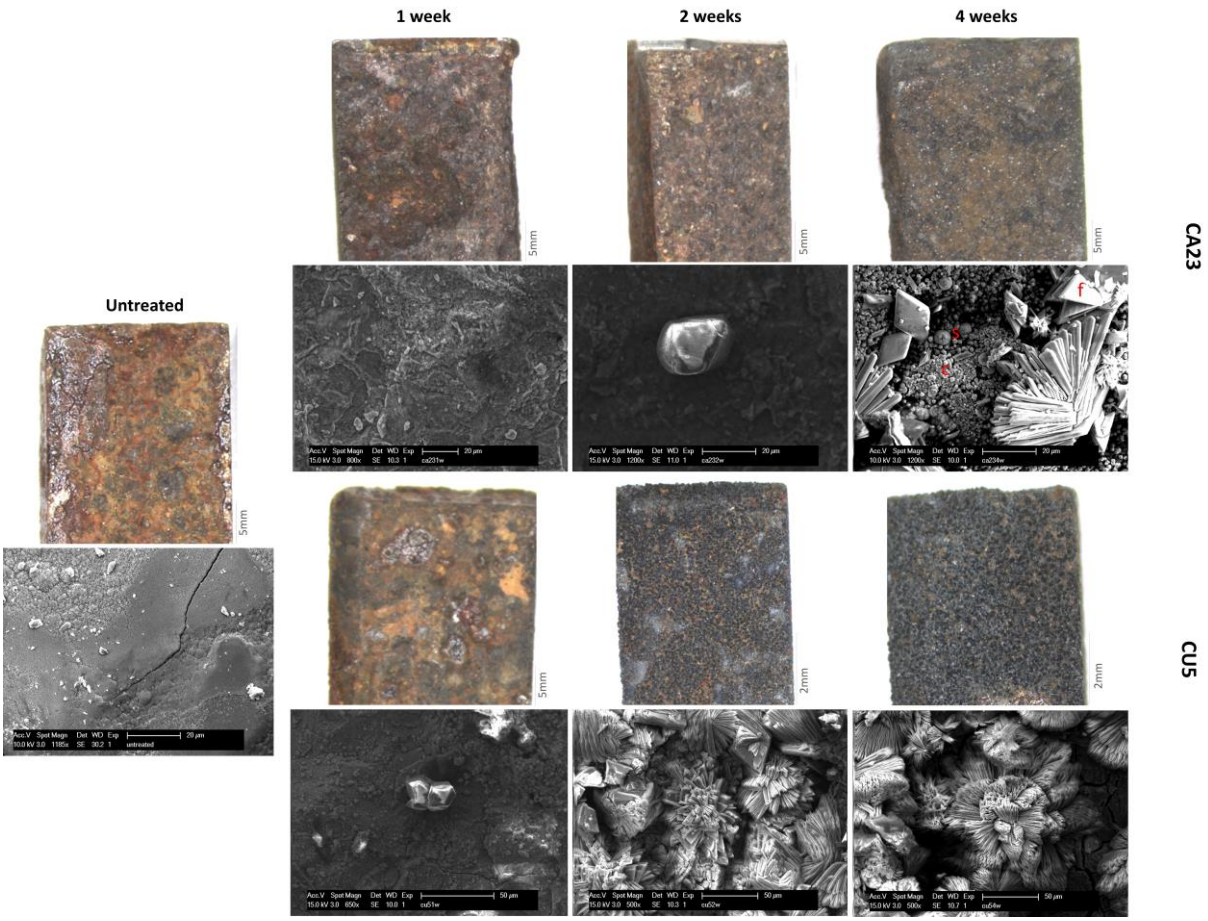

Figure 1: Iron reduction and biogenic mineral formation of corroded iron plates treated with the strains CA23 and CU5. Scanning electron microscopy (SEM) images and visual aspect of the iron coupons treated with CA23 and CU5 after 1, 2, and 4 weeks of incubation compared to an untreated

coupon. The letters f, s and c indicate foil-like biogenic mineral habita, spherical and cubical agregates respectively.

Table 6: Atomic percentages (AT%) of the elements obtained from the Energy-dispersive X-ray spectroscopy (EDS) measurements performed on the iron coupons after 1, 2 and 4 weeks of treatment with the strains CA23 and CU5 and on the untreated coupon. "f" corresponds to the foil-like aggregates indicated in Figure 1, while "s" and "c" refer to the spherical and cubical-shaped minerals respectively. "-" stands for not detected element.

Elements (AT%)	1 week		2 weeks		4 weeks				untreated iron coupon
	CA23	CU5	CA23	CU5	CA23			CU5	
					f	s	c		
C	10.33	26.96	27.98	12.96	5.56	25.78	29.73	13.30	18.75
O	23.92	56.05	55.55	57.50	60.63	47.12	45.15	39.26	43.42
Fe	63.42	-	-	16.79	21.09	27.09	23.00	30.23	36.28
P	-	-	-	12.75	12.72	-	-	17.21	-
Ca	-	16.99	16.13	-	-	-	-	-	-
Na	-	-	0.34	-	-	-	2.12	-	-
Si	2.32	-	-	-	-	-	-	-	-
Cl	-	-	-	-	-	-	-	-	1.56

X-ray diffraction analyses (XRD) were performed on the CU5 and CA23 4-week treated iron coupons in order to identify the mineral phases present on the surface (Fig. 2). The results show the presence of two Fe(II) phosphate minerals (vivianite $Fe_3(PO)_4 \cdot 8H_2O$ and $Fe_2P_20_7$), as well magnetite (Fe_3O_4). In addition, Fe(II) carbonate (siderite; $FeCO_3$), was only detected on the treated coupons with CA23. These three minerals are absent in the abiotic controls and on the untreated coupons. These results are consistent with the EDS analysis, even if aggregates composed only of Fe and O (representing magnetite) were not detected through EDS. Moreover, Fe(III) oxyhydroxides (goethite and lepidocrocite) corresponding to reactive corrosion products present as intense peaks in abiotic controls and untreated coupons are less intense in the spectrum of plates treated with the strain CA23 and absent from the spectrum of the plates treated with CU5. This result demonstrates the efficiency of the biological treatment for the transformation of the reactive corrosion products into stable biogenic minerals. The effectiveness of this bacterial treatment is confirmed also by confocal microscopy measurements (Fig. 3) where the surface of the biologically treated iron coupon is completely modified by the presence of crystals covering the entire surface as seen in a 3-dimensional reconstruction. This is also reflected in a change in the rusty colour of the untreated controls compared to a greyish colour in the treated plates. Overall the results of the reduction experiments with the corroded iron plates show the potential of using these two environmental strains for a biotechnological treatment. Therefore, we next investigated in detail the phylogenetic affiliation of the strains, as well as their potential pathogenic lifestyle.

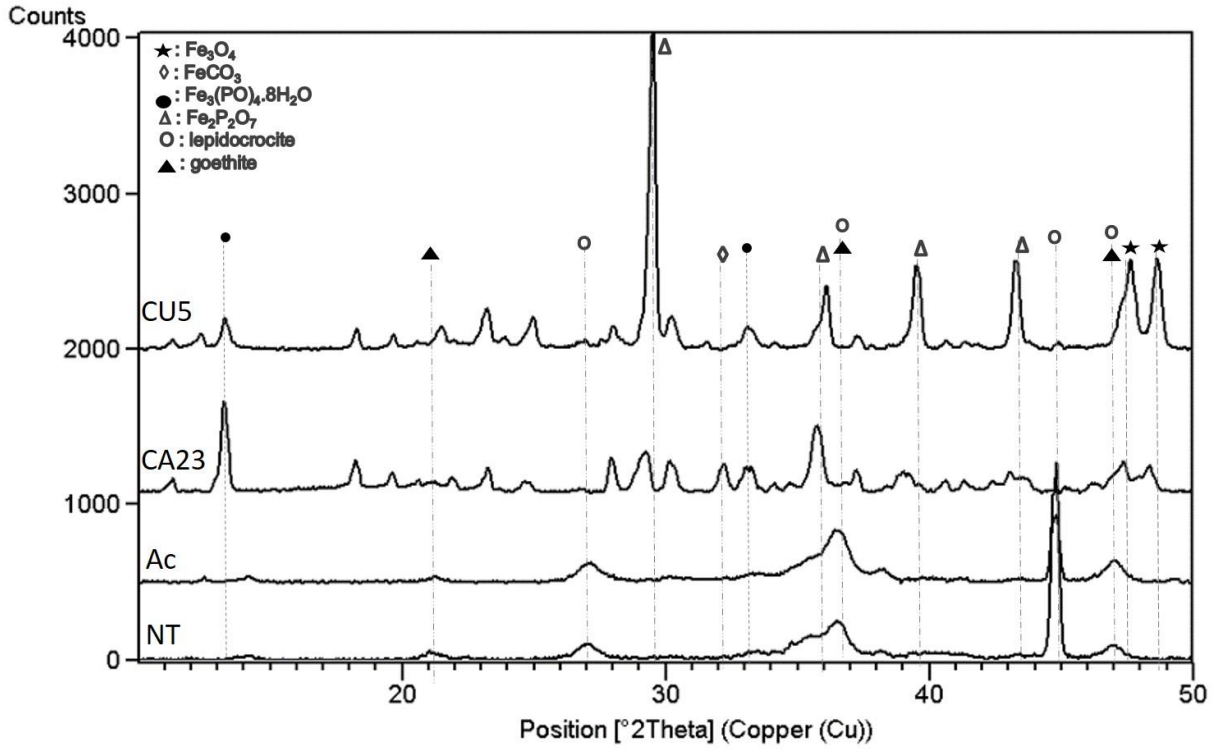

Figure 2: X-Ray diffraction (XRD) spectra of corroded iron coupons exposed in a marine environment. Spectra generated of the coupons treated with CU5 and CA23 after 4 weeks of incubation, as well as the abiotic controls (Ac), and the untreated coupons (NT). The low intensity peaks between 18-24° are difficult to identify because of their intensity and large peak width.

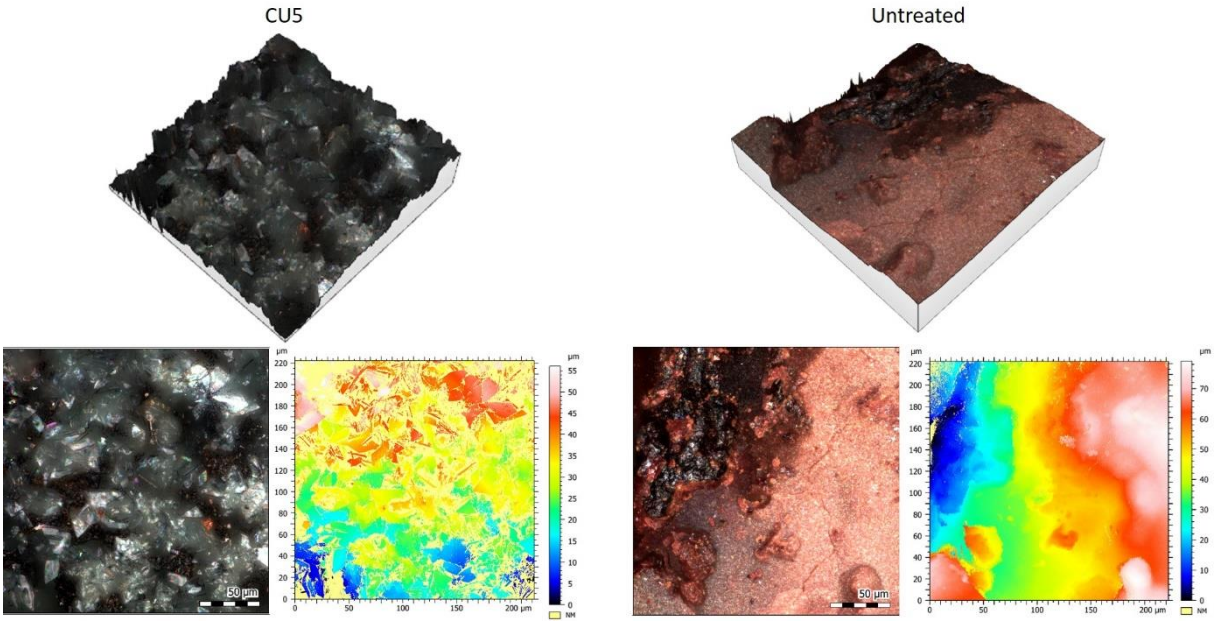

Figure 3: Confocal microscopy images of iron coupons**.** A) plate treated with the strain CU5 after 4 weeks of incubation. B) untreated plate. For each plate, we present the 3D configuration, reconstructed from a scanning of the surface made at a 50X magnification with its corresponding color-coded height map. The images were taken using the Smartproof 5 Zeiss confocal microscope (aperture correlation microscopy) with ZEISS Efficient Navigation (ZEN) and Confomap software.

Phylogenetic classification of strains CA23 and CU5

In order to classify the strains isolated we use whole genome phylogenetic analysis to compare strains CA23 and CU5 with all the available genomes of *Aeromonas* deposited in GenBank (Fig. 4). The phylogenomic tree presented in Figure 4 is in general agreement with the current classification of species within the genus [32–40]. However, incoherence in the phylogenetic placement of some isolates was observed. We suggest that the species *Aeromonas aquatica* MX16A, *Aeromonas jandaei* L14h, and *A. hydrophila* 4AK4 should be reclassified (species underlined in blue) given their misplacement in the tree. The renaming of the latter was also suggested by Hidalgo et al (2015) [41]. The phylogenomic analysis of the two isolates investigated here show that the two strains belong to different species. This difference is also confirmed by the biochemical tests performed (Table SI2) and by the average nucleotide identity (ANI) of 85.61% calculated between the two strains (Fig. SI3, A). According to the analysis strain CA23 could belong either to the species *Aeromonas bestiarum* CECT 4227 or *A. salmonicida* CBA100, given its placement in the phylogenomic analysis (Fig. 4) as well as the ANI values, which were superior to 95% in both cases (see table 2). However, since *A. salmonicida* CBA100 was not clustered within other strains belonging to *A. salmonicida* we proposed that the nomenclature of *A. salmonicida* CBA100 should be reconsidered. Both, *A. bestiarum* CECT 4227 and *A. salmonicida* CBA100 are reported as fish pathogens. The latter was the first Chilean pathogenic isolate to be sequenced and the analysis of its genome shows a diverse set of mechanisms involved in resistance to multiple antibiotics [42]. However, for none of these species information concerning iron reduction could be retrieved. Concerning CU5 the results show that this bacterial strain is closely related to *Aeromonas sobria* CECT 4245 and *Aeromonas* sp. EERV15, suggesting that it could belong to the species *A. sobria* (Fig. 4, Table 2 and Fig. SI3, B). Although *A. sobria* is also considered as an opportunistic fish pathogen, there is increasing evidence of a large phenotypic diversity within this species [43]. However, the potential of strains in this species for iron-reduction has not yet been assessed.

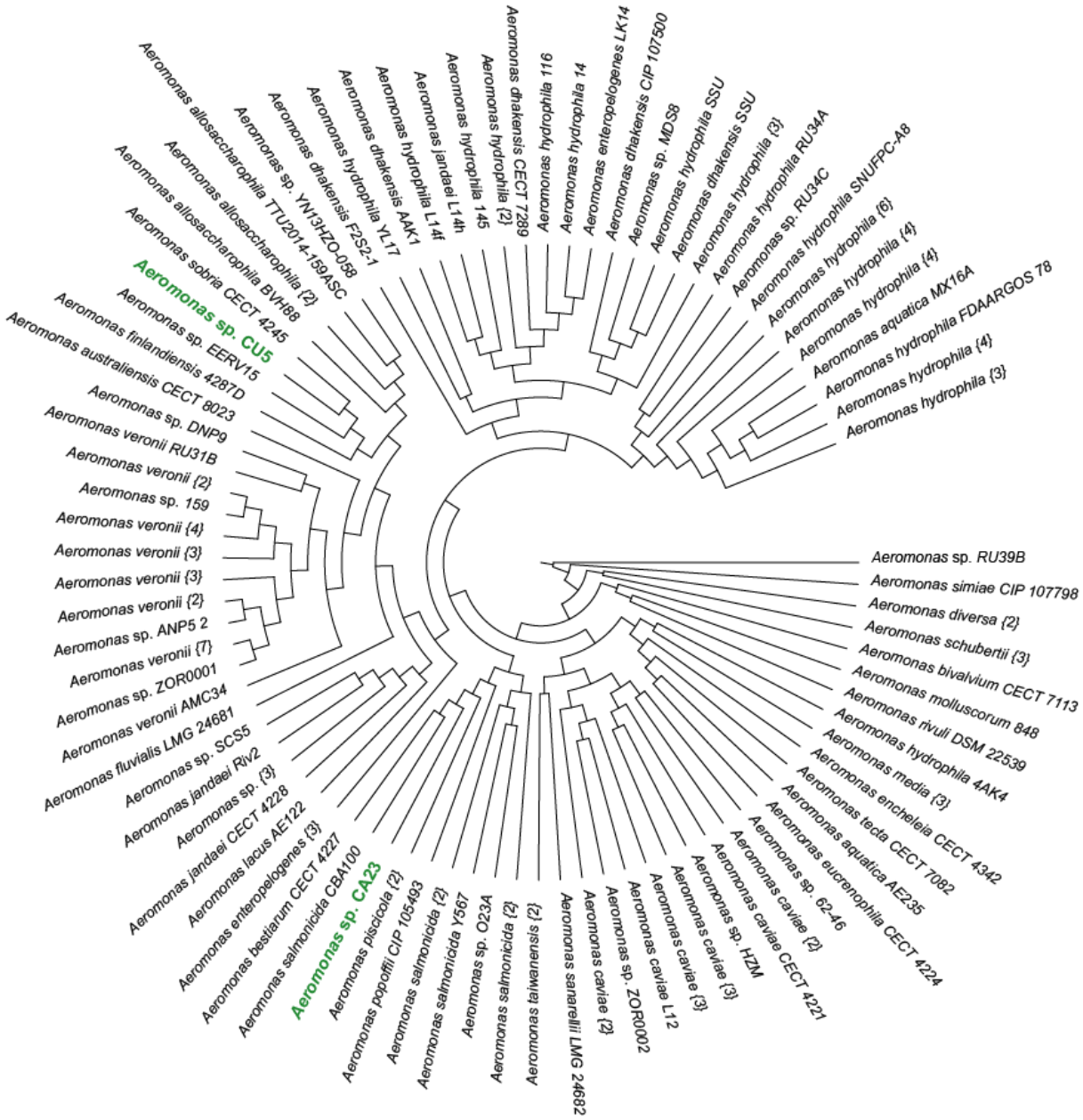

Figure 4: Phylogenomic tree indicating the phylogenetic position of the two isolates CA23 and CU5 (colored in green) within the genus *Aeromonas*.

Table 7: Average nucleotide identities (ANI) of CA23 and CU5 and the closest related strains showed in the phylogenomic tree presented in Figure 4. nd= not determined

Closest relative to CA23	**Isolation site**	**ANI %**
Aeromonas salmonicida CBA100	Skin of rainbow trout, Chile	97.04
Aeromonas bestiarum CECT 4227	nd	97.15
Closest relative to CU5	**Isolation site**	**ANI %**
Aeromonas sobria CECT 4245	nd	96.65
Aeromonas sp. EERV15	sand filter	96.34

Potential electron transport chain for solid iron reduction in CA23 and CU5

Based on the model of the electron transport to solid iron reported for *S. oneidensis* and described in the Chapters 1 and 3, as well as the information found for *A. hydrophila* [26], we analyzed the genomes of CA23 and CU5 to propose a potential electron transport chain (ETC) for the reduction of insoluble iron minerals. Using BLASTp (identities ranging from 60-80%) we proposed a model for CA23 including homologs of the *mtrCAB* complex (gene locus: CK910_RS13405, CK910_RS13415, CK910_RS13395 respectively), and a homolog of *cymA* CK910_RS20025: (Fig. 5). Interestingly, only a homolog of *cymA* (CK911_02795) and no homologues of *mtrCAB* were identified using different BLAST tools (identities below 35%) and Needleman-Wunsch (identities below 20%) in CU5, suggesting that this bacterium has a different iron reduction pathway. As the Pili has been involved in iron reduction in other bacteria such as *Geobacter sulfurreducens*, we included it in the analysis. However, a homolog of the gene *pilC* in *G. sulfurreducens* was the only gene identified in the genomes of both strains (Table SI3).

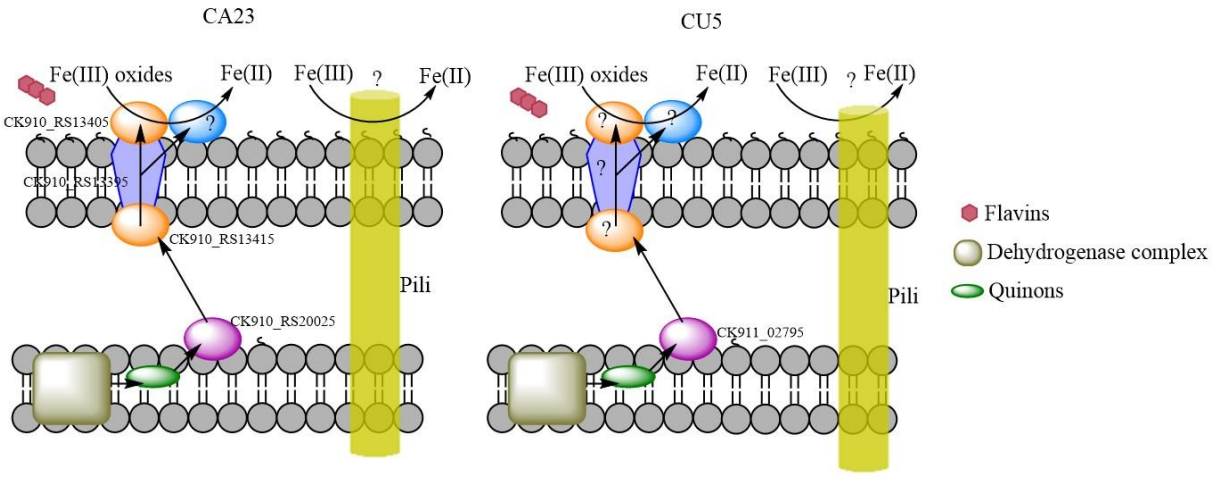

Figure 5. Potential iron reduction pathways of CA23 and CU5 and the homologs identified in their genomes based on the analysis of the genome of *A. hydrophila* and the iron reduction pathway of *S. oneidensis* [44,45].

As we have observed previously for *S. loihica* (Chapters 2 and 4) that the production of Fe(II) phosphate minerals in a medium lacking a phosphate source can be related to polyphosphate accumulation, we investigated this in *Aeromonas* [46]. Indeed, the genomes of CA23 and CU5 as well as *A. hydrophila*, *A. salmonicida* and *A. veronii* possess two genes coding for polyphosphate kinases and one gene coding for a polyphosphatase (Table 3). These genes were reported in the literature to be involved in polyphosphate accumulation [47,48]. Interestingly, even if polyphosphate accumulation in *Aeromonas* genus was reported [49], especially for *A. hydrophila* [50, 51], no extensive information on this process could be found, which is surprising as according to Table 3, polyphosphate accumulation in *Aeromonas* spp. seems to be a common trait.

Table 8: Putative genes involved in polyphosphate metabolism from the genomes of CA23, CU5, *A. hydrophila* ATCC 7966, *A. salmonicida* A449 and *A. veronii* B565

Predicted function	CA23	CU5	*A. hydrophila*	*A. salmonicida*	*A. veronii*
poly-phosphate kinase (*ppk*)	CK910_RS12780 (*ppk1*) CK910_RS19580 (*ppk2*)	CK911_RS04045 (*ppk1*) CK911_RS04810 (*ppk2*)	AHA_2829 AHA_1671	ASA_RS07565 ASA_RS13405	AMS64_RS14790 AMS64_RS15750
Exopolypho-sphatase (*ppx*)	CK910_RS12775	CK911_RS04040	AHA_2830	ASA_RS07560	AMS64_RS15755

Analysis of the pathogenic potential of the strains

Aeromonas species are known as causative agents of a wide spectrum of infections in man and animals, predominantly amphibians, fish, and reptiles [52]. They are autochthonous inhabitants of aquatic environments such as fresh and brackish water, sewage and wastewater [29] and some studies have shown that some motile *Aeromonas* species are becoming food and waterborne pathogens of increasing importance [20]. The ability of *Aeromonas* spp. to cause many diseases can be attributed to a broad range of virulence factors possessed by aeromonads. *A. hydrophila*, *A. caviae,* and *A. veronii* are considered as major *Aeromonas* pathogens [29]. These pathogens also display variable degrees of antimicrobial resistance.

Given the pathogenic lifestyle of the closest related species to our environmental isolates we performed several analyses to infer their potential pathogenicity. First, we consider the resistance of the strains to a series of antibiotics. Both CA23 and CU5 have the same antibiotic resistance profile (Table SI4). They are resistant to some *β*-lactam antibiotics such as ampicillin, amoxicillin and cefalotin, suggesting that they could have a cephalosporinase (a β-lactaminase). Indeed, some researchers demonstrated that almost all *Aeromonas* spp. are resistant to ampicillin and cefalotin [20].

Next, we investigated the pathogenic life style of the two *Aeromonas* by analyzing the genomic repertoire of virulence factors found in their genomes. According to the literature, the main pathogenic factors associated with *Aeromonas* spp. include structural features as pili and flagella, lipopolysaccharides (LPS), and S-layer. The flagella of pathogenic bacteria promote the colonization and invasion of the host's mucosa. Once bacteria reach the mucosal environment, the flagellum structure becomes necessary for motility, adhesion and invasion. This motility, coupled with chemotaxis, allows the pathogens to reach their target.

LPS are immunostimulatory and the O-antigen, which is the most surface-exposed LPS moiety, mediates pathogenicity by protecting infecting bacteria from serum complement killing and phagocytosis. S-layer is associated with many pathogenic functions like adhesion, protection against attack by phagocytes. Other extracellular factors like hemolysins, toxins (mainly enterotoxin), iron binding systems (e.g. siderophores), proteases, chitinases, amylases, secretion systems, and β- lactamases also participate in pathogenicity. Toxins and other extracellular enzymes represent an important virulence factor. Toxins interact with the membranes of erythrocytes, insert into the lipid bilayer, and create pores, damaging tissues. Indeed, hemolysin and aerolysin are considered as the main virulence factor in *A. hydrophila*, being responsible for hemolytic, cytotoxic, and enterotoxic activities [52,53]. As iron represents a limiting element in natural environments, micro-organisms developed a series of mechanisms to sequester iron from their hosts, including: reduction of ferric to ferrous iron, chelation and use of host iron compounds. This could be achieved by siderophores, ferric reductases, cytochromes and iron transporters [52,53]. Even if their involvement in pathogenicity is not always confirmed, extracellular enzymes as proteases, amylases, and chitinases, represent an interesting group of molecules for adaptation to environmental change. Proteases were reported to contribute to the pathogenicity by direct damage of host tissue [21,52,53].

The search for genes coding for potential virulence factors in the genomes of CA23 and CU5 showed that, indeed, these two *Aeromonas* species possess most of the genes reported in pathogenicity, including genes related to adherence, hemolysin and toxins, flagella and pili biosynthesis, secretion system, chitinase, collagenase and hyaluronidase, multidrug transporters, LPS, proteases and antibiotic-degrading enzymes (Table 4). However, possessing this arsenal of pathogenicity factors does not imply a pathogenic lifestyle. For example, the β-lactamases encoded in our two strains were demonstrated to be functional, as resistance to three β-lactamic antibiotics was observed *in vivo* (Table SI4). In contrast, even if in the genomes of CA23 and CU5 encode TonB siderophore receptors, a preliminary test for siderophore production using CAS medium was negative (Fig. SI8). Therefore, and given the large range of potential virulence factors, we investigated the expression of these genes using a transcriptomic analysis under the conditions that are used to convert reactive Fe(III) corrosion products to stable Fe(II) minerals. Under these conditions, none of the genes involved in pathogenicity was significantly expressed except for type II secretion system (*epsE*), multidrug transporters (*norM*) and anti-toxin (*yfjZ*) that were instead down regulated under iron reducing conditions (the latter was up regulated in CA23) (Table 4). Moreover, CU5 appears to have a less pathogenic potential as no genes coding for toxins, enterotoxins and aerolysin were found in its genome. This tends to favor CU5 for a biotechnological treatment.

Table 9: Gene loci coding for virulence factors found in genomes and transcriptomic analysis (RNAseq data) of CA23 and CU5, ns=not significant, +=found, -= not found

Virulence Function		CA23		CU5	
		Genome	Rnaseq data	Genome	Rnaseq data
Adherence and motility	Pilus assembly, MSHA pilus and type IV pili	CK910_RS01560-70 CK910_RS03095-115 CK910_RS07360 CK910_RS08660 CK910_RS08740-45 CK910_RS11045-65 CK910_RS13525 CK910_RS13830 CK910_RS17960 CK910_RS19080 CK910_RS20680-740	ns (only type IV pili)	CK911_RS05025 CK911_RS08980 CK911_RS12050-70 CK911_RS14800 CK911_RS15460-80 CK911_RS19975-80 CK911_RS19750-55 CK911_RS19970-80 CK911_RS03930-60 CK911_RS03990-4030 CK911_RS04445-65 CK911_RS10705-85	ns (only type IV pili)
	Flagella	CK910_RS12690-2765 CK910_RS18940 CK910_RS19330-50 CK910_RS21170- CK911_RS08650 CK911_RS10415 CK911_RS18840	+(downregulated)	CK911_RS14955-15130 CK911_RS20715 CK911_RS01545 CK911_RS02440 CK911_RS10425 CK911_RS10495 CK911_RS17675	+(downregulated)
	LPS	CK910_RS12525 CK910_RS12555	ns		ns
	O-antigen		-		ns
Toxins and extracellular enzymes	Toxin and enterotoxin	CK910_RS00960 (antitoxin) CK910_RS12220 CK910_RS13090 CK910_RS19835 CK910_RS12375	+ (antitoxin, upregulated) ns (Toxins)	CK911_RS01110 (antitoxin)	+(downregulated)
	Hemolysin	CK910_RS09570 CK910_RS10940 CK910_RS20415	ns	CK911_RS00740 CK911_RS09825 CK911_RS12215	ns
	Aerolysin	CK910_RS02845	ns	-	-
	Chitinase	CK910_RS00070 CK910_RS09840	ns	CK911_RS00935 CK911_RS12780	ns
	Metalloprotease	CK910_RS10490 CK910_RS01820 CK910_RS02990 CK910_RS07020	ns	CK911_RS00235 CK911_RS11850 CK911_RS15345 CK911_RS18785 CK911_RS19670	ns
	Other proteases	23 loci	ns	20 loci	+(downregulated)
	Hyaluronidase	CK910_RS20620	-	CK911_RS10170	-
	Collagenases	CK910_RS02455 CK910_RS20825	-	CK911_RS14200	-
	Phospholipase	CK910_RS03220	ns	CK911_RS15625	ns
	Alpha-amylases	CK910_RS21730 CK910_RS22255	ns	CK911_RS07125 CK911_RS11695	ns
Iron acquisition	siderophore receptors	CK910_RS02730 CK910_RS15610 CK910_RS15610 CK910_RS04745	ns	CK911_RS17235 CK911_RS18880 CK911_RS09860	ns

	Ferric reductase Ferric uptake regulator Fur Ferrous iron transporter	CK910_RS15615 CK910_RS20320 CK910_RS04080 CK910_RS13500	- ns ns	- CK911_RS09930 CK911_RS09200 CK911_RS16520	- ns ns
Antibiotic resistance	β-lactamase	CK910_RS01300 CK910_RS04830 CK910_RS11380	ns	CK911_RS11640 CK911_RS12920 CK911_RS17150	ns
	Aminoglycoside acetyltransferase et phosphotransferase	CK910_RS05645 CK910_RS05645 CK910_RS00245	-	CK911_RS20860	-
	SapABCDF peptide intake transport	CK910_RS02000 CK910_RS02555 CK910_RS12175 CK910_RS15245	ns	CK911_RS05100 CK911_RS10300 CK911_RS19460	ns
Transport	multidrug transporters MFS transporter	14 loci 32 loci	ns -	18 loci 13 loci	+(downregulated) ns
	Secretion system	CK910_RS02125-85 CK910_RS02175-85 CK910_RS03045-80 CK910_RS07355 CK910_RS08605 CK910_RS13705 CK910_RS14985-15095 CK910_RS18505-15 CK910_RS18505-15 CK910_RS21330-40	+(downregulated)	CK910_RS02125-85 CK910_RS03045 CK910_RS03075-80 CK910_RS07355 CK910_RS08605 CK910_RS14985-15095 CK910_RS20700 CK910_RS21330-40 CK910_RS22725-35	ns

As shown in supplementary data (Tables SI5 and SI6), the time frame chosen for the transcriptomic study does not show significant expression of genes involved iron reduction and energy metabolism. Nevertheless, other set of genes were differentially expressed in CA23 and CU5 mostly between the switch from aerobic to anaerobic conditions. In CA23, genes coding for HTH-type transcriptional regulator SarZ and for catalase (*katA* gene), were up regulated under anaerobic condition. It was reported that *sarZ*, is induced during anaerobiosis in comparison to aerobic growth in *Staphylococcus aureus* [54]. SarZ senses oxidative stress, and coordinates the expression of genes involved in metabolic switching but also has a regulatory role in antibiotic resistance, oxidation resistance, autolysis and virulence (particularly on proteases and hemolysins synthesis [55]) [56]. Except for *Aeromonas schubertii*, all *Aeromonas* species possess a *katA* gene. This gene codes for catalase, which acts as a safeguard against oxidative stress [57]. Our results are coherent with these findings. Concerning CU5, genes coding for sodium/proton antiporter gene *chaA*, dephospho-CoA kinase *coaE* and inner membrane ABC transporter permease gene *ynjC* were down regulated in the anaerobic condition in comparison to the aerobic phase (overnight). According to the literature, the expression of *chaA*, a gene part of the sodium extrusion system, is regulated by medium osmolarity and this gene was induced by NaCl addition. Since the anaerobic solution that we used lacks NaCl, It may be reasonable to deduce that physiologically, the induction of the sodium ion extrusion system is involved in *Aeromonas* sp. CU5 strategies to adapt to osmotic stress [58].

Treatment application on archaeological iron objects

In order to establish an "easy-to-handle" treatment that will convert the reactive corrosion layer into more stable iron minerals, we performed a first experiment using a commercial gel mixed with bacteria and applied to the archaeological iron nails. The results showed that the treatment was partially successful (Fig. SI9). Indeed, the corrosion layer of the nails was not fully converted as obtained with the iron plates (Fig. 1). In the case of a real archaeological object, the formation of biogenic iron minerals was observed after 4 weeks with the bacterium CA23 and starting from 2 weeks with the bacterium CU5. These minerals are composed of mainly O, C and P according to EDS measurements. Fourier Transform Infrared Spectroscopy (FTIR) analyses were performed to identify the minerals formed. The results showed typical vibration bands of proteins (amide I peak around 1640 cm^{-1} and amide II peak around 1420 cm^{-1}) indicating the presence of bacteria. The peaks between 1040 and 940 cm^{-1} correspond to the phosphate absorbance region [59, 60], which confirmed the formation of iron phosphates. Absorbance bands corresponding to the coordinated water associated with iron phosphates can be observed at 3161 and 795 cm^{-1} which indicates that these minerals have indeed a crystalline phase. According to the FTIR spectrum, the biogenic minerals belong to the vivianite-related group [59] with traces of sodium and potassium. In order to optimize this treatment, we performed a second test by increasing the amount of bacterial cells, the incubation time and incubating archaeological iron objects both aerobically and anaerobically (see material and methods, section: development of user-friendly treatment of archaeological iron nails). The results are shown in Fig. 6. Indeed, the optimization in bacterial cells quantity had a positive effect on the performance of the treatment, especially when comparing with the first treatment (Fig. SI9). In this case the treatment using CA23 or CU5 was successful. The reactive corrosion layer of the archaeological objects was completely covered by minerals compounds, which transformed the visual aspect of the artifacts into a velvety texture and grey-black color (Fig. 6, SI10). This result is not due to the effect of the compounds in the delivery system, as no change in the visual aspect was observed in the abiotic control without bacteria (Fig. 6).

In order to determine the nature of these grey-black compounds a Raman spectroscopy analysis was performed (Fig. 7). In comparison to the untreated archaeological iron objects, which have been characterized using Raman previously [17] , as well as the abiotic control (Fig. SI11), vivianite (shifts at 187,192, 480, 954 and 1001 cm^{-1}) and siderite (shifts at 734, 736 and 1087, 1083 cm^{-1}) were only detected in the samples treated with CU5 after one and two months of incubation. These Fe(II) minerals were also present in the treated iron coupons (Fig. 2). Likewise, Raman analysis show that in contrary to siderite, vivianite was less present in the two months sample. Goethite and lepidocrocite (reactive corrosion products) were completely transformed, as the latter was only detected in the untreated and abiotic control sample, while small pics of goethite were detected mainly in the one-month sample. The incubation under aerobic or anaerobic conditions does not seem to influence the efficiency of the treatment, which is positive, as handling of a fully aerobic treatment might be easier for application. However, the treatment is not entirely satisfactory as partial re-oxidation of the treated surfaces was observed after 48h of air exposition of the objects once the gel was removed and bacteria were cleaned off from the surface.

Figure 6: Optimised bacterial treatment on archaeological iron objects. A) Visual aspect of the iron nails treated with the bacterium CU5 (aerobically and anaerobically) in comparison to the abiotic control (gel delivery system without the bacterium) and CA23 (anaerobically) in comparison to the untreated after 1 month of incubation. B) Spectroscopic images of an archeological nail treated with CU5 anaerobically after 2 months of incubation.

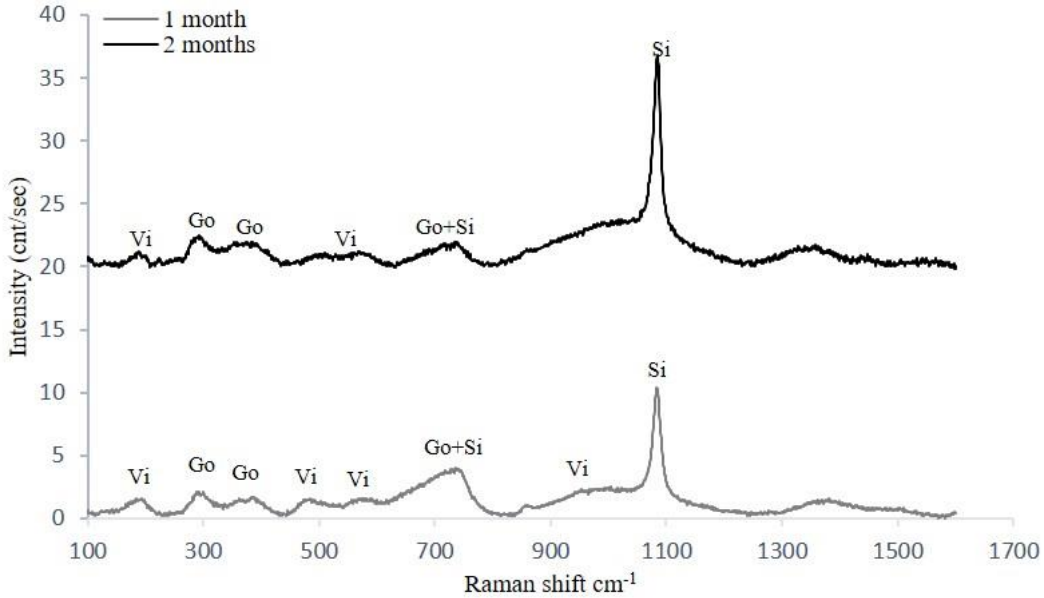

Figure 7: Raman spectrum of the treated archaeological objects after 1 and 2 months of incubation with the bacterium CU5 under anaerobic conditions. Corrosion compounds were identified as, goethite (Go), vivianite (Vi) and siderite (Si).

A stabilization treatment of archaeological iron nail was already proposed by *Comensoli et al* (2017). However, this treatment employed a strict anaerobic bacterium growing in a complex medium, which render the optimization difficult. Indeed, even if the visual characteristics and the composition of the corrosion layer were transformed, the production of undesirable products and abiotical reduction were both observed. Further optimization using the facultative anaerobe *S. loihica* facilitate the potential up-scaling of the process, but the presence of chloride ions in the medium, which is reported to enhance reactive corrosive on archaeological iron objects [17], is incompatible with real praxis. During this study, we proposed a promising *in situ* treatment, using a gel delivery system for the stabilization of surfaces corroded in marine environment as well as archaeological iron objects, this treatment was performed under aerobic conditions, without the addition of salt and the visual aspect of the objects changed due to the transformation of the unstable corrosion layer by the formation of mainly siderite and vivianite. The visual aspect resembles more to the original facet of the objects (before corrosion) which is of an interest from the conservator-restorers point of view. Nevertheless, an improvement of the long-term stability of these Fe(II) minerals formed needs to be considered as well as the eventual pathogenicity of the two bacterial strains used.

Material and methods

Bacterial strain and growth conditions

Bacterial isolates from Lake Cadagno and Lake Cudrefin (Switzerland) were used in this study. Regular cultivation was performed aerobically using Luria-Bertani medium (LB; 1% tryptone, 0.5% yeast extract, and 1% NaCl) at pH 7 and at 30°C under agitation at 130 rpm.
Iron Samples

The corroded iron coupons have the same characteristics as the same ones used in Chapter 2 and 3. Concerning the archaeological iron nails they were excavated from France, Champagne, Sol en Craie region, dating from late Roman period (3rd century A.D).

Chemical matrix for solid Fe(III) reduction

Iron reduction and biogenic mineral formation with the coupons as solid iron source was performed in a matrix composed of 20 mM PIPES, 5 mM sodium lactate, and 50 mM $NaHCO_3$. For the sterilization of the iron coupons, autoclaving was avoided as an enhancement of the corrosion layer was observed under both oxic and anoxic conditions. Instead of autoclaving, coupons were washed with 70% (v/v) ethanol and dried under UV exposure for 1 hour for each side (here we did autoclaving under anoxic conditions). A control for this sterilization method was performed by incubating UV-sterilized plates on solid LB medium under oxic and anoxic conditions, which showed no bacterial growth after one week of incubation.

Iron reduction of solid Fe(III)

In order to decouple growth from iron reduction, a culture of 50 mL of CA23 and CU5 was prepared by cultivating the bacterium under aerobic conditions in LB medium overnight at room temperature. Cell biomass was then collected by centrifugation (1700 x *g* for 10 min) and the pellet was washed with basal solution. The pellet was resuspended in a solution of 20 mM PIPES and added to the matrix containing iron. To evaluate iron reduction, samples were collected every 2 hours for 24 hours. The production of iron minerals was evaluated after 1, 2, and 4 weeks of incubation at room temperature and under agitation (120 rpm). Experiments were performed in triplicates including abiotic controls (without the bacteria).

Measurements of Fe(II) concentration

To measure the reduction of Fe(III) into Fe(II), the ferrozine assay was performed following a modified protocol from Bell *et al.*[61]. First, 100 µL of 5 M HCl were added to 900 µL of collected samples and stored at 4°C. The samples were centrifuged for 1 minute at 6700 x *g*, then 100 µL of the supernatant were taken and 900 µL of ferrozine solution (0.1% ferrozine in a 100 mM HEPES solution at pH 7) were added. Fe(II) concentration was determined by measuring the absorbance at 562 nm with a UV-Vis spectrophotometer (Thermo Fisher Scientific Genesis™ 10s). A calibration curve was obtained using serial dilutions of 1 mM ferrous ammonium sulfate solution in acidic MilliQ water (pH 2).

Scanning Electron Microscopy coupled with Energy Dispersive X-Ray Spectroscopy (SEM-EDS) analyses

The iron coupons were washed twice with deionized water and ethanol 70% (v/v) before being mounted on stubs using carbon conductive tape without gold sputtering. To avoid humidification, the stubs were stored in desiccators with silica gel. A Philips ESEM XL30 FEG environmental scanning electron microscope equipped with an energy-dispersive X-ray analyser was used. The samples and coupons were observed in secondary electrons mode at an acceleration potential of 10–25 keV and with a 10 mm working distance.

X-Ray Diffraction crystallography (XRD) analyses

XRD analyses were performed on untreated, abiotic control and bacterially-treated iron coupons after 4 weeks on incubation. The preparation of the iron coupons was the same as for SEM-EDS analyses. High-statistics θ-2θ (bulk) measurements were performed with a PANalytical X'Pert Pro MPD diffractometer equipped with a fast-linear detector and sample spinner. The measurement time was 60 hours to acquire high statistics for better signal-to-noise ratio. The sensitivity of the XRD phase analyses was about 1 % weight. ICSD codes were used for the identification of siderite (98-004-6078), vivianite (98-004-6142), magnetite (98-001-1782).

RNA extraction and rRNA removal

The RNA sequencing consisted on the extraction of RNA, removal of rRNA and library preparation and sequencing. Bacterial cell stored at -80°C were thawed on ice and then briefly centrifuged (10000 x g for 1min) prior to RNA extraction. RNA extraction was done using a Zymo Research Direct-zol kit with TRIzol® reagent according to the manufacturer's instructions. A Ribo-Zero™ Magnetic kit for Gram-negative bacteria (Illumina) was used for rRNA removal, according to the manufacturer's instructions. The concentration of RNA from the extraction was considered to calculate the reagents used for the preparation of the magnetic beads and for the treatment of total RNA with Ribo-Zero rRNA removal solution (4 µl rRNA removal solution for 0.25 to 1 µg total RNA per reaction). Samples in Ribo-Zero rRNA removal solution were incubated at 68°C for 10 minutes followed by 5 minutes of incubation at 20°C. To remove rRNA, the Ribo-Zero mix incubated previously was mixed with the prepared magnetic beads and placed at room temperature for 5 minutes, then at 50°C for 5 minutes. The rRNA-depleted samples were purified using RNeasy MinElute Kit (Qiagen). The final mRNA eluted was quantified using Qubit-IT RNA HS assay kit (ThermoFisher Scisntific) and Bioanalyzer RNA 6000 Pico kit (Agilent).

Illumina indexed library preparation

The preparation of indexed libraries from RNA and sequencing using Illumina's ScriptSeq v2 Sample Preparation Kit (Illumina) follows these steps: fragmentation of RNA and primer hybridization, cDNA synthesis where RNA is converted to cDNA, then adapter sequences and indexes are added onto the ends of the fragments to generate libraries using PCR that was run as multiplexed paired-end sequencing libraries on an Illumina sequencer. RNA fragmentation step depends on the size of the RNA fragments. As less than 40% of the RNA obtained was more than 600 nt, no fragmentation was done. Nevertheless, A maximum of 5 µg of RNA was mixed 2µL of cDNA primer (200 µM) and incubated at 65°C for 5 minutes on a thermal cycler, then placed on ice (1 µLµL of fragmentation solution was added after

incubation according to the manufacturer's instructions). 3 µLµL of the cDNA synthesis premix obtained previously was mixed with 0.5 µL DTT 100 mM and 0.5 µL StarScript Reverse Transcriptase. The reaction was incubated at 25°C for 5 minutes, by 42°C for 20 minutes and hold at 37°C. Then 1 µL of finishing solution was added and the reaction was incubated at 37°C for 10 minutes, 95°C for 3 minutes and hold at 25°C. 8 µLµL of Tagging Master mix (7.5 µL Terminal Tagging Premix and 0.5 µL DNA polymerase was added and the tubes were incubated at 25°C for 15 minutes, 95°C for 3 minutes and hold on ice. The purification of the cDNA was performed using Agencourt AMPure XP beads. PCR was performed using Failsafe PCR Enzyme Mix (Illumina). It starts by preparing a PCR Master Mix (25 µL of PCR Premix E, 1 µL of forward PCR primer and 0.5 µL of Failsafe enzyme (2.5U/µL) and adding 1 µL of Index Primer (Script Seq Index PCR primers, Illumina). The reaction was incubated in the thermocycler as follows: 95°C for 1 minute, 15 cycles of 95°C for 30 seconds, 55°C for 30 seconds and 68°C for 3 minutes. The samples were then incubated at 68°C for 7 minutes and hold at 4°C. The PCR products clean-up was done using AMPure XP beads. The validation and the control of the quality of the library was done using Qubit-IT dsDNA HS assay kit and BioAnalyzer DNA high sensitivity kit (Agilent). Accurate quantification of the amplified library products is important for the sequencing results on the Illumina next-generation sequencing platforms. A qPCR (using KAPA SYBR FAST universal qPCR kit for illumine libraries) was performed in order to obtain an accurate quantification of the amplifiable molecules in the DNA libraries.

Illumina sequencing and data analysis pipeline

Libraries were sequenced on Illumina NextSeq 500 instrument, using Nextseq Sequencing Kit HO 300 cycles (Illumina) according to the manufacturer's instruction (paired end sequencing mode).

The raw reads of RNA-seq data were processed using Pipeline for Reference based Transcriptomics (PiReT) software (https://github.com/mshakya/PyPiReT). Briefly, the reads were aligned and assigned to the reference genomes using HISAT2 version [version information is available in github repo]. Aligned reads were then analyzed and assigned to individual genes according to the genome annotations (Genbank; GCF_002587065.1 and GCF_002586745.1 for CA23 and CU5 respectively). The normalized read counts for each gene, RPKM, was calculated by an R software, package EdgeR.

Graphical representations of differential gene expression data obtained from pairwise comparison (Volcano plots, PCA, Heatmaps) were created using R software [62] including the ggplot 2 package [63].

Genomic analysis for the genes involved in solid iron reduction, polyphosphate accumulation and virulence

Genomic analysis was performed in order to identify the potential genes involved in iron reduction in CA23 and CU5. To do so, we extracted the sequences of the proteins involved in solid iron reduction in the model bacterium *S. oneidensis* MR-1 (NC_004347.2) from NCBI (MtrA NP_717386.1, MtrB NP_717385.1, MtrC NP_717387.1,OmcA NP_717388.1, CymA NP_720107.1) as well as the homologes of mtrCAB in *A. hydrophila* ATCC 7966 (AHA_2765: YP_857273.1, AHA_2766: YP_857274.1, AHA_2764: YP_857272.1) and we performed a similarity search against the proteome of CA23 and CU5 (NZ_CP023818.1 and NZ_CP023817.1 respectively) using blastp, blastp suite, blastn, tblastn [64] and Needleman Wunsh [65] similarities alignment techniques. The iron reduction pathways of both CA23 and CU5 were drown using ChemDraw Professional (version 16.0.0.82(68)) [66]. To identify the

genes involved in polyphosphate accumulation, we extracted the locus tag of these genes from the annotation files of the genomes of CA23, CU5, *A. hydrophila* ATCC 7966 (NC_008570.1, GCA_000014805.1), *A. salmonicida* A449 (NC_009348.1, GCA_000196395.1) and *A. veronii* B565 (NZ_CP012504.1, GCA_000204115.1).

Whole genome sequencing of CA23 and CU5 strains

Genomic DNA of the bacterial isolates was extracted using the Qiagen G20 for bacteria according to the manufacturer's instructions with a modification consisting on washing the bacterial pellet with PIV solution (composition, in 990 mL of nanopore water, addition of 10 mL 1M Tris-HCl, pH8 and 58.4g NaCl) before resuspension in B1 buffer. The two genomes were sequenced using PacBio RSII sequencer (Microsynth AG, Switzerland). PacBio long read library was assembled with HGAP3 [67], version 2.3.0 and the genomes were annotated using Prokka pipeline [68], version 1.11. The complete genomic sequences of CA23 and CU5 were deposited in GenBank under accession numbers of NZ_CP023818.1 and NZ_CP023817.1 respectively.

Phylogenetic analysis

Phylogenetic Analysis and Moecular Evolution (PhaME) software [69] was used to reconstruct Single Nucleotide Polymorphisms(SNPs) phylogeny of *Aeromonas* spp. Briefly, PhaME aligned the genomes of *Aeromonas*, removed regions that are not conserved across all genomes, and calculated SNPs from the conserved regions. The SNP alignment were then used to reconstruct maximum likelihood phylogeny using RAxML. *Aeromonas* genomes were downloaded from genbank (files downloaded the 07/27/2017). The resulting tree was visualized using Newick utilities [70].

Development of user-friendly treatment of archaeological iron nails

For this treatment, we tested the effect of the two bacteria CA23 and CU5 on the stabilization of archaeological iron nails in a gel delivery system**.** Before being in contact with the bacteria, the nails were sterilized using 70% (v/v) ethanol and under UV light for 1h. Phytagel™ (an agar substitute produced from a bacterial fermentation composed of glucuronic acid, rhamnose and glucose, P8169 SIGMA-ALDRICH, CAS number 71010-52-1), was chosen as delivery system. This The gelling agent in its initial powder format was sterilized under UV for 30 min before being mixed with the bacterial culture.

For each nail: 100 mL of an overnight culture at room temperature of CA23 and CU5 with an OD (measured at 600nm) of 1.080 and 1.027 respectively were centrifuged at 4000 rpm for 10 minutes. The cells' pellet was washed twice with 20 mM PIPES solution. The pellet was mixed with 1g of the gelling agent Phytagel™, and 1mL of sodium bicarbonate and 0.5mL of sodium lactate were added to this gel mixture. The system bacteria-gel was applied to the nails. These latter were then covered with cellophane and stored at room temperature. Two conditions were tested: incubation under oxic (the nails were in petri dishes) and under anoxic conditions (using Anaerocult A© bags, Merck). To test the treatment's efficiency and according to the results obtained with the iron coupons, the treatment was stopped after 1 and 2 months of incubation for each bacterium. Concerning the abiotic control: 2g of gelling agent were mixed with 10 mL of 20 mM PIPES solution amended with 5 mM sodium lactate and 50 mM sodium bicarbonate.

Genome comparison

Genomes comparison was performed using: (i) ACT (Artemis Comparison Tool) [71,72], a pairwise comparisons tool between complete genome sequences and associated annotations. DNA sequences were used to identify and analyze regions of similarity and difference between genomes. (ii) ANI (average nucleotide identity) calculator from Kostas Lab [73,74] (http://enve-omics.ce.gatech.edu/ani/ default settings) was used to measure the nucleotide-level genomic pair-wise similarity between the coding regions of the genomes.

Physiological characterization of CA23 and CU5

VITEK® 2 Compact consists on biochemical tests for the physiological identification of bacteria. It is an automated microbiology system utilizing growth-based technology in different biochemical conditions contained in colorimetric reagent cards. From a fresh culture of pure bacterial strain, 0.5 McFarland suspension was prepared using sterile physiological water. The bacterial suspension was then inoculated in wells contained in a VITEK card. Each well corresponds to an individual test substrate. Substrates measure some metabolic activities such as carbon source utilization, enzymatic activities, and resistance. A transmittance optical system allows interpretation of test reactions using different wavelengths (660 nm, 568 nm, 430 nm). During incubation at 35.5°C, each test reaction is read every 15 minutes to measure either turbidity or colored products of substrate metabolism. (See table SI2).

Antibiotic resistance of CA23 and CU5 was performed using antibiograms containing different antibiotics at defined quantities. The MIC (mg/l) and the zone diameter (mm) breakpoints were determined using broth microdilution (ISO standard 20776-1; medium: Mueller-Hinton broth, inoculum: $5x10^5$ CFU/ml, incubation: Sealed panels, air, 35±1ºC, 18±2h) and disk diffusion (EUCAST standardized disk diffusion method; medium: Mueller-Hinton agar, inoculum: McFarland 0.5, incubation: Air, 35±1ºC, 18±2h) methods respectively. The sensitivity/resistance were measured for each antibiotic tested using the machine SIRSCAN-2000. (See table SI4).

RAMAN spectroscopy analysis

Non-destructive Raman spectroscopy was performed directly on the samples to define the molecular composition of the corrosion layer before and after bacterial treatment. The analysis was carried out with a Horiba-Jobin Yvon Labram Aramis microscope equipped with a Nd:YAG laser of 532 nm at a power lower than 1 mW. The spectral interval analyzed was between 100 and 1600 cm^{-1}. Single points analyses were carried out with the following conditions: 400-µm hole, 100xLWD objective, D2 filter, 100-µm slit, and 5 accumulations of 100 s. The spectra recorded were corrected (automatic baseline correction) using LabSpec NGS spectral software. Reference spectra were used for identifying the compounds present.

Fourier Transform Infrared Spectroscopy (FTIR) analyses

FTIR measurements were performed on the minerals formed on the surface of the nails. An iS5 Thermo Scientific spectrometer with a diamond Attenuated Total Reflectance (ATR) crystal plate (iD5™ ATR accessory) was used. All spectra were acquired in the range 4000–650 cm^{-1}, at a spectral resolution of 4 cm^{-1}. A total of 32 scans were recorded and the resulting interferograms averaged. Data collection and post-run processing were carried out using Omnic™ software.

Acknowledgments

The Swiss National Science Foundation (Ambizione grant PZ00P2_142514, P.I. Dr. Edith Joseph) for the funding of MAIA project (Microbes for archaeological iron Artifacts).

The Swiss Integrative Center for Human Health (SICHH) and especially Dr Marck Ambühl and Dr Ana Raduta for the confocal microscopy analysis.

Author contribution

WMK designed and performed the experiments, analyzed the data and wrote the manuscript. TJ, MS, KD, CG, KM and PC performed the RNA sequencing data analysis; MM performed the Raman analysis, KV, OS, IM performed the XRD analysis. TM performed the antibiogram and VITEK analysis; EJ performed the Raman data analysis and corrected the manuscript and PJ designed the experiments, analyzed the data and wrote and corrected the manuscript.

References

1. Dinh, H. T. *et al.* Iron corrosion by novel anaerobic microorganisms. *Nature* **427,** 829–832 (2004).

2. Straub, K. L., Benz, M. & Schink, B. Iron metabolism in anoxic environments at near neutral pH. *FEMS Microbiol. Ecol.* **34,** 181–186 (2001).

3. S. Berg, J. *et al.* Intensive cryptic microbial iron reduction in the low iron water column of the meromictic Lake Cadagno. *Environ. Microbiol.* **18,** 5288–5302 (2016).

4. Knight, V. & Blakemore, R. Reduction of diverse electron acceptors by *Aeromonas hydrophila*. *Arch. Microbiol.* **169,** 239–248 (1998).

5. Benz, M., Brune, a. & Schink, B. Anaerobic and aerobic oxidation of ferrous iron at neutral pH by chemoheterotrophic nitrate-reducing bateria. *Arch Microbiol.* **169,** 159–165 (1998).

6. García-Balboa, C. *et al.* Bio-reduction of Fe(III) ores using three pure strains of *Aeromonas hydrophila*, *Serratia fonticola* and *Clostridium celerecrescens* and a natural consortium. *Bioresour. Technol.* **101,** 7864–7871 (2010).

7. Gadd, G. M. Metals, minerals and microbes: Geomicrobiology and bioremediation. *Microbiology* **156,** 609–643 (2010).

8. Widdel, F. *et al.* Ferrous iron oxidation by anoxygenic phototrophic bacteria. *Nature* **362,** 834–836 (1993).

9. Sarin, P., Snoeyink, V. L., Lytle, D. A. & Kriven, W. M. Iron corrosion scales: model for sclae growth, iron release and colored water formation. *J. Environ. Eng.* **130,** 364–373 (2004).

10. Tweed, C. & Sutherland, M. Built cultural heritage and sustainable urban development. *Landsc. Urban Plan.* **83,** 62–69 (2007).

11. Goral, A. Research on cultural tourism development in sacral and spiritual sites from the UNESCO World Heritage List. *Int. J. Herit. Sustain. Dev.* **1,** 49–59 (2011).

12. Chhabra, D., Healy, R. & Sills, E. Staged authenticity and heritage tourism. *Ann. Tour. Res.* **30,** 702–719 (2003).

13. Pienimäki, A. Desalination of iron. A comparison of fresh, wet finds and dry storage ones. (Helsinki Metropolia University of Applied Sciences, 2016).

14. Watkinson, D. & Lewis, M. ss Great Britain iron hull: modelling corrosion to define storage relative humidity. *Met. 2004* **44,** 88–102 (2004).

15. Chaudhuri, S. K., Lack, J. G. & Coates, J. D. Formation through Anaerobic Biooxidation of Fe (II) Biogenic Magnetite. *Appl. Environ. Microbiol.* **67,** 2844–2948 (2001).

16. Kooli, W. M. *et al.* Bacterial iron reduction and biogenic mineral formation for the stabilisation of corroded iron objects. *Sci. Rep.* **8,** 764 (2018).

17. Comensoli, L. *et al.* Use of bacteria to stabilize archaeological iron. *Appl. Environ. Microbiol.* (2017). doi:10.1128/AEM.03478-16

18. Selwyn, L. overview of archeological iron: the corrosion problem, key factors affecting

treatment and gaps in current knowledge. *Natl. museum Aust. Canberra* 294–306 (2004).

19. Selwyn, L. S., Sirois, P. J. & Argyropoulos, V. Maney Publishing The Corrosion of Excavated Archaeological Iron with Details on Weeping and Akaganéite. *Stud. Conserv.* **44,** 217–232 (1999).

20. Igbinosa, I. H., Igumbor, E. U., Aghdasi, F., Tom, M. & Okoh, A. I. Emerging *Aeromonas* Species Infections and Their Significance in Public Health. *Sci. World J.* 1–13 (2012). doi:10.1100/2012/625023

21. Seshadri, R. *et al.* Genome sequence of *Aeromonas hydrophila* ATCC 7966T: Jack of all trades. *J. Bacteriol.* **188,** 8272–8282 (2006).

22. Wang, X. J., Chen, X. P., Kappler, A., Sun, G. X. & Zhu, Y. G. Arsenic binding to iron(II) minerals produced by an iron(III)reducing *Aeromonas* strain isolated from paddy soil. *Environ. Toxicol. Chem.* **28,** 2255–2262 (2009).

23. Woźnica, A., Dzirba, J., Mańka, D. & Łabuzek, S. Effects of electron transport inhibitors on iron reduction in *Aeromonas hydrophila* strain KB1. *Anaerobe* **9,** 125–130 (2003).

24. Cao, F. *et al.* Enhanced biotransformation of DDTs by an iron- and humic-reducing bacteria *Aeromonas hydrophila* HS01 upon addition of goethite and anthraquinone-2,6-disulphonic disodium salt (AQDS). *J. Agric. Food Chem.* **60,** 11238–11244 (2012).

25. Pham, C. A. *et al.* A novel electrochemically active and Fe(III)-reducing bacterium phylogenetically related to *Aeromonas hydrophila*, isolated from a microbial fuel cell. *FEMS Microbiol. Lett.* **223,** 129–134 (2003).

26. Shi, L., Rosso, K. M., Zachara, J. M. & Fredrickson, J. K. Mtr extracellular electron-transfer pathways in Fe(III)-reducing or Fe(II)-oxidizing bacteria: a genomic perspective. *Biochem. Soc. Trans.* **40,** 1261–1267 (2012).

27. Bullen, J. J., Rogers, H. J., Spalding, P. B. & Ward, C. G. Iron and infection: The heart of the matter. *FEMS Immunol. Med. Microbiol.* **43,** 325–330 (2005).

28. Janda, J. M. & Abbott, S. L. The genus *Aeromonas*: Taxonomy, pathogenicity, and infection. *Clin. Microbiol. Rev.* **23,** 35–73 (2010).

29. Ghatak, S. *et al.* Pan-genome analysis of *Aeromonas hydrophila, Aeromonas veronii and Aeromonas caviae* indicates phylogenomic diversity and greater pathogenic potential for *Aeromonas hydrophila*. *Antonie van Leeuwenhoek, Int. J. Gen. Mol. Microbiol.* **109,** 945–956 (2016).

30. Li, Y. & Cai, S. H. Identification and pathogenicity of *Aeromonas sobria* on Tail-rot disease in Juvenile Tilapia Oreochromis niloticus. *Curr. Microbiol.* **62,** 623–627 (2011).

31. Garduno, R. A. & Kay, W. W. Interaction of the fish pathogen *Aeromonas salmonicida* with rainbow trout macrophages. *Infect. Immun.* **60,** 4612–4620 (1992).

32. Lorén, J. G., Farfán, M. & Fusté, M. C. Molecular phylogenetics and temporal diversification in the genus *Aeromonas* based on the sequences of five housekeeping genes. *PLoS One* **9,** (2014).

33. Colston, S. M. *et al.* Bioinformatic genome comparisons for taxonomic and

phylogenetic assignments using *Aeromonas* as a test case. *MBio* **5,** 1–13 (2014).

34. Sanglas, A., Albarral, V., Farfán, M., Lorén, J. G. & Fusté, M. C. Evolutionary roots and diversification of the genus *Aeromonas*. *Front. Microbiol.* **8,** 1–13 (2017).

35. Uhrynowski, W. *et al.* Analysis of the genome and mobilome of a dissimilatory arsenate reducing *Aeromonas* sp. O23A reveals multiple mechanisms for heavy metal resistance and metabolism. *Front. Microbiol.* **8,** 1–12 (2017).

36. Khor, W. C., Puah, S. M., Tan, J. A. M. A., Puthucheary, S. D. & Chua, K. H. Phenotypic and genetic diversity of *Aeromonas* species isolated from fresh water lakes in Malaysia. *PLoS One* **10,** (2015).

37. Soler, L. *et al.* Phylogenetic analysis of the genus *Aeromonas* based on two housekeeping genes. *Int. J. Syst. Evol. Microbiol.* **54,** 1511–1519 (2004).

38. Beaz-Hidalgo, R. *et al. Aeromonas aquatica* sp. nov., *Aeromonas finlandiensis* sp. nov. and *Aeromonas lacus* sp. nov. isolated from Finnish waters associated with cyanobacterial blooms. *Syst. Appl. Microbiol.* **38,** 161–168 (2015).

39. Saavedra, M. J., Figueras, M. J. & Martínez-Murcia, A. J. Updated phylogeny of the genus *Aeromonas*. *Int. J. Syst. Evol. Microbiol.* **56,** 2481–2487 (2006).

40. Martínez-Murcia, A. J. *et al.* Phenotypic, genotypic, and phylogenetic discrepancies to differentiate *Aeromonas salmonicida* from *Aeromonas bestiarum*. *Int. Microbiol.* **8,** 259–269 (2005).

41. Beaz-Hidalgo, R., Hossain, M. J., Liles, M. R. & Figueras, M. J. Strategies to avoid wrongly labelled genomes using as example the detected wrong taxonomic affiliation for *Aeromonas* genomes in the genbank database. *PLoS One* **10,** 1–13 (2015).

42. Valdes, N. *et al.* Draft genome sequence of the Chilean isolate *Aeromonas salmonicida* strain CBA100. *FEMS Microbiol. Lett.* **362,** 1–4 (2015).

43. Gauthier, J., Vincent, A. T., Charette, S. J. & Derome, N. Strong genomic and phenotypic heterogeneity in the *Aeromonas sobria* species complex. *Front. Microbiol.* **8,** 1–14 (2017).

44. Weber, K. a., Achenbach, L. a. & Coates, J. D. Microorganisms pumping iron: anaerobic microbial iron oxidation and reduction. *Nat. Rev. Microbiol.* **4,** 752–764 (2006).

45. White, G. F. *et al.* in *Advances in Microbial Physiology* **68,** 87–138 (Elsevier Ltd., 2016).

46. Comeau, Y., Hall, K., Hancock, R. & Oldham, W. Biochemical model for enhanced biological phosphorus removal. *Water Res.* **20,** 1511–1521 (1986).

47. Alcántara, C., Blasco, A., Zúñiga, M. & Monedero, V. Accumulation of polyphosphate in *Lactobacillus* spp. and its involvement in stress resistance. *Appl. Environ. Microbiol.* **80,** 1650–1659 (2014).

48. Mullan, A., Quinn, J. P. & McGrath, J. W. Enhanced phosphate uptake and polyphosphate accumulation in *Burkholderia cepacia* grown under low-pH conditions. *Microb. Ecol.* **44,** 69–77 (2002).

49. Merzouki, M., Delgenès, J. P., Bernet, N., Moletta, R. & Benlemlih, M.

Polyphosphate-accumulating and denitrifying bacteria isolated from anaerobic-anoxic and anaerobic-aerobic sequencing batch reactors. *Curr. Microbiol.* **38,** 9–17 (1999).

50. Sidat, M., Bux, F. & Kasan, H. C. Polyphosphate accumulation by bacteria isolated from activated sludge. *Water SA* **25,** 175–179 (1999).

51. Merzouki, M., Bernet, N., Delgenès, J. P., Moletta, R. & Benlemlih, M. Kinetic behavior of some polyphosphate-accumulating bacteria isolates in the presence of nitrate and oxygen. *Curr. Microbiol.* **38,** 300–308 (1999).

52. Tomás, J. M. The main *Aeromonas* pathogenic factors. *ISRN Microbiol.* (2012). doi:10.5402/2012/256261

53. Janda, J. M. Recent Advances in the Study of the Taxonomy , Pathogenicity , and Infectious Syndromes Associated with the Genus *Aeromonas*. **4,** 397–410 (1991).

54. Fuchs, S., Pané-Farré, J., Kohler, C., Hecker, M. & Engelmann, S. Anaerobic gene expression in *Staphylococcus aureus*. *J. Bacteriol.* **189,** 4275–4289 (2007).

55. Ballal, A., Ray, B. & Manna, A. C. sarZ, a sarA family gene, is transcriptionally activated by MgrA and is involved in the regulation of genes encoding exoproteins in *Staphylococcus aureus*. *J. Bacteriol.* **191,** 1656–1665 (2009).

56. Chen, P. R. *et al.* A new oxidative sensing and regulation pathway mediated by the MgrA homologue SarZ in *Staphylococcus aureus*. *Mol. Microbiol.* **71,** 198–211 (2009).

57. Rio, R. V. M., Anderegg, M. & Graf, J. Characterization of a catalase gene from *Aeromonas veronii*, the digestive-tract symbiont of the medicinal leech. *Microbiology* **153,** 1897–1906 (2007).

58. Shijuku, T. *et al.* Expression of chaA, a sodium ion extrusion system of *Escherichia coli*, is regulated by osmolarity and pH. *Biochim. Biophys. Acta - Bioenerg.* **1556,** 142–148 (2002).

59. Frost, R., Martens, W., Williams, P. & Kloprogge, J. Raman and infrared spectroscopic study of the vivianite-group phosphates vivianite, baricite and bobierrite. *Mineral. Mag.* **66,** 1063–1073 (2002).

60. Frost, R. L. *et al.* Vibrational spectroscopic characterization of the phosphate mineral barbosalite Fe2+Fe3+2 (PO4)2(OH)2 -Implications for the molecular structure. *J. Mol. Struct.* **1051,** 292–298 (2013).

61. Bell, P. E., Mills, a L. & Herman, J. S. Biogeochemical Conditions Favoring Magnetite Formation during Anaerobic Iron Reduction. *Appl. Environ. Microbiol.* **53,** 2610–2616 (1987).

62. R Core Team. R Core Team (2017). R: A language and environment for statistical computing. *R Found. Stat. Comput. Vienna, Austria. URL http//www.R-project.org/*. R Foundation for Statistical Computing (2017).

63. Wickham, H. *ggplot2:Elegant Graphics for Data Analysis*. *Media* **35,** (2009).

64. Johnson, M. *et al.* NCBI BLAST: a better web interface. *Nucleic Acids Res.* **36,** 5–9 (2008).

65. Needleman, S. B. & Wunsch, C. D. A general method applicable to the search for similarities in the amino acid sequence of two proteins. *J. Mol. Biol.* **48,** 443–453 (1970).

66. Mills, N. ChemDraw Ultra 10.0. *J. Am. Chem. Soc.* **128,** 13649–13650 (2006).

67. Chin, C. S. *et al.* Nonhybrid, finished microbial genome assemblies from long-read SMRT sequencing data. *Nat. Methods* **10,** 563–569 (2013).

68. Seemann, T. Prokka: Rapid prokaryotic genome annotation. *Bioinformatics* **30,** 2068–2069 (2014).

69. Ahmed, S. A., Lo, C.-C., Li, P.-E., Davenport, K. W. & Chain, P. S. G. From raw reads to trees: Whole genome SNP phylogenetics across the tree of life. *bioRxiv* (2015). doi:10.1101/032250

70. Junier, T. & Zdobnov, E. M. The Newick utilities: high-throughput phylogenetic tree processing in the UNIX shell. *Bioinformatics* **26,** 1669–1670 (2010).

71. Carver, T. *et al.* Artemis and ACT: Viewing, annotating and comparing sequences stored in a relational database. *Bioinformatics* **24,** 2672–2676 (2008).

72. Carver, T. J. *et al.* ACT: The Artemis comparison tool. *Bioinformatics* **21,** 3422–3423 (2005).

73. Goris, J. *et al.* DNA-DNA hybridization values and their relationship to whole-genome sequence similarities. *Int. J. Syst. Evol. Microbiol.* **57,** 81–91 (2007).

74. Rodriguez-r, L. M. & Konstantinidis, K. T. Bypassing Cultivation To Identify Bacterial Species. *Microbe* **9,** 111–118 (2014).

75. Lies, D. P., Mielke, R. E., Gralnick, J. A. & Newman, D. K. *Shewanella oneidensis* MR-1 Uses overlapping Pathways for Iron Reduction at a Distance and by Direct Contact under Conditions Relevant for Biofilms. *Appl. Environ. Microbiol.* **71,** 4414–4426 (2005).

76. Saffarini, D., Brockman, K., Beliaev, A., Bouhenni, R. & Shirodkar, S. in *Bacteria-Metal Interactions* 21–40 (2015). doi:10.1007/978-3-319-18570-5

77. Cheng, Y. Y. *et al.* Promotion of iron oxide reduction and extracellular electron transfer in *Shewanella oneidensis* by DMSO. *PLoS One* **8,** (2013).

Supplementary information

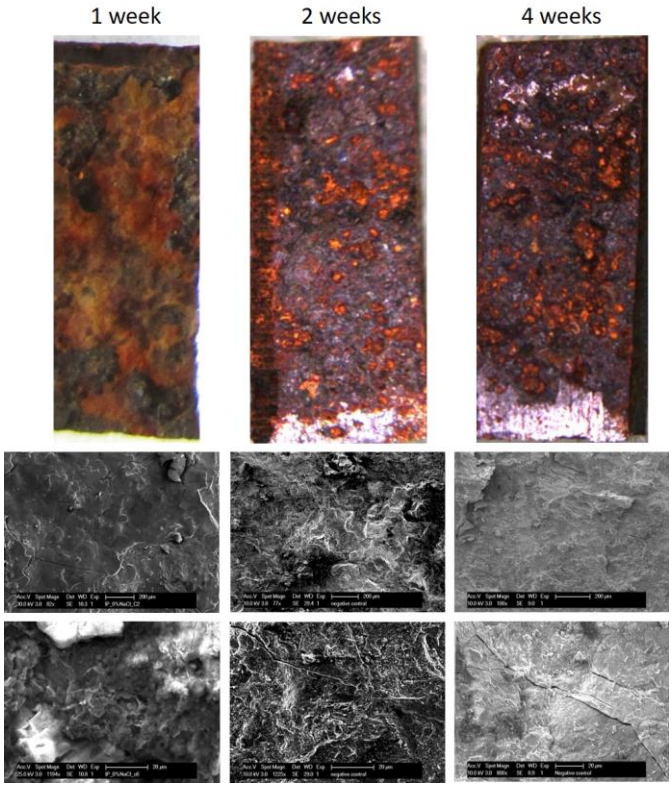

Figure SI1: Scanning electron microscopy (SEM) images and visual aspect of the abiotic control treated coupons, after 1, 2 and 4 weeks on incubation

Table SI1: Atomic percentages (AT%) of the elements obtained from the Energy-dispersive X-ray spectroscopy (EDS) measurements performed on the abiotic iron coupons after 1, 2 and 4 weeks of incubation. "-" stands for not detected

Elements (AT%)	1 week	2 weeks	4 weeks
C	16.45	10.03	11.99
O	57.93	45.03	50.58
Fe	24.58	43.06	33.40
Na	-	-	1.55
Si	0.65	1.88	2.47
S	0.40	-	-

Table SI2: Biochemical reactions of CA23 and CU5 determining their physiological characteristics

Test	CA23	CU5
Ala-Phe-Pro-Arylamidase (APPA)	-	-
Adonitol (ADO)	-	-
L-Pyrrolidonyl-arylamidase (PyrA)	-	+
L-arabitol (IARL)	-	-
D-cellobiose (dCEL)	-	-
β-galactosidase (BGAL)	-	-
H2S production	-	-
β2S productglucosaminidase (BNAG)	+	+
Glutamyl Arylamidase pNA (AGLTp)	-	-
D-glucose (dGLU)	+	+
γGGlutamyl-transferase (GGT)	-	-
Glucose fermentation (OFF)	+	-
β -glucosidase (BGLU)	-	-
D-maltose (dMAL)	+	+
D-mannitol (dMAN)	-	-
D-mannose (dMNE)	-	+
β -xylosidase (BXYL)	-	-
β(BAlanine arylamidase pNA (BAIap)	-	-
L-Proline-arylamidase (ProA)	+	+
Lipase (LIP)	+	-
Palatinose (PLE)	-	-
Tyrosine-arylamidase (TyrA)	+	+
Urease (URE)	-	-
D-sorbitol (dSor)	-	-
Saccharose/Sucrose (SAC)	+	+
D-tagatose (dTAG)	-	-
D-trehalose (dTRE)	+	+
Sodium citrate (CIT)	-	-
Malonate (MNT)	-	-
5-ceto-D-gluconate (5KG)	-	-
L-lactate alcalinization (ILATk)	-	-
α-glucosidase (AGLU)	-	-
Succinate alcalinization (SUCT)	+	-
β-N-acetyl-galactosaminidase (NAGA)	-	-
α(galactosidase (AGAL)	-	-
Phosphatase (PHOS)	-	-
Glycine arylamidase (GlyA)	-	-
Ornithine decarboxylase (ODC)	-	-
Lysine decarboxylase (LDC)	-	-
L-histidine assimilation (IHISa)	-	-
Courmarate (CMT)	+	+
β(glucuronidase (BGUR)	-	-
O/129 (comp. vibrio.) resistance (O129R)	-	+
Glu-Gly-Arg-arylamidase (GGAA)	-	-
L-malate assimilation (IMLTa)	-	-
Ellman (ELLM)	+	+
L-lactate assimilation (ILATa)	-	-

Table SI3: Genes involved in iron reduction in *S. oneidensis* MR-1 (also *pilC* and *pilN* of *G. sulfurreducens*) and their homologues in *A. hydrophila* ATCC 7966, CA23 and CU5 using blastp. Id=identity, cov= coverage, x: not found

S.oneidensis	**Function**	**Literature**	***A. hydrophila***	**CA23**	**CU5**
cymA	Cytoplasmic membrane-bound periplasmic c-type cytochrome (required for anaerobic respiratory electron transport), is a menaquinol oxidase	[44,75,76]	*napC* WP_011705485.1 (id 31%, cov 95%)	CK910_RS20025 (id 31%, cov 95%) WP_043138459.1	CK911_02795 (id 32%, cov 95%) WP_098968901.1
undA	Outer membrane 11 heme c-type cytochrome in *Shewanella* sp. strain HRCR-6 and *S. putrefaciens*	[76]	x (ncbi id 22%, low cov)	X (id 37%, cov 67)	x (id 26%, cov 13%)
mtrA	Periplasmic Decaheme c-type cytochrome (electron shuttle). Could function as terminal reductase for soluble Fe(III)	[44,75,76]	AHA_2765	CK910_RS13415 WP_098983641.1	x very low id
mtrB	Outer membrane porin	[75,76]	AHA_2766	CK910_RS13395 WP_098983638.1	x
mtrC	Decaheme c-type cytrochrome	[76,77]	AHA_2764	CK910_RS13405 WP_098983639.1 (id 95%)	x very low id (id 31%)
omcA	Outer membrane decaheme c-type cytochrome	[76]	x WP_011706572.1 (id 21%, cov97%)	x	x
mtrD	Extracellular respiratory system periplasmic decaheme cytochrome c component	[76,77]	cytochromeC WP_011706573.1 (id55%, cov87%)	cystathionine beta-synthase WP_042866040.1 (multispecies: id 51%, cov95%) cytrochrome C WP_098983922.1 (id35%, cov71%)	cytochrome C WP_09896950 4.1 (id 29%, 87%cov)
mtrE	Extracellular respiratory system outer	[75]	outer membrane protein (id 27%, cov 98%). WP_011706574.1	hypotheticl protein WP_098983638.1 (id 28%, 98%cov)	x

	membrane component				
mtrF	Decaheme c-type cytochrome	[44,75]	x cytochromeC (id 28%, cov 98%) WP_011706572.1	cytochrome C WP_098983639.1 (id 24%, cov 98%)	x
cytc 3	Tetraheme c-type cytochrome in the periplasm (electron shuttle between electron carriers)	[75]	x	x	x
menC	Encode o-succinylbenzoic acid synthase, required for Menaquinone biosynthesis (extracellular electron transfer)	[75]	AHA_0528 osuccinylbenzoate synthase WP_011704501.1 (id36%, cov71%)	menC osuccinylbenzoate synthase WP_098980880.1	osuccinylbenzoate WP_098970730.1 (id 36%, cov71%)
menF	Protein for the menaquinone synthesis, isochorismate synthase	[44,76]	isochorismate synthase WP_011704505.1 id50%, cov90%)	isochorismate synthase WP_098980876.1 (id50%, cov90%)	isochorismate synthase WP_098970723.1 (id51%, cov90%)
hmuZ	FMN binding heme iron utilization protein	genbank	hutZ heme utilization protein (id 54%, cov 90%) WP_011704904.1	hutZ heme utilization protein (id 54%, cov 90%) WP_098980622.1	hutZ heme utilization protein (id 55%, cov 90%) WP_098968667.1
pilY *mshQ*	TypeIV pili and TypeIV pili adhesion		WP_011704651.1 Pilus biosynthesis protein (id23%, cov54%) mshQ WP_011704375.1 (id 37%, cov 97%)	Hypothetical protein WP_098980775.1 (id 39%, cov 97%) mshQ WP_098980973.1 (id 39%, cov 88%)	Hypothetical protein WP_098972176.1 (id 39%, cov 97%) Hypothetical protein WP_098971018.1 (id 29%, cov 56%)
pilA	Major component of type IV pili (nanowires) in *Geobacter sulfurreducens*		TypeII secretion system WP_011704371.1 (id 47%, cov 34%)	type IV pilin protein WP_098980778.1 (id 59%, cov 24%	type IV pilin protein(id 54%, cov 25% WP_098972170.1
fcca	Periplasmic fumarate reductase (genebank)	[76]	Fumarate reductase (id29%, cov 64%) WP_011706984.1	Fumarate reductase (id29%, cov 64%) WP_043555131.1	Fumarate reductase (id29%, cov 74%) WP_042020383.1
hydA	Periplasmic [Fe-Fe] hydrogenase large subunit (genebank)	[76]	x	x	x

pilC geobacter	Type IV pilus inner membrane protein		type II secretion system F family protein (id38%, 98%) WP_011707570.1	type II secretion system F family protein WP_098981882.1 (id39%, 99%)	type II secretion system F family protein (id38%, 99%) WP_068978945.1
pilN geobacter			x	x	x

Table SI4: Antibiogram results of CA23 and CU5. The bacteria show the same antibiogram profile where there's resistance to ampicillin, amoxicillin and cefalotin. R indicates resistance while S indicates sensitive

Antibiotic tested	**MIC breakpoint (mg/L)**		**Disk content (µg)**	**Zone diameter breakpoint (mm)**		**Result**
	S ≤	**R >**		**S ≥**	**R <**	
Ampicillin	8	8	10	14	14	**R**
Amoxicillin-clavulanic acid	8	8	20-10	19	19	**R**
Piperacillin-tazobactam	8	16	30-6	20	17	S
Ticarcillin	8	16	75	23	20	S
Cefalotin	16	16	30	12	12	**R**
Cefuroxim	8	8	30	19	19	S
Ceftriaxon	1	2	30	25	22	S
Ceftazidim	1	4	10	24	21	S
Cefepim	1	4	30	27	24	S
Imipenem	2	8	10	22	16	S
Ertapenem	0.5	1	10	25	22	S
Ciprofloxacin	0.25	0.5	5	27	24	S
Levofloxacin	0.5	1	5	27	24	S
Norfloxacin	0.5	1	10	22	19	S
Moxifloxacin	0.25	0.25	5	22	22	S
Trimethoprim+Sulfamethoxazol	2	4	1.25-	19	16	S
Amikacin	8	16	30	18	15	S
Gentamicin	2	4	10	17	14	S
Tobramycin	2	4	10	17	14	S
Fosfomycin	32	32	200	24	24	S
Nitrofurantoin	64	64	100	11	11	S

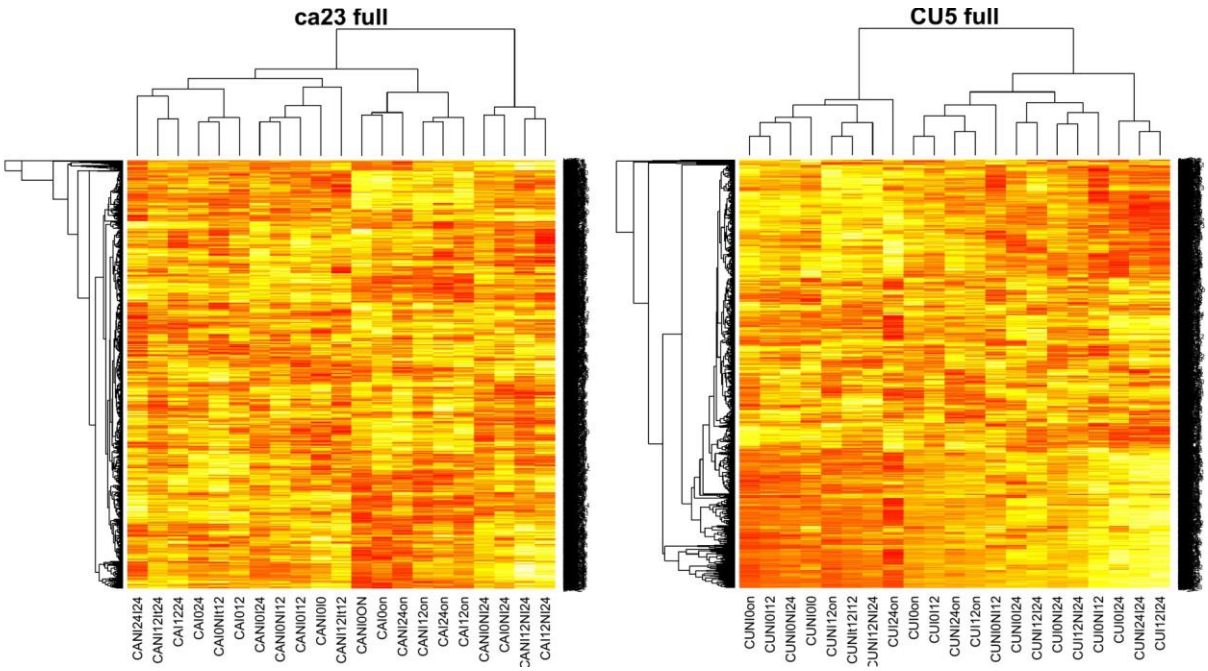

Figure SI2: Heatmap without filtering the genes with |log(FC)|>2 and selecting the interesting conditions

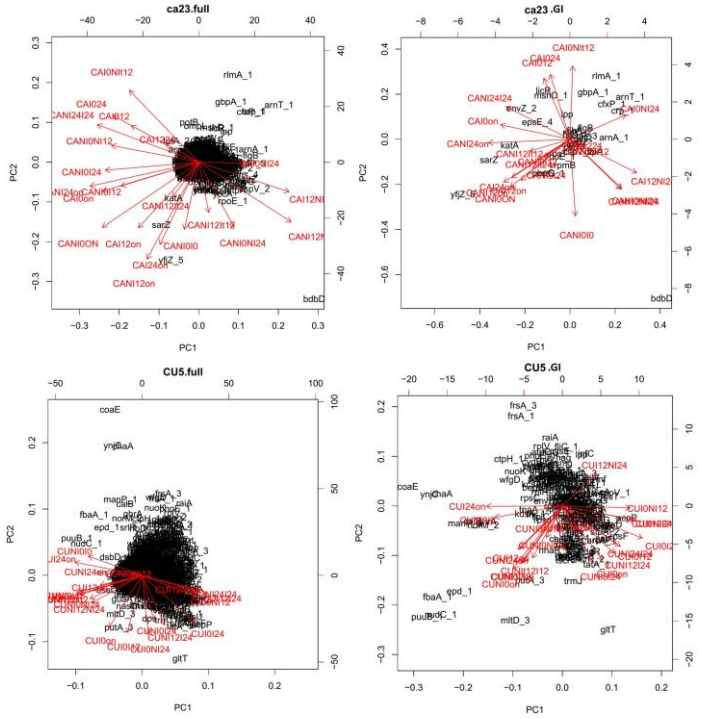

Figure SI3: PCA representation of the differential gene expression data. On the left column the entire data was presented and on the right column the data was filtered according to the |log(FC)|>2

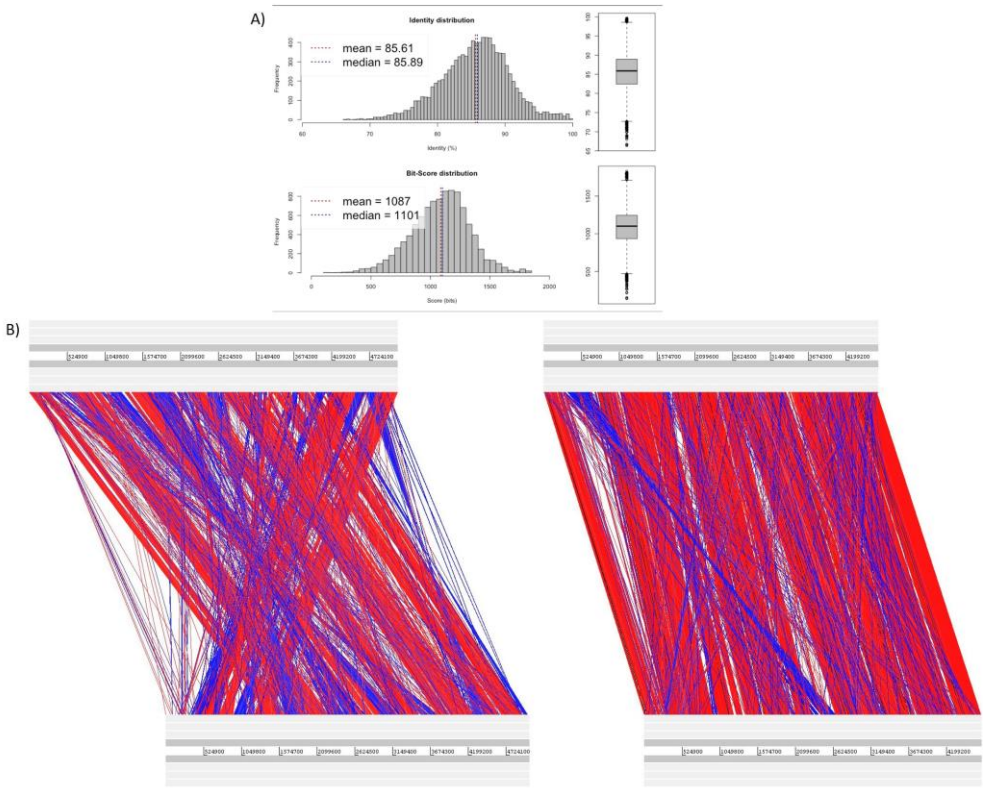

Figure SI4: Genomes comparison of CA23 and CU5. A) ANI results obtained when comparing CA23 and CU5. B) ACT results: CA23 (on the top left) and CU5 (on the top right) are compared respectively with: *A. salmonicida* CBA100 (bottom left) and *A. sobria* CECT 4245 (bottom right). The red and blue bands represent the forward and reverse matches, respectively, the white color represent the absence of matches

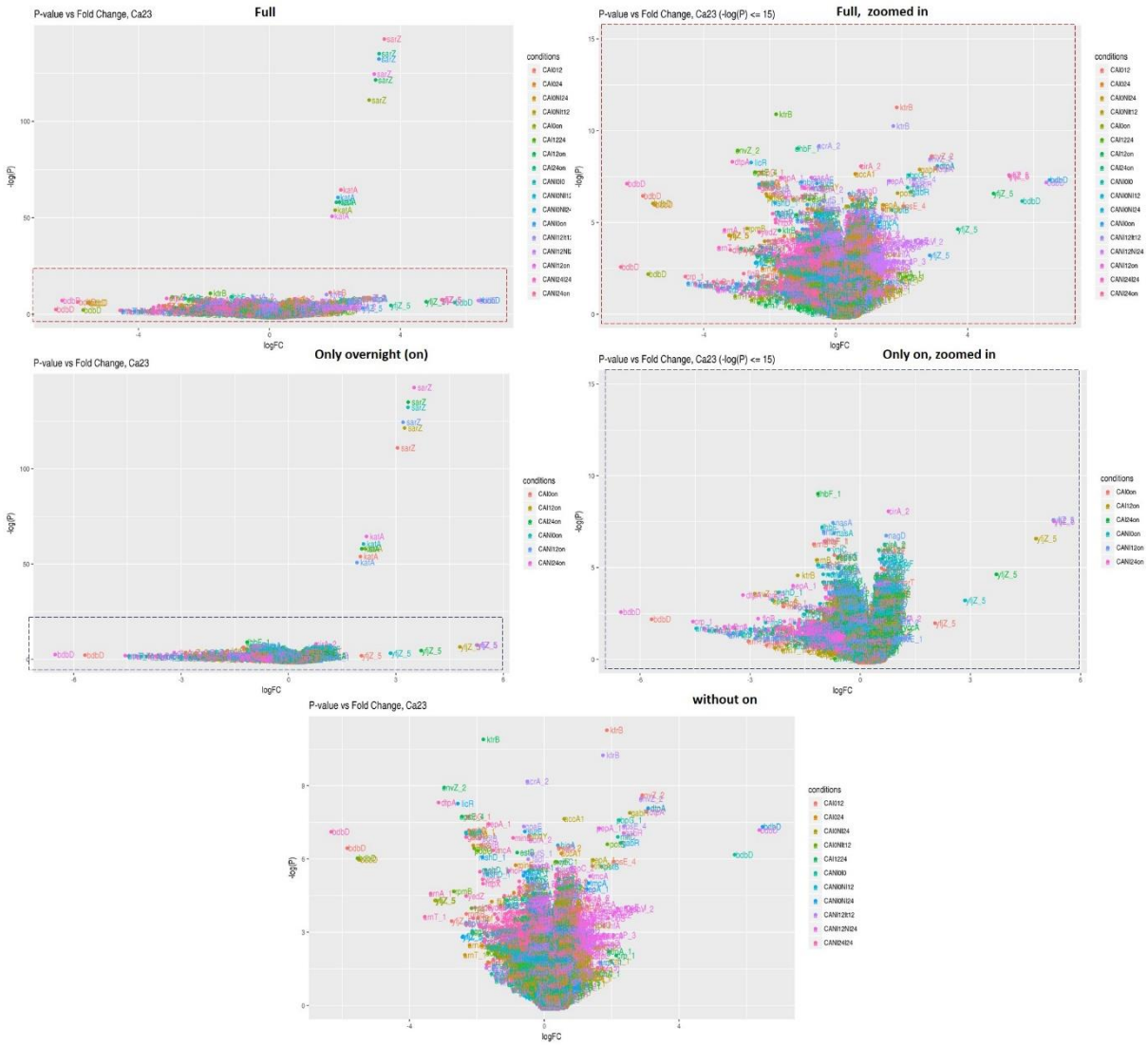

Figure SI5: Pairwise comparison on the Rna-seq data of CA23 using volcano plots (-log10Pvalue, Y axis, logFC, X axis). On the upper line, volcano plots representing the differential gene expression data without any selection. The middle line refers to the comparison of the conditions with and without iron with an overnight culture and the bottom line the pairwise comparisons of the conditions with and without iron at three different time points

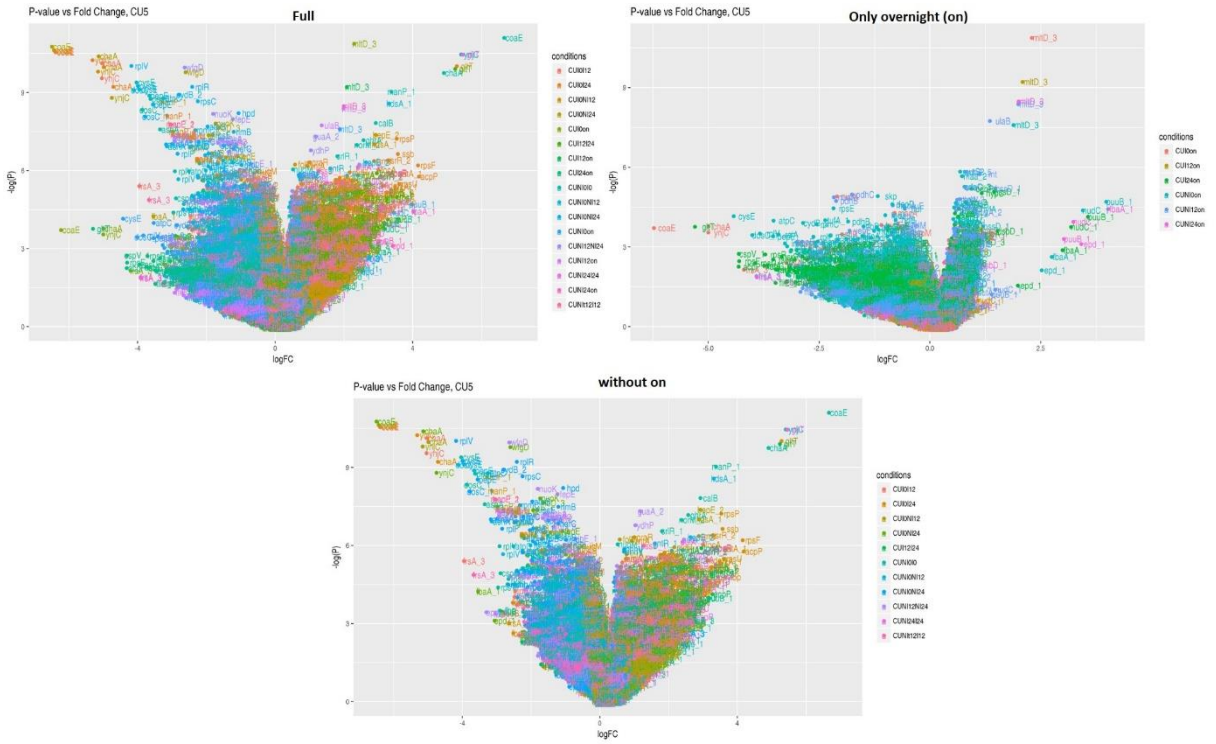

Figure SI6: Pairwise comparison on the Rna-seq data of CU5 using volcano plots (-log10Pvalue, Y axis, logFC, X axis). On the upper line, volcano plots representing the differential gene expression data without any selection. The middle line refers to the comparison of the conditions with and without iron with an overnight culture and the bottom line the pairwise comparisons of the conditions with and without iron at three different time points.

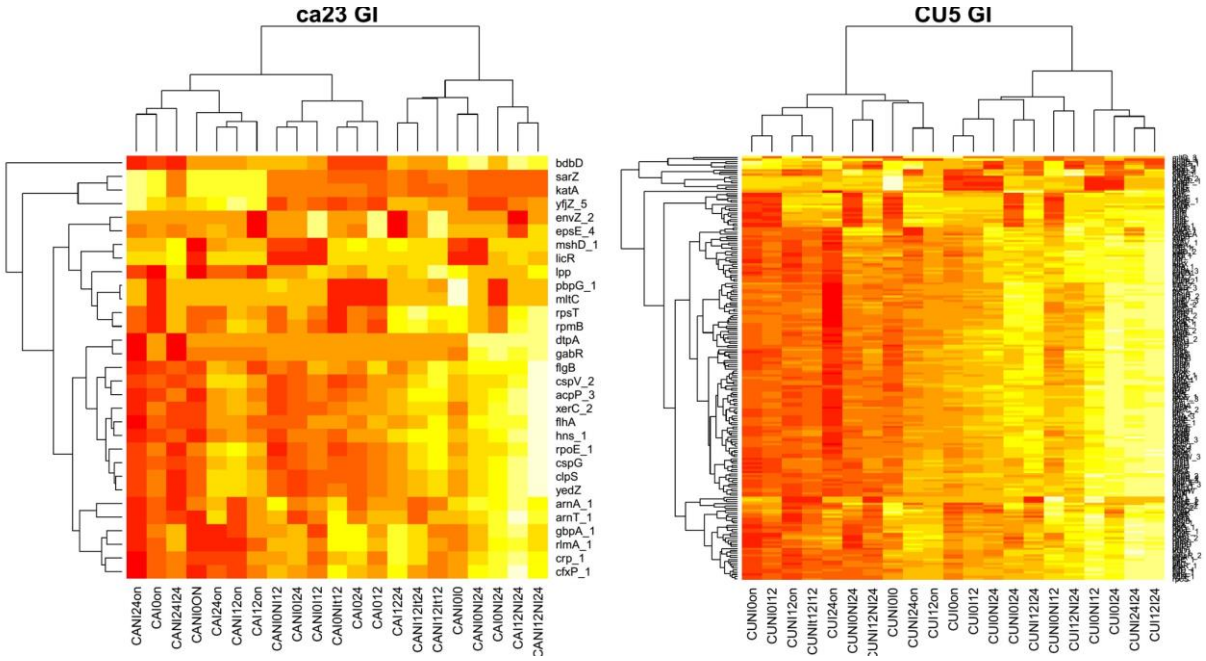

Figure SI7: Comparisons of transcriptional profiles of CA23 and CU5 across samples. Hierarchical clustering of transcripts and samples. Shown is a heatmap showing the relative expression levels of each transcript (columns) in each pairwise comparison (rows). Rows and columns are hierarchically clustered. Each cell in the matrix represents the expression level of a gene feature. Red and white in cells reflect low and high expression levels, respectively. Transcripts that are identified as significantly differentially expressed at |log(FC)|>2

Table SI10: Differential genes expression data of the comparison between iron containing and overnight conditions with CA23 and CU5 at three different time points 0, 12 and 24 hours. CAIxon=CA23, iron, xhour, overnight, CUIXon= CU5, iron, xhour, overnight. x= 0, 12 or 24 hours. |log(FC)|>2

Gene_ID	"conditions"	"logFC"	"P value"	"fonction"
"sarZ"	"CAI0on"	3.044310182	6.36E-49	"=HTH-type transcriptional regulator SarZ"
"katA"	"CAI0on"	2.004804216	3.60E-24	"=Catalase"
"pbpG_1"	"CAI0on"	-2.102925221	0.04567779	"=D-alanyl-D-alanine endopeptidase precursor"
"mltC"	"CAI0on"	-2.086679926	0.056215185	"=Membrane-bound lytic murein transglycosylase C precursor"
"bdbD"	"CAI0on"	-5.68802486	0.111690374	"=Disulfide bond formation protein D precursor"
"yfjZ_5"	"CAI0on"	2.031526504	0.138462311	"=Putative antitoxin YfjZ"
"flgB"	"CAI0on"	-2.324619156	0.174114179	"=Flagellar basal body rod protein FlgB"
"rpmB"	"CAI0on"	-2.366095971	0.195219527	"=50S ribosomal protein L28"
"rpsT"	"CAI0on"	-2.042790118	0.202635636	"=30S ribosomal protein S20"
"lpp"	"CAI0on"	-2.378498144	0.256878878	"=Major outer membrane lipoprotein Lpp precursor"
"acpP_3"	"CAI0on"	-2.114387889	0.28576533	"=Acyl carrier protein"
"crp_1"	"CAI0on"	-2.594102184	0.371326148	cAMP-activated global transcriptional regulator
"arnT_1"	"CAI0on"	-3.049590859	0.373359856	Undecaprenyl transferase
"arnA_1"	"CAI0on"	-2.285678411	0.375781517	Undecaprenyl transferase
"cfxP_1"	"CAI0on"	-2.270410192	0.412991186	Phosphoribulokinase%2C plasmid
"rlmA_1"	"CAI0on"	-2.55214254	0.462035956	23S rRNA (guanine(745)-N(1))-methyltransferase
"arnB_3"	"CAI0on"	-1.271031216	0.001872873	UDP-4-amino-4-deoxy-L-arabinose--oxoglutarate aminotransferase
"ulaF"	"CAI0on"	0.736550112	0.002670221	"=L-ribulose-5-phosphate 4-epimerase UlaF"
"cirA_2"	"CAI0on"	0.635307488	0.002762868	"=Colicin I receptor precursor"
"yfiH"	"CAI0on"	-0.707884442	0.003384923	"=Laccase domain protein YfiH"
"speG"	"CAI0on"	-0.615352177	0.00371126	"=Spermidine N(1)-acetyltransferase"
"dhbF_1"	"CAI0on"	-0.886627319	0.005766732	"=Dimodular nonribosomal peptide synthase"
"nagD"	"CAI0on"	0.579860602	0.006889189	"=Ribonucleotide monophosphatase NagD"
"sarZ"	"CAI12on"	3.23953178	1.79E-53	"=HTH-type transcriptional regulator SarZ"
"katA"	"CAI12on"	2.129205404	5.35E-26	"=Catalase"
"yfjZ_5"	"CAI12on"	4.781123675	0.001381434	"=Putative antitoxin YfjZ"
"flgB"	"CAI12on"	-2.244030962	0.189504683	"=Flagellar basal body rod protein FlgB"
"lpp"	"CAI12on"	-2.248225854	0.283057848	"=Major outer membrane lipoprotein Lpp precursor"
"arnT_1"	"CAI12on"	-2.120643573	0.609607384	Undecaprenyl transferase
"rlmA_1"	"CAI12on"	-2.329755834	0.536701056	23S rRNA (guanine(745)-N(1))-methyltransferase
"epsE_4"	"CAI12on"	-2.354820933	0.041401118	"=Type II secretion system protein E"
"envZ_2"	"CAI12on"	-2.881217877	0.027869375	"=Osmolarity sensor protein EnvZ"
"arnB_3"	"CAI12on"	-1.190672709	0.004428011	UDP-4-amino-4-deoxy-L-arabinose--oxoglutarate aminotransferase
"cirA_2"	"CAI12on"	0.671115636	0.002032403	"=Colicin I receptor precursor"
"dhbF_1"	"CAI12on"	-0.946043494	0.001611734	"=Dimodular nonribosomal peptide synthase"
"rimK_2"	"CAI12on"	0.498542635	0.002567841	"=Ribosomal protein S6 modification protein"
"sarZ"	"CAI24on"	3.341163228	2.28E-59	"=HTH-type transcriptional regulator SarZ"
"katA"	"CAI24on"	2.043556669	6.13E-26	"=Catalase"
"yfjZ_5"	"CAI24on"	3.702587614	0.009699419	"=Putative antitoxin YfjZ"
"crp_1"	"CAI24on"	-3.281695154	0.25585665	cAMP-activated global transcriptional regulator

"cfxP_1"	"CAI24on"	-2.001867994	0.454540457	Phosphoribulokinase%2C plasmid
"rlmA_1"	"CAI24on"	-3.957925563	0.206903884	23S rRNA (guanine(745)-N(1))-methyltransferase
"gbpA_1"	"CAI24on"	-2.734606502	0.226078937	"=GlcNAc-binding protein A"
"cirA_2"	"CAI24on"	0.609215764	0.00407822	"=Colicin I receptor precursor"
"speG"	"CAI24on"	-0.611833645	0.00392538	"=Spermidine N(1)-acetyltransferase"
"dhbF_1"	"CAI24on"	-1.155147567	0.000120243	"=Dimodular nonribosomal peptide synthase"
"gpt"	"CAI24on"	-0.610136293	0.006674596	"=Xanthine phosphoribosyltransferase"
"mltD_3"	"CUI0on"	2.29802083	1.89E-05	"=Membrane-bound lytic murein transglycosylase D precursor"
"nuoK"	"CUI0on"	-2.101932764	0.007429599	"=NADH-quinone oxidoreductase subunit K"
"chaA"	"CUI0on"	-4.998692267	0.022950391	"=Sodium/proton antiporter ChaA"
"coaE"	"CUI0on"	-6.231518322	0.0242956	"=Dephospho-CoA kinase"
"ynjC"	"CUI0on"	-5.000332074	0.028870268	"=Inner membrane ABC transporter permease protein YnjC"
"manP_1"	"CUI0on"	-2.973087288	0.044400171	"=PTS system mannose-specific EIIBCA component"
"wfgD"	"CUI0on"	-2.020358184	0.050455677	"=UDP-Glc:alpha-D-GlcNAc-diphosphoundecaprenol glucosyltransferase"
"calB"	"CUI0on"	-2.703333312	0.052162946	"=Coniferyl aldehyde dehydrogenase"
"norM_2"	"CUI0on"	-2.30655735	0.053528364	"=Multidrug resistance protein NorM"
"ghrA"	"CUI0on"	-2.438655876	0.055500567	"=Glyoxylate/hydroxypyruvate reductase A"
"frsA_1"	"CUI0on"	-3.241100039	0.090599354	NA
"frsA_3"	"CUI0on"	-4.201946165	0.117029601	NA
"pcp_2"	"CUI0on"	-2.564189678	0.096800549	"=Outer membrane lipoprotein pcp precursor"
"raiA"	"CUI0on"	-2.330643843	0.123500332	"=Ribosome-associated inhibitor A"
"ctpH_1"	"CUI0on"	-2.755067914	0.128908439	"=Methyl-accepting chemotaxis protein CtpH"
"fliC_1"	"CUI0on"	-2.429553776	0.173426439	"=A-type flagellin"
"phoE_1"	"CUI0on"	-2.037642253	0.178625819	"=Outer membrane pore protein E precursor"
"hag"	"CUI0on"	-2.078666712	0.260080774	"=Flagellin"
"kcsA_1"	"CUI0on"	-2.245919905	0.264249392	pH-gated potassium channel KcsA
"mltD_3"	"CUI12on"	2.088032341	9.96E-05	"=Membrane-bound lytic murein transglycosylase D precursor"
"pcp_2"	"CUI24on"	-2.128602308	0.162195094	"=Outer membrane lipoprotein pcp precursor"
"envZ_2"	"CUI24on"	-2.433321446	0.11050578	"=Osmolarity sensor protein EnvZ"
"ompA_3"	"CUI24on"	-2.825951121	0.110541947	"=Outer membrane protein A precursor"
"ompW"	"CUI24on"	-2.395422655	0.317259699	"=Outer membrane protein W precursor"
"fliC_1"	"CUI24on"	-2.510958702	0.160631697	"=A-type flagellin"
"fliN_1"	"CUI24on"	-2.001566901	0.057959211	"=Flagellar motor switch protein FliN"
"fliD_1"	"CUI24on"	-2.486529193	0.225823031	"=Flagellar hook-associated protein 2"
"fliE_1"	"CUI24on"	-3.484938549	0.192768083	"=Flagellar hook-basal body complex protein FliE"
"fliE_2"	"CUI24on"	-2.460452311	0.150781084	"=Flagellar hook-basal body complex protein FliE"
"fliA"	"CUI24on"	-2.662982417	0.218971741	"=RNA polymerase sigma factor FliA"
"fliS"	"CUI24on"	-2.180905175	0.129546467	"=Flagellar protein FliS"
"flgI_1"	"CUI24on"	-2.20531822	0.288812258	"=Flagellar P-ring protein precursor"
"flgA"	"CUI24on"	-2.893563688	0.146431274	"=Flagella basal body P-ring formation protein FlgA precursor"
"flgF_1"	"CUI24on"	-2.164729266	0.292233182	"=Flagellar basal-body rod protein FlgF"
"flgB_1"	"CUI24on"	-3.227421733	0.184966934	"=Flagellar basal body rod protein FlgB"
"flhA_1"	"CUI24on"	-2.469729088	0.209687045	"=Flagellar biosynthesis protein FlhA"
"ylxH"	"CUI24on"	-2.367522165	0.158171782	"=Flagellum site-determining protein YlxH"
"cheW_3"	"CUI24on"	-2.114028119	0.183888346	"=Chemotaxis protein CheW"

"cheR2"	"CUI24on"	-2.506073226	0.118471062	"=Chemotaxis protein methyltransferase Cher2"
"cheA_3"	"CUI24on"	-2.419184319	0.106469055	"=Chemotaxis protein CheA"
"cheV_3"	"CUI24on"	-2.370778673	0.051056832	"=Chemotaxis protein CheV"
"cheV_1"	"CUI24on"	-2.179226783	0.172503759	"=Chemotaxis protein CheV"
"cheY_3"	"CUI24on"	-2.589103199	0.171660546	"=Chemotaxis protein CheY"
"lpp"	"CUI24on"	-2.948714308	0.067477929	"=Major outer membrane lipoprotein Lpp precursor"
"rpsP"	"CUI24on"	-2.825782088	0.110792659	"=30S ribosomal protein S16"
"rpsD"	"CUI24on"	-2.105472878	0.16746824	"=30S ribosomal protein S4"
"rpsA"	"CUI24on"	-2.310665302	0.109764463	"=30S ribosomal protein S1"
"rpsN"	"CUI24on"	-2.256889596	0.101403805	"=30S ribosomal protein S14"
"rpsR"	"CUI24on"	-3.718958632	0.066022957	"=30S ribosomal protein S18"
"rpsB"	"CUI24on"	-2.354152574	0.110384112	"=30S ribosomal protein S2"
"rpsU"	"CUI24on"	-3.942959547	0.091483882	"=30S ribosomal protein S21"
"rpsT"	"CUI24on"	-3.216345791	0.141664236	"=30S ribosomal protein S20"
"rpsL"	"CUI24on"	-2.984539104	0.151479961	"=30S ribosomal protein S12"
"rpsF"	"CUI24on"	-4.306821781	0.084910999	"=30S ribosomal protein S6"
"rpsM"	"CUI24on"	-2.795612774	0.121333162	"=30S ribosomal protein S13"
"rplJ"	"CUI24on"	-3.072314863	0.120742551	"=50S ribosomal protein L10"
"rplX"	"CUI24on"	-2.867068025	0.155101287	"=50S ribosomal protein L24"
"rplU"	"CUI24on"	-2.594707514	0.196169037	"=50S ribosomal protein L21"
"rplA"	"CUI24on"	-3.041360538	0.105742285	"=50S ribosomal protein L1"
"rplM"	"CUI24on"	-2.226791499	0.176563499	"=50S ribosomal protein L13"
"rplK"	"CUI24on"	-2.161000931	0.182811197	"=50S ribosomal protein L11"
"rpmB"	"CUI24on"	-2.798427545	0.144335488	"=50S ribosomal protein L28"
"rpmA"	"CUI24on"	-2.901368041	0.110828782	"=50S ribosomal protein L27"
"rpmI"	"CUI24on"	-2.739578416	0.145619033	"=50S ribosomal protein L35"
"rpoA"	"CUI24on"	-2.084893426	0.151809296	"=DNA-directed RNA polymerase subunit alpha"
"rpoH"	"CUI24on"	-3.434733727	0.11801755	"=RNA polymerase sigma factor RpoH"
"rpoE_1"	"CUI24on"	-2.741718138	0.168069477	"=ECF RNA polymerase sigma-E factor"
"rseA"	"CUI24on"	-3.539545091	0.079840364	"=Anti-sigma-E factor RseA"
"fkpA"	"CUI24on"	-2.540532447	0.131050512	"=FKBP-type peptidyl-prolyl cis-trans isomerase FkpA precursor"
"infC"	"CUI24on"	-2.874638921	0.070903521	"=Translation initiation factor IF-3"
"infA"	"CUI24on"	-2.426087994	0.078042318	"=Translation initiation factor IF-1"
"hag"	"CUI24on"	-2.288894604	0.216122444	"=Flagellin"
"nudC_1"	"CUI24on"	3.186215337	0.023354468	NADH pyrophosphatase
"fbp"	"CUI24on"	-2.672235741	0.296651048	"=Fructose-1%2C6-bisphosphatase class 1"
"fbcH"	"CUI24on"	-2.054881801	0.123419339	"=Cytochrome b/c1"
"htpX"	"CUI24on"	-2.376643675	0.208466454	"=Protease HtpX"
"puuB_1"	"CUI24on"	3.567041129	0.015986162	"=Gamma-glutamylputrescine oxidoreductase"
"secY"	"CUI24on"	-2.124337167	0.129440344	"=Protein translocase subunit SecY"
"comEA"	"CUI24on"	-2.354344876	0.338343588	"=ComE operon protein 1"
"hflX"	"CUI24on"	-2.336301512	0.156102125	"=GTPase HflX"
"clpX"	"CUI24on"	-2.178818852	0.111166571	"=ATP-dependent Clp protease ATP-binding subunit ClpX"
"csrA"	"CUI24on"	-3.131471199	0.05590082	"=Carbon storage regulator"
"rpfG_7"	"CUI24on"	-2.7888752	0.114857216	"=Cyclic di-GMP phosphodiesterase response regulator RpfG"

"gapA"	"CUI24on"	-2.197920834	0.136836857	"=Glyceraldehyde-3-phosphate dehydrogenase A"
"hpf"	"CUI24on"	-2.95666135	0.116364879	"=Ribosome hibernation promoting factor"
"nhaR_2"	"CUI24on"	-2.032975768	0.044743715	"=Transcriptional activator protein NhaR"
"nhaA"	"CUI24on"	-2.407458388	0.166350794	"=Na(+)/H(+) antiporter NhaA"
"cspV_1"	"CUI24on"	-4.313896321	0.06439423	"=Cold shock protein CspV"
"cspG"	"CUI24on"	-2.355070099	0.214453157	"=Cold shock-like protein CspG"
"cspD"	"CUI24on"	-2.135989405	0.271287269	"=Cold shock-like protein CspD"
"ybaB"	"CUI24on"	-2.043639551	0.049594208	"=Nucleoid-associated protein YbaB"
"fbaA_1"	"CUI24on"	2.990218419	0.056097519	Fructose-bisphosphate aldolase class 2
"ssb"	"CUI24on"	-3.163423006	0.104707248	"=Single-stranded DNA-binding protein"
"ihfB"	"CUI24on"	-2.649789105	0.075490344	"=Integration host factor subunit beta"
"kinA"	"CUI24on"	-2.573283615	0.139426	"=Sporulation kinase A"
"dosC_2"	"CUI24on"	-3.028683081	0.128939043	"=Diguanylate cyclase DosC"
"ycf3"	"CUI24on"	-2.343504563	0.053692827	"=Photosystem I assembly protein Ycf3"
"stpA_2"	"CUI24on"	-3.03531429	0.18684797	"=DNA-binding protein StpA"
"hfq_2"	"CUI24on"	-2.848466487	0.11123429	"=RNA-binding protein Hfq"
"dksA_3"	"CUI24on"	-2.092085203	0.102365326	"=RNA polymerase-binding transcription factor DksA"
"crr"	"CUI24on"	-2.782632095	0.115836723	"=Glucose-specific phosphotransferase enzyme IIA component"
"tusB"	"CUI24on"	-2.967888005	0.15916807	"=Protein TusB"
"aroK"	"CUI24on"	-2.139337897	0.13889574	"=Shikimate kinase 1"
"ihfA"	"CUI24on"	-2.032605945	0.207885447	"=Integration host factor subunit alpha"
"engB"	"CUI24on"	-2.186618139	0.134213608	"=putative GTP-binding protein EngB"
"tatA_1"	"CUI24on"	-3.480338213	0.116501607	"=Sec-independent protein translocase protein TatA"
"dnaQ"	"CUI24on"	-2.137572189	0.113735143	"=DNA polymerase III subunit epsilon"
"kdgR"	"CUI24on"	-2.989186533	0.130170681	"=Transcriptional regulator KdgR"
"pflB"	"CUI24on"	-2.558084072	0.06637875	"=Formate acetyltransferase 1"
"yhcB"	"CUI24on"	-2.250085537	0.152429697	"=Inner membrane protein YhcB"
"pyrH"	"CUI24on"	-2.010198279	0.092458158	"=Uridylate kinase"
"rlmE"	"CUI24on"	-2.349608695	0.150127339	"=Ribosomal RNA large subunit methyltransferase E"
"trmJ"	"CUI24on"	-2.766607898	0.080218787	"=tRNA (cytidine/uridine-2'-O-)-methyltransferase TrmJ"
"glnA"	"CUI24on"	-2.115673483	0.156814155	"=Glutamine synthetase"
"tabA_2"	"CUI24on"	-2.583760938	0.134482066	"=Toxin-antitoxin biofilm protein TabA"
"stpA_1"	"CUI24on"	-2.224357766	0.124235149	"=DNA-binding protein StpA"
"ybgC"	"CUI24on"	-2.306010128	0.122792106	"=Acyl-CoA thioester hydrolase YbgC"
"zapB"	"CUI24on"	-2.501111279	0.239663781	"=Cell division protein ZapB"
"rmf"	"CUI24on"	-2.67756214	0.212723134	"=Ribosome modulation factor"
"trxA_3"	"CUI24on"	-2.473373038	0.163865483	"=Thioredoxin-1"
"thrS"	"CUI24on"	-3.179143009	0.123070638	"=Threonine--tRNA ligase"
"ptsH"	"CUI24on"	-2.239902261	0.124465061	"=Phosphocarrier protein HPr"
"pglF_1"	"CUI24on"	-2.488914449	0.245570657	"=UDP-N-acetyl-alpha-D-glucosamine C6 dehydratase"
"pyrG"	"CUI24on"	-2.284026531	0.081492102	"=CTP synthase"
"upp"	"CUI24on"	-2.03638253	0.096960907	"=Uracil phosphoribosyltransferase"
"fabG_2"	"CUI24on"	-3.675222764	0.103421395	"=3-oxoacyl-[acyl-carrier-protein] reductase FabG"
"arcA_1"	"CUI24on"	-3.741864559	0.100334556	"=Aerobic respiration control protein ArcA"
"acpP"	"CUI24on"	-4.318856809	0.104579092	"=Acyl carrier protein"

"menH"	"CUI24on"	-2.223031215	0.077559357	"=2-succinyl-6-hydroxy-cyclohexadiene-1-carboxylate synthase"
"iscR"	"CUI24on"	-2.172833674	0.108873545	"=HTH-type transcriptional regulator IscR"
"zraR_3"	"CUI24on"	-2.868412986	0.103987804	"=Transcriptional regulatory protein ZraR"
"nsrR_2"	"CUI24on"	-3.347751975	0.071698741	"=HTH-type transcriptional repressor NsrR"
"focA"	"CUI24on"	-3.04923518	0.08002511	"=putative formate transporter 1"
"gltT"	"CUI24on"	-5.302800758	0.023284334	"=Proton/sodium-glutamate symport protein"
"bssD_1"	"CUI24on"	1.447357835	0.006207224	"=Benzylsuccinate synthase activating enzyme"
"cdhR"	"CUI24on"	0.941271631	0.00557416	"=HTH-type transcriptional regulator CdhR"
"hypC"	"CUI24on"	1.167956902	0.006592531	"=Hydrogenase isoenzymes formation protein HypC"

Table SI6: Differential genes expression data of the comparison between iron and non-iron containing conditions with CA23 and CU5 at three different time points 0, 12 and 24 hours. CAIxx=CA23, iron, xhour, xhour, CANIxx=CA23, no iron, xhour, xhour, CAIxNIx= CA23 ,iron, xhour, no iron, xhour, CUIxx= CU5,iron,xhour, xhour, CUNIxx=CU5, no iron, xhour, xhour, CUIxNIx= CU5 ,iron, xhour, no iron, xhour. x= 0, 12 or 24 hours. |log(FC)|>2

"Gene_ID"	"conditions"	"logFC"	"P"	"fonction"
"pbpG_1"	"CAI012"	-2.260475559	0.000436785	"=D-alanyl-D-alanine endopeptidase precursor"
"pbpG_1"	"CAI024"	-2.138447761	0.0008032	"=D-alanyl-D-alanine endopeptidase precursor"
"pbpG_1"	"CAI0NI24"	-2.10569905	0.000955838	"=D-alanyl-D-alanine endopeptidase precursor"
"pbpG_1"	"CANI0I0"	2.224853647	0.000505691	"=D-alanyl-D-alanine endopeptidase precursor"
"mltC"	"CAI012"	-2.239008003	0.000763738	"=Membrane-bound lytic murein transglycosylase C precursor"
"mltC"	"CAI024"	-2.106486498	0.00142055	"=Membrane-bound lytic murein transglycosylase C precursor"
"mltC"	"CAI0NIt12"	-2.082885005	0.001593161	"=Membrane-bound lytic murein transglycosylase C precursor"
"mltC"	"CAI0NI24"	-2.206903893	0.000880953	"=Membrane-bound lytic murein transglycosylase C precursor"
"mltC"	"CANI0I0"	2.179575704	0.000999849	"=Membrane-bound lytic murein transglycosylase C precursor"
"bdbD"	"CAI012"	-5.849726205	0.001580642	"=Disulfide bond formation protein D precursor"
"bdbD"	"CAI024"	-5.497294153	0.002544262	"=Disulfide bond formation protein D precursor"
"bdbD"	"CAI0NIt12"	-5.544852846	0.002386921	"=Disulfide bond formation protein D precursor"
"bdbD"	"CANI0I0"	5.645429415	0.002084699	"=Disulfide bond formation protein D precursor"
"bdbD"	"CANI0NI24"	6.477665366	0.000660198	"=Disulfide bond formation protein D precursor"
"bdbD"	"CANI12NI24"	6.377072011	0.000760012	"=Disulfide bond formation protein D precursor"
"bdbD"	"CANI24I24"	-6.329508159	0.000812272	"=Disulfide bond formation protein D precursor"
"yfjZ_5"	"CAI012"	-2.749364865	0.031351219	"=Putative antitoxin YfjZ"
"yfjZ_5"	"CAI0NIt12"	-3.221135163	0.01345209	"=Putative antitoxin YfjZ"
"yfjZ_5"	"CAI0NI24"	-3.239711443	0.013501156	"=Putative antitoxin YfjZ"
"yfjZ_5"	"CANI0NI12"	-2.409811627	0.058221783	"=Putative antitoxin YfjZ"
"yfjZ_5"	"CANI0NI24"	-2.429523535	0.060478891	"=Putative antitoxin YfjZ"
"flgB"	"CANI24I24"	-2.106089434	0.028117109	"=Flagellar basal body rod protein FlgB"
"rpmB"	"CAI012"	-2.312850338	0.023412874	"=50S ribosomal protein L28"
"rpmB"	"CAI0NIt12"	-2.689618237	0.009284026	"=50S ribosomal protein L28"
"rpsT"	"CAI0NIt12"	-2.157892848	0.018578048	"=30S ribosomal protein S20"
"acpP_3"	"CANI0NI12"	-2.139247338	0.047023473	"=Acyl carrier protein"
"acpP_3"	"CANI12NI24"	2.053639836	0.055917756	"=Acyl carrier protein"
"cspV_2"	"CAI0NIt12"	-2.12877821	0.049910471	"=Cold shock protein CspV"
"cspV_2"	"CANI0NI12"	-2.320913274	0.033725601	"=Cold shock protein CspV"

"cspV_2"	"CANI12NI24"	2.587071632	0.019110268	"=Cold shock protein CspV"
"cspV_2"	"CANI24I24"	-2.302235351	0.035048936	"=Cold shock protein CspV"
"crp_1"	"CAI1224"	2.134011346	0.128687886	NA
"arnT_1"	"CAI024"	-2.354150308	0.126000946	NA
"arnT_1"	"CANI24I24"	-3.544694326	0.026388316	NA
"arnA_1"	"CAI024"	-2.216587788	0.083684803	NA
"arnA_1"	"CANI24I24"	-3.375681053	0.010135325	NA
"cspG"	"CANI12NI24"	2.090187558	0.02192457	"=Cold shock-like protein CspG"
"yedZ"	"CANI12NI24"	2.041859263	0.024543476	"=Sulfoxide reductase heme-binding subunit YedZ"
"yedZ"	"CANI24I24"	-2.322355396	0.011305729	"=Sulfoxide reductase heme-binding subunit YedZ"
"xerC_2"	"CANI12NI24"	2.168161146	0.018725091	"=Tyrosine recombinase XerC"
"clpS"	"CANI24I24"	-2.052637645	0.01813196	"=ATP-dependent Clp protease adapter protein ClpS"
"rpoE_1"	"CANI12NI24"	2.415306444	0.017847749	"=ECF RNA polymerase sigma-E factor"
"epsE_4"	"CAI012"	2.052439939	0.002752215	"=Type II secretion system protein E"
"epsE_4"	"CAI1224"	-2.445475697	0.000435282	"=Type II secretion system protein E"
"epsE_4"	"CANI12It12"	2.365726211	0.000642035	"=Type II secretion system protein E"
"envZ_2"	"CAI012"	2.904690217	0.000181261	"=Osmolarity sensor protein EnvZ"
"envZ_2"	"CAI1224"	-2.970305563	0.000132348	"=Osmolarity sensor protein EnvZ"
"envZ_2"	"CANI12It12"	2.868263691	0.000209768	"=Osmolarity sensor protein EnvZ"
"dtpA"	"CAI0NI24"	3.077025878	0.000314771	"=Dipeptide and tripeptide permease A"
"dtpA"	"CANI0NI24"	3.079657999	0.000308942	"=Dipeptide and tripeptide permease A"
"dtpA"	"CANI12NI24"	3.039974047	0.00036004	"=Dipeptide and tripeptide permease A"
"dtpA"	"CANI24I24"	-3.13700897	0.000246068	"=Dipeptide and tripeptide permease A"
"licR"	"CANI0I0"	-2.314119696	0.000889542	"=putative licABCH operon regulator"
"licR"	"CANI0NI12"	-2.324833156	0.000830717	"=putative licABCH operon regulator"
"licR"	"CANI0NI24"	-2.567640205	0.000256028	"=putative licABCH operon regulator"
"gabR"	"CAI0NI24"	2.540154801	0.000375332	"=HTH-type transcriptional regulatory protein GabR"
"gabR"	"CANI0NI24"	2.270137274	0.001276102	"=HTH-type transcriptional regulatory protein GabR"
"gabR"	"CANI12NI24"	2.356867234	0.000852792	"=HTH-type transcriptional regulatory protein GabR"
"gabR"	"CANI24I24"	-2.320709899	0.001005262	"=HTH-type transcriptional regulatory protein GabR"
"chaA"	"CUI0I12"	-5.0382038	3.99E-05	"=Sodium/proton antiporter ChaA"
"chaA"	"CUI0I24"	-4.709470947	9.88E-05	"=Sodium/proton antiporter ChaA"
"chaA"	"CUI0NI12"	-4.991513021	4.62E-05	"=Sodium/proton antiporter ChaA"
"chaA"	"CUI0NI24"	-5.138057594	3.06E-05	"=Sodium/proton antiporter ChaA"
"chaA"	"CUNI0I0"	4.904391915	5.81E-05	"=Sodium/proton antiporter ChaA"
"coaE"	"CUI0I12"	-6.388908835	2.61E-05	"=Dephospho-CoA kinase"
"coaE"	"CUI0I24"	-6.410005071	2.51E-05	"=Dephospho-CoA kinase"
"coaE"	"CUI0NI12"	-6.436205003	2.41E-05	"=Dephospho-CoA kinase"
"coaE"	"CUI0NI24"	-6.495361762	2.11E-05	"=Dephospho-CoA kinase"
"coaE"	"CUNI0I0"	6.661891215	1.50E-05	"=Dephospho-CoA kinase"
"ynjC"	"CUI0I12"	-5.043371548	7.14E-05	"=Inner membrane ABC transporter permease protein YnjC"
"ynjC"	"CUI0I24"	-5.317311617	3.55E-05	"=Inner membrane ABC transporter permease protein YnjC"
"ynjC"	"CUI0NI12"	-5.154097815	5.52E-05	"=Inner membrane ABC transporter permease protein YnjC"
"ynjC"	"CUI0NI24"	-4.752117126	0.000150426	"=Inner membrane ABC transporter permease protein YnjC"
"ynjC"	"CUNI0I0"	5.411488929	2.85E-05	"=Inner membrane ABC transporter permease protein YnjC"

"manP_1"	"CUI0I12"	-3.05359359	0.000416239	"=PTS system mannose-specific EIIBCA component"
"manP_1"	"CUI0I24"	-3.140517242	0.000302915	"=PTS system mannose-specific EIIBCA component"
"manP_1"	"CUI0NI12"	-3.282687332	0.000177115	"=PTS system mannose-specific EIIBCA component"
"manP_1"	"CUI0NI24"	-2.979258991	0.000553438	"=PTS system mannose-specific EIIBCA component"
"manP_1"	"CUNI0I0"	3.378413879	0.00011912	"=PTS system mannose-specific EIIBCA component"
"wfgD"	"CUI0NI24"	-2.604460556	5.62E-05	"=UDP -glucosyltransferase WfgD"
"wfgD"	"CUNI12NI24"	-2.63587297	4.69E-05	"=UDP-glucosyltransferase WfgD"
"calB"	"CUI0I12"	-2.807438706	0.000619221	"=Coniferyl aldehyde dehydrogenase"
"calB"	"CUI0I24"	-2.80367389	0.000645271	"=Coniferyl aldehyde dehydrogenase"
"calB"	"CUI0NI12"	-2.803194132	0.000647276	"=Coniferyl aldehyde dehydrogenase"
"calB"	"CUI0NI24"	-2.793924867	0.000662821	"=Coniferyl aldehyde dehydrogenase"
"calB"	"CUNI0I0"	2.926453622	0.000398518	"=Coniferyl aldehyde dehydrogenase"
"norM_2"	"CUI0I12"	-2.250318754	0.001627311	"=Multidrug resistance protein NorM"
"norM_2"	"CUI0I24"	-2.264186123	0.001574472	"=Multidrug resistance protein NorM"
"norM_2"	"CUI0NI12"	-2.455929281	0.000677376	"=Multidrug resistance protein NorM"
"norM_2"	"CUI0NI24"	-2.242390604	0.001713371	"=Multidrug resistance protein NorM"
"norM_2"	"CUNI0I0"	2.380381731	0.000923141	"=Multidrug resistance protein NorM"
"ghrA"	"CUI0I12"	-2.58432329	0.000678623	"=Glyoxylate/hydroxypyruvate reductase A"
"ghrA"	"CUI0I24"	-2.092390066	0.005268736	"=Glyoxylate/hydroxypyruvate reductase A"
"ghrA"	"CUI0NI12"	-2.214474847	0.003220357	"=Glyoxylate/hydroxypyruvate reductase A"
"ghrA"	"CUI0NI24"	-2.48677285	0.001028905	"=Glyoxylate/hydroxypyruvate reductase A"
"ghrA"	"CUNI0I0"	2.569782291	0.000768051	"=Glyoxylate/hydroxypyruvate reductase A"
"frsA_1"	"CUI0I12"	-2.480709239	0.017800892	NA
"frsA_1"	"CUI0I24"	-2.530317066	0.022271351	NA
"frsA_1"	"CUNIt12I12"	-2.418975327	0.024384673	NA
"frsA_1"	"CUNI24I24"	-2.203356586	0.04671152	NA
"pcp_2"	"CUNIt12I12"	-2.353788689	0.007696026	"=Outer membrane lipoprotein pcp precursor"
"pcp_2"	"CUNI12NI24"	-2.114909997	0.015938944	"=Outer membrane lipoprotein pcp precursor"
"frsA_3"	"CUI0I12"	-3.956072233	0.004505366	NA
"frsA_3"	"CUI0I24"	-2.649128768	0.048955424	NA
"frsA_3"	"CUNI0I0"	2.715891034	0.044662361	NA
"frsA_3"	"CUNI0NI12"	2.438305078	0.073453421	NA
"frsA_3"	"CUNI0NI24"	2.420346571	0.07241964	NA
"frsA_3"	"CUNIt12I12"	-3.677360113	0.007657372	NA
"frsA_3"	"CUNI24I24"	-2.353595846	0.077933191	NA
"raiA"	"CUNI0NI24"	-2.993117576	0.000880502	"=Ribosome-associated inhibitor A"
"raiA"	"CUNI12NI24"	-2.322888675	0.008057662	"=Ribosome-associated inhibitor A"
"ctpH_1"	"CUI0I12"	-2.464833429	0.014187561	"=Methyl-accepting chemotaxis protein CtpH"
"ctpH_1"	"CUI0I24"	-2.335334023	0.02188407	"=Methyl-accepting chemotaxis protein CtpH"
"ctpH_1"	"CUNI0I0"	2.317134239	0.02109743	"=Methyl-accepting chemotaxis protein CtpH"
"ctpH_1"	"CUNI0NI24"	2.200374134	0.02994632	"=Methyl-accepting chemotaxis protein CtpH"
"ctpH_1"	"CUNIt12I12"	-2.112409454	0.035478663	"=Methyl-accepting chemotaxis protein CtpH"
"ctpH_1"	"CUNI24I24"	-2.218685215	0.028108378	"=Methyl-accepting chemotaxis protein CtpH"
"ompR_2"	"CUNI12NI24"	-2.164242285	0.007528806	"=Transcriptional regulatory protein OmpR"
"phoE_1"	"CUNI0NI24"	-2.399569598	0.006736002	"=Outer membrane pore protein E precursor"

"phoE_1"	"CUNI12NI24"	-2.171927614	0.013475634	"=Outer membrane pore protein E precursor"
"rplO"	"CUNI0NI24"	-2.249438373	0.003229578	"=50S ribosomal protein L15"
"envZ_2"	"CUNI24I24"	2.010348677	0.020722012	"=Osmolarity sensor protein EnvZ"
"rpsS"	"CUNI0NI24"	-2.037315805	0.00136764	"=30S ribosomal protein S19"
"kcsA_1"	"CUI0I12"	-2.042449976	0.057439804	NA
"kcsA_1"	"CUNIt12I12"	-2.079000144	0.049523002	NA
"cydB_2"	"CUNI0NI24"	-2.798135825	0.000133397	"=Cytochrome bd-I ubiquinol oxidase subunit 2"
"rpmC"	"CUNI0NI24"	-2.32556965	0.000522848	"=50S ribosomal protein L29"
"rplP"	"CUNI0NI24"	-2.455864128	0.000810635	"=50S ribosomal protein L16"
"atpC"	"CUNI0I0"	-2.251216571	0.005886768	"=ATP synthase epsilon chain"
"atpC"	"CUNI0NI12"	-2.516005237	0.002544779	"=ATP synthase epsilon chain"
"atpC"	"CUNI0NI24"	-3.255601483	0.000153207	"=ATP synthase epsilon chain"
"flgG_1"	"CUNI0NI24"	-2.401130626	0.018146967	"=Flagellar basal-body rod protein FlgG"
"flgI_1"	"CUNI0NI24"	-2.172327768	0.052879007	"=Flagellar P-ring protein precursor"
"nudC_1"	"CUI0I24"	-2.173057999	0.081443241	NA
"nudC_1"	"CUI0NI24"	-2.219426521	0.068680999	NA
"nudC_1"	"CUI12I24"	-2.111173833	0.081421867	NA
"nudC_1"	"CUNI0I0"	2.434111186	0.047811616	NA
"rpmD"	"CUNI0NI24"	-2.474872367	0.000983514	"=50S ribosomal protein L30"
"ompA_3"	"CUI12I24"	2.182857772	0.025654234	"=Outer membrane protein A precursor"
"ompA_3"	"CUNI0NI24"	-2.082294063	0.032729044	"=Outer membrane protein A precursor"
"ompA_3"	"CUNIt12I12"	-2.005383116	0.039176982	"=Outer membrane protein A precursor"
"ompA_3"	"CUNI24I24"	2.120179315	0.029903061	"=Outer membrane protein A precursor"
"fbp"	"CUI0I24"	3.652289626	0.008324884	"=Fructose-1%2C6-bisphosphatase class 1"
"fbp"	"CUI0NI12"	2.576420382	0.051656831	"=Fructose-1%2C6-bisphosphatase class 1"
"fbp"	"CUI12I24"	2.59222192	0.050302761	"=Fructose-1%2C6-bisphosphatase class 1"
"fbp"	"CUNI0I0"	-2.906434625	0.030225878	"=Fructose-1%2C6-bisphosphatase class 1"
"fbp"	"CUNI24I24"	2.156976628	0.098019229	"=Fructose-1%2C6-bisphosphatase class 1"
"putA_3"	"CUI0I12"	2.043486936	0.007412981	NA
"putA_3"	"CUI0NI24"	2.086331209	0.006612244	NA
"putA_3"	"CUNIt12I12"	2.404417482	0.002154878	NA
"putA_3"	"CUNI12NI24"	2.446314741	0.001966605	NA
"atpH"	"CUNI0NI24"	-2.20178021	0.001869771	"=ATP synthase subunit delta"
"puuB_1"	"CUI0I24"	-2.781035904	0.033296587	"=Gamma-glutamylputrescine oxidoreductase"
"puuB_1"	"CUI0NI24"	-2.237550587	0.076463297	"=Gamma-glutamylputrescine oxidoreductase"
"puuB_1"	"CUI12I24"	-2.846416993	0.031435173	"=Gamma-glutamylputrescine oxidoreductase"
"puuB_1"	"CUNI0I0"	3.191157612	0.018857196	"=Gamma-glutamylputrescine oxidoreductase"
"puuB_1"	"CUNI0NI12"	2.57287112	0.059012464	"=Gamma-glutamylputrescine oxidoreductase"
"rpsP"	"CUI0I24"	3.536960631	0.000728126	"=30S ribosomal protein S16"
"rpsP"	"CUI12I24"	2.515303073	0.010668075	"=30S ribosomal protein S16"
"rpsP"	"CUNI0I0"	-2.660426805	0.008939295	"=30S ribosomal protein S16"
"rpsP"	"CUNI24I24"	2.629838415	0.008371072	"=30S ribosomal protein S16"
"rplF"	"CUNI0NI24"	-2.842187055	0.001298374	"=50S ribosomal protein L6"
"flgF_1"	"CUNIt12I12"	-2.113955736	0.05672593	"=Flagellar basal-body rod protein FlgF"
"flgF_1"	"CUNI12NI24"	-2.046236411	0.064634715	"=Flagellar basal-body rod protein FlgF"

"csrA"	"CUI0I24"	2.170390833	0.016762768	"=Carbon storage regulator"
"csrA"	"CUI12I24"	2.628086102	0.004401496	"=Carbon storage regulator"
"flgB_1"	"CUI12I24"	2.411594764	0.055347705	"=Flagellar basal body rod protein FlgB"
"flgB_1"	"CUNIt12I12"	-2.058556991	0.097735707	"=Flagellar basal body rod protein FlgB"
"rpsD"	"CUNI0I0"	-2.104068111	0.016488345	"=30S ribosomal protein S4"
"rpsD"	"CUNI0NI24"	-2.417677741	0.006470411	"=30S ribosomal protein S4"
"fliD_1"	"CUI12I24"	2.006016021	0.06895609	"=Flagellar hook-associated protein 2"
"rpsJ"	"CUNI0I0"	-2.100124083	0.003517134	"=30S ribosomal protein S10"
"cheR2"	"CUI12I24"	2.083391296	0.021812048	"=Chemotaxis protein methyltransferase Cher2"
"rpfG_7"	"CUI12I24"	2.398458473	0.015031252	"=Cyclic di-GMP phosphodiesterase response regulator RpfG"
"hpf"	"CUI12I24"	2.220721065	0.030553003	"=Ribosome hibernation promoting factor"
"rplV"	"CUNI0I0"	-2.918727167	0.002541257	"=50S ribosomal protein L22"
"rplV"	"CUNI0NI12"	-2.819875909	0.003441853	"=50S ribosomal protein L22"
"rplV"	"CUNI0NI24"	-4.185260084	4.43E-05	"=50S ribosomal protein L22"
"rplJ"	"CUI0I24"	2.019305018	0.057041711	"=50S ribosomal protein L10"
"rplJ"	"CUI12I24"	2.235294716	0.035782271	"=50S ribosomal protein L10"
"rplJ"	"CUNI0I0"	-2.078259376	0.05032676	"=50S ribosomal protein L10"
"rplJ"	"CUNI0NI24"	-2.210845362	0.037910854	"=50S ribosomal protein L10"
"rplJ"	"CUNI24I24"	2.151892709	0.043199586	"=50S ribosomal protein L10"
"cheV_3"	"CUI12I24"	2.035811472	0.0045374	"=Chemotaxis protein CheV"
"cspV_1"	"CUI0I24"	3.144919818	0.00962825	"=Cold shock protein CspV"
"cspV_1"	"CUI12I24"	3.077331253	0.011037515	"=Cold shock protein CspV"
"cspV_1"	"CUNI24I24"	2.397218553	0.042031318	"=Cold shock protein CspV"
"flgE_1"	"CUNI0NI24"	-2.179635228	0.037197697	"=Flagellar hook protein FlgE"
"rseA"	"CUI0I24"	2.51077338	0.020188428	"=Anti-sigma-E factor RseA"
"rseA"	"CUI12I24"	2.425983631	0.024181902	"=Anti-sigma-E factor RseA"
"arsD"	"CUI0NI12"	2.020669418	0.030757504	"=Arsenical resistance operon trans-acting repressor ArsD"
"rplR"	"CUNI0NI24"	-2.419082455	9.93E-05	"=50S ribosomal protein L18"
"fbaA_1"	"CUI0I24"	-2.514805659	0.072324249	NA
"fbaA_1"	"CUI0NI24"	-3.543260307	0.014471787	NA
"fbaA_1"	"CUI12I24"	-2.262915667	0.101004151	NA
"fbaA_1"	"CUNI0I0"	2.273605639	0.095233563	NA
"fbaA_1"	"CUNI12NI24"	-3.03874345	0.034380369	NA
"ssb"	"CUI0I24"	3.568919761	0.001302664	"=Single-stranded DNA-binding protein"
"ssb"	"CUI0NI12"	2.287972758	0.029954543	"=Single-stranded DNA-binding protein"
"ssb"	"CUI12I24"	2.764675857	0.009892889	"=Single-stranded DNA-binding protein"
"ssb"	"CUNI24I24"	2.71549981	0.011149942	"=Single-stranded DNA-binding protein"
"phhA"	"CUNI0NI24"	-2.492738782	0.011044198	"=Phenylalanine-4-hydroxylase"
"phhA"	"CUNI12NI24"	-2.609757179	0.008080979	"=Phenylalanine-4-hydroxylase"
"ihfB"	"CUI12I24"	2.351887679	0.005995037	"=Integration host factor subunit beta"
"fliE_1"	"CUI0I24"	2.187457391	0.101458244	"=Flagellar hook-basal body complex protein FliE"
"fliE_1"	"CUI12I24"	2.734378274	0.044745644	"=Flagellar hook-basal body complex protein FliE"
"fliE_1"	"CUNIt12I12"	-2.172903873	0.10353142	"=Flagellar hook-basal body complex protein FliE"
"fliE_1"	"CUNI24I24"	2.363513621	0.078631354	"=Flagellar hook-basal body complex protein FliE"
"dosC_2"	"CUI0I24"	2.090083767	0.050388853	"=Diguanylate cyclase DosC"

"dosC_2"	"CUI12I24"	2.538578718	0.019355031	"=Diguanylate cyclase DosC"
"dosC_2"	"CUNI24I24"	2.105897746	0.048858047	"=Diguanylate cyclase DosC"
"rpsA"	"CUNI0I0"	-2.098052865	0.012141135	"=30S ribosomal protein S1"
"stpA_2"	"CUI0I24"	3.422401757	0.006639099	"=DNA-binding protein StpA"
"stpA_2"	"CUI12I24"	2.439447728	0.043903809	"=DNA-binding protein StpA"
"stpA_2"	"CUNI0I0"	-2.17335954	0.070255377	"=DNA-binding protein StpA"
"hfq_2"	"CUI0I24"	2.030658234	0.038499616	"=RNA-binding protein Hfq"
"hfq_2"	"CUI12I24"	2.417913673	0.014988979	"=RNA-binding protein Hfq"
"hfq_2"	"CUNI24I24"	2.043728558	0.037354158	"=RNA-binding protein Hfq"
"rpsN"	"CUNI0I0"	-2.233137253	0.005905223	"=30S ribosomal protein S14"
"rpsN"	"CUNI0NI24"	-2.192444665	0.006595192	"=30S ribosomal protein S14"
"epd_1"	"CUI0NI24"	-3.061017142	0.044517851	NA
"epd_1"	"CUNI0I0"	2.168773738	0.144683526	NA
"epd_1"	"CUNI0NI12"	2.410783898	0.10888073	NA
"epd_1"	"CUNI12NI24"	-3.301256691	0.032264922	NA
"cspD"	"CUI0I24"	2.465289443	0.022247554	"=Cold shock-like protein CspD"
"cspD"	"CUI0NI12"	2.167262784	0.042229743	"=Cold shock-like protein CspD"
"rpsH"	"CUNI0NI24"	-2.100633269	0.012396874	"=30S ribosomal protein S8"
"crr"	"CUI0I24"	2.053561468	0.035357508	"=Glucose-specific phosphotransferase enzyme IIA component"
"crr"	"CUI12I24"	2.373703356	0.016108114	"=Glucose-specific phosphotransferase enzyme IIA component"
"tusB"	"CUI0I24"	3.242375196	0.005671803	"=Protein TusB"
"tusB"	"CUI0NI12"	2.425145728	0.03288484	"=Protein TusB"
"tusB"	"CUI12I24"	2.315895472	0.040055012	"=Protein TusB"
"ackA_1"	"CUI0I24"	2.07229342	0.024882156	"=Acetate kinase"
"rpmE"	"CUI0I24"	2.005275596	0.016361446	"=50S ribosomal protein L31"
"aroK"	"CUI0I24"	2.361451402	0.005405165	"=Shikimate kinase 1"
"cspG"	"CUI0I24"	2.580822821	0.015016788	"=Cold shock-like protein CspG"
"cspG"	"CUI12I24"	2.328897978	0.026573522	"=Cold shock-like protein CspG"
"cspG"	"CUNI0I0"	-2.889735332	0.007160509	"=Cold shock-like protein CspG"
"rpsI"	"CUNI0I0"	-2.104300526	0.005379099	"=30S ribosomal protein S9"
"rpsI"	"CUNI0NI12"	-2.038213766	0.007029183	"=30S ribosomal protein S9"
"rpsI"	"CUNI0NI24"	-2.256442619	0.00305366	"=30S ribosomal protein S9"
"rplX"	"CUI0I24"	2.116555868	0.051232212	"=50S ribosomal protein L24"
"rplX"	"CUI12I24"	2.07868476	0.054633194	"=50S ribosomal protein L24"
"rplX"	"CUNI24I24"	2.111710783	0.051212027	"=50S ribosomal protein L24"
"asnA"	"CUNI0I0"	-3.350580442	0.000508929	"=Aspartate--ammonia ligase"
"asnA"	"CUNI0NI12"	-3.151734821	0.000981427	"=Aspartate--ammonia ligase"
"asnA"	"CUNI0NI24"	-3.175182357	0.000904522	"=Aspartate--ammonia ligase"
"kdsA_1"	"CUI0NI12"	2.887485967	0.0009043	"=2-dehydro-3-deoxyphosphooctonate aldolase"
"kdsA_1"	"CUNI0NI12"	3.314154878	0.000188379	"=2-dehydro-3-deoxyphosphooctonate aldolase"
"kdsA_1"	"CUNIt12I12"	-2.976674927	0.000635541	"=2-dehydro-3-deoxyphosphooctonate aldolase"
"kdsA_1"	"CUNI12NI24"	-2.9236401	0.000800171	"=2-dehydro-3-deoxyphosphooctonate aldolase"
"engB"	"CUI0I24"	2.382560609	0.005391076	"=putative GTP-binding protein EngB"
"engB"	"CUI12I24"	2.011380251	0.017156225	"=putative GTP-binding protein EngB"
"rpsC"	"CUNI0NI24"	-2.249072028	0.000172394	"=30S ribosomal protein S3"

"nhaA"	"CUNI12NI24"	-2.058698529	0.034071237	"=Na(+)/H(+) antiporter NhaA"
"nhaA"	"CUNI24I24"	2.251918745	0.021276399	"=Na(+)/H(+) antiporter NhaA"
"tatA_1"	"CUI0I24"	3.662111433	0.002776024	"=Sec-independent protein translocase protein TatA"
"tatA_1"	"CUI12I24"	3.369637047	0.005269118	"=Sec-independent protein translocase protein TatA"
"tatA_1"	"CUNI24I24"	3.037653592	0.010755036	"=Sec-independent protein translocase protein TatA"
"kdgR"	"CUI0I24"	3.152528956	0.004392099	"=Transcriptional regulator KdgR"
"kdgR"	"CUI12I24"	2.666045839	0.013959933	"=Transcriptional regulator KdgR"
"kdgR"	"CUNI24I24"	2.510685142	0.01988091	"=Transcriptional regulator KdgR"
"pflB"	"CUI0I24"	2.103087868	0.008965551	"=Formate acetyltransferase 1"
"pflB"	"CUI12I24"	2.302835478	0.004465747	"=Formate acetyltransferase 1"
"pflB"	"CUNI24I24"	2.063801725	0.010216701	"=Formate acetyltransferase 1"
"rplU"	"CUI0I24"	2.750619701	0.013421108	"=50S ribosomal protein L21"
"rplU"	"CUI0NI12"	2.009758884	0.063515401	"=50S ribosomal protein L21"
"rplU"	"CUI12I24"	2.15228919	0.047788243	"=50S ribosomal protein L21"
"yhcB"	"CUNI24I24"	2.294092926	0.011431273	"=Inner membrane protein YhcB"
"pyrH"	"CUI0I24"	2.170010367	0.002646642	"=Uridylate kinase"
"udp_1"	"CUI0I24"	2.102582352	0.008851779	"=Uridine phosphorylase"
"trmJ"	"CUI0I24"	2.87745702	0.001720908	"=tRNA (cytidine/uridine-2'-O-)-methyltransferase TrmJ"
"trmJ"	"CUI12I24"	2.651338463	0.003484856	"=tRNA (cytidine/uridine-2'-O-)-methyltransferase TrmJ"
"trmJ"	"CUNI24I24"	2.646949597	0.00358994	"=tRNA (cytidine/uridine-2'-O-)-methyltransferase TrmJ"
"glnA"	"CUI0I24"	2.219365086	0.010662179	"=Glutamine synthetase"
"glnA"	"CUNI24I24"	2.025230511	0.018906653	"=Glutamine synthetase"
"pepE"	"CUNI0I0"	-3.626176938	0.000157462	"=Peptidase E"
"pepE"	"CUNI0NI12"	-3.665036138	0.000138597	"=Peptidase E"
"pepE"	"CUNI0NI24"	-3.557322563	0.000195979	"=Peptidase E"
"fliA"	"CUI0I24"	2.698729518	0.021761625	"=RNA polymerase sigma factor FliA"
"fliA"	"CUI12I24"	2.498046691	0.032285854	"=RNA polymerase sigma factor FliA"
"fliA"	"CUNI24I24"	2.32017888	0.0453818	"=RNA polymerase sigma factor FliA"
"ompW"	"CUNIt12I12"	-2.057108466	0.096732994	"=Outer membrane protein W precursor"
"ompW"	"CUNI12NI24"	-2.228643539	0.07363974	"=Outer membrane protein W precursor"
"ompW"	"CUNI24I24"	2.127486572	0.086600927	"=Outer membrane protein W precursor"
"flgJ_1"	"CUNI0NI24"	-2.068870746	0.042180997	"=Peptidoglycan hydrolase FlgJ"
"tabA_2"	"CUI0I24"	2.653776707	0.006858826	"=Toxin-antitoxin biofilm protein TabA"
"tabA_2"	"CUI12I24"	2.649052169	0.006878245	"=Toxin-antitoxin biofilm protein TabA"
"tabA_2"	"CUNI24I24"	2.087245311	0.029814342	"=Toxin-antitoxin biofilm protein TabA"
"stpA_1"	"CUI0I24"	2.297473886	0.006705148	"=DNA-binding protein StpA"
"stpA_1"	"CUI12I24"	2.272233891	0.007210423	"=DNA-binding protein StpA"
"ybgC"	"CUI0I24"	2.380586156	0.006216789	"=Acyl-CoA thioester hydrolase YbgC"
"ybgC"	"CUI12I24"	2.116056792	0.013809406	"=Acyl-CoA thioester hydrolase YbgC"
"zapB"	"CUI0I24"	2.521951631	0.02922493	"=Cell division protein ZapB"
"zapB"	"CUI12I24"	2.140911863	0.060153423	"=Cell division protein ZapB"
"rmf"	"CUI0I24"	2.106677811	0.065418002	"=Ribosome modulation factor"
"rmf"	"CUNI0I0"	-2.063532213	0.070716035	"=Ribosome modulation factor"
"cheY_3"	"CUI0I24"	2.60182163	0.013841802	"=Chemotaxis protein CheY"
"cheY_3"	"CUI12I24"	2.36068858	0.024055083	"=Chemotaxis protein CheY"

"cheY_3"	"CUNI24I24"	2.037011268	0.049062088	"=Chemotaxis protein CheY"
"rplA"	"CUI0I24"	2.568807866	0.013214227	"=50S ribosomal protein L1"
"rplA"	"CUI12I24"	2.550561004	0.013630832	"=50S ribosomal protein L1"
"rplA"	"CUNI24I24"	2.41581841	0.019022077	"=50S ribosomal protein L1"
"fkpA"	"CUI0I24"	2.14157045	0.023623992	"=FKBP-type peptidyl-prolyl cis-trans isomerase FkpA precursor"
"fkpA"	"CUI12I24"	2.095990871	0.026323595	"=FKBP-type peptidyl-prolyl cis-trans isomerase FkpA precursor"
"trxA_3"	"CUI0I24"	2.049767766	0.037641353	"=Thioredoxin-1"
"trxA_3"	"CUI12I24"	2.04719772	0.037755348	"=Thioredoxin-1"
"thrS"	"CUI0I24"	2.69836607	0.01582151	"=Threonine--tRNA ligase"
"thrS"	"CUI12I24"	2.497912732	0.024355758	"=Threonine--tRNA ligase"
"thrS"	"CUNI24I24"	2.204888342	0.044583481	"=Threonine--tRNA ligase"
"cysE"	"CUNI0I0"	-4.036826012	8.32E-05	"=Serine acetyltransferase"
"cysE"	"CUNI0NI12"	-3.954999021	0.000109568	"=Serine acetyltransferase"
"cysE"	"CUNI0NI24"	-3.993704247	9.62E-05	"=Serine acetyltransferase"
"rpmB"	"CUI0I24"	2.358302057	0.024542836	"=50S ribosomal protein L28"
"rpmB"	"CUI12I24"	2.249965802	0.030119072	"=50S ribosomal protein L28"
"rpmB"	"CUNI0I0"	-2.235090027	0.031796902	"=50S ribosomal protein L28"
"ptsH"	"CUI12I24"	2.05120535	0.01527084	"=Phosphocarrier protein HPr"
"pglF_1"	"CUI0I24"	2.073433239	0.069533186	"=UDP-N-acetyl-alpha-D-glucosamine C6 dehydratase"
"pglF_1"	"CUI12I24"	2.169269803	0.058348954	"=UDP-N-acetyl-alpha-D-glucosamine C6 dehydratase"
"pyrG"	"CUI0I24"	2.076711669	0.007093455	"=CTP synthase"
"pyrG"	"CUI12I24"	2.250227642	0.003684702	"=CTP synthase"
"pyrG"	"CUNI24I24"	2.191279597	0.004618149	"=CTP synthase"
"rpsR"	"CUI0I24"	3.304717448	0.002775012	"=30S ribosomal protein S18"
"rpsR"	"CUI12I24"	2.835711982	0.008549226	"=30S ribosomal protein S18"
"rpsR"	"CUNI0I0"	-2.027804531	0.056346676	"=30S ribosomal protein S18"
"rpsR"	"CUNI0NI24"	-2.03308611	0.054784241	"=30S ribosomal protein S18"
"rpsR"	"CUNI24I24"	3.310172609	0.002690066	"=30S ribosomal protein S18"
"rpoE_1"	"CUI0I24"	2.40103912	0.027067125	"=ECF RNA polymerase sigma-E factor"
"rpoE_1"	"CUI12I24"	2.32461006	0.03182267	"=ECF RNA polymerase sigma-E factor"
"rplD"	"CUNI0I0"	-2.118456457	0.003591008	"=50S ribosomal protein L4"
"rplD"	"CUNI0NI24"	-2.427643042	0.000967454	"=50S ribosomal protein L4"
"rpoH"	"CUI0I24"	3.080471997	0.00943843	"=RNA polymerase sigma factor RpoH"
"rpoH"	"CUI12I24"	2.667253278	0.022240026	"=RNA polymerase sigma factor RpoH"
"rpoH"	"CUNI24I24"	2.541588116	0.028607502	"=RNA polymerase sigma factor RpoH"
"guaB_2"	"CUNI0NI24"	-2.048408749	0.051356845	"=Inosine-5'-monophosphate dehydrogenase"
"rplM"	"CUI12I24"	2.222232043	0.017867157	"=50S ribosomal protein L13"
"rplM"	"CUNI0I0"	-2.087413064	0.02567441	"=50S ribosomal protein L13"
"rpsU"	"CUI0I24"	3.607307421	0.004117937	"=30S ribosomal protein S21"
"rpsU"	"CUI12I24"	2.864784232	0.01847007	"=30S ribosomal protein S21"
"rpsU"	"CUNI24I24"	2.660407746	0.027592289	"=30S ribosomal protein S21"
"flgA"	"CUI0I24"	2.634314026	0.016038308	"=Flagella basal body P-ring formation protein FlgA precursor"
"flgA"	"CUI12I24"	2.528831733	0.020239329	"=Flagella basal body P-ring formation protein FlgA precursor"
"flgA"	"CUNI24I24"	2.095111181	0.050763829	"=Flagella basal body P-ring formation protein FlgA precursor"
"fabG_2"	"CUI0I24"	3.370709496	0.005746865	"=3-oxoacyl-[acyl-carrier-protein] reductase FabG"

"fabG_2"	"CUI12I24"	3.245334308	0.007456828	"=3-oxoacyl-[acyl-carrier-protein] reductase FabG"
"fabG_2"	"CUNI24I24"	3.116153103	0.009834213	"=3-oxoacyl-[acyl-carrier-protein] reductase FabG"
"arcA_1"	"CUI0I24"	3.488930008	0.004631177	"=Aerobic respiration control protein ArcA"
"arcA_1"	"CUI12I24"	3.356877598	0.006127989	"=Aerobic respiration control protein ArcA"
"arcA_1"	"CUNI24I24"	2.995937081	0.013011346	"=Aerobic respiration control protein ArcA"
"rpsT"	"CUI0I24"	3.005342711	0.011249818	"=30S ribosomal protein S20"
"rpsT"	"CUI12I24"	2.595315843	0.02595407	"=30S ribosomal protein S20"
"rpsT"	"CUNI0I0"	-2.962012411	0.012376466	"=30S ribosomal protein S20"
"rpmA"	"CUI0I24"	2.696508333	0.008008349	"=50S ribosomal protein L27"
"rpmA"	"CUI0NI12"	2.120997657	0.033643745	"=50S ribosomal protein L27"
"rpmA"	"CUI12I24"	2.23560855	0.024654412	"=50S ribosomal protein L27"
"rpmA"	"CUNI24I24"	2.179038677	0.028178607	"=50S ribosomal protein L27"
"rpsL"	"CUI0I24"	2.792306209	0.013997087	"=30S ribosomal protein S12"
"rpsL"	"CUI0NI12"	2.081547127	0.059961651	"=30S ribosomal protein S12"
"rpsL"	"CUI12I24"	2.384155107	0.032819582	"=30S ribosomal protein S12"
"rpsL"	"CUNI24I24"	2.217884667	0.045874937	"=30S ribosomal protein S12"
"rpmI"	"CUI0I24"	2.547095239	0.015040758	"=50S ribosomal protein L35"
"rpmI"	"CUI12I24"	2.854378696	0.00689553	"=50S ribosomal protein L35"
"rpmI"	"CUNI0I0"	-2.684079881	0.010932834	"=50S ribosomal protein L35"
"rpmI"	"CUNI0NI24"	-2.667109327	0.011089658	"=50S ribosomal protein L35"
"rpmI"	"CUNI24I24"	2.530149477	0.015486344	"=50S ribosomal protein L35"
"rpsF"	"CUI0I24"	4.1528976	0.002018797	"=30S ribosomal protein S6"
"rpsF"	"CUI12I24"	3.53223536	0.006891341	"=30S ribosomal protein S6"
"rpsF"	"CUNI0I0"	-2.118145511	0.087085387	"=30S ribosomal protein S6"
"rpsF"	"CUNI24I24"	3.441266639	0.008224865	"=30S ribosomal protein S6"
"dosC_1"	"CUNI0I0"	-3.865336489	0.000239443	"=Diguanylate cyclase DosC"
"dosC_1"	"CUNI0NI12"	-4.113774634	0.000111925	"=Diguanylate cyclase DosC"
"dosC_1"	"CUNI0NI24"	-3.780695848	0.000310153	"=Diguanylate cyclase DosC"
"acpP"	"CUI0I24"	4.183927824	0.003105402	"=Acyl carrier protein"
"acpP"	"CUI0NI12"	2.526475664	0.05552221	"=Acyl carrier protein"
"acpP"	"CUI12I24"	3.271380004	0.016044325	"=Acyl carrier protein"
"acpP"	"CUNI0I0"	-2.155049824	0.09790774	"=Acyl carrier protein"
"acpP"	"CUNI24I24"	2.753858955	0.038432721	"=Acyl carrier protein"
"menH"	"CUI0I24"	2.100787857	0.005065363	"=2-succinyl-6-hydroxy-2%2C4-cyclohexadiene-1-carboxylate synthase"
"menH"	"CUI12I24"	2.053828399	0.005817393	"=2-succinyl-6-hydroxy-2%2C4-cyclohexadiene-1-carboxylate synthase"
"iscR"	"CUI0I24"	2.05159502	0.010146681	"=HTH-type transcriptional regulator IscR"
"iscR"	"CUI12I24"	2.223522095	0.005495192	"=HTH-type transcriptional regulator IscR"
"rplK"	"CUI0I24"	2.051955759	0.02642592	"=50S ribosomal protein L11"
"rplK"	"CUI12I24"	2.136536734	0.020590195	"=50S ribosomal protein L11"
"zraR_3"	"CUI0I24"	2.766003337	0.005500653	"=Transcriptional regulatory protein ZraR"
"zraR_3"	"CUI12I24"	2.650547407	0.007504781	"=Transcriptional regulatory protein ZraR"
"zraR_3"	"CUNI24I24"	2.765148883	0.005507084	"=Transcriptional regulatory protein ZraR"
"bepE_2"	"CUI0NI12"	2.925420618	0.00062802	"=Efflux pump membrane transporter BepE"
"bepE_2"	"CUNI0NI12"	2.640070924	0.001804201	"=Efflux pump membrane transporter BepE"
"bepE_2"	"CUNIt12I12"	-3.030123377	0.000419778	"=Efflux pump membrane transporter BepE"

"bepE_2"	"CUNI12NI24"	-2.901071581	0.000689151	"=Efflux pump membrane transporter BepE"
"fliS"	"CUI0I24"	2.106924196	0.011971558	"=Flagellar protein FliS"
"fliS"	"CUI12I24"	2.13942318	0.010632777	"=Flagellar protein FliS"
"nsrR_2"	"CUI0I24"	3.291022079	0.001667195	"=HTH-type transcriptional repressor NsrR"
"nsrR_2"	"CUI12I24"	3.055489662	0.003176515	"=HTH-type transcriptional repressor NsrR"
"nsrR_2"	"CUNI24I24"	3.070534781	0.00305359	"=HTH-type transcriptional repressor NsrR"
"rplC"	"CUNI0NI12"	-2.017953584	0.002456236	"=50S ribosomal protein L3"
"rplC"	"CUNI0NI24"	-2.234520915	0.000820618	"=50S ribosomal protein L3"
"focA"	"CUI0I24"	3.00325093	0.002404033	"=putative formate transporter 1"
"focA"	"CUI12I24"	2.952538141	0.002750265	"=putative formate transporter 1"
"focA"	"CUNI24I24"	2.80314294	0.004268116	"=putative formate transporter 1"
"fhs"	"CUI0NI12"	2.025372944	0.003965621	"=Formate--tetrahydrofolate ligase"
"fhs"	"CUNI0NI12"	2.088429771	0.00302589	"=Formate--tetrahydrofolate ligase"
"gltT"	"CUI0I24"	5.283068217	4.46E-05	"=Proton/sodium-glutamate symport protein"
"gltT"	"CUI12I24"	5.238858553	4.97E-05	"=Proton/sodium-glutamate symport protein"
"gltT"	"CUNI24I24"	5.459263886	2.87E-05	"=Proton/sodium-glutamate symport protein"
"fliE_2"	"CUI0I24"	2.442080396	0.01193667	"=Flagellar hook-basal body complex protein FliE"
"fliE_2"	"CUI12I24"	2.452718947	0.011096975	"=Flagellar hook-basal body complex protein FliE"
"fliE_2"	"CUNI24I24"	2.528472354	0.009336366	"=Flagellar hook-basal body complex protein FliE"
"infA"	"CUI0I24"	2.415172604	0.002926712	"=Translation initiation factor IF-1"
"infA"	"CUI12I24"	2.404229188	0.002969637	"=Translation initiation factor IF-1"
"rpsM"	"CUI0I24"	2.791039302	0.006200775	"=30S ribosomal protein S13"
"rpsM"	"CUI12I24"	2.440487546	0.015000584	"=30S ribosomal protein S13"
"rpsM"	"CUNI0I0"	-2.292796884	0.021920836	"=30S ribosomal protein S13"
"rpsM"	"CUNI24I24"	2.23567111	0.025022758	"=30S ribosomal protein S13"
"pspC"	"CUI0NI12"	2.158424677	0.042528161	"=Phage shock protein C"
"pspC"	"CUNI0I0"	-2.063403325	0.051970471	"=Phage shock protein C"

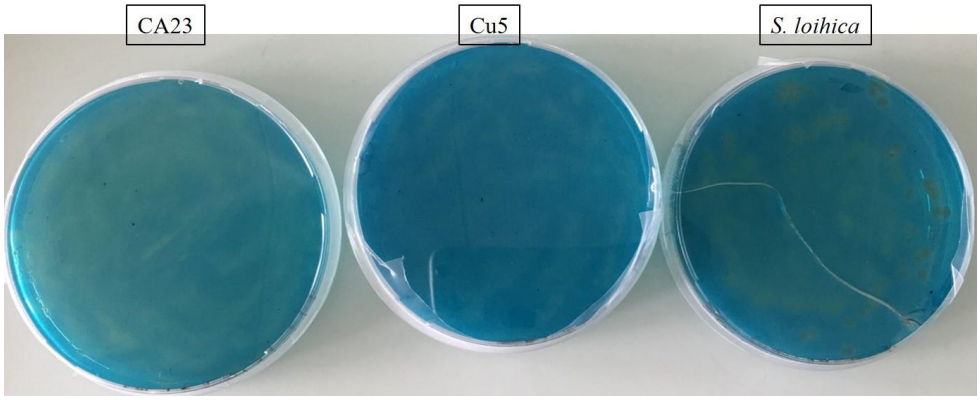

Figure SI8: Culture of CA23 and CU5 on CAS medium

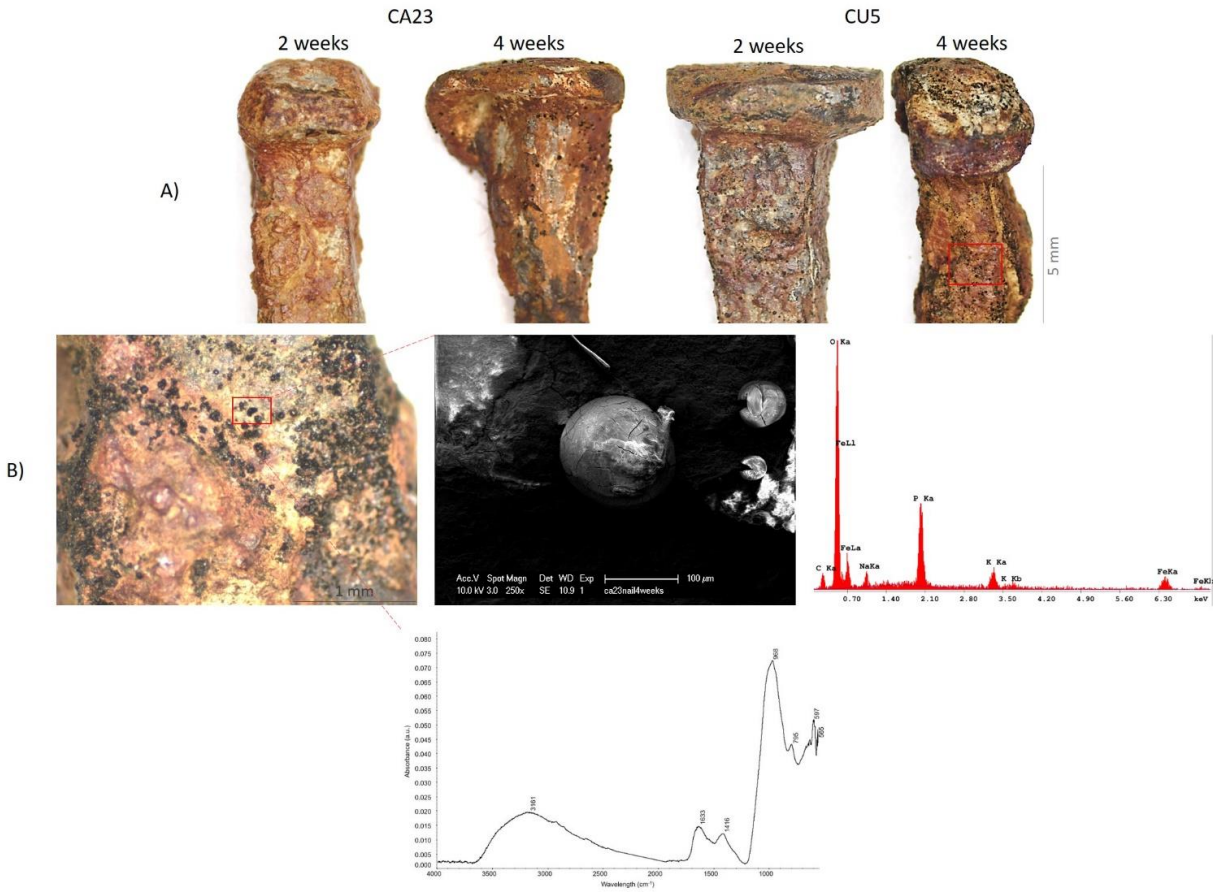

Figure SI9: First test of biogenic mineral formation on archaeological iron nails. A) Visual aspect of the iron nails treated with CA23 and CU5 after 2 and 4 weeks of incubation. B) visual aspect of the red square in part A) (CU5/4weeks) and its corresponding Scanning electron microscopy (SEM) images, EDS and FTIR spectra.

Figure SI10: Visual observations of archaeological iron objects before and after treatment with CA23 and CU5. These are the photos of the objects treated (Aerobic and /or Anaerobic) and before treatment (untreated). This figure represents the remaining results that were not presented in Fig. 6.

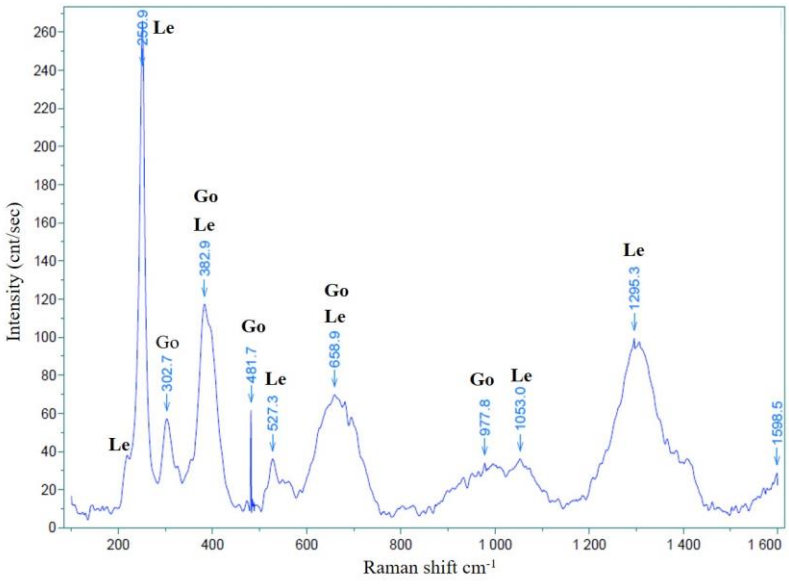

Figure SI11: Raman spectrum of abiotic control archaeological iron objects after 1 month of incubation in the gel delivery system without bacteria. Corrosion compounds were identified as, goethite (Go), and lepidocrocite (Le).

Chapter 7

General Discussion and Perspectives

"Strong minds discuss ideas, average minds discuss events, weak minds discuss people." Socrates

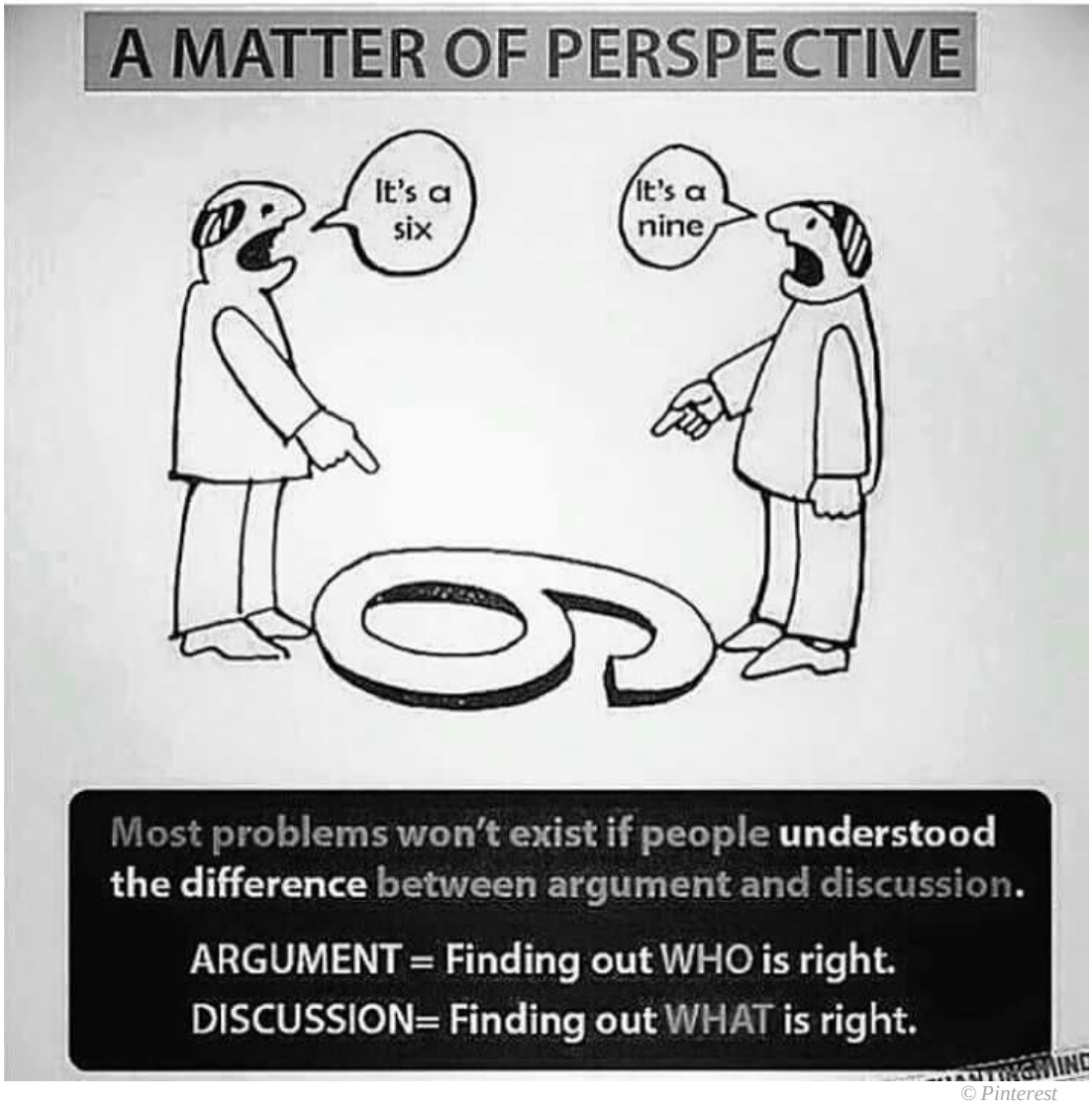

© Pinterest

Iron is an essential nutrient for all organisms studied to date. Its valuable nature is due to the many roles that this element plays within the cell, from being incorporated into proteins for essential cellular activities (e.g. ribonucleotide reductase enzymes), to acting as oxidative stress sensors (e.g. superoxide dismutases). In addition, iron incorporated as heme is essential for various energy generating process key in respiration. Iron scarcity can lead to death of an organism, while an excess of it can cause damage in the cellular machineries through free radical formation via the Fenton reaction [1]. Nevertheless, in natural environments, iron is mostly present in the form of Fe(III) insoluble minerals, like Fe(III) oxyhydroxides and thus is not instantly available for uptake [1,2]. Microorganisms have developed many strategies to cope with iron limitation. Iron-reducing bacteria are considered as the main actor in the reductive dissolution of Fe(III)-bearing minerals in biogeochemical environments. Often microbial activity is linked to the biocorrosion of metallic materials. If the impact of iron-oxidizing bacteria leads to the enhancement of the corrosion rate of iron objects, iron-reducing bacteria, could reduce Fe (III) oxide layers and passivate the objects through the conversion of Fe(III) oxides into more stable minerals (e.g. magnetite) [3]. This process, generally performed by dissimilatory Fe(III)-reducing bacteria, couples the oxidation of organic matter or hydrogen to the formation of Fe(II)-bearing minerals [4]. The formation of bacterial mediated Fe(II) minerals is relevant in bioremediation and natural attenuation of heavy metals and radionuclides [5,6].

Iron corrosion is an important threat in many fields. In cultural heritage, enhancing the stability and preserving archaeological iron objects is a main concern [7]. Corrosion in terrestrial burial environments forms dense corrosion product layer covering the metal core [8]. The contact of this layer with oxygen, humidity and /or chloride ions lead to the damage and break-up of the object [8]. Even if many conventional methods exist for the treatment of recently corroded or archaeological iron objects [7], the disadvantages of these latter as well as their non-optimal efficiency engender the need for the development of a biotechnological stabilizing treatment. Accordingly, the overall aim of this study was the development of a method for the stabilization of marine corroded iron objects and archaeological iron artifacts based on the utilization of dissimilatory bacterial iron reduction properties and the formation of stable Fe(II) minerals.

We started our study by evaluating solid iron reduction and biogenic iron mineral formation using *Shewanella loihica* strain PV-4, a halophilic facultative anaerobe that was reported to reduce iron and was involved in magnetite production [9,10]. *S. loihica* was used to produce biogenic iron minerals, as by-products of iron reduction, in defined chemical conditions. To demonstrate the performance of the proposed treatment, conditions leading to the formation of biogenic minerals were applied on corroded iron coupons that were previously corroded under a marine environment. The results obtained were promising; we indeed demonstrated that producing biomass under aerobic conditions facilitates the practical use of bacteria, compared to strict anaerobes [11], but most importantly, we proved that *S. loihica* is able to reduce solid Fe(III) oxides and oxyhydroxides present on the surface of the iron coupons. This led to the decrease of these minerals from the surface of the object and in return, to the increase of siderite and vivianite, stable Fe(II) carbonate and phosphate minerals. Interestingly the formation of Fe(II) phosphate minerals was not expected, as there was no supply of phosphate in the solution used for iron reduction and mineral formation. Moreover, *S. loihica* was able to reduce insoluble Fe(III) phase only when 1% NaCl was amended to the iron reductive solution, which could be problematic if we consider that chlorine enhances iron corrosion on objects. In the iron reducing solution without salt (0% NaCl), there was no iron reduction but the integrity of the bacterial cells was preserved. These results generate two mains questions: what is the origin of the phosphate that was incorporated in the Fe(II) minerals obtained?

And what is the effect of NaCl on solid iron reduction mechanism of *S. loihica*? We tried to answer to these questions in Chapters 3 and 4.

Concerning the effect of NaCl on iron reduction, there is a general lack of information in the literature, which is surprising, given the potential importance of iron reduction in the oxidation of organic matter in environments with a high salt content, for example, low sulphate marine sediments [2,12]. In addition, this is a clear knowledge gap in the overall body of information concerning the impact of salt on the metabolic and physiological functions of living organisms [13–16]. Interestingly we found that *S. loihica* recovered completely its iron reduction capabilities after amending 1% NaCl, to a culture of this bacterium that was exposed for 24 hours to a solution without NaCl. Moreover, some genes coding for transcriptional regulators, *c*-type cytochromes and porins were only activated in presence of NaCl, suggesting that they play a key role in the physiological iron reduction observed in 1% NaCl and 1% NaCl-amended conditions. Nevertheless, due to the minimal composition of the iron reduction solution, the bacterial cells were confronted to severe stresses and thus, the conditions tested were not ideal for determining the effect of salt on the genes involved in solid iron reduction in *S. loihica*. In this case, further research needs to be performed with the same model organism by evaluating the use of iron under growing conditions.

The investigation on the source of phosphate present in the Fe(II) minerals was based on the hypothesis that *S. loihca* could accumulate polyphosphate granules and release it in the form of orthophosphates when confronted to phosphate-depleted environments. This behaviour was reported for some bacterial species [17–19] but was not studied for *Shewanella* spp. Interestingly, we report, for the first time that *S. loihica* was able to accumulate polyphosphate granules inside the cells. In addition, we also demonstrated an increase of the orthophosphate release in the iron-reducing anaerobic solution used for biogenic mineral formation (a solution lacking phosphate in its initial composition). Moreover, when comparing *S. loihica* with *S. oneidensis* (representative model for *Shewanella* spp.), using the same iron-reducing solution, we found that the latter was not able to accumulate polyphosphates and release orthophosphate, in contrast to *S. loihica*. This was most probably due to the mutation observed in the *ppk* gene, a gene encoding the enzyme reported to be involved in polyphosphate accumulation [20]. As the results of the comparison of polyphosphate accumulation between *S. loihica* and *S. oneidensis* are preliminary, more investigations need to be performed. The formation of vivianite using *Shewanella* spp. like *S. oneidensis* and *S. putrefaciens* was previously reported in the literature [3,21]. However, even if for the latter, the authors hypothesized the polyphosphate accumulation potential, the media used for mineral formation contained a phosphate source. It is known that iron reduction contributes to the immobilization and removal of toxic metals and phosphates from aerobic zones into the anaerobic sediments [5]. This contributes to the biogeochemical cycling of phosphorus, which impacts on the speciation and the fate of this element in anoxic subsurface environments [6]. However, the link between microorganisms that accumulate polyphosphate and natural phosphate minerals present in the environment is poorly investigated. Our findings raise an important question as to the role of polyphosphates and give a new perspective concerning polyphosphate accumulating-bacteria and their role in the formation of phosphate minerals in nature.

Even if the results of these studies have demonstrated the feasibility of the biotechnological concept in terms of the conversion of reactive corrosion products, the use of *S. loihica* could not be ideal due to the need of NaCl to perform iron reduction, considered as corrosive product in the conservation and restoration fields. That is the reason we also considered the possibility to use other bacterial candidates. A screening campaign to isolate new environmental bacterial strains that fulfil the following criteria was conducted: the strain should be facultative anaerobe, halotolerant and reduce solid Fe(III) phases without the need

of salt addition. The screening performed allowed us to select two promising candidates, both belonging to *Aeromonas* genus, strains CA23 and CU5. These two bacterial strains were used for further investigation of the biotechnological stabilization process of corroded iron objects.

The results obtained with the two *Aeromonas* isolates show that they are able to convert reactive iron corrosion products in biogenic Fe(II) minerals on corroded iron coupons. The layer of reactive corrosion products was completely converted into stable Fe(II) minerals. As with *S. loihica*, these biogenic minerals were vivianite and siderite. This suggests that the condition used are suitable for phosphate release and Fe(II) phosphate mineral formation. Since we observed previously that the conditions used for performing iron reduction are not optimal in terms of investigating the iron reduction pathway, we focused our transcriptomic analysis in the case of *Aeromonas* sp. CA23 and CU5 into their pathogenic life style, which is a relevant question if we want to use these strains in an applied biotechnological treatment for archaeological iron objects. We demonstrated through physiological and phylogenetic analyses that CA23 and CU5 are two different species. Even if using genomic data mining, it was not possible to deduce the potential iron reduction pathway of CU5, this strain seems to have a lesser pathogenic potential as no genes coding for toxins were found in its genome. This tends to favor CU5 for our treatment. Using CU5 and also CA23 we scaled up the treatment by using a gel delivery system with minimal compounds to treat archaeological iron objects in oxic conditions. This allowed us to obtain promising results as the surface appearance and composition of the artifacts. The reactive corrosion composed of lepidocrocite and goethite decreased with the increase of vivianite and siderite. Nevertheless, the stability of the Fe(II) mineral layer needs to be optimized.

Iron corrosion has a major impact in man-made ecosystems and cause large economic loses in fields as diverse as water supply, transport, and cultural heritage [22,23]. The global aim of this biotechnological treatment consists in the stabilization of corroded/archaeological objects by transforming the reactive corrosion layer present in a corroded iron object by forming biogenic Fe(II) minerals as by-products of Fe(III) reduction of reactive Fe(III) oxyhydroxides. This needs to be performed in a solution without NaCl addition, as the negative effect of chloride ions on the stability of iron objects has been well established [7]. Overall, during our study we succeeded in transforming reactive corrosion products into Fe(II) minerals using bacteria and the elaboration of praxis and an easy to use biotechnological treatment. However, more investigations on the bacterial strains used need to be considered. Even if CA23 and CU5 did not express virulence factors in our treatment, assessing their *in vivo* pathogenicity needs to be included to rule out the potential virulence of the stains. If the pathogenic potential is confirmed, genetically modifying these strains could be considered in order to attenuate their virulence. Another possibility could be testing the iron reduction capabilities of *S. loihica* with amendment of other sodium salts, knowing that these salts could change the nature of the biogenic minerals formed. Iron reduction with *S. loihica* in presence of NaCl could still be considered as a treatment, and in this case, an evaluation of the effect of chlorine needs to be done to make sure that it does not embed in the corrosion layer of the iron objects. The formation of Fe(II) minerals is interesting and allows us to raise important questions but it also demonstrates that the control of the minerals produced could be improved. Polyphosphate-accumulating bacteria can store around 12% phosphorus on a dry-weight basis, compared to 1%-3% for “normal” bacteria [24]. The use of *S. oneidensis* or other bacterial species that do not accumulate polyphosphate could be considered as a possibility to better control the biogenic minerals formed. Nonetheless, there is no evidence of bacteria that do not accumulate polyphosphate, as polyphosphate accumulation is involved in many other cellular processes. Scaling up of the process and assessing the stability of the biogenic minerals produced (for example by enhancing incubation time, increasing bacterial concentration,

testing other delivery systems) and their long-term protective effect on corroded iron surfaces as well as the effective removal of chloride ions are required for the application of this stabilization method into real conservation-restoration praxis. However, stabilizing the corroded iron object by converting the reactive corrosion products into more stable Fe(II) minerals could lead to some interrogations: would the production of these stable minerals change irreversibly the composition of the object? To which extend such a change could be problematic considering future interventions and studies of the object? The stability of the minerals formed, which depends also on the initial reactive corrosion products present on the object, could not guarantee that future maintenance is not required. An alternative to these issues could be the use of biological systems to remove most of the corrosion products and to "clean" the object without producing a Fe(II) protective layer to allow a better readability of the object (decorations and manufacturing traces). In this case, the object could recover its original shape. The problem here is, if the object is fragile or heavily corroded (which is the case for many of the archaeological iron artifacts), the exposition to an uncontrolled environment will likely enhance its deterioration and further consolidation and/or storage conditions would be required.

Even if there are still open questions and optimizations concerning the proposed treatment, exploiting bacterial metabolic activity to stabilize corroded iron objects can be considered as an innovative biotechnological process that can have a significantly positive impact on the preservation and maintenance of iron-based surfaces. The use of bacterial iron reduction, phosphate mineral formation and study the effect of salt on these mechanisms in the environment as well as in fields, like in agriculture and bioremediation could be considered as another perspective of this work.

References

1. Lau, C. K. Y., Krewulak, K. D. & Vogel, H. J. Bacterial ferrous iron transport: The Feo system. *FEMS Microbiol. Rev.* **40,** 273–298 (2016).

2. Weber, K. a., Achenbach, L. a. & Coates, J. D. Microorganisms pumping iron: anaerobic microbial iron oxidation and reduction. *Nat. Rev. Microbiol.* **4,** 752–764 (2006).

3. Schütz, M. K. *et al.* Combined geochemical and electrochemical methodology to quantify corrosion of carbon steel by bacterial activity. *Bioelectrochemistry* **97,** 61–68 (2014).

4. Schütz, M. K., Bildstein, O., Schlegel, M. L. & Libert, M. Biotic Fe(III) reduction of magnetite coupled to H2 oxidation: Implication for radioactive waste geological disposal. *Chem. Geol.* **419,** 67–74 (2015).

5. Beliaev, A. S. & Saffarini, D. a. *Shewanella putrefaciens* mtrB encodes an outer membrane protein required for Fe(III) and Mn(IV) reduction. *J. Bacteriol.* **180,** 6292–6297 (1998).

6. Roh, Y. *et al.* Biogeochemical and environmental factors in Fe biomineralization: magnetite and siderite formartion. *Clays Clay Miner.* **51,** 83–95 (2003).

7. Selwyn, L. overview of archeological iron: the corrosion problem, key factors affecting treatment and gaps in current knowledge. *Natl. museum Aust. Canberra* 294–306 (2004).

8. Watkinson, D. Measuring effectiveness of washing methods for corrosion control of archaeological iron: problems and challenges. *Corros. Eng. Sci. Technol.* **45,** 400–406 (2010).

9. Gao, H. *et al. Shewanella loihica* sp. nov., isolated from iron-rich microbial mats in the Pacific Ocean. *Int. J. Syst. Evol. Microbiol.* **56,** 1911–1916 (2006).

10. Moon, J.-W. *et al.* Microbial preparation of metal-substituted magnetite nanoparticles. *J. Microbiol. Methods* **70,** 150–158 (2007).

11. Comensoli, L. *et al.* Use of bacteria to stabilize archaeological iron. *Appl. Environ. Microbiol.* (2017). doi:10.1128/AEM.03478-16

12. Lovley, D. R. Dissimilatory Fe(III) and Mn(IV) reduction. *Microbiol. Rev.* **55,** 259–287 (1991).

13. Mudryk, Z. & Donderski, W. Effect of Sodium Chloride on the Metabolic Activity of Halophilic Bacteria Isolated From the Lake Gardno Estuary. *Estuaries* **14,** 495–496 (1991).

14. Wichern, J., Wichern, F. & Joergensen, R. G. Impact of salinity on soil microbial communities and the decomposition of maize in acidic soils. *Geoderma* **137,** 100–108 (2006).

15. Yan, N., Marschner, P., Cao, W., Zuo, C. & Qin, W. Influence of salinity and water content on soil microorganisms. *Int. soil water Conserv. Res.* **3,** 316–323 (2015).

16. Urbina, M. A. & Glover, C. N. Effect of salinity on osmoregulation, metabolism and nitrogen excretion in the amphidromous fish, inanga (*Galaxias maculatus*). *J. Exp.*

Mar. Bio. Ecol. **473,** 7–15 (2015).

17. Tumlirsch, T., Sznajder, A. & Jendrossek, D. Formation of Polyphosphate by Polyphosphate kinases and its Relationship to PHB Accumulation in *Ralstonia eutropha* H16. *Appl. Environ. Microbiol.* **81,** 8277–8293 (2015).

18. Zhang, H. *et al. Gemmatimonas aurantiaca* gen. nov., sp. nov., a Gram-negative, aerobic, polyphosphate-accumulating micro-organism, the first cultured representative of the new bacterial phylum *Gemmatimonadetes* phyl. nov. *Int. J. Syst. Evol. Microbiol.* **53,** 1155–1163 (2003).

19. Sidat, M., Bux, F. & Kasan, H. C. Polyphosphate accumulation by bacteria isolated from activated sludge. *Water SA* **25,** 175–179 (1999).

20. Alcántara, C., Blasco, A., Zúñiga, M. & Monedero, V. Accumulation of polyphosphate in *Lactobacillus* spp. and its involvement in stress resistance. *Appl. Environ. Microbiol.* **80,** 1650–1659 (2014).

21. Jorand, F. *et al.* Assessment of vivianite formation in *Shewanella putrefaciens* culture. *Environ. Technol.* **21,** 1001–1005 (2000).

22. Sarin, P., Snoeyink, V. L., Lytle, D. A. & Kriven, W. M. Iron corrosion scales: model for sclae growth, iron release and colored water formation. *J. Environ. Eng.* **130,** 364–373 (2004).

23. Dinh, H. T. *et al.* Iron corrosion by novel anaerobic microorganisms. *Nature* **427,** 829–832 (2004).

24. vanLoosdrecht, M. C. M., Hooijmans, C. M., Brdjanovic, D. & Heijnen, J. J. Biological phosphate removal processes. *Appl Microbiol Biotechnol* **48,** 289–296 (1997).

Annex

Publications

Presentations at national and international conferences

Curriculum Vitae

Publications (*: equal contributions of the authors)

Kooli, W.M, Comensoli L. Maillard J., Albini M., Gelb A., Junier P.* and Joseph E.*. *Bacterial iron reduction and biogenic mineral formation for the stabilisation of corroded iron objects*. *Sci. Rep.* **8,** 764 (2018).

Albini, M., Comensoli, L., Brambilla, L., Domon Beuret, E., Kooli, W.M.., Mathys, L., Letardi, P. and Joseph, E. (2016), *Innovative biological approaches for metal conservation*. Materials and Corrosion, 67: 200–206.

Joseph E., Letardi P., Albini M., Comensoli L., Kooli W.M., Mathys L., Domon Beuret E., Brambilla L., Cevey C., Bertholon R., Job D., and Junier P. *Innovative biological approaches for metal conservation*. EUROCORR 2014, European Corrosion Congress « Improving materials durabilty: from cultural heritageto industrial applications » Pisa, Italy, 8th-12th September 2014. DECHEMA e.V., Frankfurt and AIM – Associazione Italiana di Metallurgia, Milano, 2014; ISBN 9783897461598, 1-10

Simon A., Bindschedler S.,Job D.,Wick L.Y., Filippidou S., Kooli W.M., Verrecchia E.P.,Junier P. (2015). *Exploiting the fungal highway: development of a novel tool for the in situ isolation of bacteria migrating along fungal mycelium*, *FEMS Microbiology Ecology*, Volume 91, Issue 11, 1 November 2015.

Deng X., Petitjean M., Teste MA, Kooli W.M., Tranier S., François JM. And Parrou JL. (2014). *Similarities and differences in the biochemical and enzymological properties of the four isomaltases from Saccharomyces cerevisiae.* Published by Elsevier B.V. on behalf of the Federation of European Biochemical Societies. FEBS Open Bio 4: 200-212.

Comensoli L., Albini M.*, Kooli W.M.*, Maillard J., Woerle M., Junier P.,Joseph E.. *Spectroscopic characterization of an innovative green treatment for corroded iron.* Status: submitted

Filippidou S., Junier T., Wunderlin T., Kooli W.M., Palmeri I., Al-Dourobi A., Molina V., Lienhard R., Spangenberg J.E., Johnson S.L., Chain P.S., Dorador C., Junier P.. *Adaptive strategies in a poly-extreme environment: differentiation of vegetative cells in Serratia ureilytica and resistance to extreme conditions.* Status: submitted.

Bergottini V., Filippidou S., Kooli W.M., Junier T., Herve V., Otegui M.B., Zapata P. and Junier P.. *Rot competent and plant growth promotion of Kosakonia radicincitans in Yerba Maté (Ilex paraguariensis A.St.-Hil.).* Status: in preparation.

Kooli W.M., Maillard J., Li P., Joseph E., Chain P. and Junier P.. *Investigations for polyphosphate accumulation by Shewanella loihica and comparison with the model bacterium Shewanella oneidensis.* Status: in preparation.

Kooli W.M., Junier T., Shakya M., Monachon M., Davenport K., Vaideeswaran K., Sereda O., Monrouzeau T., Chain P.S., Joseph E. and Junier P.. *Reductive treatment of corroded iron objects by environmental Aeromonas isolates*. Status: in preparation.

Kooli W.M, Junier T., Shakya M., Maillard J., Davenport K., Li P., Joseph E., Chain P.S. and Junier P.. *Effect of NaCl on solid iron reduction capabilities of Shewanella loihica PV-4*. Status: in preparation.

Participation at national or international conference

Poster presentation at Annual Ph.D. students meeting from doctoral School of Organismal Biology, Neuchatel, Switzerland, May 2014.

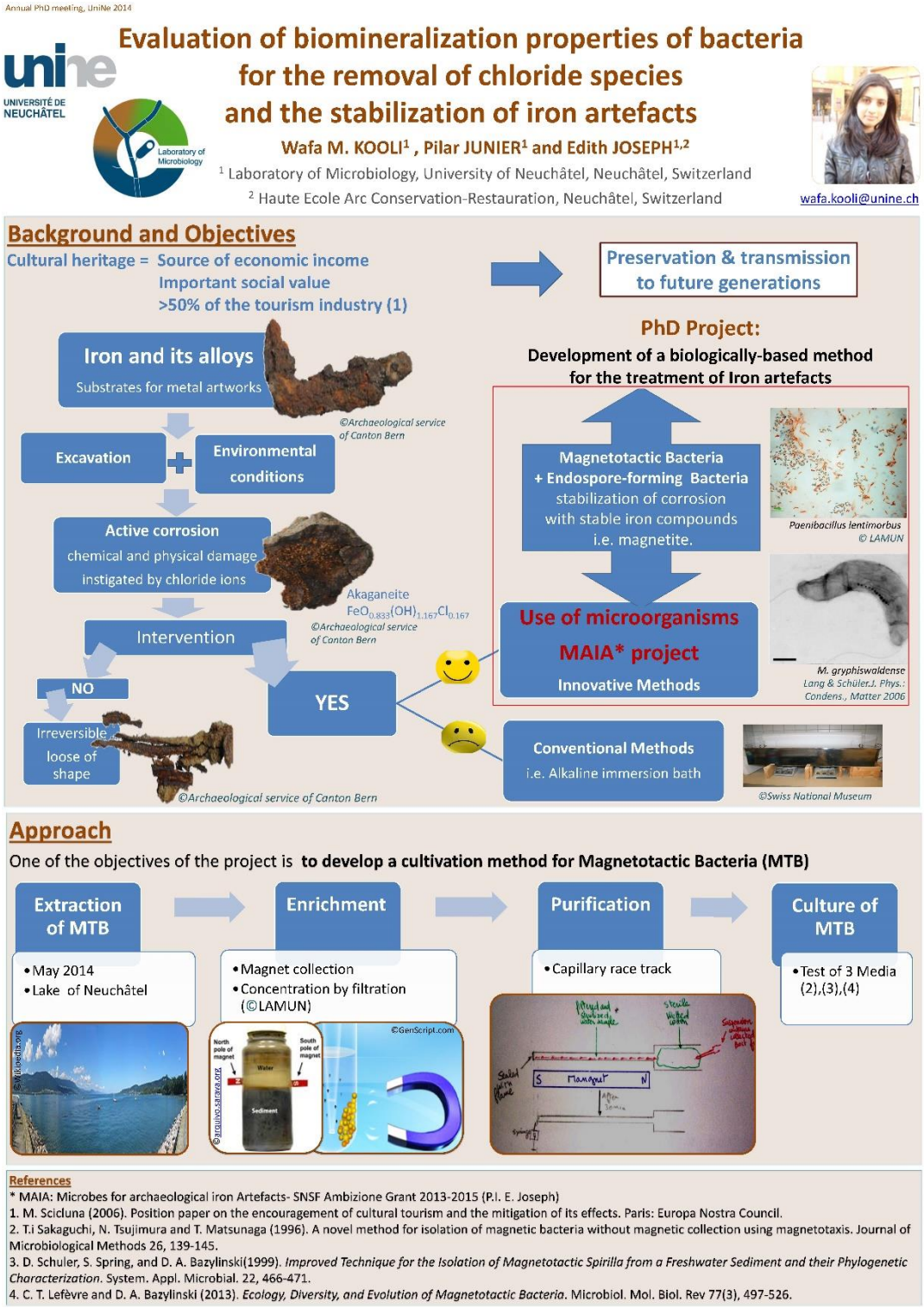

Poster presentation at Annual Meeting of the Swiss Society for Microbiology, Fribourg, Switzerland, June 2014 and Biomineralization Short Course, Paris, France, December 2014.

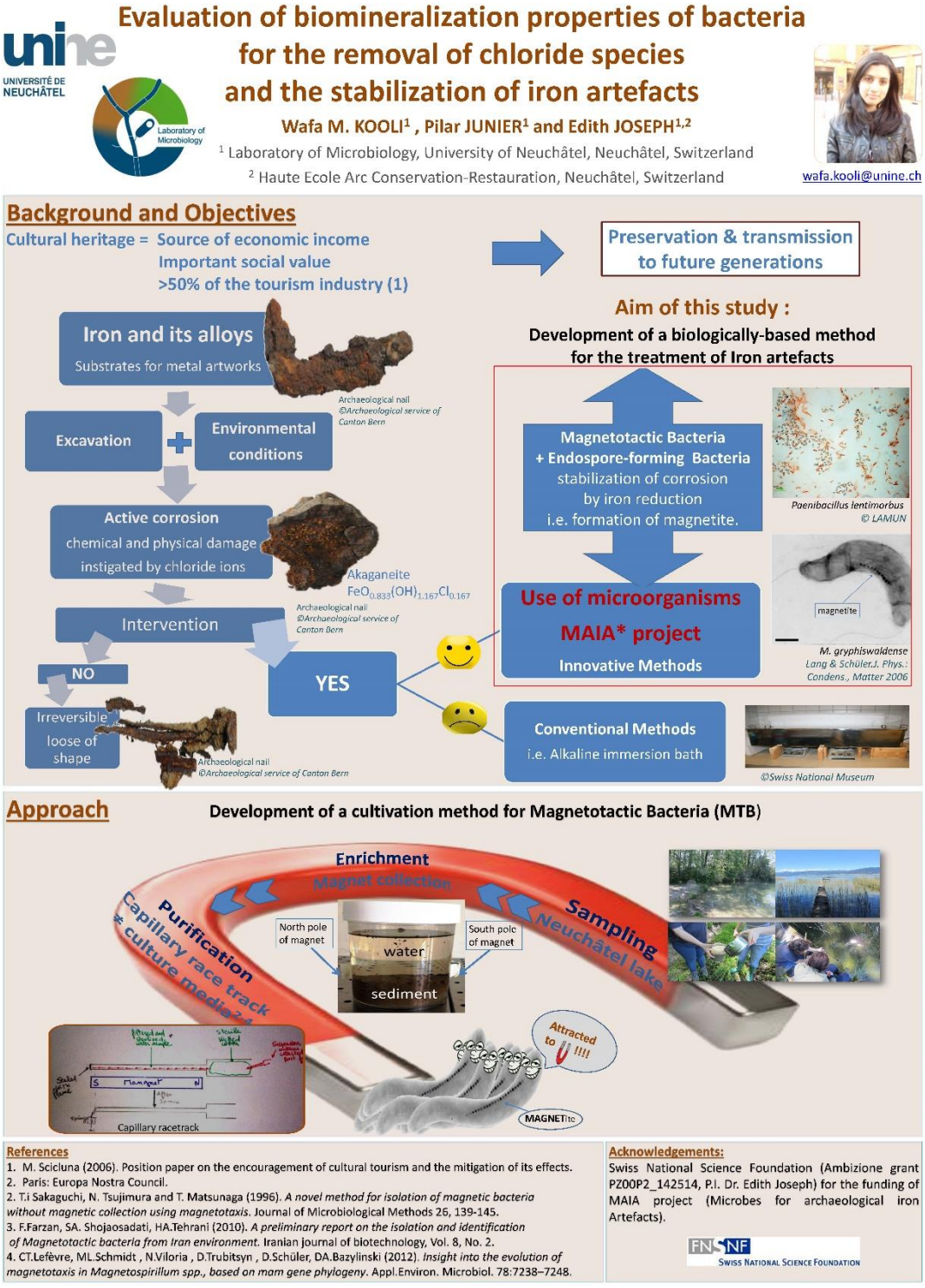

Poster presentation at ISME 15th International Microbial ecology symposium, Seoul, South-Korea, August 2014

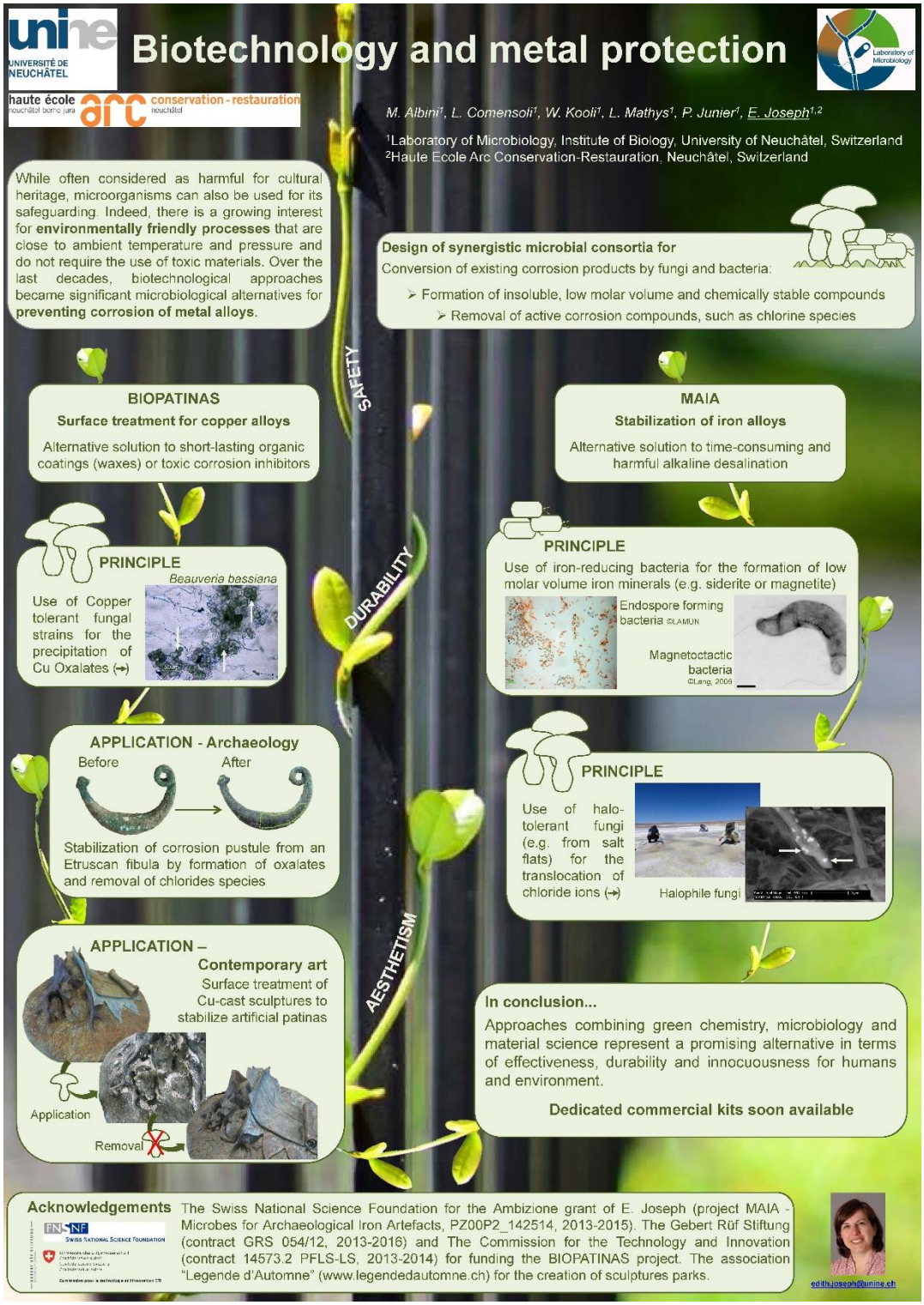

Poster presentation at 73rd Annual Meeting of the Swiss Society for Microbiology, Lugano, Switzerland, May 2015.

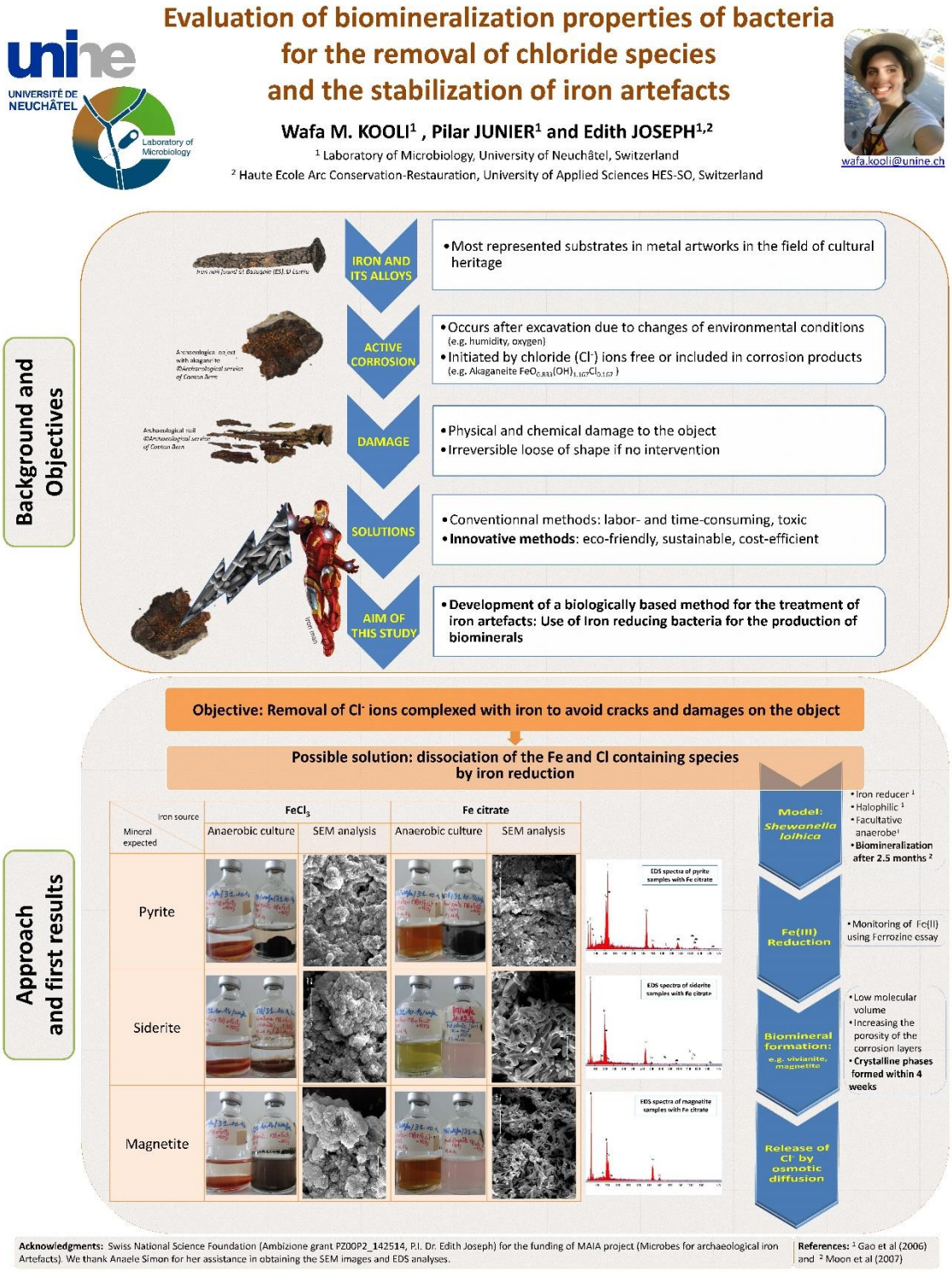

Poster presentation at 6th Swiss Microbial Ecology Meeting, Ascona, Switzerland, September 2015.

Evaluation of biomineralization properties of bacteria for the removal of chloride species and the stabilization of iron artefacts

Wafa M. KOOLI[1] , Pilar JUNIER[1] and Edith JOSEPH[1,2]

[1] Laboratory of Microbiology, University of Neuchâtel, Switzerland

[2] Haute Ecole Arc Conservation-Restauration, University of Applied Sciences HES-SO, Switzerland

wafa.kooli@unine.ch

Objectives and approach

IRON AND ITS ALLOYS
- Most represented substrate in metal artworks

ACTIVE CORROSION
- Occurs after excavation due to changing environmental conditions (e.g. humidity, oxygen)
- Initiated by chloride ions (Cl^-) free or included in corrosion products (e.g. Akaganeite $FeO_{0.83}(OH)_{1.37}Cl_{0.197}$)

DAMAGE
- Physical and chemical damage to the object
- Irreversible loose of shape if no intervention

SOLUTIONS
- Conventional methods: labor- and time-consuming, toxic
- **Innovative methods**: eco-friendly, sustainable, cost-efficient

AIM OF THIS STUDY
- **Development of a biologically-based method for the treatment of iron artefacts: Use of iron-reducing bacteria for the production of stable biominerals**

Proposition
Dissociation of Fe- and Cl-containing species by iron reduction

Objectives
Removal of Cl^- ions
Formation of stable iron biominerals

Shewanella loihica
- Iron reducer [1]
- Halophilic [1]
- Facultative anaerobe [1]
- **Iron bio-mineralization after 2.5 months** [2]

Fe(III) Reduction
- Monitoring of Fe(II) using Ferrozine essay

Biomineral formation: e.g. vivianite, magnetite
- Low molar volume
- Increasing the porosity of the corrosion layers
- **Crystalline phases formed within 1 week**

Release of Cl^- by osmotic diffusion

Results

Iron source	Iron III citrate (soluble phase) *		Iron plates (solid phase) **	
Analysis	Experiment with *S.loihica*	Negative control	Negative control	Experiment with *S.loihica*
Visual observations				
SEM observations	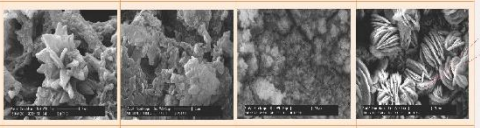			
EDS analysis	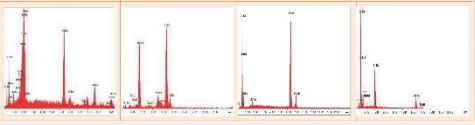			

Experimental conditions: *S.loihica* incubated under anaerobic conditions with 1) soluble iron phases (iron III citrate and iron III chloride) or 2) solid iron phases (aged iron plates in a marine environment) and 0% or 1 % NaCl. SEM pictures and EDS spectra were recorded after one week of incubation. * no crystal phases were formed with Fe chloride, ** no crystal phases were formed with 0%NaCl (data not shown)

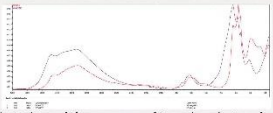

FTIR Analysis showed the presence of iron phosphates when using Fe citrate as iron source. These compounds could be probably vivianite.

Biominerals formed after **1 week only!**

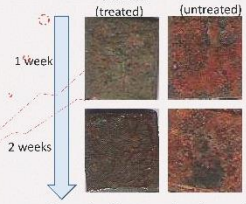

Treated and untreated marine aged iron plates, after 1 and 2 weeks of incubation with *S.loihica*.

Iron reduction monitoring

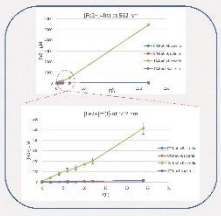

Curves showing the increase of iron (II) concentration during the incubation of aged iron plates with *S.loihica* after 24h and 1 week.

Acknowledgments: Swiss National Science Foundation (Ambizione grant PZ00P2_142514, PI. Dr. Edith Joseph) for the funding of MAIA project (Microbes for archaeological Iron Artefacts).

References: [1] Gao et al (2006) and [2] Moon et al (2007)

Oral presentation at Green conservation of cultural heritage workshop, Rome, Italy, October 2015.

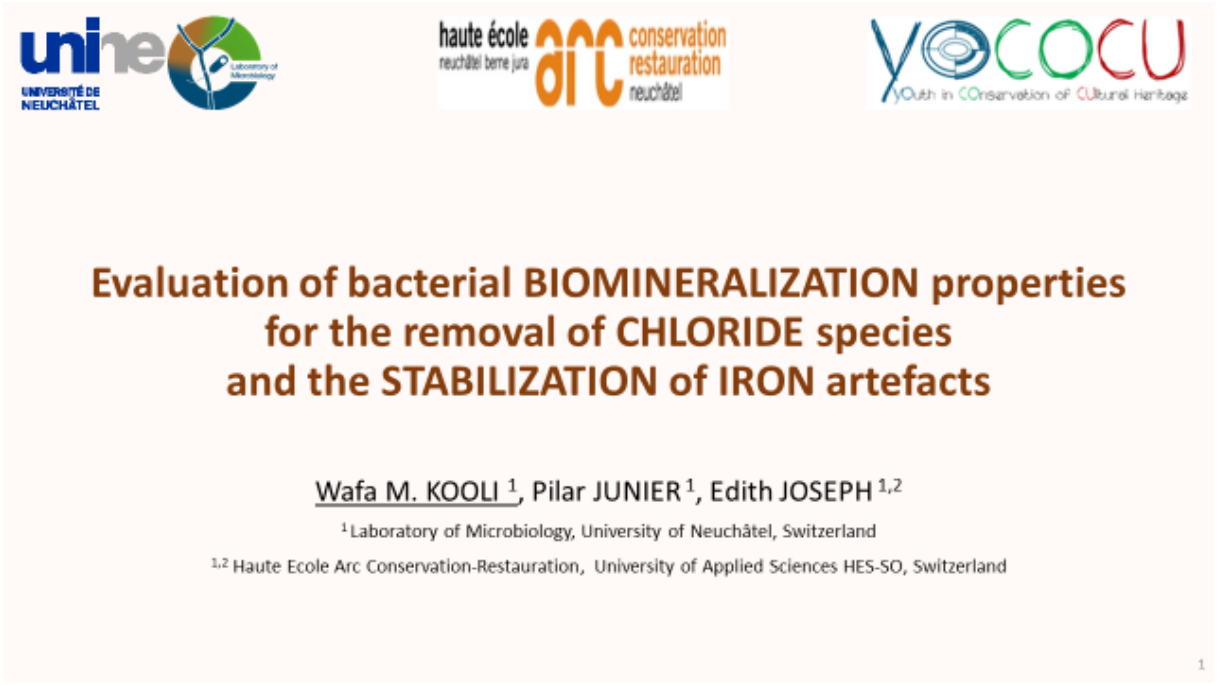

Oral presentation at Swiss Society for Microbiology meeting, Berne, Switzerland, June 2016

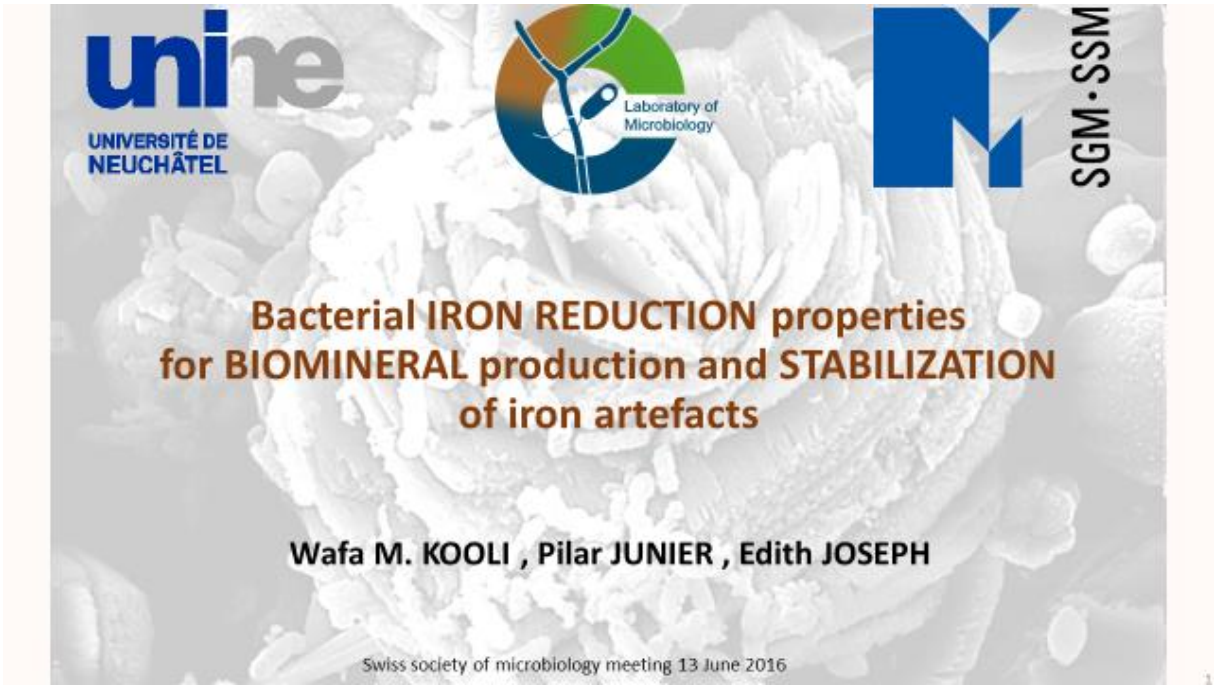

Curriculum Vitae

Education

January 2014-June 2018	**Ph.D. Microbiology** "Bacterial iron reduction properties for the stabilization of corroded iron artefacts"	**LAMUN – Laboratory of microbiology of the University of Neuchâtel** **Neuchâtel, Switzerland.** Supervisors: Pr Pilar Junier and Dr Edith Joseph
2010-2011	**M.Sc. Microbiology** Master thesis: " purification and biochemical caracterisation of a *S.cerevisiae*'s isomaltase	**National Institute of applied sciences (Insa), Toulouse, France.** Supervisor: Dr Claude Maranges
2004-2009	**Engineering studies in bio-industries**	**National Institute of applied sciences and technologies (INSAT) of Tunis, Tunisia.**

Research experience

March-August 2017	Internship focused on bioinformatic skills and especially on genomics analysis and RNA sequencing	**Los Alamos National Lab (Lanl). New Mexico, United States of America (USA).** Supervisor : Dr Patrick Chain
January-Februrary 2017	Collaboration on Protein extraction and Protein Pattern determination of bacteria under different parameters	**Ecole Polytechnique Fédérale de Lausanne (EPFL)**. Switzerland Supevisor : Dr Julien Maillard
January-March 2016	Collaboration focused on polyphosphate detection in bacteria	**Ecole polytechnique Federale de Lausanne (EPFL)**. Switzerland Supevisor : Dr Julien Maillard
March- June 2013	Internship focused on molecular biology and especially on Real-Time PCR	**Pasteur Institute of Tunis** Supervisor: Pr Aida bouratbine
March- July 2012	Internship on microbiological analysis of various food, drinks and bathing water	**Regional laboratory of public health, Nabeul, Tunisia** Supervisor: Dr Abdelhamid Gharbi
September 2009 - January 2010	Engineering end of studies thesis " Study about biochemicals and metabolic inhibition mechanisms of the yeast *S.Cerevisiae* growth by 2-Phényléthanol"	**National Institute of applied sciences (Insa) –Toulouse, France** Supervisor: Dr Philippe Blanc
June-August 2006	Internship focused on food microbial analysis	**Regional laboratory of Public Health, Nabeul, Tunisia.** Supervisor: Dr A. Gharbi
September-October 2006	Internship:" Study of the cellular viability of *Lactobacillus plantarum* on preserved shape"	**National Institute of Applied sciences and technologies (INSAT) of Tunis, Tunisia.** Supervisor: Dr Hamdi Mokhtar

Technical skills

Biochemistry	- Enzymatic assays
Molecular biology	- DNA extractions, cloning - PCR, RT qPCR
Microscopy	- Optical microscopy - Scanning Electron Microscopy (SEM)
Microbiology	- Culture, isolation and characterization (bacteria, fungi) - Microbial extraction from Lakes
Chemistry	- Spectrophotometry - X-ray Diffraction (XRD) - Energy-dispersive X-ray spectroscopy (EDS) - Raman spectroscopy
Scientific communication	- Member of the CUSO transversal program - Member of the museum "histoire naturelle" of Neuchâtel - Co-organization of the annual PhD meeting, University of Neuchâtel
Languages	- French (fluent) - English (fluent) - Arabic (native language)

Training workshops attended

- Blogging and using Twitter for scientific communication, University of Lausanne, March 2014
- Effective public speaking, University of Neuchâtel, Switzerland, October 2014
- Scanning electronic microscopy, University of Neuchâtel, Switzerland, April 2014
- 5th international course in microbial ecology, Venice, Italy, October 2014
- Introduction to chromatography and mass spectrometry for biologists, November 2014
- Biomineralization short course, Paris, France, December 2014
- Introduction to bioinformatics, May-June 2015
- Symposium in RNAseq data gathering and analysis - a joint course with CUSO, November 2015

Teaching and supervising

- University of Neuchâtel for the Bachelor students (2014-2017): Practical teaching in bacteriology
- Supervision of interns and master students